

AD-A237 988



DTIC  
ELECTE  
JUL 10 1991  
S C D

2

# NAVAL POSTGRADUATE SCHOOL Monterey, California



Accession For	
DTIC Report	<input checked="" type="checkbox"/>
DTIC Tab	<input type="checkbox"/>
Unclassified	<input type="checkbox"/>
Justification	
by	
Distribution/	
Availability Codes	
Dist	Avail and/or Special
A-1	

## THESIS



**EFFECTS OF IMPOSED BULK FLOW OSCILLATIONS  
AT 1, 2, 3 AND 4 HZ ON TRANSITION IN A STRAIGHT  
CHANNEL WITH 40 TO 1 ASPECT RATIO**

by

**Howard E. Koth**

**June 1990**

**Thesis Advisor: Phillip M. Ligrani  
Co-Advisor: Chelakara S. Subramanian**

Approved for public release; distribution is unlimited.

91-04474



Unclassified

Security Classification of this page

REPORT DOCUMENTATION PAGE

1a Report Security Classification <b>Unclassified</b>		1b Restrictive Markings	
2a Security Classification Authority		3 Distribution Availability of Report	
2b Declassification/Downgrading Schedule		Approved for public release; distribution is unlimited.	
4 Performing Organization Report Number(s)		5 Monitoring Organization Report Number(s)	
6a Name of Performing Organization Naval Postgraduate School	6b Office Symbol (If Applicable) 33	7a Name of Monitoring Organization Naval Postgraduate School	
6c Address (city, state, and ZIP code) Monterey, CA 93943-5000		7b Address (city, state, and ZIP code) Monterey, CA 93943-5000	
8a Name of Funding/Sponsoring Organization NPS Direct Funding	8b Office Symbol	9 Procurement Instrument Identification Number (If Applicable)	
8c Address (city, state, and ZIP code) Monterey, CA 93943-5000		10 Source of Funding Numbers	
Program Element Number		Project No	Task No
			Work Unit Accession No

11 Title (Include Security Classification) **THE EFFECTS OF 1, 2, 3 AND 4 HZ IMPOSED BULK FLOW OSCILLATIONS ON LAMINAR TO TURBULENT TRANSITION IN A STRAIGHT CHANNEL**

12 Personal Author(s) <b>Howard E. Koth</b>			
13a Type of Report Master's Thesis	13b Time Covered From To	14 Date of Report (year, month, day) June 1990	15 Page Count 244
16 Supplementary Notation <b>The views expressed in this thesis are those of the author and do not reflect the official policy or position of the Department of Defense or the U.S. Government.</b>			

17 Cosati Codes			18 Subject Terms (continue on reverse if necessary and identify by block number) Imposed Oscillations, Tollmien-Schlichting Waves, Klebanoff Type Waves, Phase-Averaged Velocity, Longitudinal Velocity Fluctuations, Intermittency, Center Mode of Secondary Instability
Field	Group	Subgroup	

19 Abstract (continue on reverse if necessary and identify by block number)  
 A channel with 40 to 1 aspect ratio and rectangular cross-section is used to study the effects of imposed oscillations on transition from laminar to turbulent flow. Oscillations are imposed using a single rotating vane located in the flow downstream of the test section. Flows with Reynolds numbers ranging from 1100 to 3580 and Strouhal numbers from 0.0211 to 0.2418 are studied. For all cases, time-averaged velocity profiles are unaffected by imposed oscillations. Imposed oscillations have a destabilizing effect on the flow near the edge of the Stokes layer. Turbulence intensity magnitudes with imposed oscillations show that transition to turbulence begins at lower Reynolds numbers and extends over a wider range of Reynolds numbers than when no imposed oscillations are present. In addition, higher levels of intermittency are present with imposed oscillations for Reynolds numbers 1900 to 2200 at  $y/d = 0.90$ . At Reynolds numbers from 1450 to 1800, frequency spectra evidence high intensity intermittent turbulent fluctuations, followed and preceded by quiescent flow, both with and without imposed oscillations. A center mode of secondary instability is evidenced by high values of normalized longitudinal turbulence intensity measured in the channel center when no oscillations are imposed on the flow. Imposed oscillations are found to suppress this center mode of secondary instability, as evidenced by reductions in longitudinal turbulence intensity values near the channel center.

20 Distribution/Availability of Abstract <input checked="" type="checkbox"/> unclassified/unlimited <input type="checkbox"/> same as report <input type="checkbox"/> DTIC users		21 Abstract Security Classification <b>Unclassified</b>	
22a Name of Responsible Individual <b>Phillip M. Ligrani</b>		22b Telephone (Include Area code) <b>(408) 646-3382</b>	22c Office Symbol <b>69Li</b>

Approved for public release; distribution is unlimited.

**Effects of 1, 2, 3 and 4 Hz Imposed Bulk Flow Oscillations on  
Transition in a Straight Channel with 40 to 1 Aspect Ratio.**

by

**Howard Edwin Koth  
Lieutenant, United States Navy  
B.S., University of Wisconsin-Eau Claire, 1981**

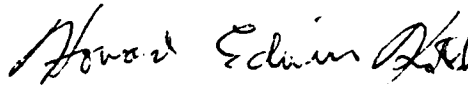
Submitted in partial fulfillment of the requirements  
for the degree of

**MASTER OF SCIENCE IN MECHANICAL  
ENGINEERING**

from the

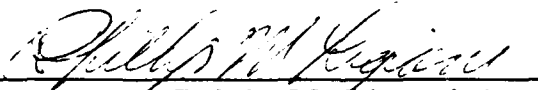
**NAVAL POSTGRADUATE SCHOOL  
June 1990**

Author:



**Howard Edwin Koth**

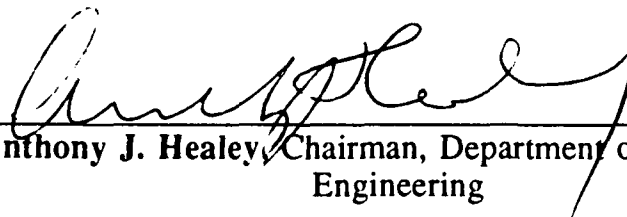
Approved by:



**Phillip M. Ligrani, Thesis Advisor**



**Chelakara. S. Subramanian, Co-Advisor**



**Anthony J. Healey, Chairman, Department of Mechanical  
Engineering**

## ABSTRACT

A channel with 40 to 1 aspect ratio and rectangular cross-section is used to study the effects of imposed oscillations on transition from laminar to turbulent flow. Oscillations are imposed using a single rotating vane located in the flow downstream of the test section. Flows with Reynolds numbers ranging from 1100 to 3580 and Strouhal numbers from 0.0211 to 0.2418 are studied. For all cases, time-averaged velocity profiles are unaffected by imposed oscillations.

Imposed oscillations have a destabilizing effect on the flow near the edge of the Stokes layer. Turbulence intensity magnitudes with imposed oscillations show that transition to turbulence begins at lower Reynolds numbers and extends over a wider range of Reynolds numbers than when no imposed oscillations are present. In addition, higher levels of intermittency are present with imposed oscillations for Reynolds numbers 1900 to 2200 at  $y/d = 0.90$ . At Reynolds numbers from 1450 to 1800, frequency spectra evidence high intensity intermittent turbulent fluctuations, followed and preceded by quiescent flow, both with and without imposed oscillations. A center mode of secondary instability is evidenced by high values of normalized longitudinal turbulence intensity measured in the channel center when no oscillations are imposed on the flow. Imposed oscillations are found to suppress this center mode of secondary instability, as evidenced by reductions in longitudinal turbulence intensity values near the channel center.

## TABLE OF CONTENTS

I. INTRODUCTION.....	1
A. BACKGROUND.....	1
B. OBJECTIVES.....	5
C. THESIS ORGANIZATION.....	6
II. EXPERIMENTAL FACILITIES.....	7
A. CHANNEL.....	7
B. UNSTEADINESS DEVICE.....	9
C. FLOW MEASURING INSTRUMENTS.....	11
1. Hot-wire Probe and Probe Positioning.....	11
2. Hot-wire Bridge.....	12
3. Signal Conditioner.....	12
4. High Speed Data Acquisition System.....	12
5. Data Storage.....	14
D. FLOW VISUALIZATION.....	14
1. Smoke Wire System.....	14
2. Video Equipment.....	15
III. EXPERIMENTAL PROCEDURES.....	16
A. HOT-WIRE CALIBRATION.....	16
B. DATA PROCESSING.....	16
1. Bulk Velocity.....	16
2. Instantaneous Velocity.....	17
3. Phase Averaging.....	17
C. SPECTRAL MEASUREMENTS.....	19

IV. RESULTS AND DISCUSSION.....	20
A. CHANNEL FLOW VALIDATION.....	20
B. EFFECT OF IMPOSED OSCILLATIONS ON MEAN VELOCITY PROFILE AT VARIOUS REYNOLDS NUMBERS.....	20
C. EFFECT OF IMPOSED OSCILLATIONS ON RMS VELOCITY PROFILES AT VARIOUS REYNOLDS NUMBERS .....	21
D. EFFECT OF IMPOSED OSCILLATIONS ON NORMALIZED RMS VELOCITY AS A FUNCTION OF REYNOLDS NUMBER....	23
1. Near-Wall Region.....	23
2. Center of the Channel.....	24
E. EFFECT OF REYNOLDS NUMBER ON PHASE-AVERAGED VELOCITY TRACES.....	25
F. EFFECT OF IMPOSED OSCILLATIONS ON INTERMITTENCY AT VARIOUS REYNOLDS NUMBERS.....	26
G. EFFECT OF IMPOSED OSCILLATIONS ON FREQUENCY SPECTRA AT VARIOUS REYNOLDS NUMBERS.....	28
H. FLOW VISUALIZATION RESULTS.....	30
I. UNCERTAINTY ANALYSIS.....	31
V. SUMMARY AND CONCLUSIONS.....	32
APPENDIX A. (SOFTWARE DIRECTORY).....	34
APPENDIX B. (FIGURES).....	37
LIST OF REFERENCES.....	219
INITIAL DISTRIBUTION LIST.....	223

## LIST OF FIGURES

- Figure 1. Schematic of straight channel.
- Figure 2. Schematic of the unsteadiness generating device.
- Figure 3. Illustration of velocity variation with vane position during imposed oscillations for quasi-steady flow.
- Figure 4. Schematic of flow measurement equipment.
- Figure 5. Bulk velocity versus orifice differential pressure.
- Figure 6. Instantaneous and phase-averaged velocity variations with imposed unsteadiness at  $f_{osc} = 2$  Hz,  $v_{blk} = 4.38$  m/s.
- Figure 7. Typical settings for Dynamic Signal Analyzer.
- Figure 8. Theoretical and measured mean velocity profiles for laminar flow.
- Figure 9. Mean velocity profiles without imposed oscillations and with imposed oscillations for  $f_{osc} = 1$  Hz at Reynolds number 1103.
- Figure 10. Mean velocity profiles without imposed oscillations and with imposed oscillations for  $f_{osc} = 1$  Hz at Reynolds number 1579.
- Figure 11. Mean velocity profiles without imposed oscillations and with imposed oscillations for  $f_{osc} = 1$  Hz at Reynolds number 2005.

- Figure 12. Mean velocity profiles without imposed oscillations and with imposed oscillations for  $f_{osc} = 1$  Hz at Reynolds number 2197.
- Figure 13. Mean velocity profiles without imposed oscillations and with imposed oscillations for  $f_{osc} = 1$  Hz at Reynolds number 2548.
- Figure 14. Mean velocity profiles without imposed oscillations and with imposed oscillations for  $f_{osc} = 1$  Hz at Reynolds number 3584.
- Figure 15. Normalized RMS velocity profiles without imposed oscillations and with imposed oscillations for  $f_{osc} = 1$  Hz at Reynolds number 1103.
- Figure 16. Normalized RMS velocity profiles without imposed oscillations and with imposed oscillations for  $f_{osc} = 1$  Hz at Reynolds number 1579.
- Figure 17. Normalized RMS velocity profiles without imposed oscillations and with imposed oscillations for  $f_{osc} = 1$  Hz at Reynolds number 2005.
- Figure 18. Normalized RMS velocity profiles without imposed oscillations and with imposed oscillations for  $f_{osc} = 1$  Hz at Reynolds number 2197.
- Figure 19. Normalized RMS velocity profiles without imposed oscillations and with imposed oscillations for  $f_{osc} = 1$  Hz at Reynolds number 2548.



- Figure 20. Normalized RMS velocity profiles without imposed oscillations and with imposed oscillations for  $f_{osc} = 1$  Hz at Reynolds number 3584.
- Figure 21. Longitudinal velocity fluctuations versus Reynolds number without imposed oscillations and with imposed oscillations for  $f_{osc} = 1$  Hz at  $y/d = 0.90$ .
- Figure 22. Longitudinal velocity fluctuations versus Reynolds number without imposed oscillations and with imposed oscillations for  $f_{osc} = 2$  Hz at  $y/d = 0.90$ .
- Figure 23. Longitudinal velocity fluctuations versus Reynolds number without imposed oscillations and with imposed oscillations for  $f_{osc} = 3$  Hz at  $y/d = 0.90$ .
- Figure 24. Longitudinal velocity fluctuations versus Reynolds number without imposed oscillations and with imposed oscillations for  $f_{osc} = 4$  Hz at  $y/d = 0.90$ .
- Figure 25. Longitudinal velocity fluctuations versus Reynolds number without imposed oscillations and with imposed oscillations for  $f_{osc} = 1$  Hz at  $y/d = 0.50$ .
- Figure 26. Longitudinal velocity fluctuations versus Reynolds number without imposed oscillations and with imposed oscillations for  $f_{osc} = 1$  Hz at  $y/d = 0.50$  ( Coumes Data ).
- Figure 27. Phase-averaged velocity and rms velocity traces at  $y/d = 0.90$  for  $Re = 1579$ ,  $f_{osc} = 1$  Hz,  $Str = 0.04222$ .
- Figure 28. Phase-averaged velocity and rms velocity traces at  $y/d = 0.90$  for  $Re = 1693$ ,  $f_{osc} = 1$  Hz,  $Str = 0.03939$ .

- Figure 29. Phase-averaged velocity and rms velocity traces at  $y/d = 0.90$  for  $Re = 1796$ ,  $f_{osc} = 1$  Hz,  $Str = 0.03711$ .
- Figure 30. Phase-averaged velocity and rms velocity traces at  $y/d = 0.90$  for  $Re = 1905$ ,  $f_{osc} = 1$  Hz,  $Str = 0.035$ .
- Figure 31. Phase-averaged velocity and rms velocity traces at  $y/d = 0.90$  for  $Re = 2005$ ,  $f_{osc} = 1$  Hz,  $Str = 0.03325$ .
- Figure 32. Phase-averaged velocity and rms velocity traces at  $y/d = 0.90$  for  $Re = 2106$ ,  $f_{osc} = 1$  Hz,  $Str = 0.03166$ .
- Figure 33. Phase-averaged velocity and rms velocity traces at  $y/d = 0.90$  for  $Re = 22197$ ,  $f_{osc} = 1$  Hz,  $Str = 0.03034$ .
- Figure 34. Phase-averaged velocity and rms velocity traces at  $y/d = 0.90$  for  $Re = 2548$ ,  $f_{osc} = 1$  Hz,  $Str = 0.02616$ .
- Figure 35. Phase-averaged velocity and rms velocity traces at  $y/d = 0.90$  for  $Re = 3584$ ,  $f_{osc} = 1$  Hz,  $Str = 0.0186$ .
- Figure 36. Phase-averaged velocity and rms velocity traces at  $y/d = 0.90$  for  $Re = 2047$ ,  $f_{osc} = 3$  Hz,  $Str = 0.09771$ .
- Figure 37. Phase-averaged velocity and rms velocity traces at  $y/d = 0.90$  for  $Re = 2126$ ,  $f_{osc} = 4$  Hz,  $Str = 0.1254$ .
- Figure 38. Intermittency versus Reynolds number at  $y/d = 0.90$
- Figure 39. Intermittency versus Reynolds number at  $y/d = 0.50$
- Figure 40. Phase-averaged velocity and intermittency traces at  $y/d = 0.90$  for  $Re = 1212$ ,  $f_{osc} = 1$  Hz.
- Figure 41. Phase-averaged velocity and intermittency traces at  $y/d = 0.90$  for  $Re = 1579$ ,  $f_{osc} = 1$  Hz.

- Figure 42. Phase-averaged velocity and intermittency traces at  $y/d = 0.90$  for  $Re = 1604$ ,  $f_{osc} = 1$  Hz.
- Figure 43. Phase-averaged velocity and intermittency traces at  $y/d = 0.90$  for  $Re = 1693$ ,  $f_{osc} = 1$  Hz.
- Figure 44. Phase-averaged velocity and intermittency traces at  $y/d = 0.90$  for  $Re = 1796$ ,  $f_{osc} = 1$  Hz.
- Figure 45. Phase-averaged velocity and intermittency traces at  $y/d = 0.90$  for  $Re = 1905$ ,  $f_{osc} = 1$  Hz.
- Figure 46. Phase-averaged velocity and intermittency traces at  $y/d = 0.90$  for  $Re = 2005$ ,  $f_{osc} = 1$  Hz.
- Figure 47. Phase-averaged velocity and intermittency traces at  $y/d = 0.90$  for  $Re = 2043$ ,  $f_{osc} = 1$  Hz.
- Figure 48. Phase-averaged velocity and intermittency traces at  $y/d = 0.90$  for  $Re = 2106$ ,  $f_{osc} = 1$  Hz.
- Figure 49. Phase-averaged velocity and intermittency traces at  $y/d = 0.90$  for  $Re = 2156$ ,  $f_{osc} = 1$  Hz.
- Figure 50. Phase-averaged velocity and intermittency traces at  $y/d = 0.90$  for  $Re = 2197$ ,  $f_{osc} = 1$  Hz.
- Figure 51. Phase-averaged velocity and intermittency traces at  $y/d = 0.90$  for  $Re = 2252$ ,  $f_{osc} = 1$  Hz.
- Figure 52. Phase-averaged velocity and intermittency traces at  $y/d = 0.90$  for  $Re = 2302$ ,  $f_{osc} = 1$  Hz.
- Figure 53. Phase-averaged velocity and intermittency traces at  $y/d = 0.50$  for  $Re = 1103$ ,  $f_{osc} = 1$  Hz.

Figure 54. Phase-averaged velocity and intermittency traces at  $y/d = 0.50$  for  $Re = 1579$ ,  $f_{osc} = 1$  Hz.

Figure 55. Phase-averaged velocity and intermittency traces at  $y/d = 0.50$  for  $Re = 2005$ ,  $f_{osc} = 1$  Hz.

Figure 56. Phase-averaged velocity and intermittency traces at  $y/d = 0.50$  for  $Re = 2197$ ,  $f_{osc} = 1$  Hz.

Figure 57. Phase-averaged velocity and intermittency traces at  $y/d = 0.50$  for  $Re = 2548$ ,  $f_{osc} = 1$  Hz.

Figure 58. Phase-averaged velocity and intermittency traces at  $y/d = 0.50$  for  $Re = 3584$ ,  $f_{osc} = 1$  Hz.

Figures 59 to 78. Frequency Spectra of Hot-Wire Probe Voltage Squared Divided by Hz versus Hz for Ranges 0.1 to 200 Hz and 0.1 to 20 Hz for 20 Averages at various Reynolds numbers without imposed oscillations.

Figure 59.  $Re = 1103$ .

Figure 60.  $Re = 1212$ .

Figure 61.  $Re = 1308$ .

Figure 62.  $Re = 1396$ .

Figure 63.  $Re = 1496$ .

Figure 64.  $Re = 1542$ .

Figure 65.  $Re = 1604$ .

Figure 66.  $Re = 1650$ .

Figure 67.  $Re = 1697$ .

Figure 68.  $Re = 1742$ .

Figure 69.  $Re = 1796$ .

Figure 70.  $Re = 1905$ .

Figure 71.  $Re = 2005$ .

Figure 72.  $Re = 2097$ .

Figure 73.  $Re = 2198$ .

Figure 74.  $Re = 2298$ .

Figure 75.  $Re = 2402$ .

Figure 76.  $Re = 2498$ .

Figure 77.  $Re = 2599$ .

Figure 78.  $Re = 2699$ .

Figures 79 to 98. Frequency Spectra of Hot-Wire Probe Voltage

Squared Divided by Hz versus Hz for Ranges 0.1 to  
200 Hz and 0.1 to 20 Hz for 20 Averages at various  
Reynolds numbers with imposed oscillations.

Figure 79.  $Re = 1103$ ,  $f_{osc} = 1$  Hz.

Figure 80.  $Re = 1212$ ,  $f_{osc} = 1$  Hz.

Figure 81.  $Re = 1308$ ,  $f_{osc} = 1$  Hz.

Figure 82.  $Re = 1396$ ,  $f_{osc} = 1$  Hz.

Figure 83.  $Re = 1496$ ,  $f_{osc} = 1$  Hz.

Figure 84.  $Re = 1542$ ,  $f_{osc} = 1$  Hz.

Figure 85.  $Re = 1604$ ,  $f_{osc} = 1$  Hz.

Figure 86.  $Re = 1650$ ,  $f_{osc} = 1$  Hz.

Figure 87.  $Re = 1696$ ,  $f_{osc} = 1$  Hz.

Figure 88.  $Re = 1742$ ,  $f_{osc} = 1$  Hz.

Figure 89.  $Re = 1796$ ,  $f_{osc} = 1$  Hz.

Figure 90.  $Re = 1905$ ,  $f_{osc} = 1$  Hz.

Figure 91.  $Re = 2005, f_{osc} = 1 \text{ Hz}$ .

Figure 92.  $Re = 2097, f_{osc} = 1 \text{ Hz}$ .

Figure 93.  $Re = 2197, f_{osc} = 1 \text{ Hz}$ .

Figure 94.  $Re = 2298, f_{osc} = 1 \text{ Hz}$ .

Figure 95.  $Re = 2402, f_{osc} = 1 \text{ Hz}$ .

Figure 96.  $Re = 2498, f_{osc} = 1 \text{ Hz}$ .

Figure 97.  $Re = 2599, f_{osc} = 1 \text{ Hz}$ .

Figure 98.  $Re = 2699, f_{osc} = 1 \text{ Hz}$ .

Figures 99 to 107. Frequency Spectra of Hot-Wire Probe Voltage

Squared Divided by Hz versus Hz for Ranges 0.1 to  
200 Hz and 0.1 to 20 Hz for 40 Averages at various  
Reynolds numbers without imposed oscillations.

Figure 99.  $Re = 1396$ .

Figure 100.  $Re = 1454$ .

Figure 101.  $Re = 1496$ .

Figure 102.  $Re = 1542$ .

Figure 103.  $Re = 1604$ .

Figure 104.  $Re = 1650$ .

Figure 105.  $Re = 1697$ .

Figure 106.  $Re = 1742$ .

Figure 107.  $Re = 1796$ .

Figures 108 to 116. Frequency Spectra of Hot-Wire Probe Voltage Squared Divided by Hz versus Hz for Ranges 0.1 to 200 Hz and 0.1 to 20 Hz for 40 Averages at various Reynolds numbers with imposed oscillations.

Figure 108.  $Re = 1396, f_{osc} = 1 \text{ Hz}$ .

Figure 109.  $Re = 1454, f_{osc} = 1 \text{ Hz}$ .

Figure 110.  $Re = 1496, f_{osc} = 1 \text{ Hz}$ .

Figure 111.  $Re = 1542, f_{osc} = 1 \text{ Hz}$ .

Figure 112.  $Re = 1604, f_{osc} = 1 \text{ Hz}$ .

Figure 113.  $Re = 1650, f_{osc} = 1 \text{ Hz}$ .

Figure 114.  $Re = 1696, f_{osc} = 1 \text{ Hz}$ .

Figure 115.  $Re = 1742, f_{osc} = 1 \text{ Hz}$ .

Figure 116.  $Re = 1796, f_{osc} = 1 \text{ Hz}$ .

Figures 117 to 131. Frequency Spectra of Hot-Wire Probe Voltage Squared Divided by Hz versus Hz for Range 0.1 to 200 Hz and plot of voltage versus time for 0 to 3.2 seconds at various Reynolds numbers without imposed oscillations.

Figure 117.  $Re = 1396$ .

Figure 118.  $Re = 1454$ .

Figure 119.  $Re = 1496$ .

Figure 120.  $Re = 1542$ .

Figure 121.  $Re = 1604$ .

Figure 122.  $Re = 1650$ .

Figure 123.  $Re = 1697$ .

Figure 124.  $Re = 1742$ .

Figure 125.  $Re = 1796$ .

Figure 126.  $Re = 1905$ .

Figure 127.  $Re = 2005$ .

Figure 128.  $Re = 2097$ .

Figure 129.  $Re = 2198$ .

Figure 130.  $Re = 2298$ .

Figure 131.  $Re = 2402$ .

Figures 132 to 147. Frequency Spectra of Hot-Wire Probe Voltage

Squared Divided by Hz versus Hz for Range 0.1 to 20 Hz and plot of voltage versus time for 0 to 3.2 seconds at various Reynolds numbers without imposed oscillations.

Figure 132.  $Re = 1396$ .

Figure 133.  $Re = 1454$ .

Figure 134.  $Re = 1496$ .

Figure 135.  $Re = 1542$ .

Figure 136.  $Re = 1604$ .

Figure 137.  $Re = 1650$ .

Figure 138.  $Re = 1697$ .

Figure 139.  $Re = 1742$ .

Figure 140.  $Re = 1796$ .

Figure 141.  $Re = 1905$ .

Figure 142.  $Re = 2005$ .



Figure 143.  $Re = 2097$ .

Figure 144.  $Re = 2198$ .

Figure 145.  $Re = 2298$ .

Figure 146.  $Re = 2402$ .

Figures 147 to 161. Frequency Spectra of Hot-Wire Probe Voltage Squared Divided by Hz versus Hz for Range 0.1 to 200 Hz and plot of voltage versus time for 0 to 3.2 seconds at various Reynolds numbers with imposed oscillations.

Figure 147.  $Re = 1396, f_{osc} = 1$  Hz.

Figure 148.  $Re = 1454, f_{osc} = 1$  Hz.

Figure 149.  $Re = 1496, f_{osc} = 1$  Hz.

Figure 150.  $Re = 1542, f_{osc} = 1$  Hz.

Figure 151.  $Re = 1604, f_{osc} = 1$  Hz.

Figure 152.  $Re = 1650, f_{osc} = 1$  Hz.

Figure 153.  $Re = 1696, f_{osc} = 1$  Hz.

Figure 154.  $Re = 1742, f_{osc} = 1$  Hz.

Figure 155.  $Re = 1796, f_{osc} = 1$  Hz.

Figure 156.  $Re = 1905, f_{osc} = 1$  Hz.

Figure 157.  $Re = 2005, f_{osc} = 1$  Hz.

Figure 158.  $Re = 2097, f_{osc} = 1$  Hz.

Figure 159.  $Re = 2197, f_{osc} = 1$  Hz.

Figure 160.  $Re = 2298, f_{osc} = 1$  Hz.

Figure 161.  $Re = 2402, f_{osc} = 1$  Hz.

Figures 162 to 176. Frequency Spectra of Hot-Wire Probe Voltage Squared Divided by Hz versus Hz for Range 0.1 to 200 Hz and plot of voltage versus time for 0 to 3.2 seconds at various Reynolds numbers with imposed oscillations.

Figure 162.  $Re = 1396, f_{osc} = 1$  Hz.

Figure 163.  $Re = 1454, f_{osc} = 1$  Hz.

Figure 164.  $Re = 1496, f_{osc} = 1$  Hz.

Figure 165.  $Re = 1542, f_{osc} = 1$  Hz.

Figure 166.  $Re = 1604, f_{osc} = 1$  Hz.

Figure 167.  $Re = 1650, f_{osc} = 1$  Hz.

Figure 168.  $Re = 1696, f_{osc} = 1$  Hz.

Figure 169.  $Re = 1742, f_{osc} = 1$  Hz.

Figure 170.  $Re = 1796, f_{osc} = 1$  Hz.

Figure 171.  $Re = 1905, f_{osc} = 1$  Hz.

Figure 172.  $Re = 2005, f_{osc} = 1$  Hz.

Figure 173.  $Re = 2097, f_{osc} = 1$  Hz.

Figure 174.  $Re = 2197, f_{osc} = 1$  Hz.

Figure 175.  $Re = 2298, f_{osc} = 1$  Hz.

Figure 176.  $Re = 2402, f_{osc} = 1$  Hz.

Figure 177. Smoke-wire patterns for  $Re = 1604$ , steady flow

Figure 178. Smoke-wire patterns for  $Re = 1696$ , steady flow

Figure 179. Smoke-wire patterns for  $Re = 1696, f_{osc} = 1$  Hz

Figure 180. Smoke-wire patterns for  $Re = 1905, f_{osc} = 1$  Hz

Figure 181. Smoke-wire patterns for  $Re = 1604, f_{osc} = 2$  Hz, 3 Hz

## TABLE OF SYMBOLS

$d$	channel height
$f_{osc}$	frequency of imposed oscillation
$n_{cycl}$	number of imposed oscillation cycles
$Re$	Reynolds number, $v_{blk} d/n$
$Str$	Strouhal number, $2\pi f_{osc} d/v_{blk}$
$t_{st}$	Stokes layer thickness, $\sqrt{\frac{\nu}{2\pi f_{osc}}}$
$U$	instantaneous longitudinal velocity
$v_{blk}$	bulk mean velocity
$\bar{u}$	mean streamwise velocity
$\hat{u}$	phase-averaged streamwise velocity
$\tilde{u}$	periodic streamwise velocity component from imposed oscillations
$u'$	instantaneous streamwise fluctuating velocity
$x$	longitudinal coordinate, measured from the nozzle exit
$y$	normal coordinate, measured from the bottom wall
$z$	spanwise coordinate, measured from the channel centerline
$D$	difference
$\Omega$	Stokes number, $d/2t_{st}$
$\nu$	kinematic viscosity

## **ACKNOWLEDGEMENTS**

This work is sponsored by the Office of Naval Research and the Naval Postgraduate School. Dr. Spiro Lekoudis is the program monitor.

The author wishes to acknowledge, with gratitude, Professors Ligrani and Subramanian for their guidance in the conducting of the research and the drafting of this document.

## I. INTRODUCTION

### A. BACKGROUND

Flow oscillations and unsteadiness are present in many practical flow situations occurring in aerodynamics, naval engineering, bio-engineering, and wind engineering. Most of these flows, especially those of technological interest, also undergo transition from a laminar state to a turbulent state. Transition is extremely complex by itself and when it also interacts with flow oscillations and unsteadiness, accurate prediction of the location and extent of transition and the accompanying changes of important flow properties is even farther beyond present modelling and computational abilities. Consequently, experiments are needed to elucidate flow behavior. According to Shemer [Ref. 1], such experiments should be "restricted to the simplest and most well-defined conditions," in order to "obtain a clear physical description of a fluid dynamical process."

The present study employs a straight channel not only to investigate a situation consistent with Shemer's [Ref. 1] suggestion, but also because this flow has not yet been studied experimentally. Even though some experimental results are available for pipe flows and some analytic and numeric results are available for channel flows, the author knows of no other experiments, other than the current work, performed to study the stability or transition of plane channel flow with imposed oscillations.

The imposed flow oscillations are induced in the present study using a single rotating vane located in the flow downstream of the test section. The device is similar to the rotating profiled sleeves employed by Tu and Ramaprian [Ref. 2], Ramaprian and Tu [Ref. 3] and Stettler and Hussain [Ref. 4] to study the influences of sinusoidal oscillations on pipe flows. Their sleeves are used in water and operate simply by altering the exit flow area. Other studies of the influences of imposed oscillations on pipe flows use reciprocating pistons in cylinders to produce the unsteadiness [Ref. 1], [Ref. 5] to [Ref. 11]. Simpson et al [Ref. 12] use a rotating blade damper system at the inlet of their wind tunnel, upstream of screens and honeycomb, in order to study the effects of unsteadiness on turbulent boundary layer flows. By changing the motion of the five individual damper blades, sinusoidal perturbations to the flow are produced with amplitudes amounting to 11-93 % of the maximum velocity over frequencies from 0.6-2 Hz.

Of the experimental studies of transitional flows in pipes, Merkli and Thomann [Ref.5], Sergeev [Ref. 6], Hino and Sawamoto [Ref. 7], Hino et al [Ref. 8], Gerrard [Ref.9], Gilbrech and Combs [Ref. 10], Sarpakaya [Ref. 11], Ramaprian and Tu [Ref.3], Shemer [Ref. 1], and Stettler and Hussain [Ref. 4] also examine the effects of imposed oscillations. Of these studies, [Ref. 5] to [Ref. 8] investigate the instability of sinusoidally modulated pipe flow with zero mean flow. Gerrard [Ref. 9] conducts his experiments at the transition Reynolds number of 3770. He relates variations of turbulent flow over individual flow oscillations to magnitudes of vorticity diffusion. Diffusion rates

are then determined by a Stokes number equal to the ratio of the pipe radius to distance the vorticity diffuses during the period of one oscillation cycle. Gerrard also suggests that, with high oscillation frequency, viscous effects are confined to a very thin Stokes layer near the wall where the fluid is retarded. Gilbrech and Combs [Ref. 10] and Sarpakaya [Ref. 11] examine the effects of amplitude and frequency of imposed oscillations on the growth rate of artificially introduced plugs. Both investigators indicate that oscillations increase the critical Reynolds number as long as they are not so large as to cause local flow reversals. Ramaprian and Tu [Ref. 3] study transitional pipe flow at a mean Reynolds number of 2100. They indicate that flow oscillations at frequencies ranging from 0.05 to 1.75 Hz increase the critical Reynolds number only when the turbulent intermittency is small. With higher intermittency levels, the authors suggest that imposed oscillations affect the flow only when the oscillation frequency is near the characteristic frequency of the turbulence. Shemer's [Ref. 1] work focuses on large oscillation amplitudes at a single low frequency. For a mean Reynolds number of about 4000 and an oscillation frequency of 0.37 Hz, he concludes that transition is governed primarily by the instantaneous Reynolds number. Stettler and Hussain [Ref.4] present results for Stokes numbers as high as 70. The authors provide a three-dimensional map of the stability-transition boundary, and also indicate that transition in pipes is associated with plugs of turbulence which can grow or shrink in size.

Numerical and analytical investigations of the influences of imposed unsteadiness on flow in a plane channel are described by Grosch and Salwen [Ref. 13], Herbert [Ref.14], Hall [Ref. 15], von Kerczek [Ref. 16] and Singer, et al [Ref. 17,Ref. 18]. In addition to these studies, Tozzi [Ref. 19] provides results of a numerical investigation of the influences of imposed unsteadiness on flow in a pipe, and Davies [Ref. 20] provides a review of much work done on the stability of time periodic flows. Of the above mentioned analytic studies of plane channel flow, Grosch and Salwen [Ref. 13] solve a set of linearized equations by integrating through one period of oscillation. They conclude that flows with small amplitudes of imposed unsteadiness are more stable than steady flows, where the degree of stabilization depends upon interactions between shear waves generated by the imposed oscillation and flow disturbances. A modified version of Grosch and Salwen's energy analysis is described by Herbert [Ref. 14]. Hall [Ref. 15] reports results obtained with high frequency oscillations and concludes that such oscillations are slightly destabilizing irrespective of amplitude. von Kerczek [Ref. 16] modulates the pressure gradient in a perturbation analysis, and shows that the oscillating flow is more stable than the steady flow for frequencies of imposed oscillations greater than about one tenth of the frequency of the steady flow neutral disturbance. However, at both very low and very high frequencies of imposed oscillations, the flow is slightly unstable. Singer et al [Ref. 17, Ref. 18] describe results from a direct Navier-Stokes simulation of flow in a plane channel with imposed



unsteadiness and indicate that imposed sinusoidal oscillations provide a stabilizing effect at all but very low frequencies. Significant variations in the amplitudes of Tollmien-Schlichting waves are also noted which depend upon the Strouhal number and amplitude of the oscillations, as well as on initial amplitudes of the Tollmien-Schlichting waves. Tozzi's [Ref. 19] study of pipe flow shows that imposed oscillations are stabilizing up to very high amplitudes of imposed oscillation, a result in contradiction to a number of experimental studies which show that flow is destabilized even at low amplitudes.

## **B. OBJECTIVES**

This study is undertaken to obtain experimental data which shows the influences of 1 Hz, 2 Hz, 3 Hz, and 4 Hz imposed oscillations on laminar, transitional, and turbulent flows in a rectangular cross-section channel with 40 to 1 aspect ratio and 4.27 meter test section length. The results presented here are an extension of works by LCDRs T. Coumes, F. Greco, and J. Longest at NPS. Their studies found that imposed oscillations at 1 Hz and 2 Hz have a destabilizing effect on the longitudinal velocity fluctuations in the Stokes layer at some Reynolds numbers.

With a rotating vane assembly located downstream of the test section to produce the oscillations, Strouhal numbers from 0.0211 to 0.2418 are produced at Reynolds numbers ranging from 1100 to 3580, where each of these quantities is based on bulk mean velocity and channel height. With these conditions, experimental results in

the transition regime are included, which is important since the author knows of no other experimental studies, other than the current ones, in this area. In addition to providing a better understanding of some of the physical mechanisms which occur, data are also given on: (1) interactions between the imposed unsteadiness and flow phenomena which result in modifications to the waveform of the imposed unsteadiness, as well as (2) effect of imposed oscillations on the spectra and intermittency variations in the flow. Compared to existing numerical and analytical studies of transition phenomena [Ref. 13] to [Ref. 18], the present work thus provides a basis of comparison, and includes experimental conditions, such as the level of inlet disturbance, which are difficult to include accurately in numerical and analytic analyses.

### **C. THESIS ORGANIZATION**

In the sections which follow, details of the experimental facilities, the unsteadiness generating device, the data acquisition system, and the flow visualization equipment are given in section II. The experimental procedure, including calibration of the Hot-Wire Probe, channel validation, flow measurement, spectral analysis, and flow visualization are described in Section III. Results and discussion, including an uncertainty analysis are given in section IV. Section V contains the summary and conclusions.

## II. EXPERIMENTAL FACILITIES

### A. CHANNEL

The channel employed was designed especially for the present study. The facility is located in the laboratories of the Department of Mechanical Engineering of the Naval Postgraduate School, and is shown schematically in Figure 1. This figure also includes the coordinate system employed, where  $x$  is the longitudinal coordinate measured from the downstream edge of the nozzle,  $y$  is normal to the top and bottom surfaces of the channel and measured from the bottom wall, and  $z$  is the transverse coordinate, measured from the spanwise centerline of the channel.

The straight test section of the channel is 4.27 m in length with inside dimensions of 1.27 cm in height and 50.8 cm in width, giving an aspect ratio of 40 to 1. The top and bottom walls of the channel are made of 6.35 mm thick Plexiglass, and supported by ribs and cross beams along the length of the straight section. The side walls are removable in order to gain access to the inside of the channel. The inlet flow is managed using a honeycomb, screens and a 20:1 contraction ratio nozzle. Two layers of cheese cloth are also placed at the inlet to remove dust and dirt from the air entering the channel. The turbulence level of the flow at the nozzle exit is estimated to be about 0.06 % at a bulk speed of 3.4 m/s, based on a measurement in another similar facility.

At the exit of the 4.27 m long test section are three 10.16 cm long frames. Between the flanges of these frames are a total of four screens, in addition to a honeycomb placed just upstream of the last screen. The middle frame houses the device used to impose unsteadiness onto the flow. A 45.72 cm long two-dimensional diffuser with a total angle of 3 degrees is located downstream of the honeycomb section. This diffuser connects to the exit plenum chamber which provides a volume of uniform low-pressure air at the diffuser exit. Inside dimensions of the plenum are 60.96 cm  $\times$  60.96 cm  $\times$  60.96 cm. The plenum chamber is connected to the suction side of a 5 H.P blower using 5.08 cm inside diameter piping. Flow through the channel is metered using a 3.81 cm orifice plate assembly located between the plenum chamber and the blower.

Bulk flow velocities  $v_{blk}$  up to 15 m/s may be achieved in the channel. However, in the present experiments,  $v_{blk}$  ranges only from 1.3 m/s to 4.4 m/s. The channel is designed such that transition occurs after the laminar flow in the channel becomes fully developed, as indicated by normalized parabolic velocity profiles which are self-similar with respect to streamwise development. The initial flow development length is estimated to be vary between 0.56 m and 1.86 m for Reynolds numbers from 1100 to 3660 (Schlichting [Ref. 21]). This leaves 3.71 m to 2.41 m of fully developed flow in the straight portion of the channel.

## **B. UNSTEADINESS DEVICE**

Periodic variations of the flow rate can be induced in the test sections of wind tunnels, channel flows and pipe flows by introducing a periodic blockage at the inlet or exit of flow passages. The most important requirement of such an unsteady device is the ability to produce controlled deterministic and periodic unsteadiness without adding other disturbances. To achieve this in an open circuit induction channel, the unsteady device is best located just downstream of the test section. With this approach, wakes and other flow disturbances resulting from the operation of the unsteady device are not convected into the test section.

Such an approach is employed in the present study. The present design is shown in Figure 2. Since the height of the channel interior is only 1.27 cm, a single rotating vane is used to impose the required unsteadiness in the flow. Because the vane is located between the straight test section and the exit plenum (Figure 1), the rotating vane varies the amount of suction applied to the test section by varying the amount of flow resistance at the vane location.

The vane is made of a 3.2 mm thick brass strip with rounded edges, and Figure 2 shows that it spans a portion of the channel height when oriented normal to the flow. The vane is supported at the ends by a 3.2 mm diameter shaft and bushings that are fitted to the side walls of the frame. Three intermediate spanwise struts are provided to increase the rigidity of the vane as it rotates. One of the shafts is extended to accommodate a 48 tooth spur gear. This gear is driven by

a spur pinion with 12 teeth, which is mounted on the shaft of a Superior Electric, M092-FD310 Stepper Motor. The motor is driven by a Modulynx MITAS PMS085-D050 Drive, which is controlled by a Modulynx MITAS PMS085-C2AR Drive Controller. With this arrangement, the motor shaft may be positioned at 1/200th increments of one motor shaft revolution, and operated at speeds up to 100 revolutions per second. With a gearing ratio of 1 to 4 and two cycles of imposed flow oscillations per vane rotation, one motor revolution corresponds to one half of one cycle of an imposed flow oscillation. The imposed oscillation frequency is set by programming the Drive Controller for a particular motor speed which then sets the vane rotation rate. The amplitude of the imposed unsteadiness is altered by changing the width of the vane. A vane width of 8.7 mm is employed in the present study.

When the vane produces a quasi-steady flow, the flow behaves as if the vane rotation rate is infinitely small, or as if the vane is fixed at each position and allowed to reach steady-state behavior. The variation of the mean velocity under such circumstances is approximately sinusoidal, as illustrated in Figure 3. This waveform results because, momentarily, mass flow rates (and resulting velocities in the straight test section) are roughly proportional to the flow passage area provided by the vane as it rotates. In Figure 3, flow resistance is maximum and velocity in the straight section is minimum when the vane is normal to the flow with position 2. With vane

position 4, the flow resistance is minimum and the velocity is maximum.

Under actual conditions, the flow around the rotating vane is quite complex. Velocity and pressure variations are affected not only by the varying flow resistance from the vane, but also by other fluid dynamic effects such as dynamic flow separation and flow inertia. At large vane speeds, the vane rotations will likely result in a local swirl with blockage like a solid cylinder and minimal bulk flow periodicity. Imposed oscillatory flow behavior is thus different and difficult to predict compared to quasi-steady flow. The assessment of the performance of the rotating vane as it produces imposed velocity oscillations in the test section is given in Subramanian, et al. [Ref. 22].

### **C. FLOW MEASURING INSTRUMENTS**

A schematic of the flow measurement equipment is presented in Figure 4.

#### **1. Hot-wire Probe and Probe Positioning**

A DANTEC 55P51 hot-wire probe, with sensor diameter of  $5 \mu\text{m}$  and sensor length of 1.25 mm, is used for instantaneous velocity measurements. The probe is mounted with the wire horizontal and normal to the flow direction. The probe position is controlled by a rotatable lever arm which can adjust it through a range from  $y/d$  of 0.25 to 0.90. The lever arm is calibrated for probe positioning with an accuracy of approximately 0.5 mm. The probe is fixed with respect to

the longitudinal and horizontal axes at 3.81m from beginning of channel and 97.6 mm left of spanwise center.

## **2. Hot-wire Bridge**

A DISA 55M10 constant-temperature bridge is used to operate the hot-wire probe at an overheat ratio of 1.8. When connected to this bridge with the same settings used for measurements, the hot-wire is calibrated in the potential flow of a wind tunnel. The DC voltage from hot-wire bridge is measured using a Hewlett-Packard (HP) 3466A digital multimeter.

## **3. Signal Conditioner**

A DANTEC Model 56N20 signal conditioner is also used to amplify and filter the voltage from the bridge. During measurements, an amplifier gain of 10 is used, the low-pass filter is set to 10 kHz, and the high pass filter is set at 0.1 Hz, to reduce the high frequency noise signal and the D.C. bias.

## **4. High Speed Data Acquisition System**

The output of the signal conditioner is fed into a HP 6944 Multiprogrammer with a buffered high speed A/D conversion system. The Multiprogrammer cards are driven using HP CAT 14752A software on a HP 9000 Series Model 310 computer.

For phase sampling, data acquisition must be triggered so that data are obtained at different phases of each cycle of flow oscillation. In most studies, the trigger source is derived from the device used to oscillate the flow or from the motor drive assembly used to move this device. Ramaprian and Tu [Ref. 3] used a pulse trigger produced by a



magnetic pickup at the instant of maximum slot opening during each revolution of their rotating sleeve. Their data acquisition system was programmed to sample the flow every 1/100 of the period of a sleeve revolution, starting from the instant when the pulse trigger is received.

In the present experimental set-up, the motor used to drive the vane generates voltage pulses sequentially in each of the four field windings used to step the motor. 50 pulses are available to each field winding for each revolution of the motor shaft, giving a total of 200 pulses per revolution. The pulses from one of the four field windings are used to trigger the data acquisition system providing a situation in which data acquisition is precisely synchronized with the vane rotation. Then, for a given vane imposed oscillation frequency,  $f_{osc}$ , the data sampling rate (TR) is given by

$$\begin{aligned} \text{TR (samples/sec.)} &= f_{osc} \times (\text{pulses/motor shaft rev.}) \times \\ &\quad (\text{motor shaft rev./imposed flow oscillations}) \\ &= f_{osc} \times 50 \times 2 \\ &= 100 \times f_{osc} \end{aligned}$$

With this approach, 100 samples of data are obtained, spaced uniformly, over each period of flow oscillation, providing a phase resolution of 1/100 of the imposed oscillation cycle. Data are acquired for 640 flow oscillations to fill the memory buffer of the computer (64 kbytes), after which, data are stored in the computer memory. In the memory, they are packed into 640 arrays of 100 samples each and stored on a disk for later processing. In many cases this acquisition

procedure is repeated up to 8 times, with a similar vane starting position each time to insure that data acquisition is always initiated at the same phase of the flow oscillation. Because non-uniform width voltage pulses are generated by the motor drive as the motor is started and stopped, the first 6000 points are ignored as data are processed, and all acquisitions are completed well before the vane motor is stopped. When no unsteadiness is imposed on the flow, data acquisition is triggered by the signal from a square-wave function generator set to the same frequency as employed with imposed unsteadiness.

### **5. Data Storage**

A data acquisition program, HOTWIREPAV, is used in the Hewlett-Packard microcomputer to acquire the output of the A/D converter. The instantaneous voltage is then stored on 3.5 inch diskettes for further processing. The heading to each data set includes the time and date, the bulk velocity, the oscillation frequency, and the average voltage from the digital multimeter.

## **D. FLOW VISUALIZATION**

### **1. Smoke Wire System**

Flow visualization results are obtained using a modified Vertical Smoke Wire Instrument, manufactured by Flow Visualization Systems of Bolingbrook, IL. The wire is made of 0.127 mm diameter nicrome, and is placed across the span of the channel at  $y/d = 0.90$ . In order to ensure that the wire is held taut as it is energized, a tension device is

installed at one end. The wire is then connected to an AC/DC converter whose voltage is supplied by a Calrad 45-740 variac. As the wire is energized, a thin sheet of smoke is produced for 2-8 seconds.

## **2. Video Equipment**

Smoke patterns are then recorded on video film using a Sony DXC-M3 Video Camera with VCL-914BY Zoom Lens and VO-6800 Portable Videocassette Recorder and then replayed on a Sony Trinitron video monitor using a Sony model VO-5800 Videocassette Recorder with a still-frame feature. The frames are photographed using a Nikon F-3 SLR camera with Kodak Tri-Xpan film, using the method described by Longest [Ref. 23], Coumes [Ref. 24], and Greco [Ref. 25]. The video camera is set on filter number 1 with the zoom lens set for 0.7 m and focused to optimum clarity. The still photos are taken in a darkened room with the monitor intensity set low and the contrast set high to show the smoke patterns. The still camera is set on f8 with shutter speed 1/15 sec., using ASA 400 film.

### **III. EXPERIMENTAL PROCEDURES**

#### **A. HOT-WIRE CALIBRATION**

The hot-wire is calibrated in the freestream of the wind tunnel located in the laboratories of the Mechanical Engineering Department of the Naval Postgraduate School. During calibration the hot-wire probe is mounted normal to the flow in the potential freestream flow of the wind tunnel. The hot-wire is connected to the same hot-wire bridge previously discussed. Output from the hot-wire bridge is read on a Keithly 169 Digital Multimeter. Freestream velocity in the wind tunnel is measured utilizing a Kiel pressure probe, a wall static pressure tap, and a Validyne PS 309 Digital Manometer. Voltage and differential pressure readings are taken for a range of pressure drops corresponding to velocities between 1.0 and 4.0 m/s. The computer program HWCAL is run on the Naval Postgraduate School's IBM 310 main frame computer to calculate all calibration constants. Following the calibration, the hot-wire is installed in the straight channel.

#### **B. DATA PROCESSING**

##### **1. Bulk Velocity**

The bulk flow velocity is calculated from the pressure drop across the orifice plate located in the outlet piping which connects the outlet plenum and the blower. The delta P is measured in inches of water using a Validyne Model PS 309 Digital Manometer . Figure 5

shows the relationship of bulk velocity to delta P. The bulk velocity is used to compute the Reynolds number and the Strouhal number in the channel.

## 2. Instantaneous Velocity

Instantaneous voltages are converted into instantaneous velocities using a look-up table that accounts for hot-wire calibration coefficients, amplifier gains and mean voltage levels. Such instantaneous velocity data are shown in Figure 6 for  $Re = 3660$  ( $v_{blk} = 4.38$  m/s) and a Strouhal number of 0.036 ( $f_{osc}$  is 2 Hz) along with the corresponding phase-averaged velocity trace.

With imposed periodic flow, instantaneous velocities can be considered to be the sum of three components such that  $U = \bar{U} + \tilde{U} + u'$ , where  $\bar{U}$  is the time-averaged velocity,  $\tilde{U}$  is the periodic velocity and  $u'$  is the fluctuating component.

## 3. Phase Averaging

In the present study  $\tilde{U}$  and  $\bar{U}$  are combined as the phase-averaged velocity ( $\hat{U}$ ), such that  $U = \hat{U} + u'$ , following Ramaprian and Tu [Ref. 3]. Thus, for a steady flow with no periodic velocity,  $\hat{U}$  is then equal to  $\bar{U}$ .  $\hat{U}$  is then determined from phase-averaging instantaneous velocity results using the equation given by

$$\hat{U}(n) \Big|_{n=1}^{100} = \frac{1}{ncycl} \sum_{m=1}^{ncycl} U(m, n) \Big|_{n=1}^{100}$$

Here, m and n correspond, respectively, to the number of cycles and to the number of locations across each phase where data are sampled.

Typically 580 to 4640 cycles are ensemble averaged to obtain a phase-averaged velocity trace, depending on the magnitude of the fluctuations relative to the amplitude of the phase-averaged velocity. With laminar flows, the former number are used. With fully turbulent and transitioning flows, signals like the one in Figure 4 are present and 4640 cycles are averaged. With this approach, statistically stable samples are obtained even for higher Reynolds numbers where fluctuation levels are significant with respect to the local mean velocity. When time-averaged velocity  $\bar{U}$  is determined, averages are obtained from 58 thousand to 464 thousand points depending upon the amount of unsteadiness in the signal.

When noise causes individual data samples to drop-out or deviate significantly from expected behavior, they are replaced using the sample acquisitioned 100 points before, which, with phase-averaging, is the point at the same phase from the previous flow oscillation. Because such occurrences happen less than 1 % of the data sampling time, no evidence of these corrections is found in ensemble- and time-averaged results.

The program for processing the data and calculating the phase-averaged velocity, the phase-averaged rms velocity, the mean velocity, and the time-averaged rms velocity, and for plotting the phase-averaged velocities versus Reynolds number is called DATAP.

### **C. SPECTRAL MEASUREMENTS**

The spectra of the analog voltages from the hot-wire bridge are analyzed using a Hewlett-Packard Model 3562A Dynamic Signal Analyzer (DSA). The display parameters are set on voltage squared divided by Hz versus frequency from 0.1 to 20 Hz or from 0.1 to 200 Hz. A typical setting of the other parameters are shown in Figure 7. Internal integrating and storage capacities of the DSA are used to take and average 20 sets of readings to produce time-averaged frequency spectra at each flow velocity. Time-averaged frequency spectra were produced using 40 sets of readings for Reynolds numbers between 1400 and 1800. A split screen display is also used to simultaneously show voltage squared divided by Hz versus frequency and voltage versus time from 0 to 3.2 seconds. The time plot is limited to 3.2 seconds of display by the design of the DSA.

## IV. RESULTS AND DISCUSSION

### A. CHANNEL FLOW VALIDATION

To partially validate measurement procedures as well as the behavior of the flow in the channel, the mean velocity profile is measured when the flow is laminar. The normalized mean velocity profile is then compared to the theoretical velocity profile for fully developed laminar channel flow given by Schlichting [Ref. 21] as:

$$\bar{U} / u_{\max} = 4.0[y/d - (y/d)^2]$$

Here,  $\bar{U}$  is the local mean velocity and  $u_{\max}$  is the maximum of this velocity, which occurs at the center ( $y/d = 0.5$ ) of the channel. The velocity profile taken at  $x/d = 300$ , at Reynolds number of 1103 is shown in Figure 8. The bulk flow velocity is 1.32 m/s as measured from the orifice pressure drop. The maximum centerline velocity is 1.51 m/s. The normalized velocity profile is parabolic in shape and agrees closely with the theoretical relationship. The profiles at this and other Reynolds numbers are also consistent with those measured by Coumes [Ref. 24] and Greco [Ref. 25].

### B. EFFECT OF IMPOSED OSCILLATIONS ON MEAN VELOCITY PROFILES AT VARIOUS REYNOLDS NUMBERS

Mean velocity profiles, with and without imposed oscillations at 1 Hz are shown in Figures 9 to 14 for Reynolds numbers from 1103 to 3584. The local mean velocities normalized by  $u_{\max}$  are plotted on the vertical axis and the normal distances measured from the bottom



wall,  $y$ , normalized by the the channel depth,  $d$ , are plotted on the horizontal axis. Without the oscillations, profiles change from a laminar parabolic shape at  $Re = 1103$  to a fuller shape typical of a turbulent flow at  $Re = 3584$ . At Reynolds numbers of 2005 and 2197, shapes of profiles are qualitatively between the ones which exist for fully laminar conditions and fully turbulent conditions. For all Reynolds numbers studied, profiles with 1 Hz imposed oscillations are nearly identical to those with no imposed oscillations. This observation is consistent with the the results of Coumes [Ref. 24] and others (e. g. Ramaprian and Tu [Ref 3]) for small amplitudes of imposed oscillations.

### **C. EFFECT OF IMPOSED OSCILLATIONS ON RMS VELOCITY PROFILES AT VARIOUS REYNOLDS NUMBERS**

Profiles of the normalized longitudinal turbulence intensity, with and without 1 Hz oscillations, are shown versus  $y/d$  in Figures 15 to 20. The quantity on the ordinate is the intensity (hereafter referred to as rms velocity) normalized by  $u_{max}$ . The figures show how normalized rms velocity profiles change with Reynolds number. At  $Re = 1103$  (Figure 15), the flow is laminar, and the rms profile is due to very low intensity fluctuations indicated by the small rms values. With oscillations imposed at 1 Hz, fluctuations are lower than without imposed oscillations. At  $Re = 1579$ , Figures 16 shows that normalized rms velocities are greater near the center of the channel than near the walls. Little change in the profile is evident with imposed oscillations.

At Reynolds numbers of 2005 and 2197, Figures 17 and 18 show that flows without imposed oscillations have rms velocity profiles which are similar in character to the ones which exist at  $Re = 1579$ . To the best of the author's knowledge, this is the first time that normalized rms velocities which are higher in the center of the channel than near the wall are experimentally observed when no imposed oscillations are present. From a direct numerical simulation of transition in plane Poiseuille flow, Zang and Krist [Ref 26] indicate that a "center mode" of secondary instability ( i. e. the disturbances that grow near center of the channel) is an important feature of the flow at Reynolds number near the critical value. They show that the amplitude of fluctuations increases significantly in the center of the channel when this secondary instability occurs. Other studies (e.g., Stettler and Hussain [Ref 4], Coles [Ref 27], Wygnanski and Champagne [Ref 28] and Rubin, Wygnanski and Haritonidis [Ref 29]) of transition in pipe flows indicate that flow disturbances originate near the center of the pipe in the form of "plugs or puffs". It is conjectured that a the center mode instability in the channel flow is similar to the "plug" type transition phenomena. With the 1 Hz imposed oscillations at Reynolds numbers of 2005 and 2197, the normalized rms velocity is decreased in the center of the channel. Thus, the imposed oscillations suppress the growth of secondary disturbances in the center of the channel at these two Reynolds numbers. It is interesting to note that imposed oscillations have a stabilizing influence on plug type transition

phenomena in the experiments of Gilbrech and Combs [Ref. 10] and Sarpkaya [Ref. 11].

With Reynolds numbers of 2548 and 3584 when flow is fully turbulent, Figures 19 and 20 show normalized rms values which are higher near the wall than near the center of the channel. When 1 Hz oscillations are imposed on the flow, results at the same Reynolds numbers are similar to data obtained without imposed oscillations.

#### **D. EFFECT OF IMPOSED OSCILLATIONS ON NORMALIZED RMS VELOCITY AS A FUNCTION OF REYNOLDS NUMBER**

##### **1. Near-Wall Region**

Figures 21 to 24 are plots of the rms velocity normalized by local mean velocity as a function of Reynolds number. These data were obtained near the edge of the Stokes layer at  $y/d = 0.90$ . The Coumes [Ref. 24] and Greco [Ref. 25] data labelled  $y/d = 0.90$  are actually for a probe position of  $y/d = 0.89$ . The data in Figures 21 to 24 are shown for flow with no imposed oscillations and with imposed oscillations at 1 Hz, 2 Hz, 3 Hz, and 4 Hz. Sampling frequencies used to obtain the results without imposed oscillations shown in each figure match sampling frequencies used to obtain the results with imposed oscillations, which is 100 times the imposed oscillation frequency.

In each plot, the normalized rms velocity generally increases in magnitude as Reynolds number increases from 1100, until a maximum is reached at a Reynolds number ranging from 2000 to 2400. As Reynolds number increases further, normalized rms values then

decrease. Local maximum Reynolds numbers are believed to indicate the upper limit of transition phenomena, and the subsequent decrease is nearly linear and mostly due to increasing local mean velocity with Reynolds number. Referring to data obtained without imposed oscillations, maxima in Figures 21 to 24 show a slight increase with sampling frequency. This is because more turbulent energy is captured as higher sampling frequencies are used to acquire data. When imposed oscillations are present, data in each figure show that maximum values of the normalized rms velocity occur at a lower Reynolds numbers compared to results obtained without imposed oscillations. Thus for the range of experimental conditions examined, imposed oscillations have a destabilizing influence on transition events.

## **2. Center of the Channel**

Figures 25 and 26 show the variation of the rms velocity normalized with respect to the local mean velocity as a function of Reynolds number, with and without imposed oscillations at 1 Hz for a probe position of  $y/d = 0.50$ . The results in Figure 26 are from the study of Coumes [Ref. 24]. The plots show that the rms velocity increases in the flow without oscillations from  $Re = 1100$  until  $Re = 2100$  to  $2200$ , and then decreases to the same values which exist in the flow with imposed oscillations. The increase and decrease which occurs without imposed oscillations occurs rather abruptly over the Reynolds numbers range from 1600 to 2550. It is believed that this type of behavior is due to strong nonlinear amplification of

subharmonic secondary instabilities, as suggested by Zang and Krist [Ref 26] and Herbert [Ref 14]. With the present situation, the effects of secondary instabilities (near the channel center) appear to overwhelm the effects of primary instabilities (near the wall) and provide a route for sudden transition to turbulence.

With imposed oscillations at 1 Hz, the rms velocities in the center of the channel are lower than without imposed oscillation. Thus, a comparison of results in Figures 25 and 26 to results in Figures 21 to 24 indicates that fluctuating intensities in the mid-portion of the channel are more readily altered (reduced) by imposed oscillations at 1 Hz than flow nearer the wall at  $y/d = 0.90$ .

#### **E. EFFECT OF REYNOLDS NUMBER ON PHASE-AVERAGED VELOCITY TRACES**

Figures 27 to 35 show traces of phase-averaged velocity,  $\hat{u}$ , obtained with imposed oscillations at 1 Hz for Reynolds numbers from 1579 to 3584.  $\hat{u}$  is calculated using the multi-run averaging technique as explained in Section III B 3. In each figure, the phase-averaged velocity versus phase angle is shown on top and the phase-averaged rms velocity versus phase angle is shown on the bottom. Figures 27 and 31 present results obtained from averages of 2320 cycles. Figures 28 to 30, and 32 to 35, present results obtained from averages of 4640 cycles.

At  $Re = 1579$  and  $2548$ ,  $\hat{u}$  variations are qualitatively sinusoidal. However, at Reynolds numbers of  $1693$ ,  $2005$  and  $2197$ ,  $\hat{u}$  variations

are non-sinusoidal evidencing interactions between imposed oscillation and transitional flow structures. Figures 36 and 37 show phase-averaged distributions obtained with oscillations imposed at 3 Hz and 4 Hz, respectively. Even greater distortion from a sinusoid is evident if these data are compared to 1 Hz data, which is partially because of interactions between flow structures and imposed oscillations, and partially because averages are obtained using only 580 phases.

Phase-averaged normalized rms velocity versus phase angle in Figures 27 to 37 generally do not show any significant influences of either Reynolds number or the imposed oscillation frequency. The only exceptions are evident in Figures 27 and 32, which show sinusoidal traces that appear to be synchronized with the traces of phase-averaged velocity.

#### **F. EFFECT OF IMPOSED OSCILLATIONS ON INTERMITTENCY AT VARIOUS REYNOLDS NUMBERS**

The intermittency factor,  $\gamma$ , is defined as the fraction of time that flow is turbulent. If  $\gamma$  is 1.0 then the flow is turbulent 100 percent of the time. If  $\gamma$  is 0.0 then the flow is non-turbulent 100 percent of the time. The intermittency factor is determined by identifying turbulent and the non-turbulent portions of velocity-time traces. In this study, the second time-derivative of the instantaneous velocity is used to determine  $\gamma$ . An on-off temporal identification function, ID, is defined such that,

$$ID = 1, \text{ if } \frac{\partial^2 U}{\partial t^2} > Thr, \text{ and}$$

$$ID = 0, \text{ otherwise.}$$

The threshold factor, Thr, is determined for different Reynolds numbers using the correlation,

$$Thr = (105 - (64.66 * (V_{blk} - 1.89)))$$

If the Thr value falls less than 20 then its value is reset to 20. This correlation is employed because it leads to intermittency values which are consistent with turbulent events detected visually from flow visualization results. The intermittency factor is obtained by averaging ID values over a sampling time of 580 seconds. Phase averaged ID distributions are obtained in a fashion similar to that described in Section III B 3.

Figures 38 and 39 show the intermittency factor plot as a function of Reynolds number for probe positions of  $y/d = 0.90$  and  $0.50$ , respectively. Figure 38 shows that the intermittency factor at  $Re = 1212$  is close to zero and increases as Reynolds number increases to 1697. Further increases in Reynolds number result in sharp increases of the intermittency factor until a Reynolds number of about 2100 is reached. Beyond this Reynolds number, the intermittency factor varies very little with  $Re$  as data asymptote to  $\gamma = 1.0$ . The intermittency factor of the flow with imposed oscillations is the same as that for flow with no imposed oscillations at all Reynolds numbers except those in the high transition range ( $Re = 2005$  to  $2100$ ). Within

this Reynolds number range, the intermittency factor is increased by up to 10 percent when imposed oscillations are present. With oscillations imposed at 1 Hz, this type of event occurs at the same Reynolds number as when normalized rms velocities are maximum.

Figure 39 shows variations of the intermittency factor with Reynolds number for  $y/d = 0.50$ . Here, the variation of the intermittency with Reynolds number is the same whether or not imposed oscillations are present. Comparing these results to the ones in Figure 38 indicates that the change of intermittency factor from a value near 0.1 to 1.0 occurs over a smaller range of Reynolds numbers for  $y/d = 0.50$  than when  $y/d = 0.90$ . Typical time traces of velocity signals for these experimental conditions are shown in Figures 40 to 45.

Figures 46 to 58 show plots of phase-averaged ID and phase-averaged velocity versus phase angle for  $y/d = 0.90$  and various Re. The only noticeable dependence of ID on phase angle occurs for  $Re = 2005$ .

## **G. EFFECT OF IMPOSED OSCILLATIONS ON FREQUENCY SPECTRA AT VARIOUS REYNOLDS NUMBERS**

The effects of imposed oscillations on frequency spectra of the voltage signal from hot-wire probes are now discussed. Figures 59 to 98 are plots of the spectral power density (voltage squared divided by Hertz) versus Hz. Each figure contains two plots, one for a frequency bandwidth of 0 to 200 Hz and another for a frequency bandwidth of 0



to 20 Hz. Figures 59 to 78 show the spectra for flow with no imposed oscillations and Figures 79 to 98 show spectra for flow when oscillations are imposed at 1 Hz . All of these figures are plots of ensemble averages of 20 spectra. Each spectra used to construct the ensembles is obtained over a 3.2 second time interval. Plots of 40 averages for flow with no imposed oscillations are shown in Figures 99 to 107. Figures 108 to 116 are plots of 40 averages taken in flow with oscillations imposed at 1 Hz.

Spectra show energy level increases as the flow velocity and Reynolds number increase. In the low transition range ( $Re = 1450$ ) Figure 62 shows a particularly large energy increase compared to the plot of the next lower Reynolds number. This is also seen in Figures 99, 100, 108, and 109. At these Reynolds numbers, time traces show intermittent, large-amplitude fluctuations probably due to passage of energy containing eddies or packets in otherwise quiescent flow. These fluctuations are spiky on the time-traces and bear semblance to a Dirac delta function. Consequently, spectra exhibit a wavy character. The number of packets of turbulence increases as the flow velocity increases, as evidenced by results in Figures 117 to 176.

With imposed oscillations, shapes of spectra are not significantly different from ones obtained with no imposed oscillations. Figures 117, 132, 147 and 162 show results with imposed oscillations which evidence of passage of turbulent packets in flows which are otherwise quiescent.

## H. FLOW VISUALIZATION RESULTS

Smoke patterns produced using a smoke wire placed at  $y/d = 0.90$  were recorded using a video camera at Reynolds numbers ranging from 1600 to 2300 without imposed oscillations and with oscillations imposed at 1, 2, 3 and 4 Hz. Some transition events are illustrated by still photographs of video frames presented in Figures 177 to 181. In each photograph, flow is moving from bottom to top, and a spanwise/streamwise plane of the channel is shown from the left wall to the spanwise center. The arrow in the lower left of each photograph indicates the position of the hot-wire probe and the dark line extending from the upper left indicates the position of the hot-wire support arm. Two photographs are shown in each figure, both obtained at the same Reynolds number, spaced  $1/15$  of a second apart.

Figures 177 to 179 show the smoke pattern at Re of 1604 and 1696 with no imposed oscillations, and at Re of 1696 with oscillations imposed at 1 Hz. In all three cases some evidence of the Klebanoff mode of Tollmien-Schlichting (T-S) waves is apparent. In the last of these three figures, the Klebanoff mode of T-S waves are seen on the left and Tollmien-Schlichting waves and ribbon patterns of smoke are seen on the right. Figure 180 shows flow at Re of 1905 with 1 Hz imposed oscillations. Ribbon patterns of smoke are evident. Figure 181 shows the flow at Re of 1604. The upper photograph is taken with 2 Hz imposed oscillations and the lower is with 3 Hz imposed oscillations. The lower photograph shows evidence of the formation of

the Klebanoff mode of T-S waves on the left and more two-dimensional Tollmien-Schlichting waves on the right. The upper photograph shows ribbons of smoke which probably evidence a packet of vortices in the flow.

## I. UNCERTAINTY ANALYSIS

Uncertainty estimates are based on 95 percent confidence levels, and determined using the methods described by Kline and McClintock [Ref. 30] and by Moffat [Ref. 31]. The uncertainty of the phase-averaged velocity  $\hat{u}$  is 2.9 %, which, for a nominal value of 2.22 m/s amounts to 0.064 m/s. Uncertainties of  $\bar{u}$  and  $\bar{u}_{\max}$  are both 1.2 %. For a nominal value of 2.22 m/s, this is equivalent to 0.027 m/s. The uncertainty of the phase angle is 5 degrees. If this quantity equals 180 degrees, then this uncertainty is 2.8%. Uncertainties of  $v_{bik}$  and Re are both 3.5%. For respective values of 1.30-3.00 m/s and 1100-2400, corresponding dimensional uncertainties are .046-.105 m/s and 40-85.

## V. SUMMARY AND CONCLUSIONS

The influences of imposed oscillations at 1, 2, 3 and 4 Hz on transition from laminar to turbulent flow in a straight channel has been studied for Reynolds numbers between 1100 and 3600 and Strouhal numbers between 0.0211 and 0.2418.

Results from the study show that mean (time-averaged) profiles are unaffected by the imposed oscillations at a particular Reynolds number for all amplitudes and frequencies of imposed oscillation and for the entire range of Reynolds numbers studied, regardless of whether the flow is laminar, transitional or fully turbulent. For all three types of flow, mean profiles additionally exhibit quantitative trends typical of laminar, transitional and turbulent flows.

Phase-averaged velocity traces show sinusoidal behavior when oscillations are imposed both at 1, 2,3 and 4 Hz when flow is laminar ( $Re = 1103$ ), transitional ( $Re = 1604$ ), and turbulent ( $Re = 2548$  and  $Re = 3584$ ) at all probe positions tested. Phase-averaged velocity traces of flow with imposed oscillations are less sinusoidal for transition Reynolds numbers from 1700 to 2150, than for flow conditions at all other Reynolds numbers. This distortion of phase-averaged velocity waveforms is of particular interest because it gives evidence of viscous interactions between the imposed oscillations and flow phenomena.

Imposed oscillations have a destabilizing effect on the flow near the edge of the Stokes layer. Turbulence intensity magnitudes with imposed oscillations show that transition to turbulence begins at lower Reynolds numbers and extends over a wider range of Reynolds numbers than when no imposed oscillations are present. In addition, higher levels of intermittency are present with imposed oscillations for Reynolds numbers 1900 to 2200 at  $y/d = 0.90$ . At Reynolds numbers from 1450 to 1800, frequency spectra evidence high intensity intermittent turbulent fluctuations, followed and preceded by quiescent flow, both with and without imposed oscillations. A center mode of secondary instability is evidenced by high values of normalized longitudinal turbulence intensity measured in the channel center when no oscillations are imposed on the flow. Imposed oscillations are found to suppress this center mode of secondary instability, as evidenced by reductions in longitudinal turbulence intensity values near the channel center.

## APPENDIX A

### SOFTWARE DIRECTORY

1. **HWCAL** : This program determines the constants for the King's Law calibration of the hot-wire. The program also provides a polynomial fit of the calibration data.
2. **HOTWIREPAV** : This program is used to read the data stored in the A/D buffer of the high speed data acquisition system and stores the information on micro diskettes. Manual inputs are: triggering frequency, hot-wire DC voltage (ungained), oscillation frequency (flow blockage), bulk velocity and date and time of run.
3. **DATAP** : This program calculates instantaneous and phase averaged velocities. Initially a look up table is created. Here, effective velocities are calculated from the effective voltage values and stored for follow on calculations. The hot-wire calibration constants obtained from HWCAL, and the amplifier gain are incorporated into these calculations. The velocity calibration is given by the equation:

$$U_{\text{eff}} = k(E_{\text{eff}}^2 - E_0^2)^{1/N}$$

where  $k$  is the proportionality constant,  $E_{\text{eff}}$  is the effective voltage, and  $E_0$  is the reference voltage at no flow.  $N$  is a constant value of 0.45 for moderate Reynolds numbers. Once the look up table is created the program reads the instantaneous voltage values from the data file and converts them to instantaneous velocities. At this point a plot of the

instantaneous velocity versus time can be generated for any of 580 cycles (The first 60 cycles are discarded to allow for flow stabilization as the unsteady device is started.)

Next the program phase averages the 580 cycles, and velocity versus phase angle (of the flow blockage) plots are available. Two plots are available from the averaged values;  $\bar{u}$  versus phase angle and  $\sqrt{\bar{\Delta}^2}$  divided by  $\bar{U}$ , versus phase angle, where  $\bar{u}$  is the phase averaged velocity,  $\sqrt{\bar{\Delta}^2}$  is the phase averaged root mean squared velocity, and  $\bar{U}$  is the average velocity. In the case where there is no imposed unsteadiness, the phase averaged velocity,  $\bar{u}$ , is equal to the time averaged velocity,  $\bar{U}$ .

The program can also be used to process a set of data when multi-run averaging is desired. In this case the averaged values are written to and stored in the computer hard disk memory. Once each of the desired data sets has been averaged and stored in the computer memory.

4. **AVGPLOT** : The program AVGPLOT is used to average any number of data sets. A maximum of eight sets of data (or 4,640 cycles) were averaged for this study. The program AVGPLOT provides the same graphs as those available from DATAP. Phase averaged data sets are copied to micro diskettes prior to purging them from the computers memory.

5. **INTRMTCY** : This program takes the data recorded by HOTWIREPAV and computes the intermittency. It uses the second time derivative of the instantaneous velocity, which is calculated

numerically using the finite difference method. This value is then compared to a threshold value in an on-off temporal identification function,  $ID$ , is defined such that,

$$ID = 1, \text{ if } \frac{\partial^2 U}{\partial t^2} > Thr, \text{ and}$$
$$ID = 0, \text{ otherwise.}$$

The threshold factor,  $Thr$ , is determined for a different Reynolds numbers using a correlation,

$$Thr = \{105 - (64.66 * (V_{blk} - 1.89)a)\}$$

If the  $Thr$  value falls less than 20 then its value is reset to 20. This correlation is found to give the best correspondence between the computer detected and visually detected turbulent events.

The values of  $ID$  are then phase-averaged and time-averaged for the traces and the mean intermittency value,  $\gamma$ .



**APPENDIX B**

**FIGURES**

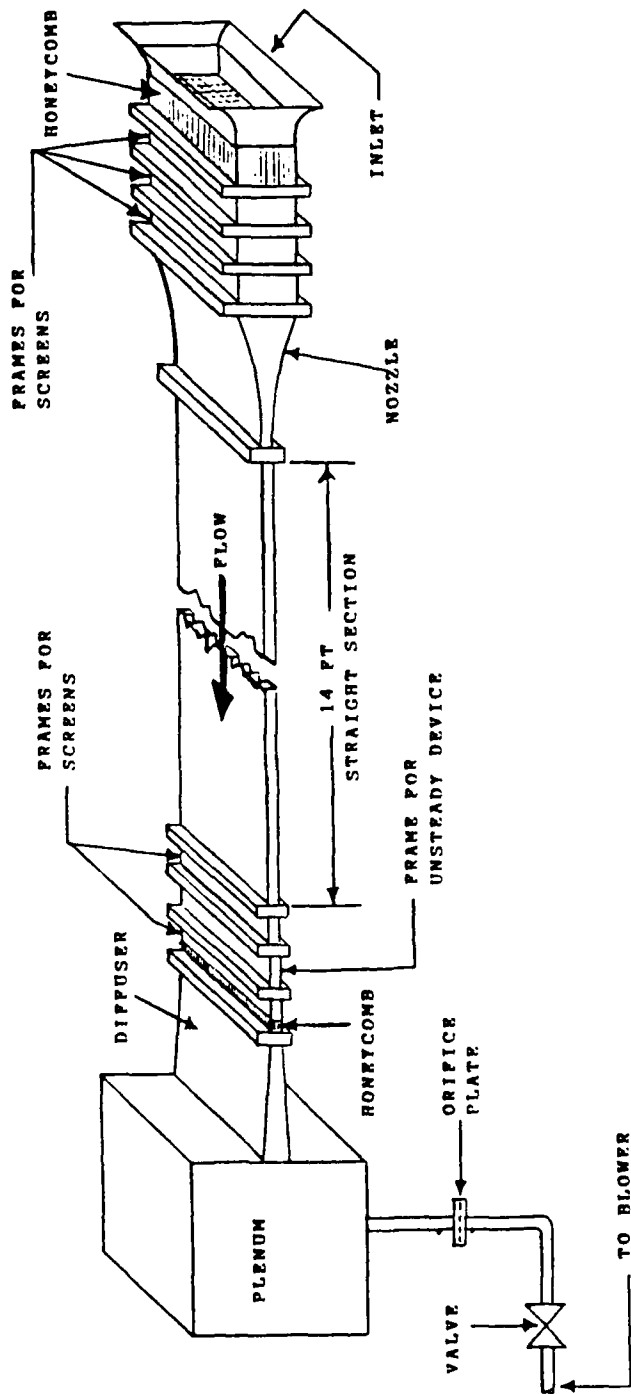


Figure 1.

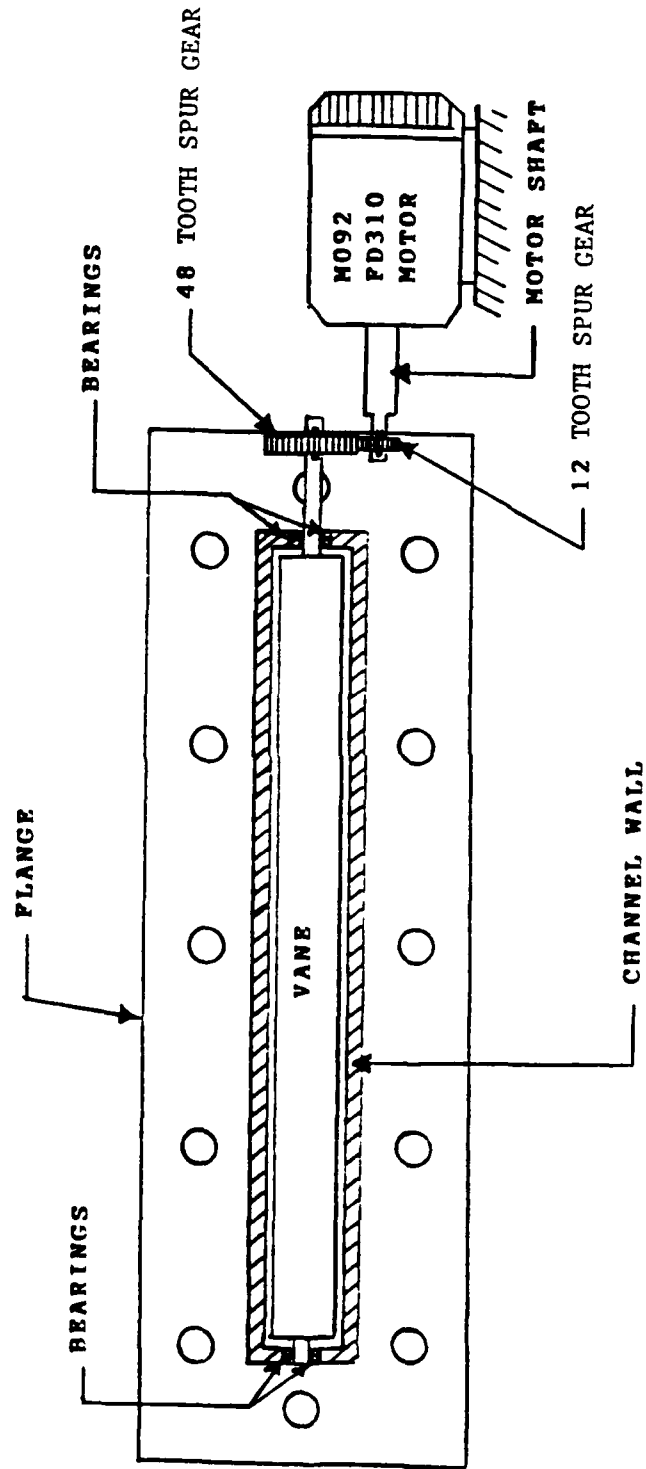


Figure 2.

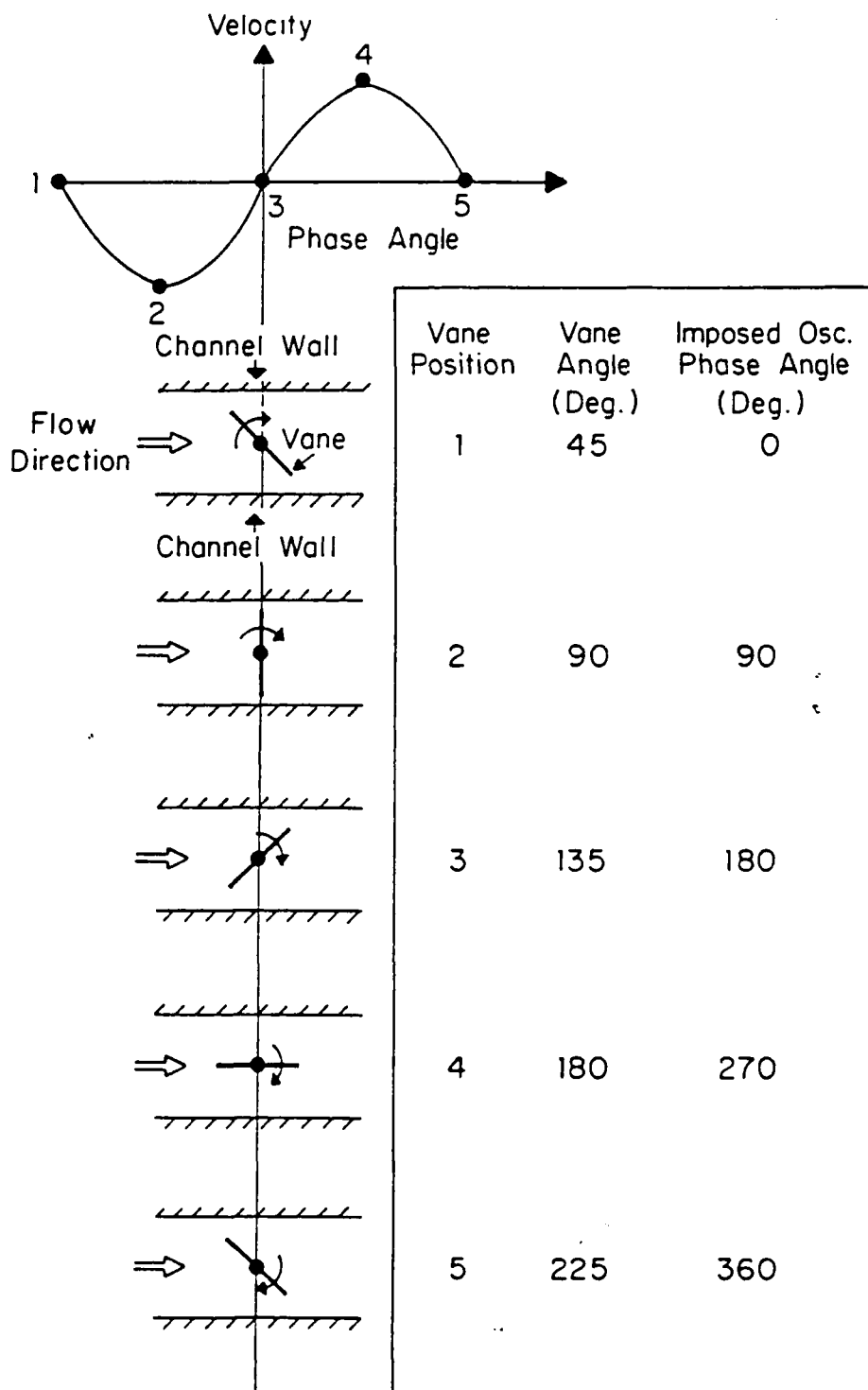


Figure 3.

## SCHMATIC OF FLOW MEASUREMENT EQUIPMENT

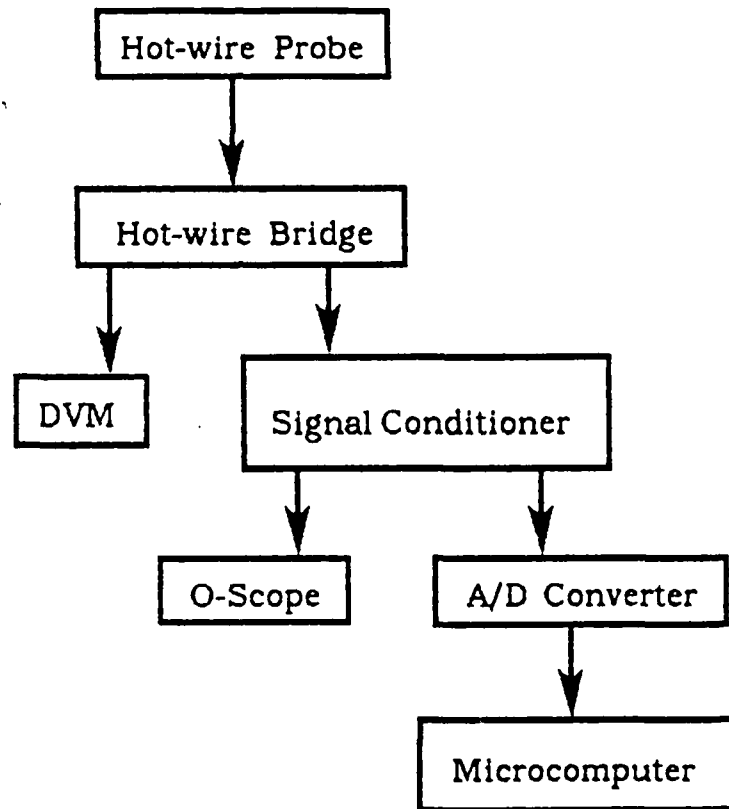


Figure 4. Schematic of flow measurement equipment

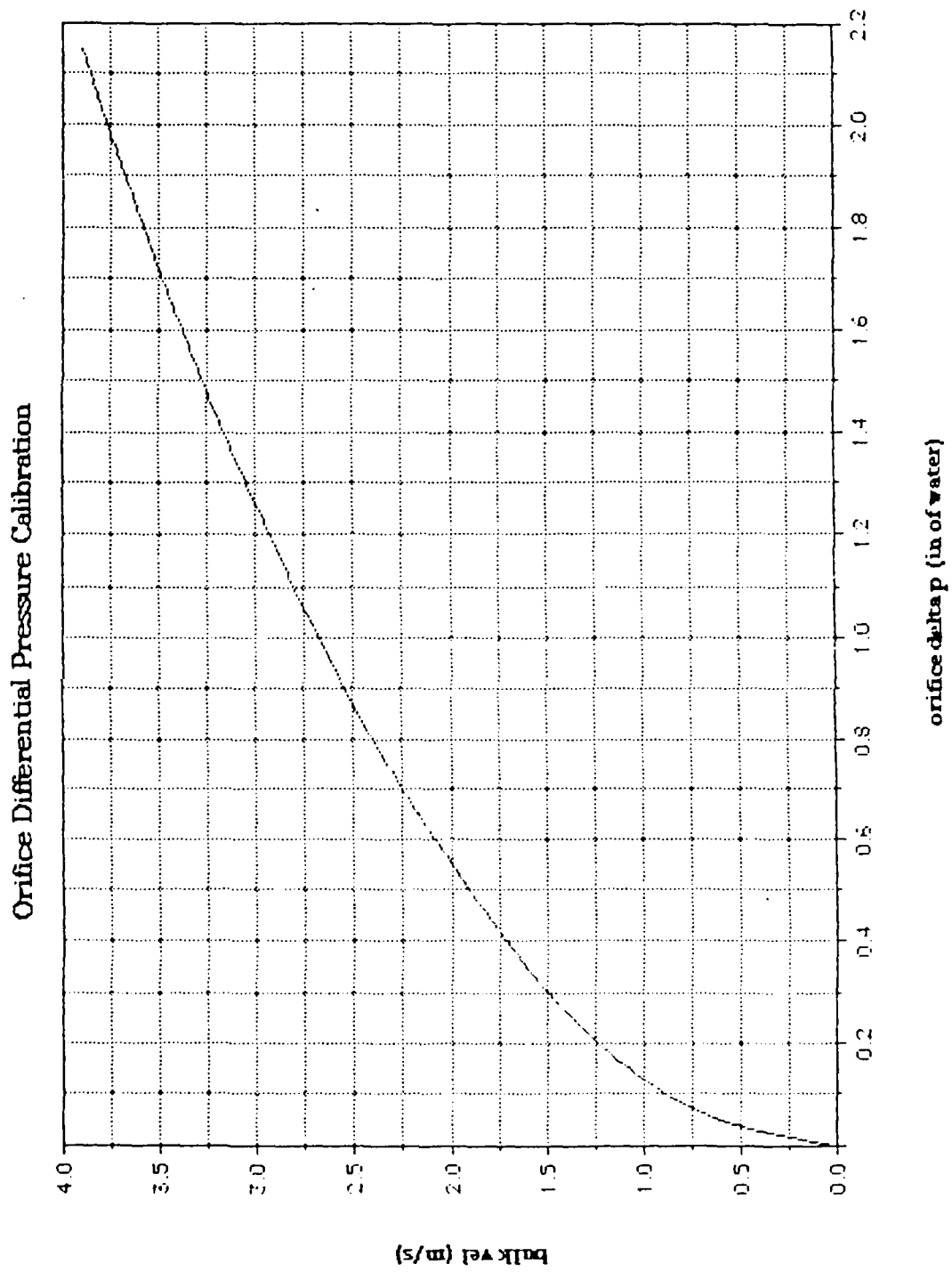


Figure 5.

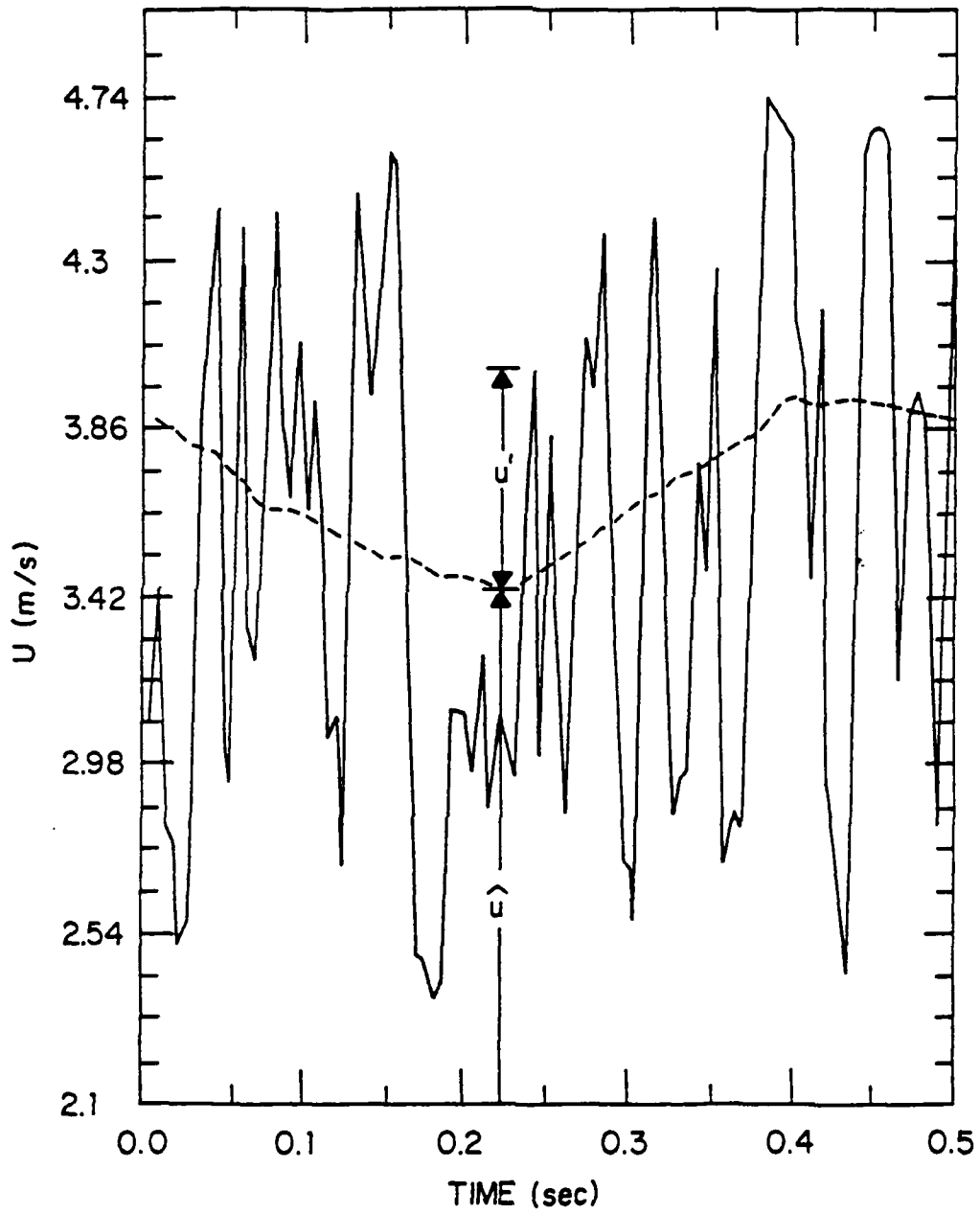


Figure 6.

## Linear Resolution

MEASURE:	CHAN 1 Power Spec	CHAN 2 Off
WINDOW:	CHAN 1 Hanning	CHAN 2 Hanning
AVERAGE:	TYPE AVG Off	OVERLAP 0%
	# AVGS 10	TIME AVG Off
FREQ:	CENTER 125 Hz	SPAN 250 Hz
	REC LGTH 3.2 S	BW 469mHz
	$\Delta t$ 1.56ms	
TRIGGER:	TYPE FreeRun	SLOPE Pos
	LEVEL 0.0 Vpk	PREVIEW Off
INPUT:	RANGE 502mVpk	COUPLING DC (Fit)
CH 1	Autorng↑	DELAY 0.0 S
CH 2		DC (Fit)
SOURCE:	TYPE Off	LEVEL 0.0 Vpk
		OFFSET 0.0 Vpk

Figure 7. Typical settings for Dynamic Signal Analyzer



Measured Profile and Theoretical Profile  
at Reynolds Number 1103

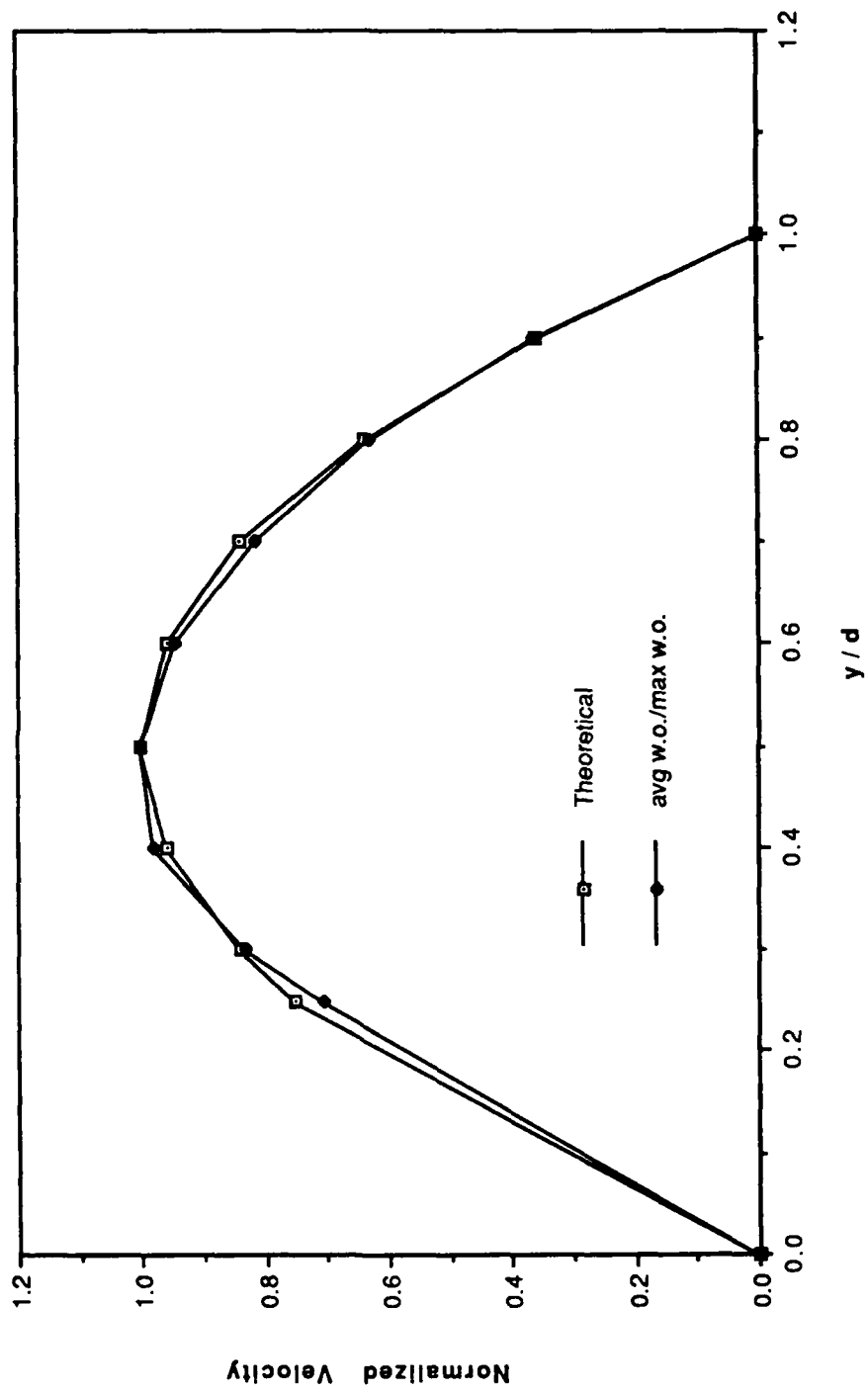


Figure 8.

Profile Re 1103

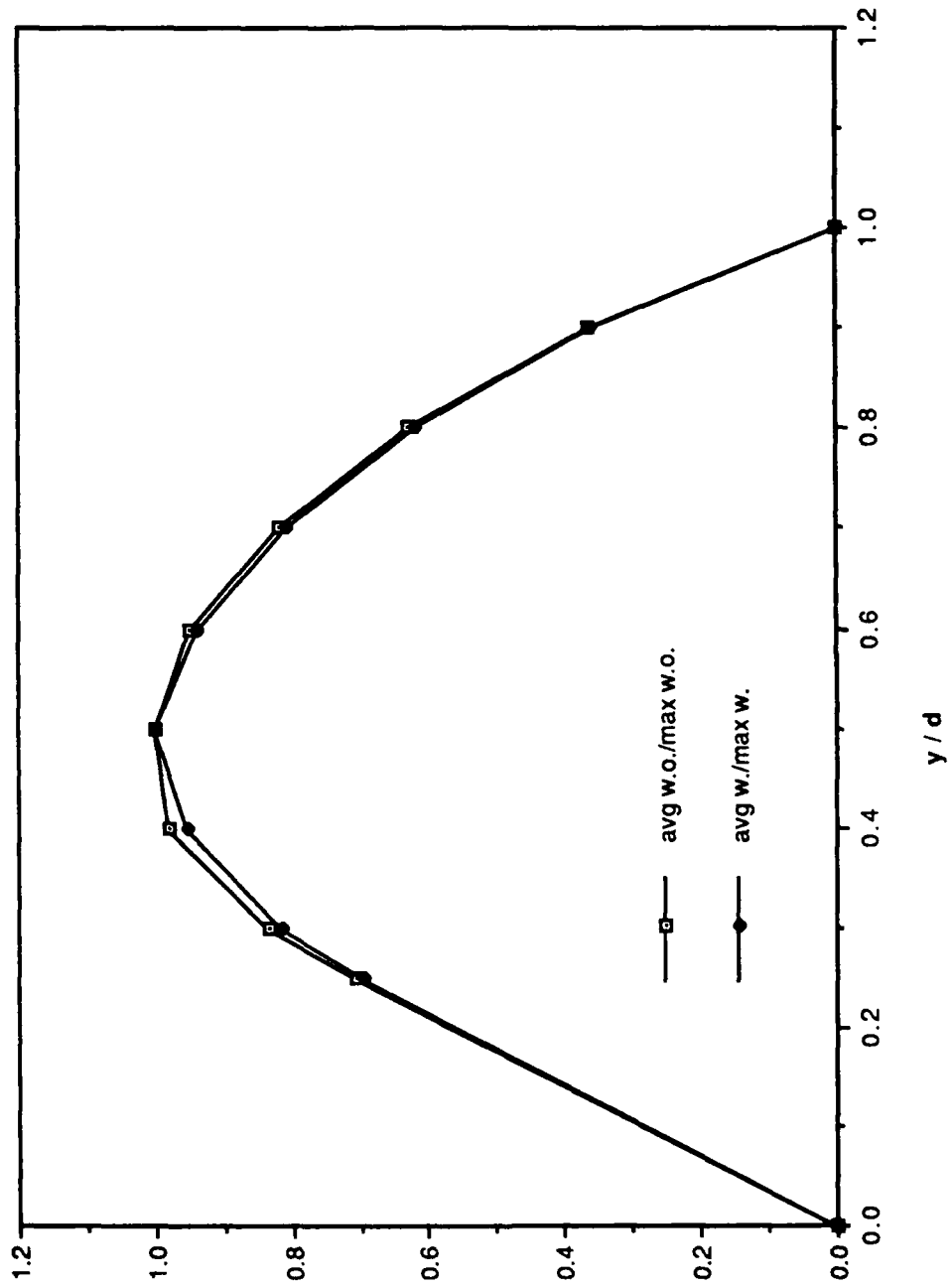


Figure 9.

avg vel / max vel

Profile Re 1579

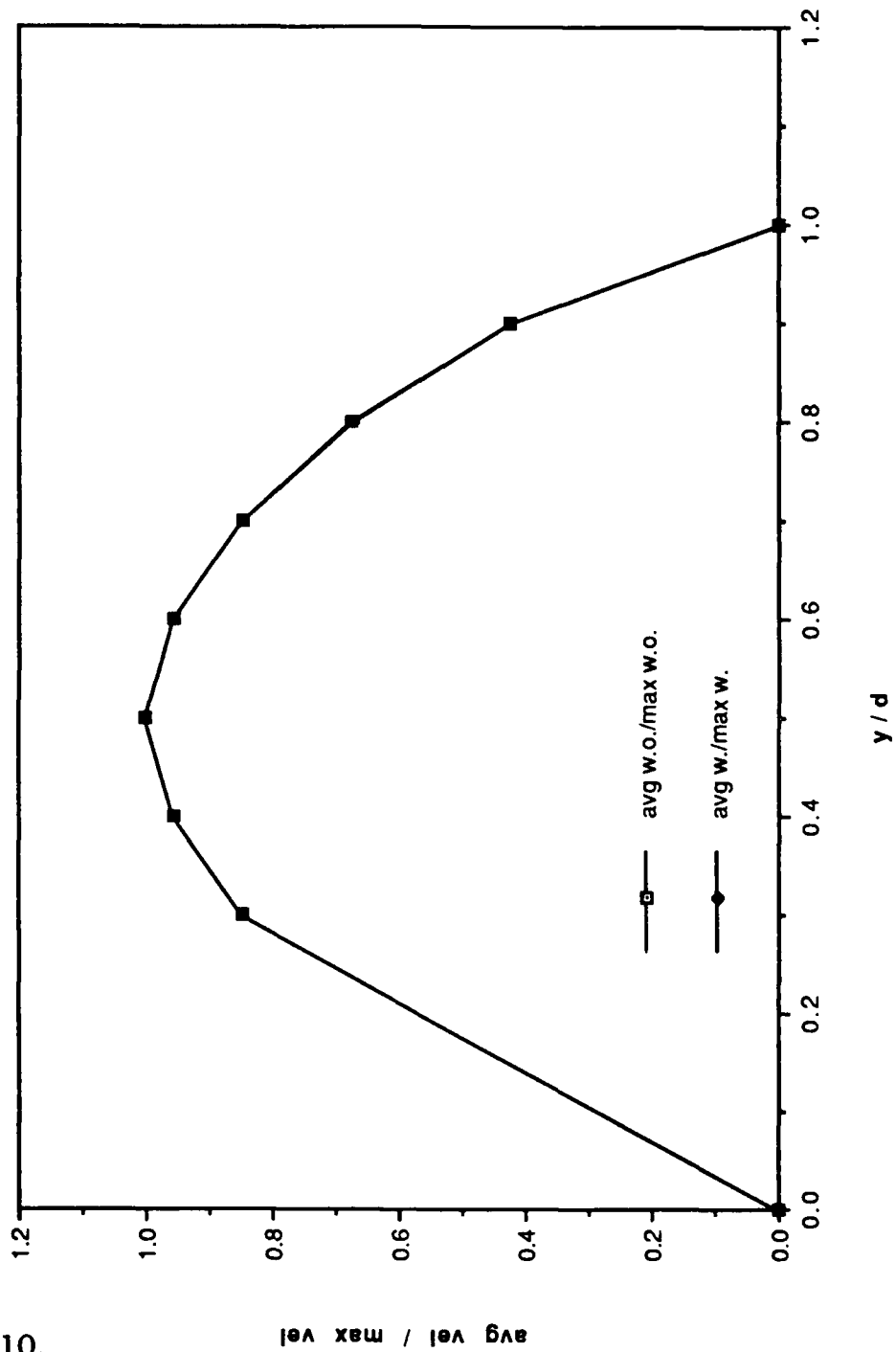


Figure 10.

Profile Re 2005

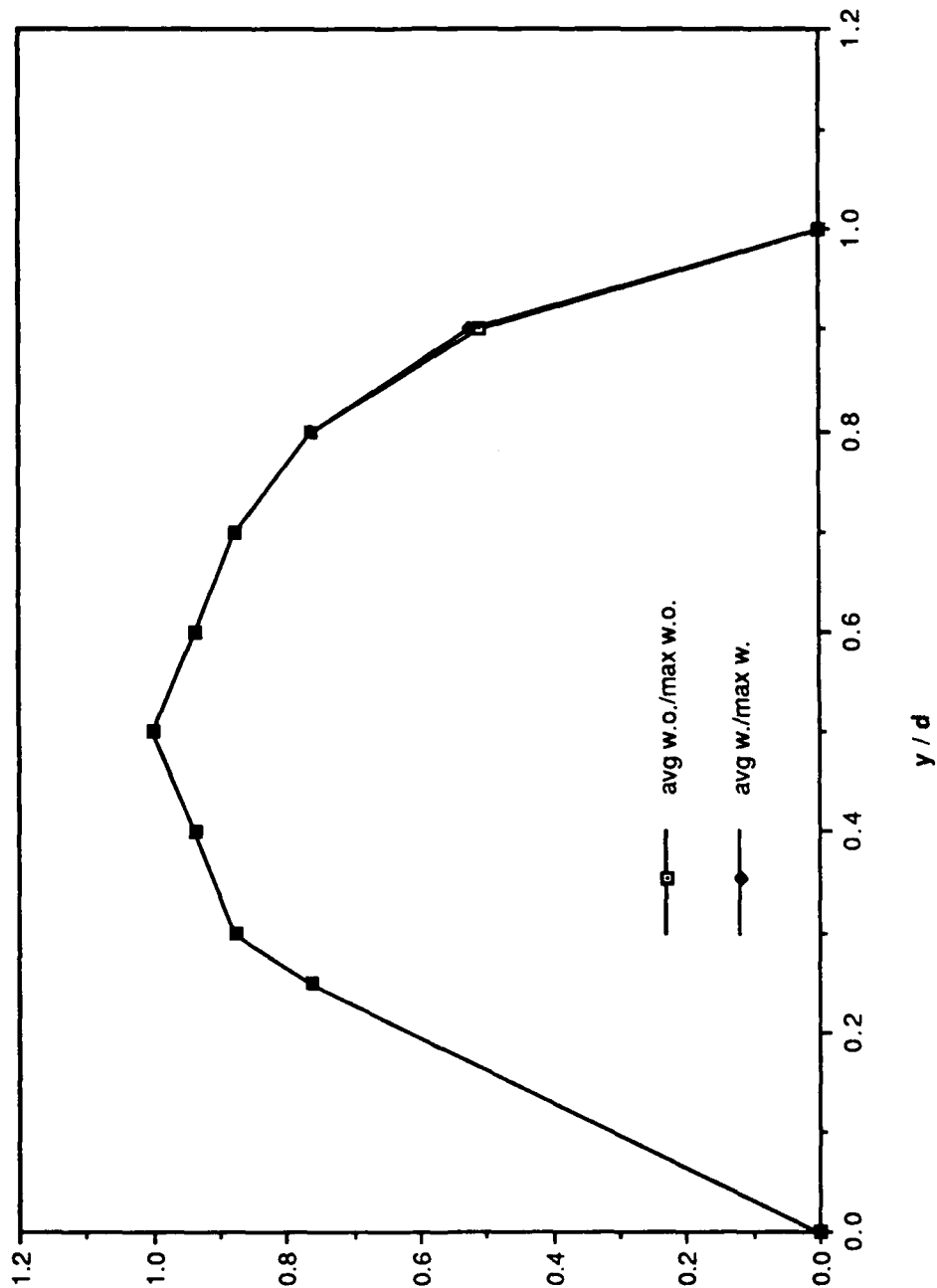


Figure 11.

avg vel / max vel

Profile Re 2197

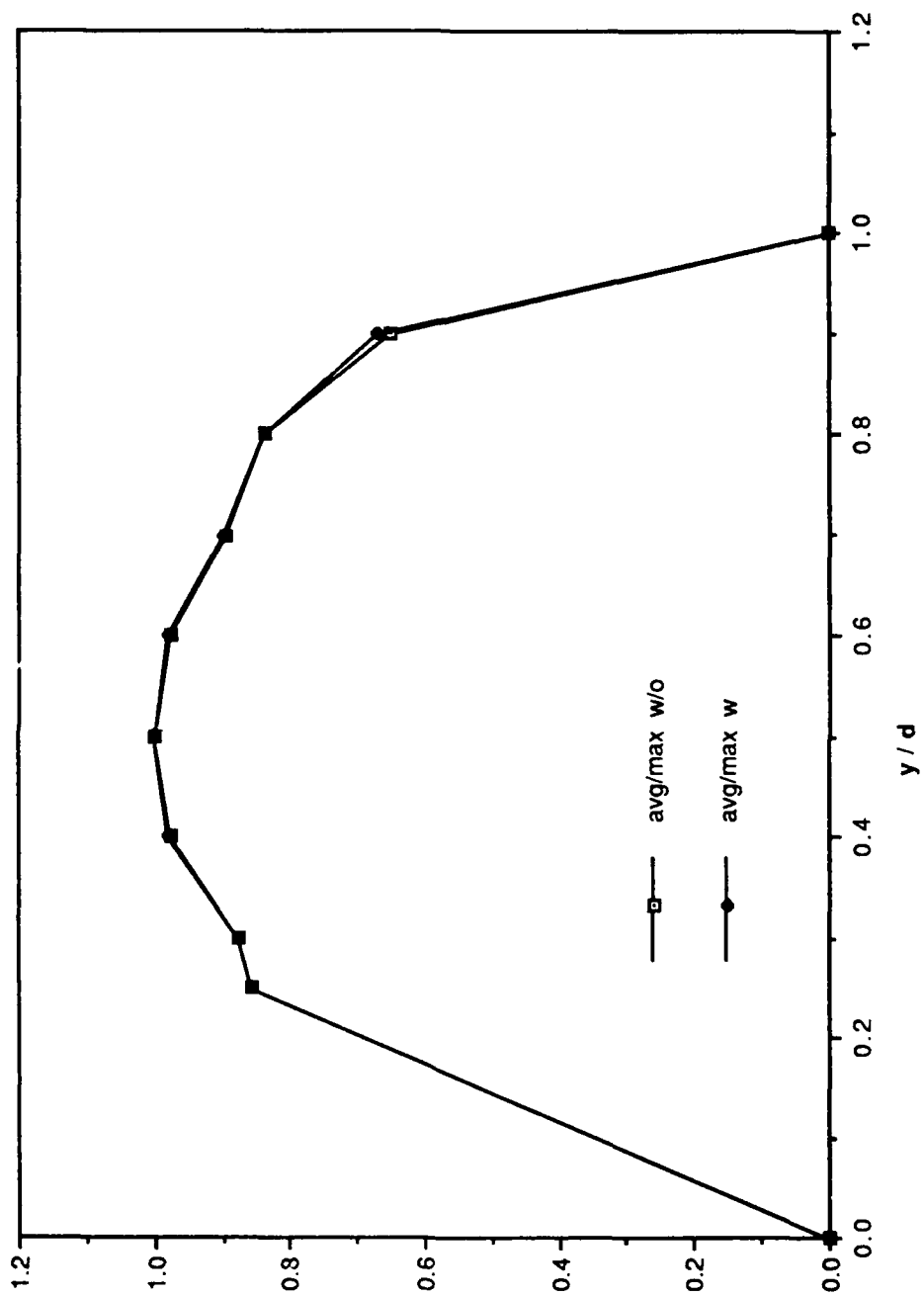


Figure 12.

avg vel / max vel

Profile Re 2548

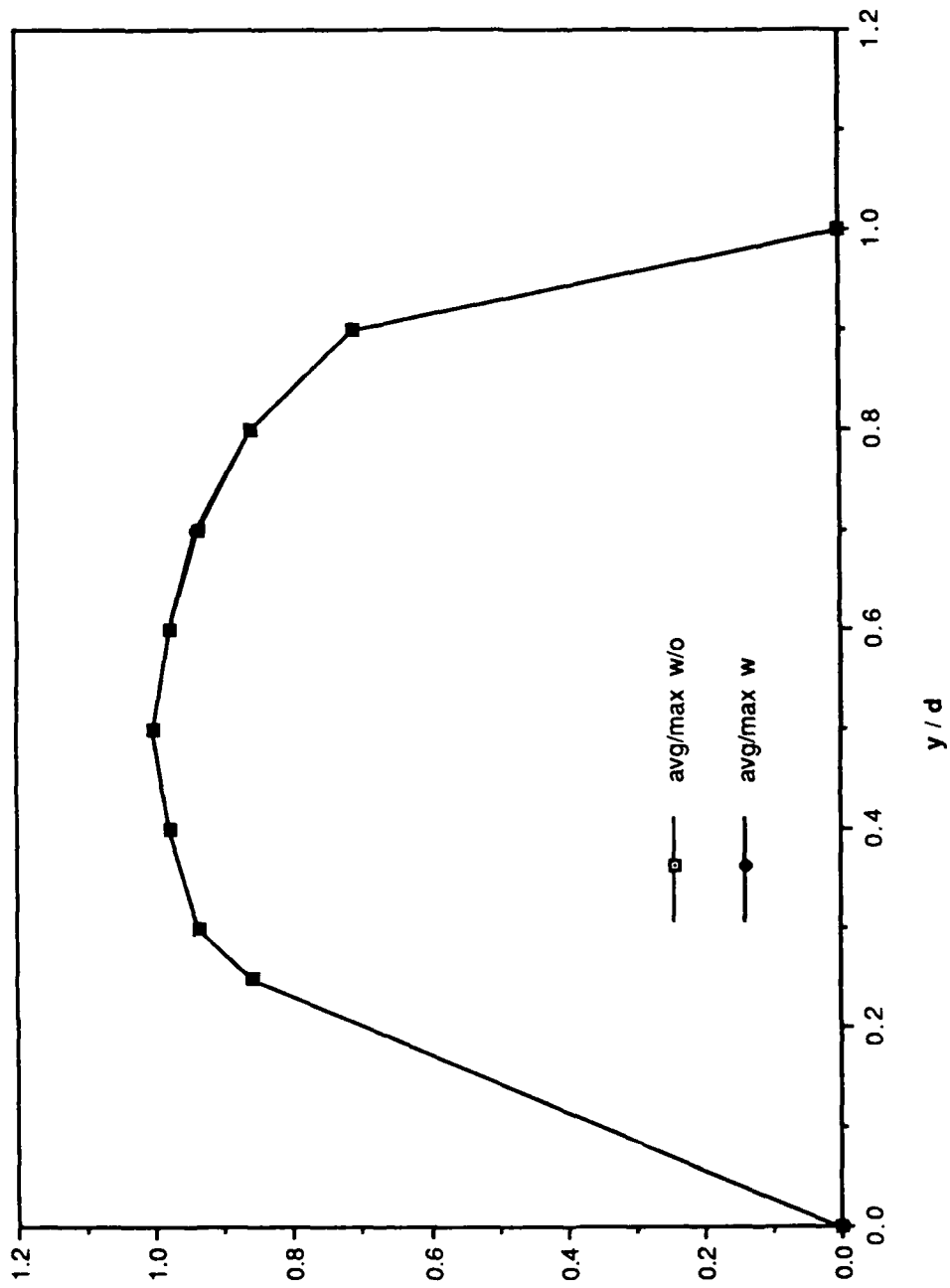


Figure 13.

avg vel / max vel

Profile Re 3584

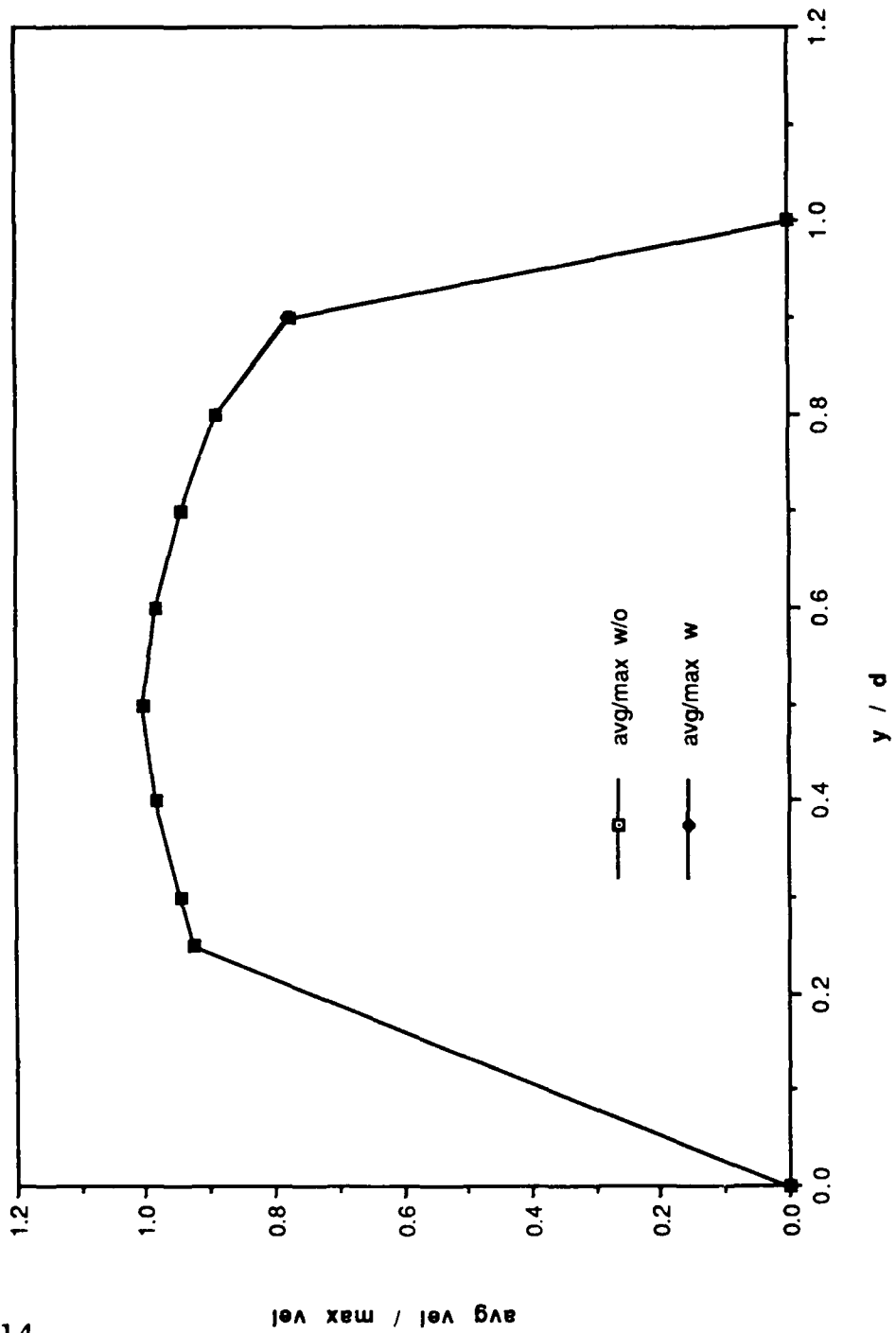


Figure 14.

rms / max Profile Re 1103

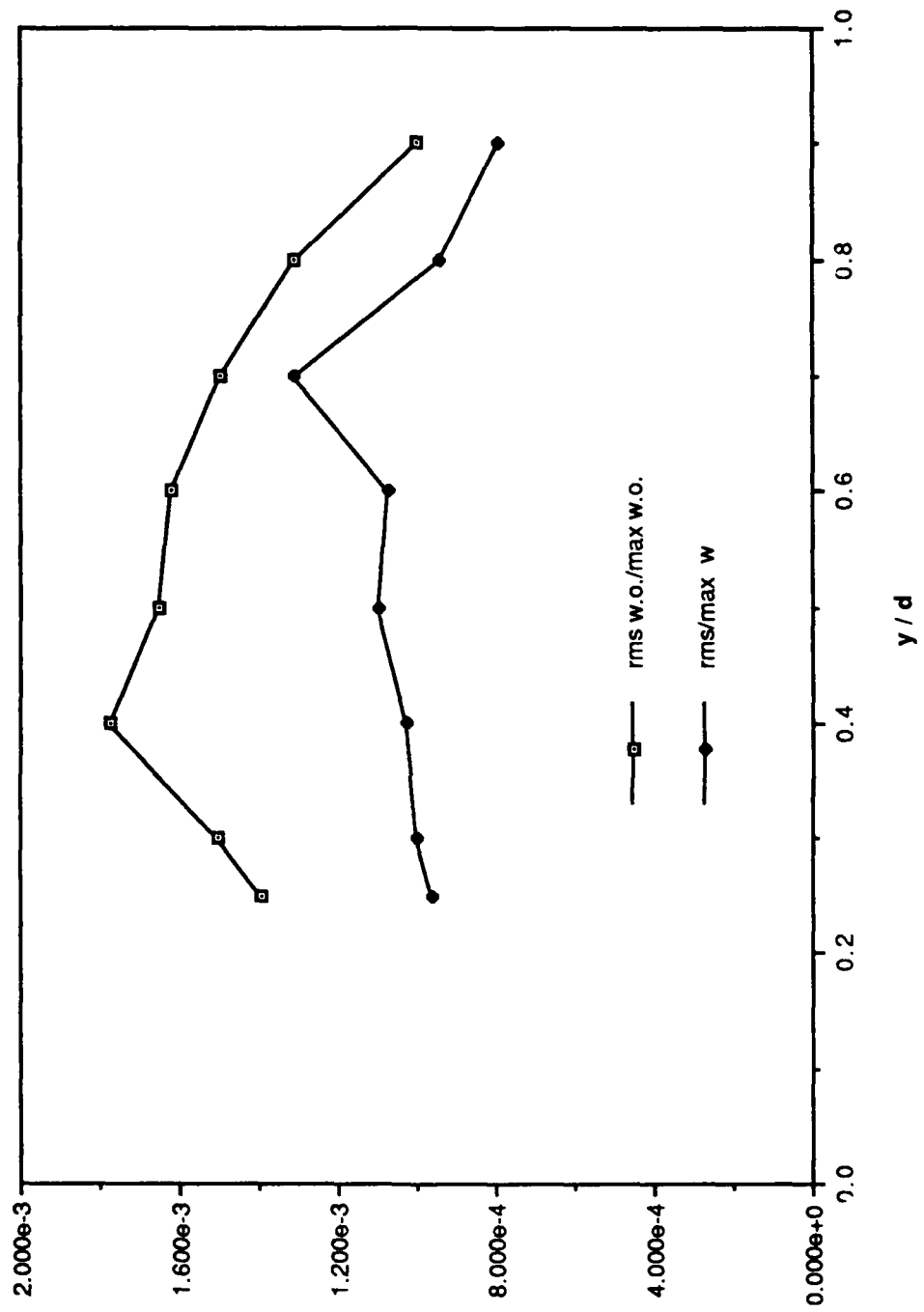


Figure 15.

rms vel / max vel



rms / max Profile 1579

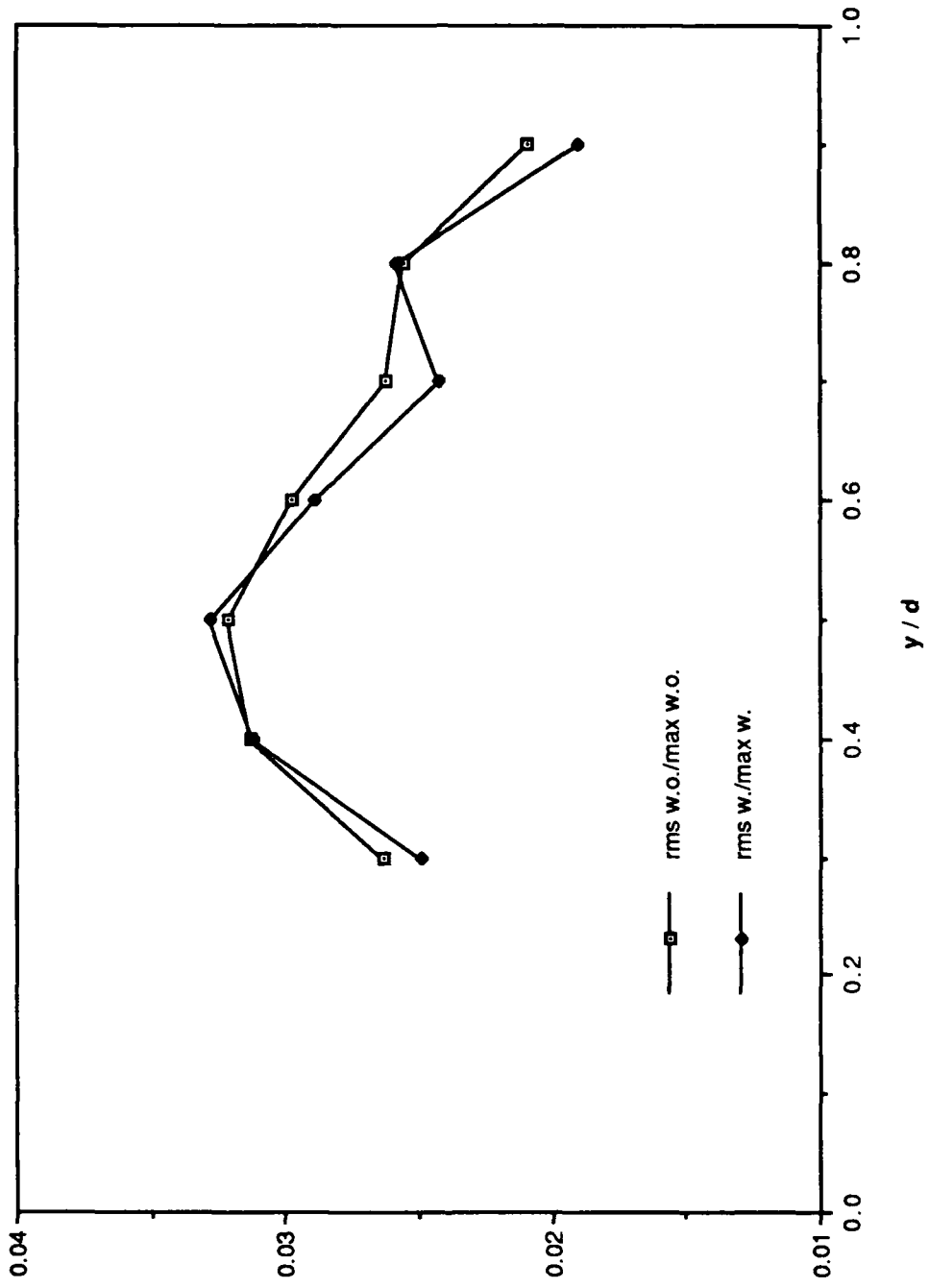


Figure 16.

rms vel / max vel

rms / max Profile Re 2005

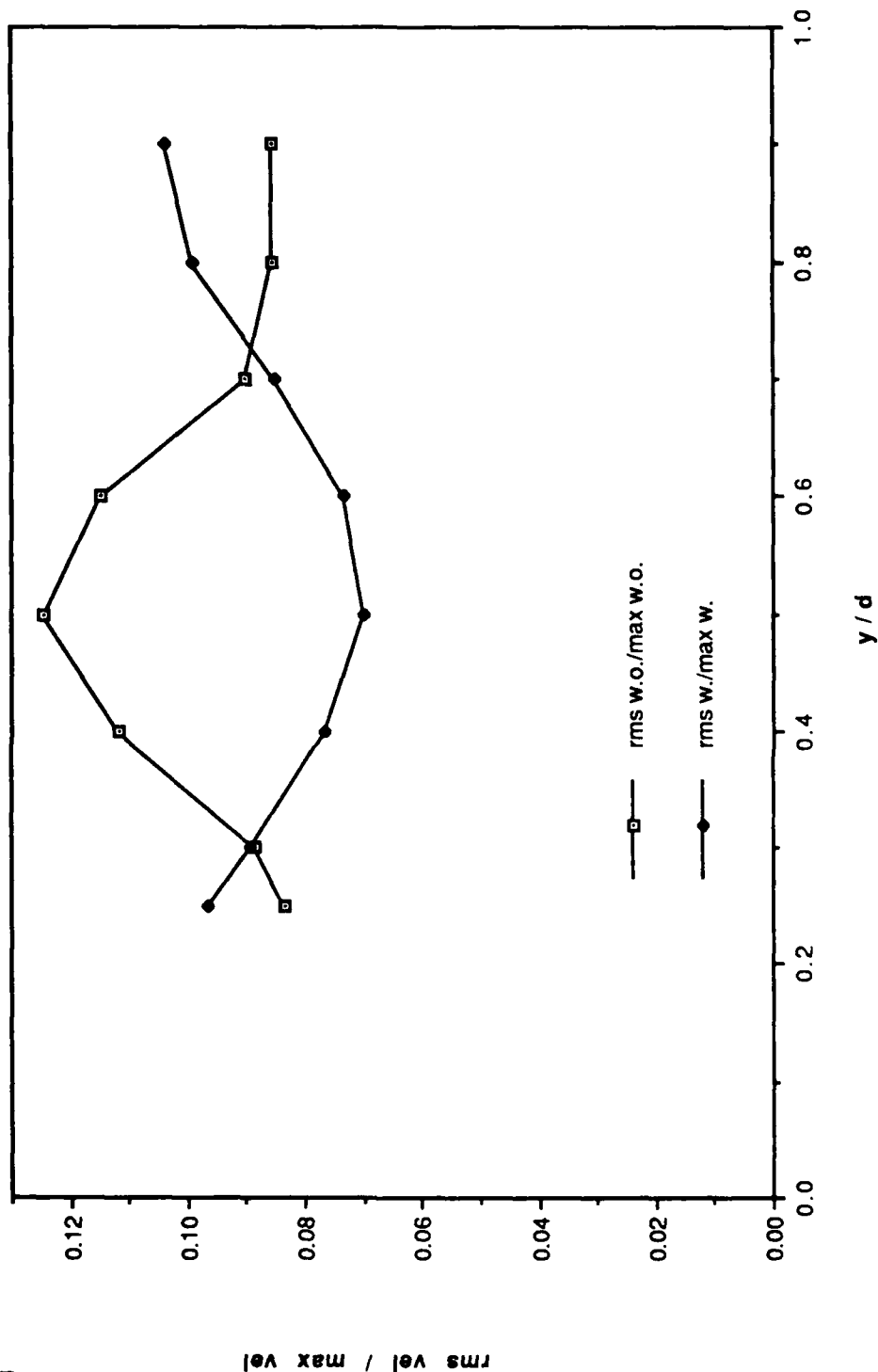


Figure 17.

rms / max Profile Re 2197

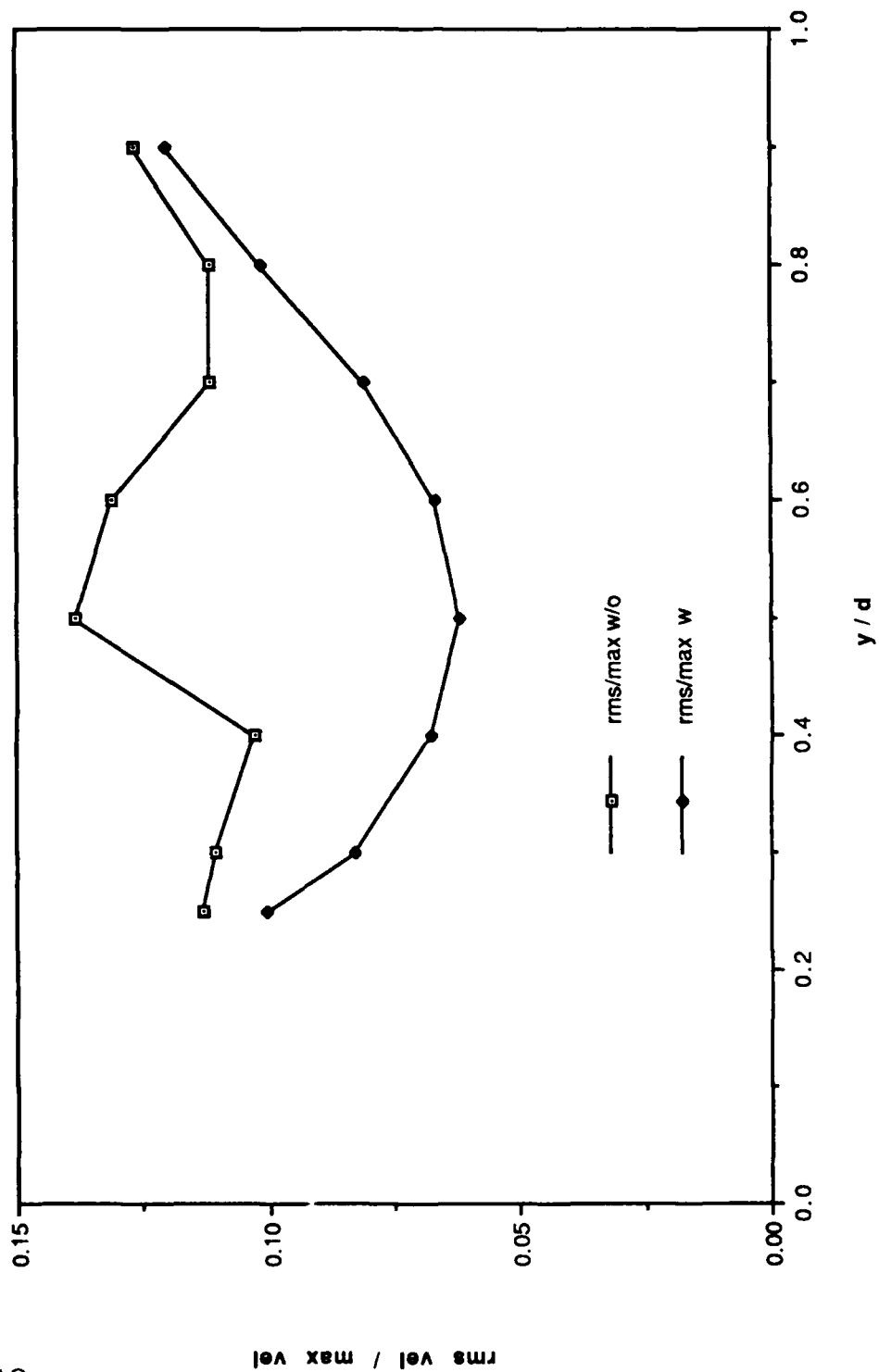


Figure 18.

rms / max Profile Re 2548

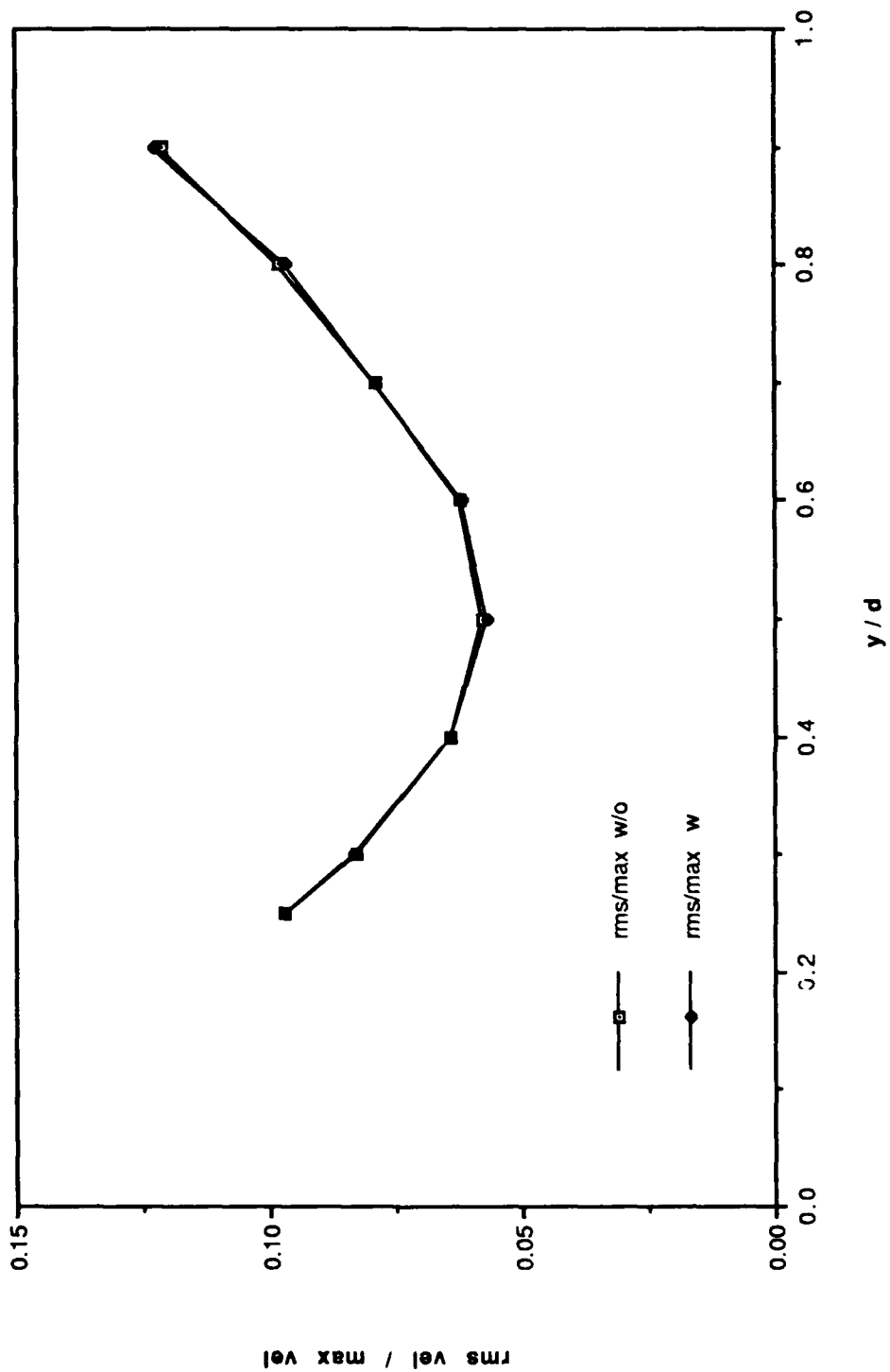


Figure 19.

rms / max Profile Re 3584

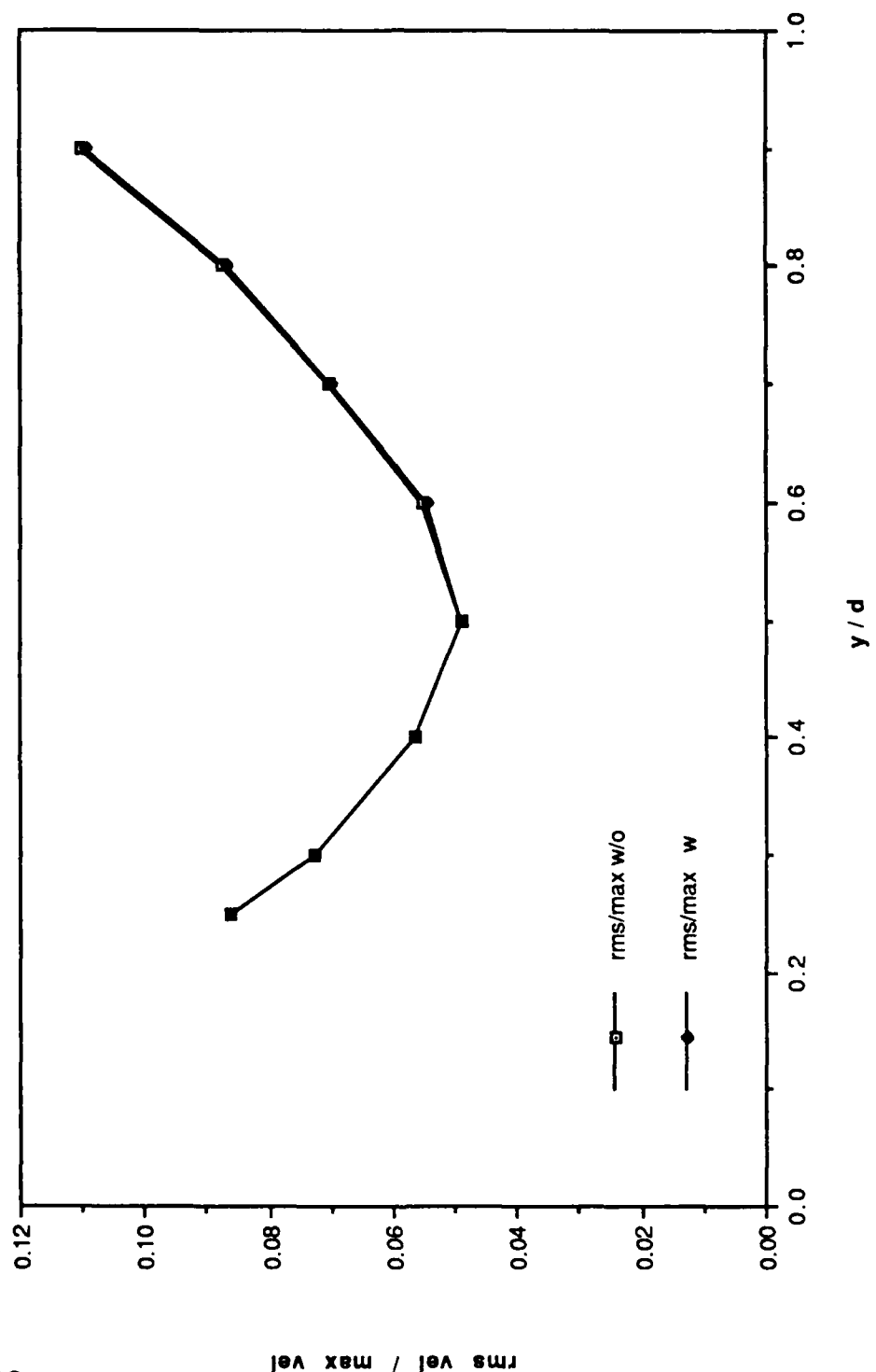


Figure 20.

1 hz rms/avg survey

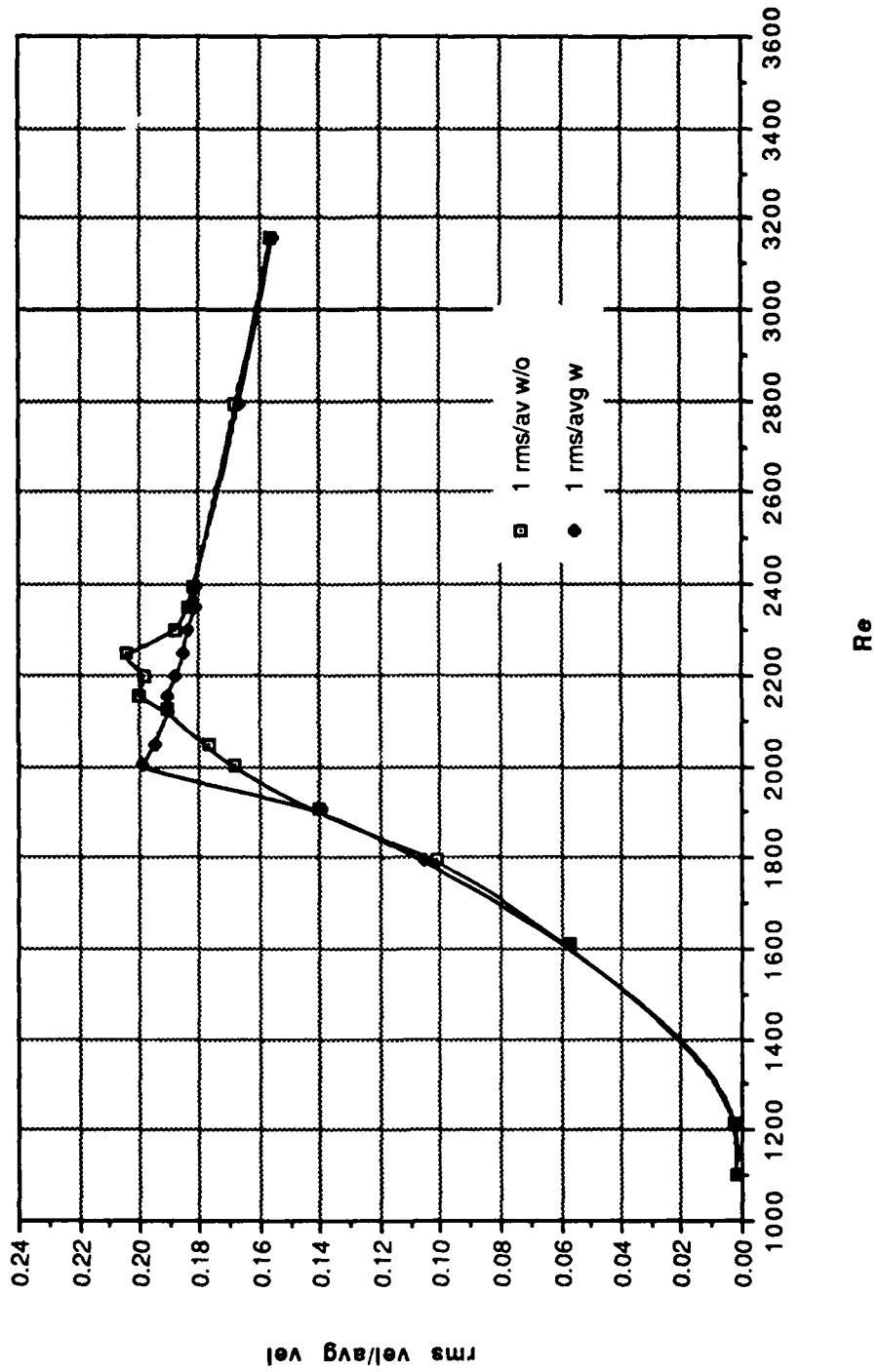


Figure 21.

2 Hz rms/avg survey

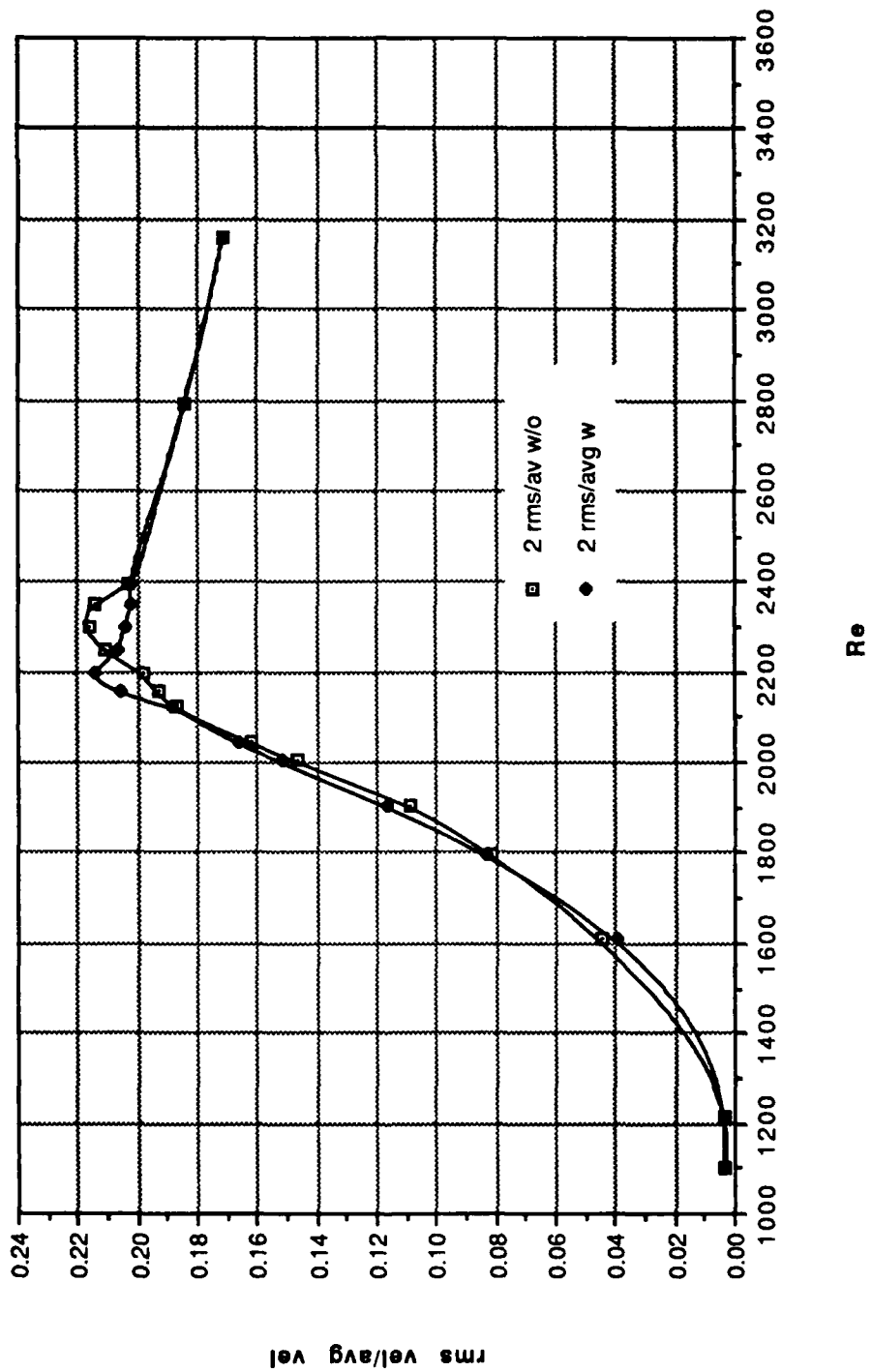


Figure 22.

3 hz rms/avg survey

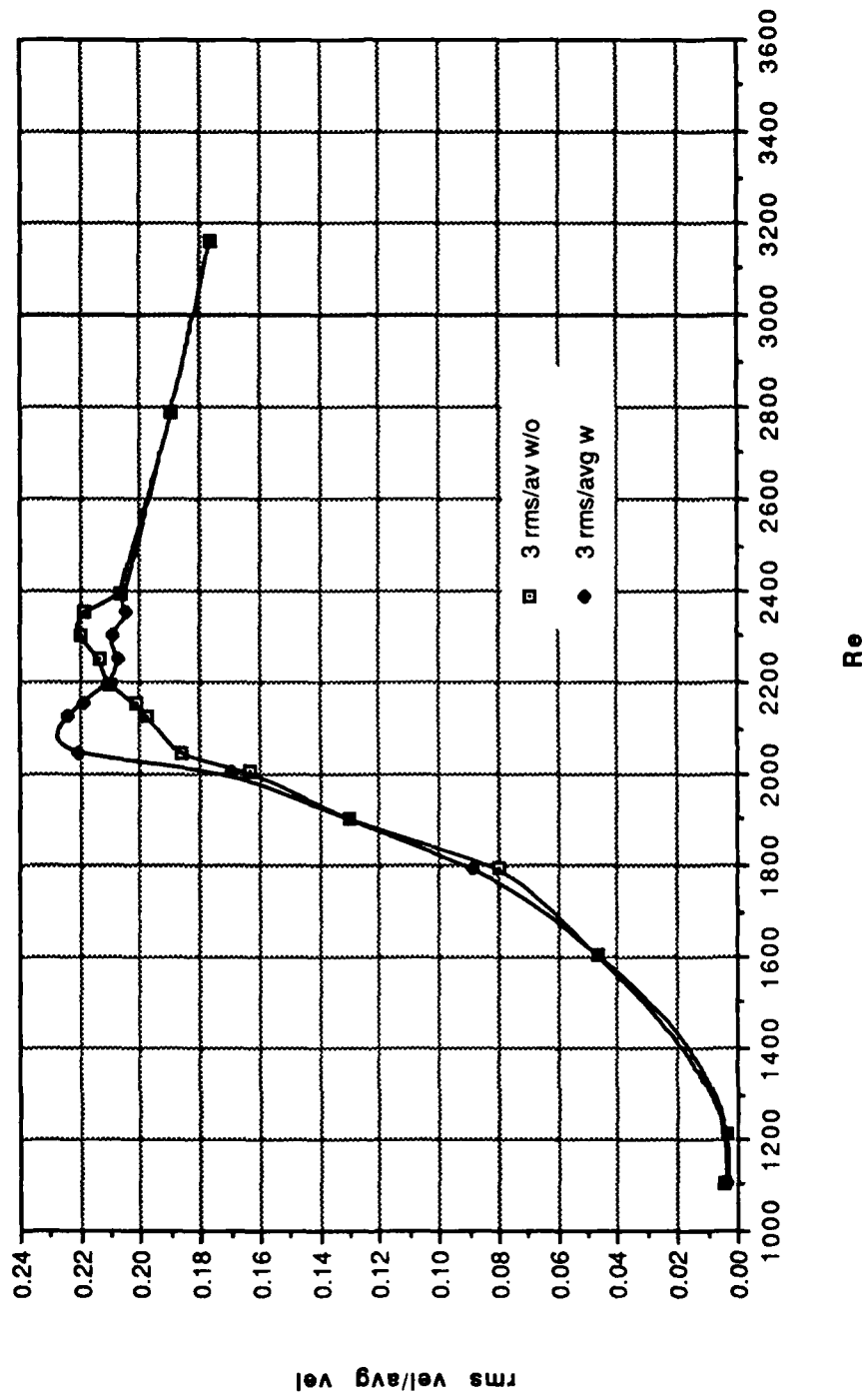


Figure 23.



4 Hz rms/avg survey

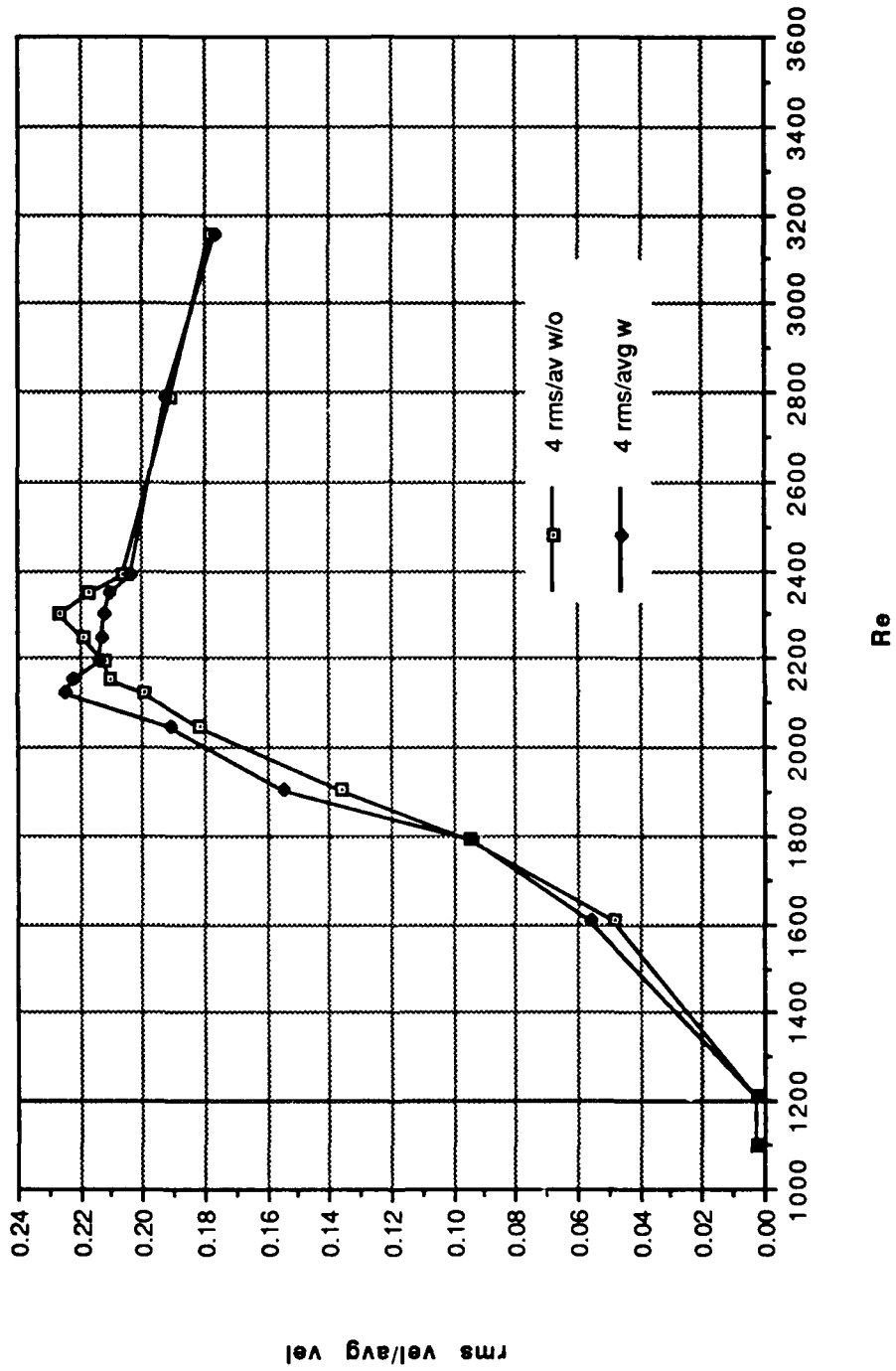


Figure 24.

1 Hz rms/avg survey (probe position 0.50)

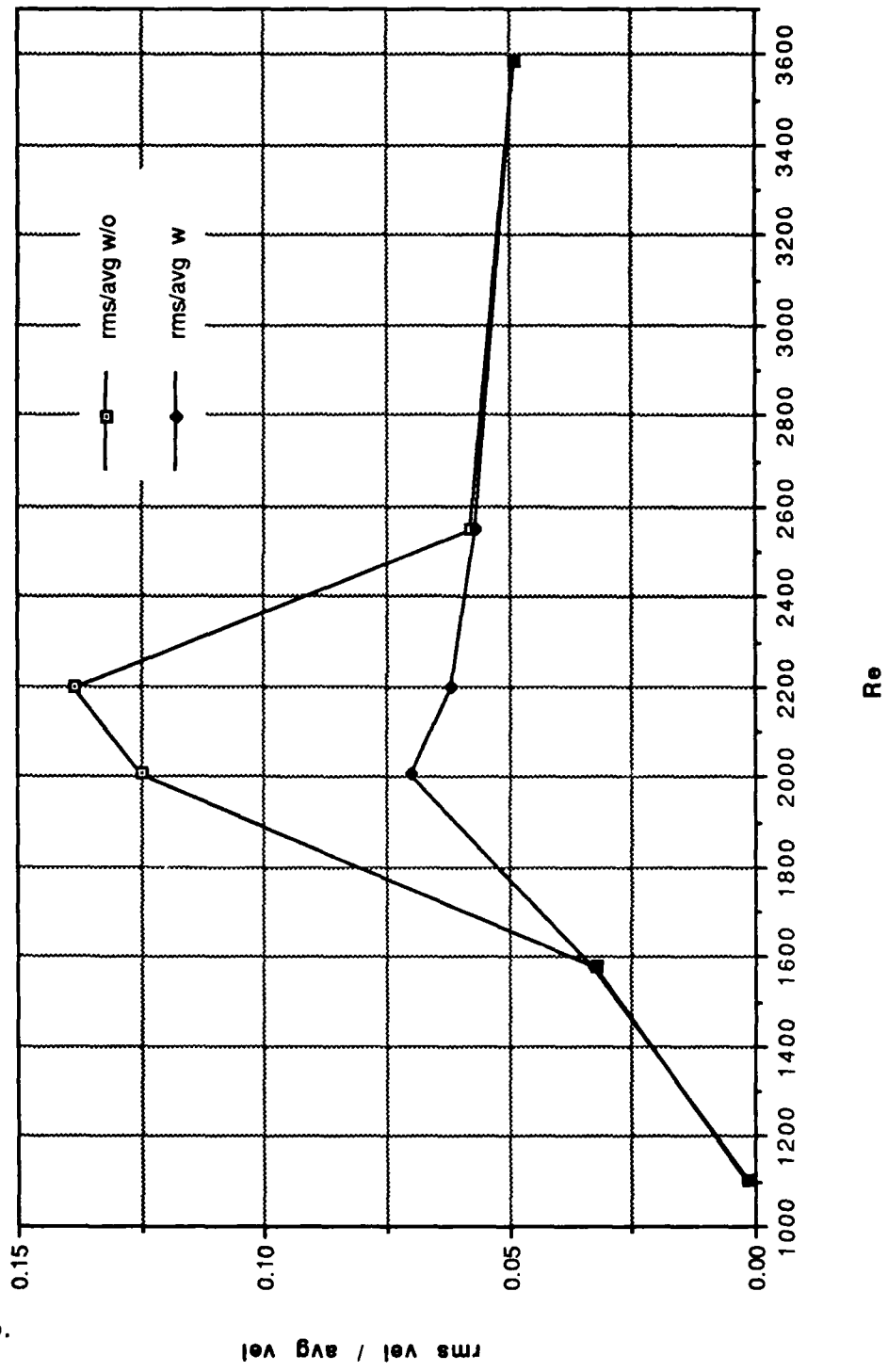


Figure 25.

1 Hz rms/avg survey (0.50, Coumes)

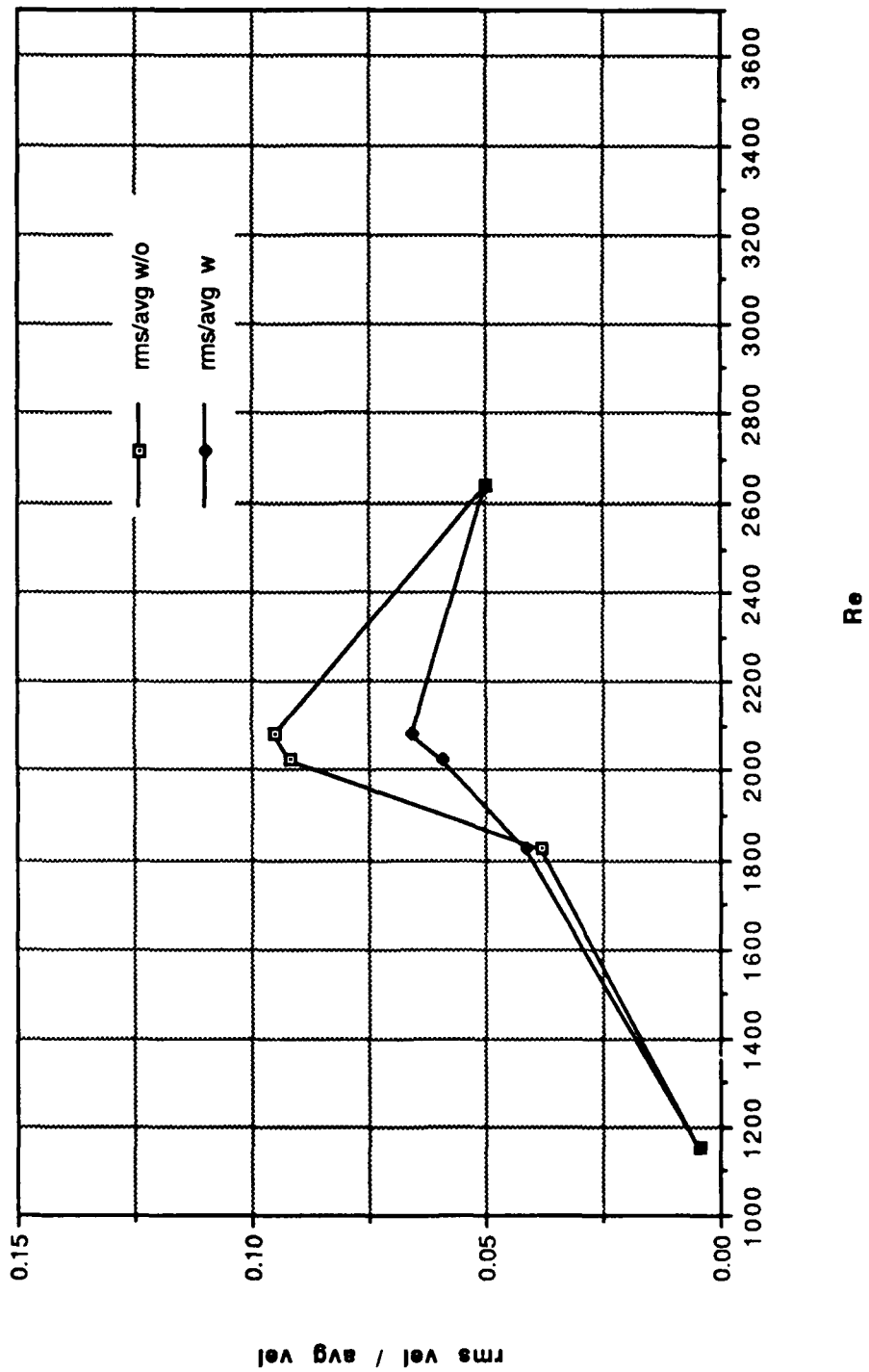
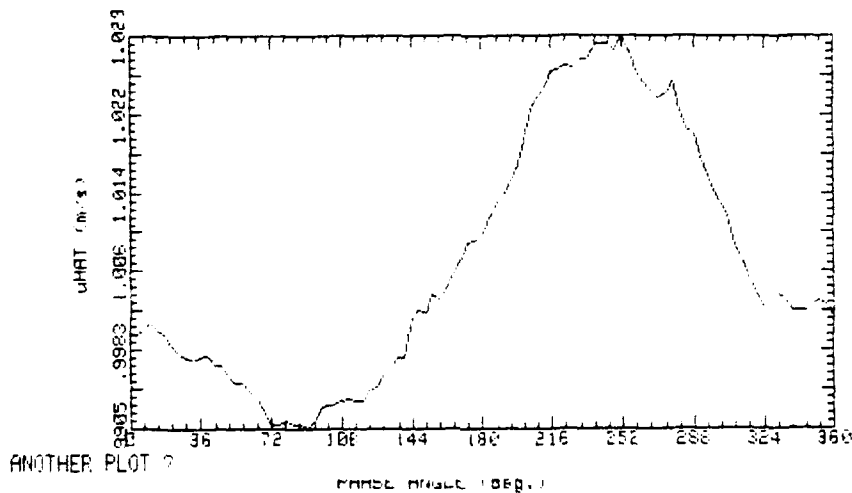


Figure 26.

MULTIRUN (, 4 RUNS) PH. AVE.,30390.1  
AVG. VEL 1.007m/s RMS VEL .06137m/s  
OSC. FREQ. 1Hz STR. # .04222  
BULK VEL. 1.89m/s REY. # 1578



MULTIRUN (, 4 RUNS) PH. AVE.,30390.1  
AVG. VEL 1.007m/s RMS VEL .06137m/s  
OSC. FREQ. 1Hz STR. # .04222  
BULK VEL. 1.89m/s REY. # 1578

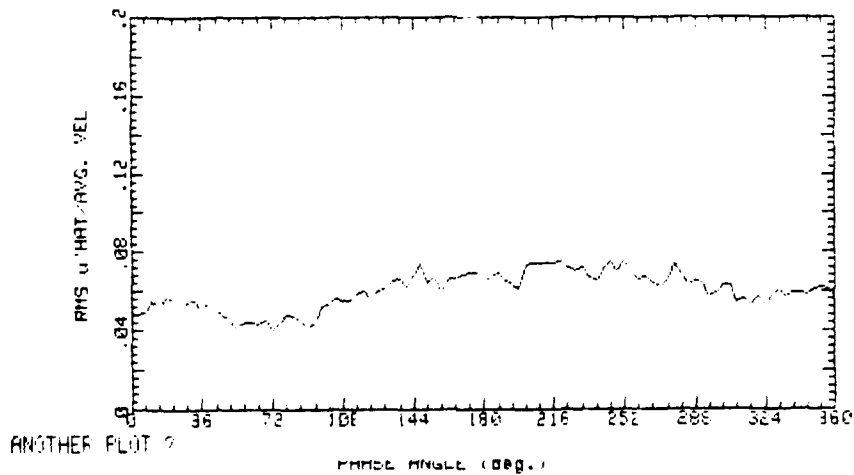
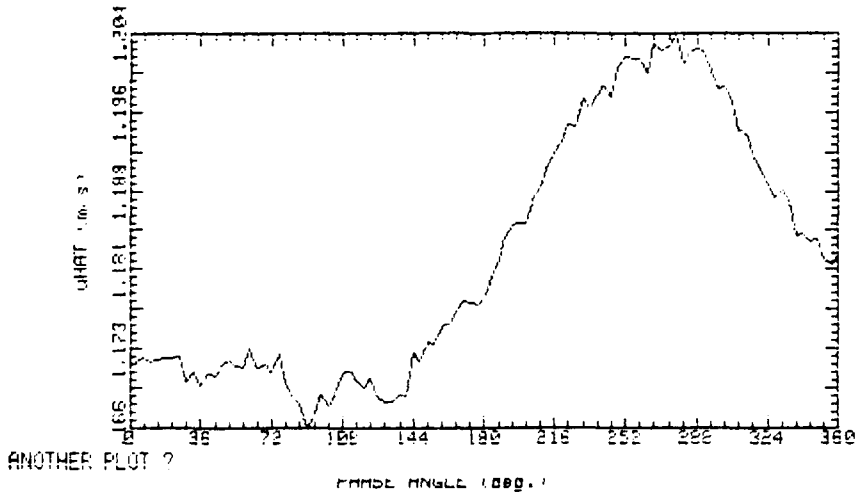


Figure 27.

MULTIRUN (, 8 RUNS) PH. AVE.,170390  
 AVG. VEL 1.182m/s RMS VEL .13m/s  
 OSC. FREQ. 1Hz STR. # .03939  
 BULK VEL. 2.026m/s REY. # 1693



MULTIRUN (, 8 RUNS) PH. AVE.,170390  
 AVG. VEL 1.182m/s RMS VEL .13m/s  
 OSC. FREQ. 1Hz STR. # .03939  
 BULK VEL. 2.026m/s REY. # 1693

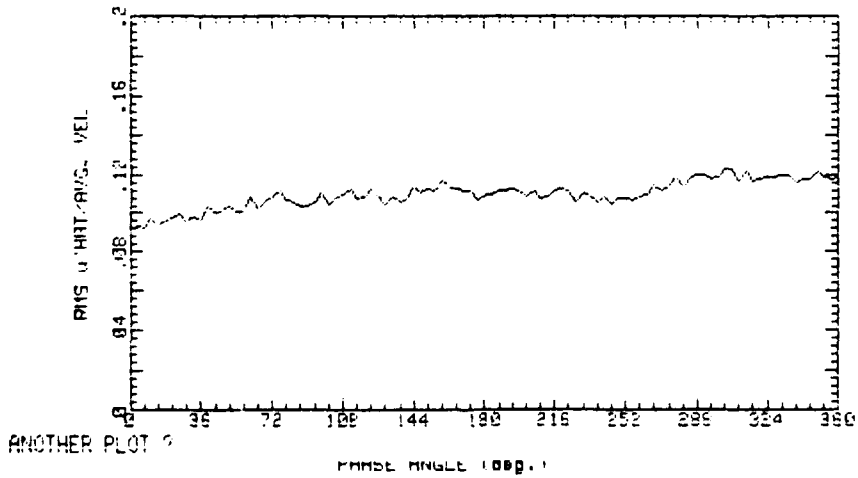
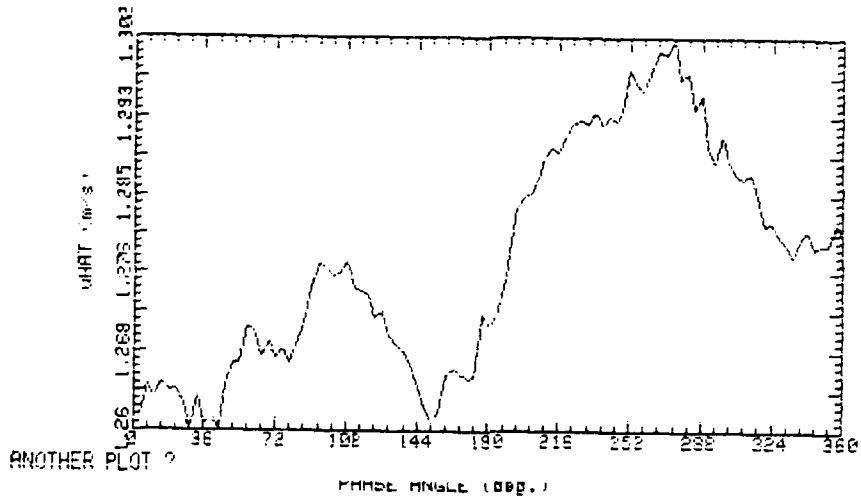
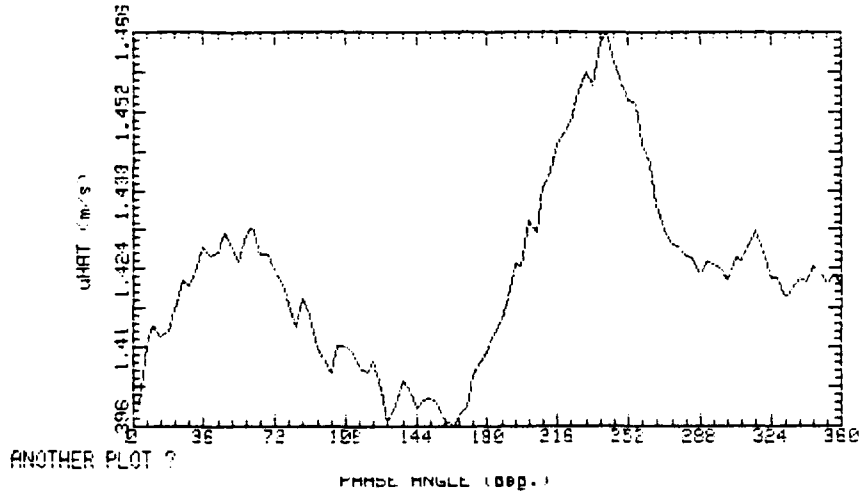


Figure 28.

MULTIRUN (. 8 RUNS) PH. AVE.,170390  
 AVG. VEL 1.278m/s RMS VEL .1919m/s  
 OSC. FREQ. 1Hz STR. # .03711  
 BULK VEL. 2.15m/s REY. # 1796



MULTIRUN (, 8 RUNS) PH. AVE.,110390  
 AVG. VEL 1.423m/s RMS VEL .2709m/s  
 OSC. FREQ. 1Hz STR. # .035  
 BULK VEL. 2.26m/s REY. # 1905



MULTIRUN (, 8 RUNS) PH. AVE.,110390  
 AVG. VEL 1.423m/s RMS VEL .2709m/s  
 OSC. FREQ. 1Hz STR. # .035  
 BULK VEL. 2.26m/s REY. # 1905

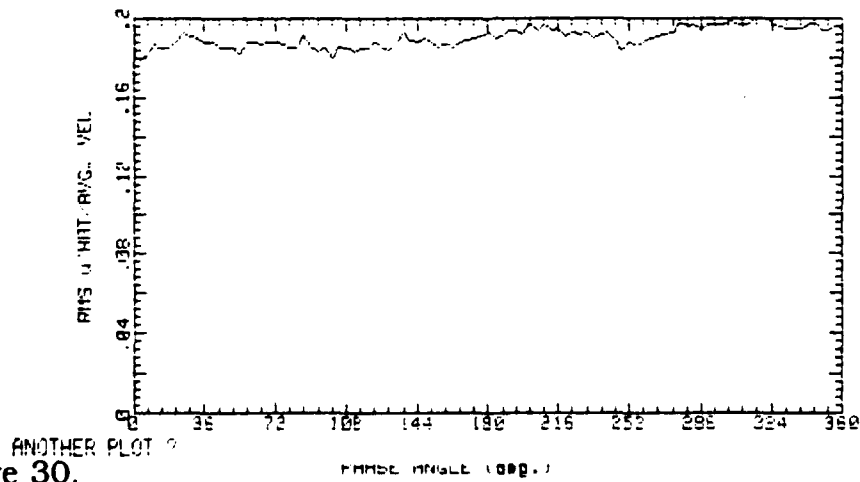
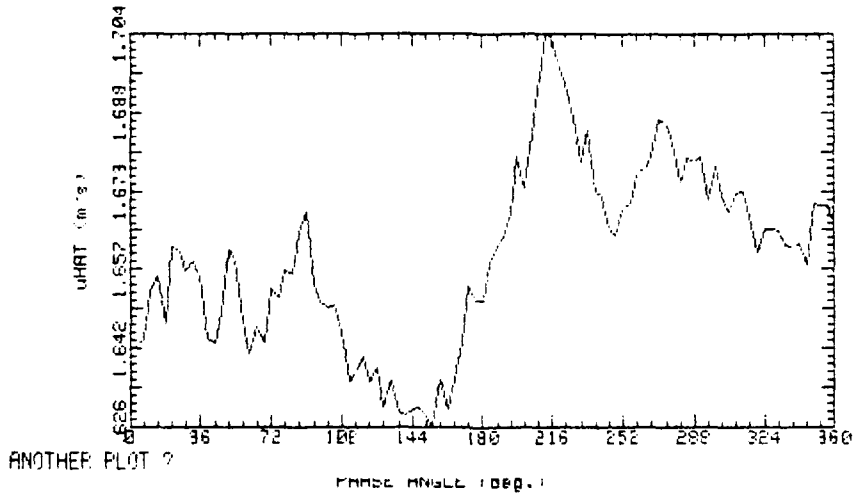


Figure 30.

MULTIRUN (, 4 RUNS) PH. AVE., 40390  
 AVG. VEL 1.66m/s RMS VEL .3585m/s  
 OSC. FREQ. 1Hz STR. # .03325  
 BULK VEL. 2.4m/s RET. # 2005



MULTIRUN (, 4 RUNS) PH. AVE., 40390  
 AVG. VEL 1.66m/s RMS VEL .3585m/s  
 OSC. FREQ. 1Hz STR. # .03325  
 BULK VEL. 2.4m/s RET. # 2005

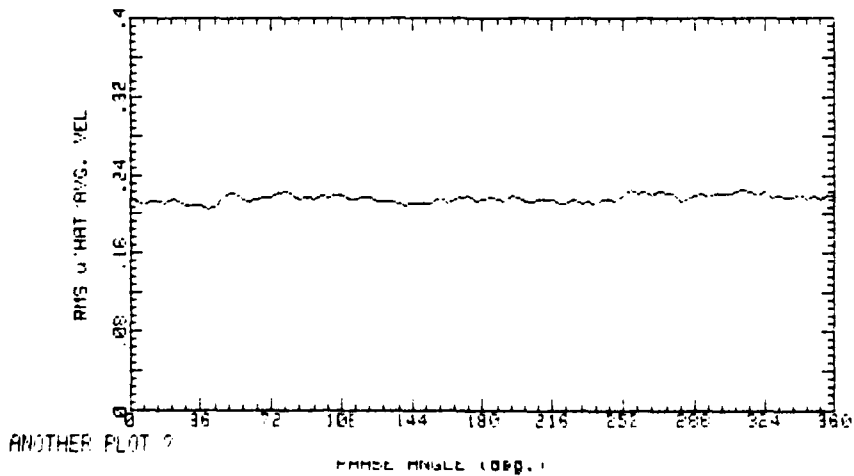
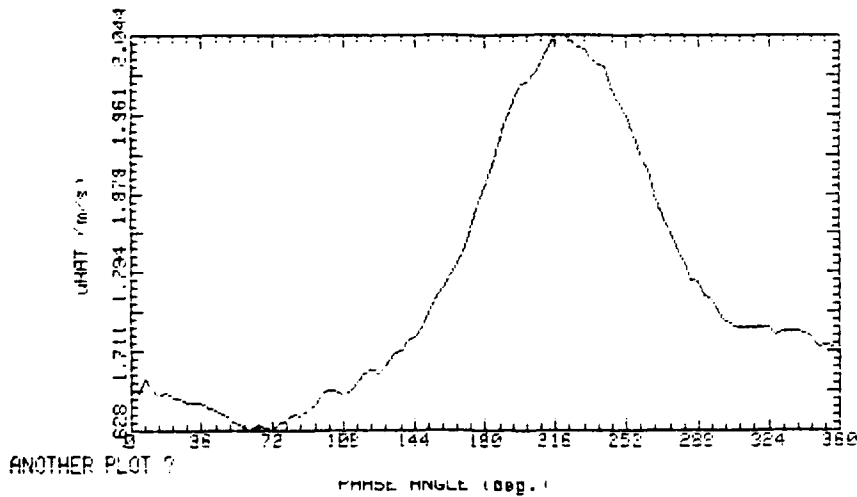


Figure 31.



MULTIRUN (, 8 RUNS) PH. AVE., 110390  
 AVG. VEL 1.778m/s RMS VEL .3689m/s  
 OSC. FREQ. 1Hz STR. # .03166  
 BULK VEL. 2.52m/s REY. # 2106



MULTIRUN (, 8 RUNS) PH. AVE., 110390  
 AVG. VEL 1.778m/s RMS VEL .3689m/s  
 OSC. FREQ. 1Hz STR. # .03166  
 BULK VEL. 2.52m/s REY. # 2106

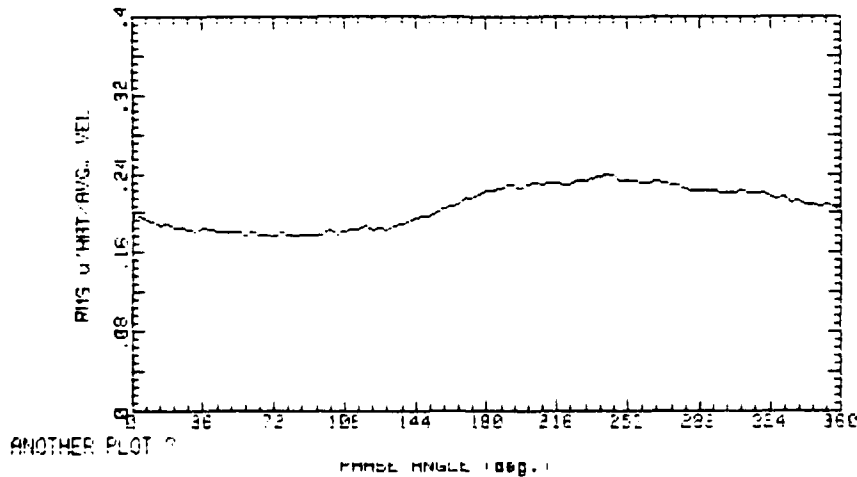
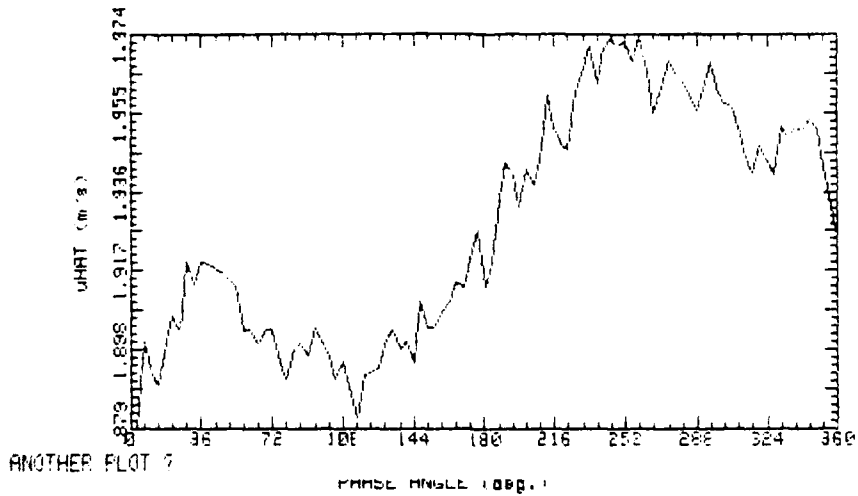


Figure 32.

MULTIRUN (, 8 RUNS) PH. AVE., 40390.1  
 AVG. VEL 1.928m/s RMS VEL .3633m/s  
 OSC. FREQ. 1Hz STR. # .03034  
 BULK VEL. 2.63m/s REY. # 2197



MULTIRUN (, 8 RUNS) PH. AVE., 40390.1  
 AVG. VEL 1.928m/s RMS VEL .3633m/s  
 OSC. FREQ. 1Hz STR. # .03034  
 BULK VEL. 2.63m/s REY. # 2197

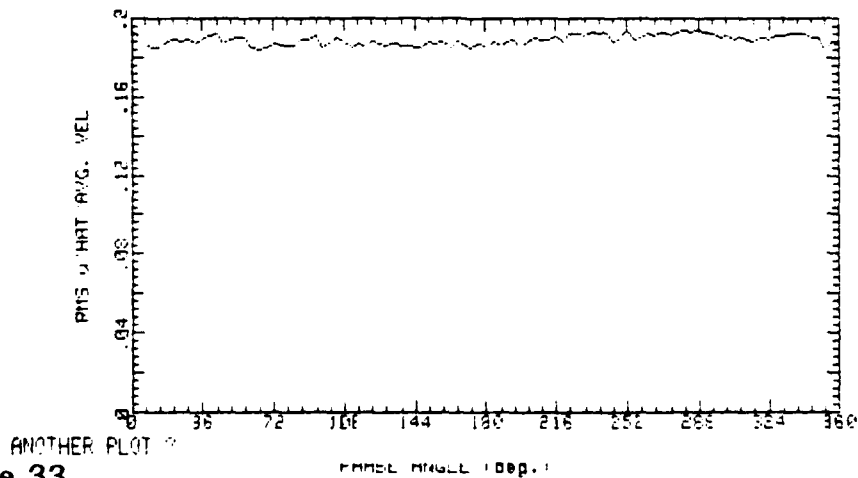
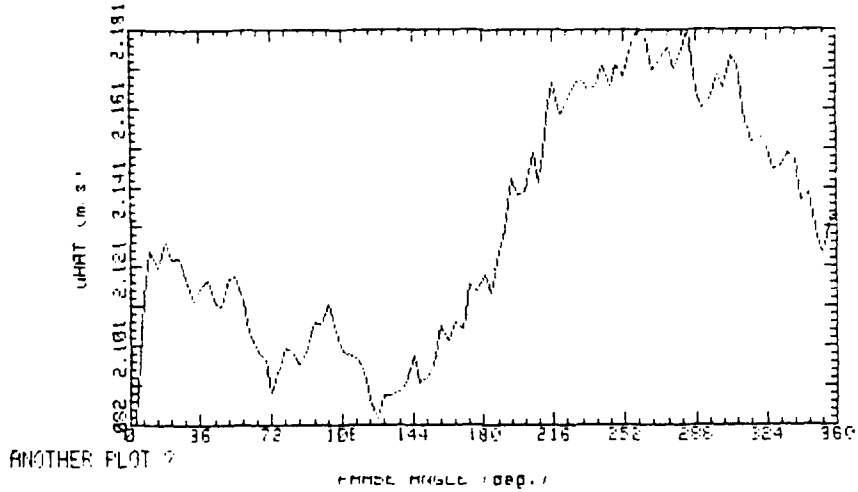


Figure 33.

MULTIRUN (, 8 RUNS) PH. AVE. .100390  
 AVG. VEL 2.131m/s RMS VEL .381m/s  
 OSC. FREQ. 1Hz STP. # .02616  
 BULK VEL. 3.05m/s REY. # 2546



MULTIRUN (, 8 RUNS) PH. AVE. .100390  
 AVG. VEL 2.131m/s RMS VEL .381m/s  
 OSC. FREQ. 1Hz STP. # .02616  
 BULK VEL. 3.05m/s REY. # 2546

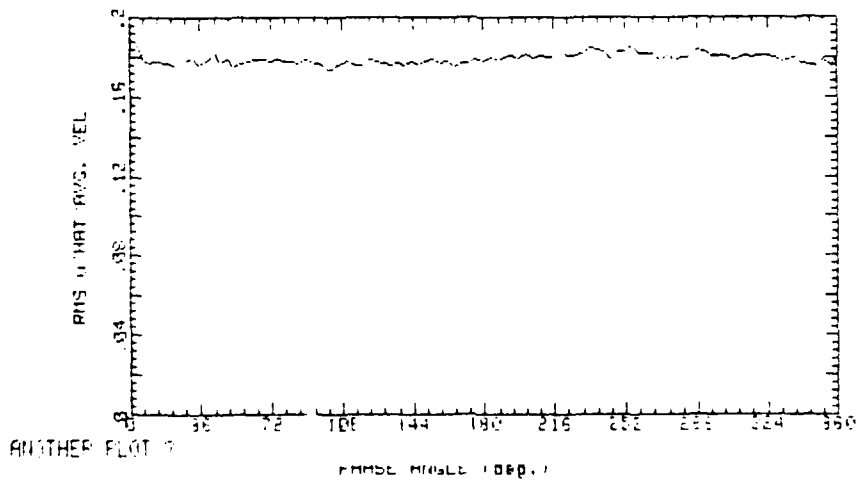
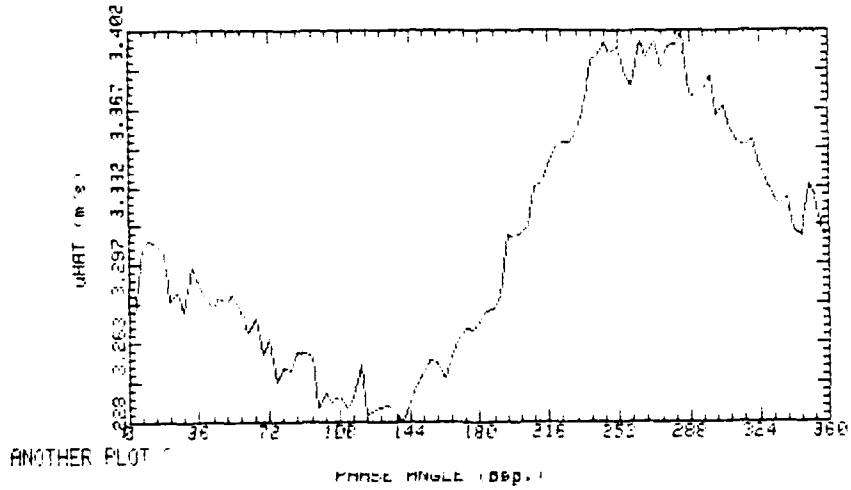


Figure 34.

MULTIRUN (, 8 RUNS) PH. AVE., 100390  
 AVG. VEL 3.306m/s RMS VEL .481m/s  
 OSC. FREQ. 1Hz STR. # .0186  
 BULK VEL. 4.29m/s REY. # 3584



MULTIRUN (, 8 RUNS) PH. AVE., 100390  
 AVG. VEL 3.306m/s RMS VEL .481m/s  
 OSC. FREQ. 1Hz STR. # .0186  
 BULK VEL. 4.29m/s REY. # 3584

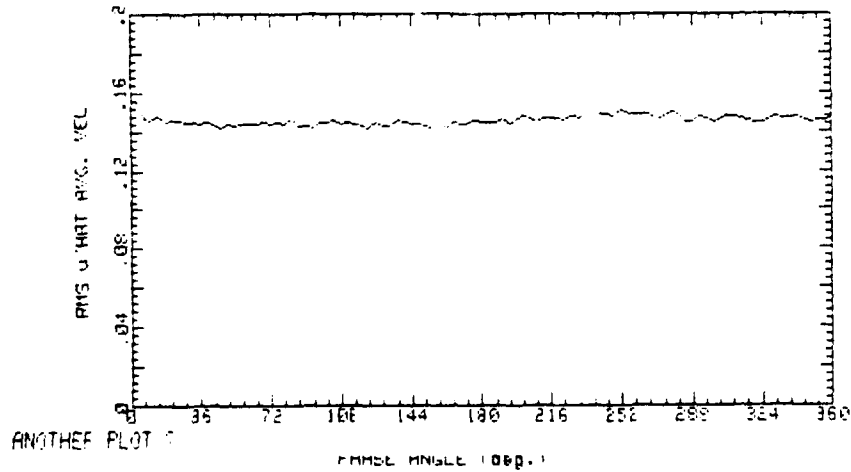
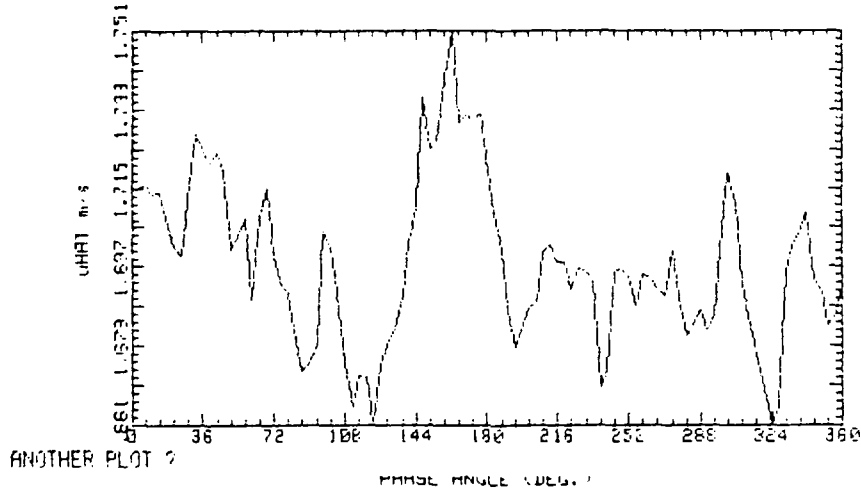


Figure 35.

RUNR10 220490.1751  
 AVG. VEL 1.698m/s RMS VEL .3745m/s  
 OSC. FREQ. 3Hz STR. # .09771  
 BULK VEL. 2.45m/s REY. # 2047



RUNR10 220490.1751  
 AVG. VEL 1.698m/s RMS VEL .3745m/s  
 OSC. FREQ. 3Hz STR. # .09771  
 BULK VEL. 2.45m/s REY. # 2047

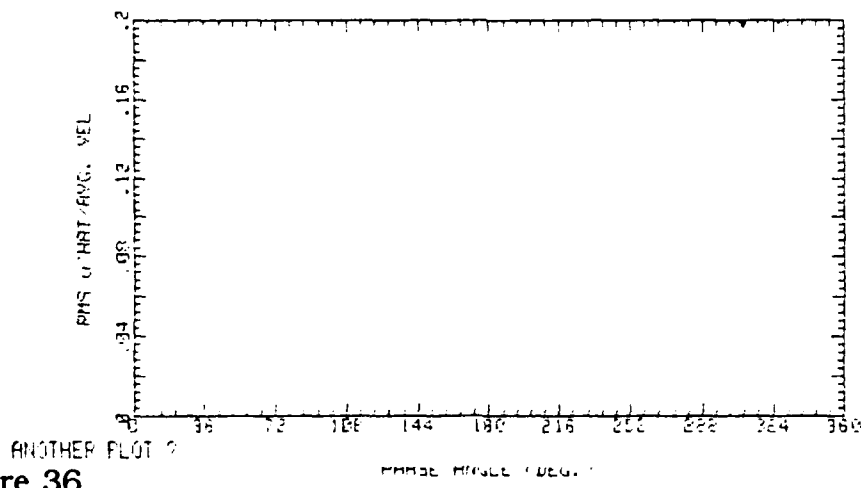
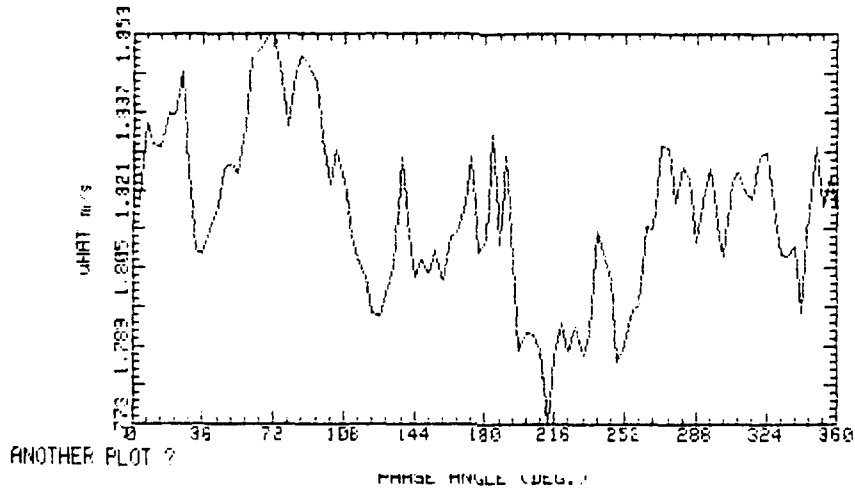


Figure 36.

RUNTIME 240490.0433  
 AVG. VEL 1.816m/s RMS VEL .4086m/s  
 OSC. FREQ. 4Hz STR. # .1254  
 BULK VEL. 2.545m/s REY. # 2126



RUNTIME 240490.0433  
 AVG. VEL 1.816m/s RMS VEL .4086m/s  
 OSC. FREQ. 4Hz STR. # .1254  
 BULK VEL. 2.545m/s REY. # 2126

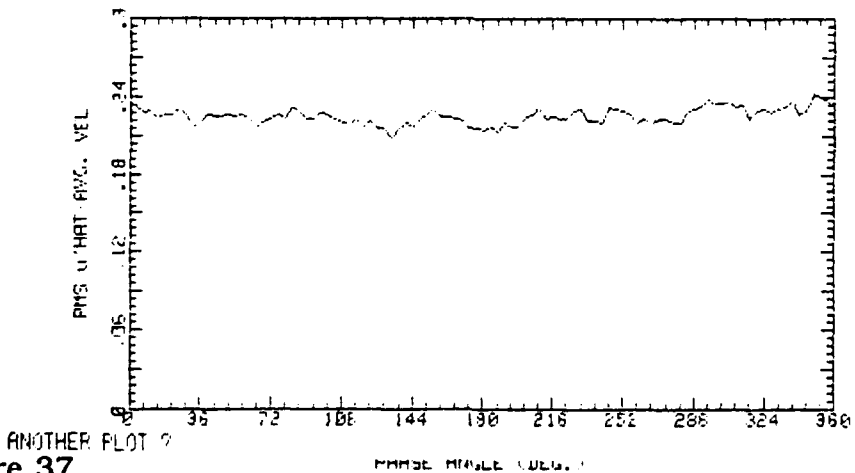


Figure 37.

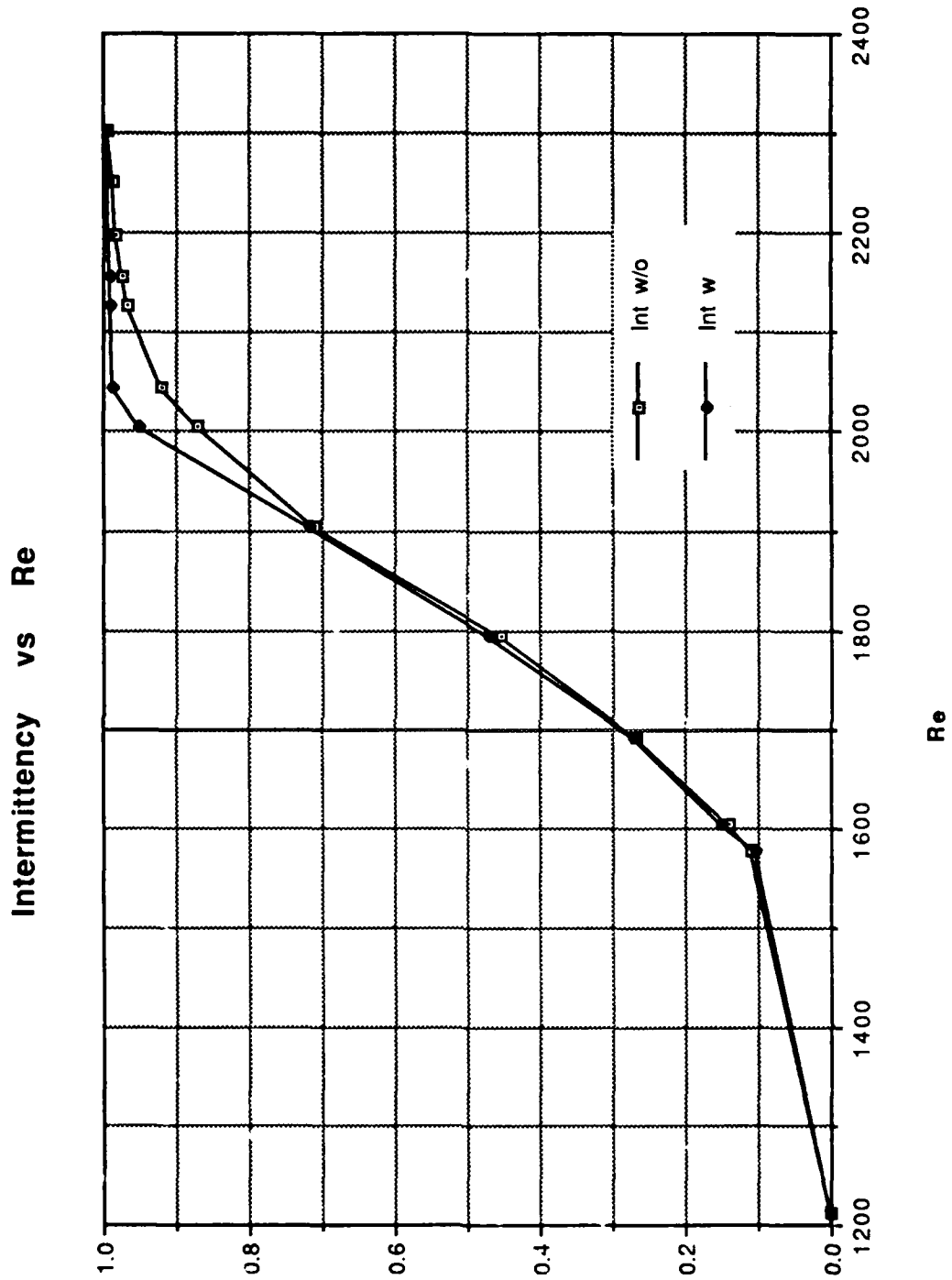


Figure 38.

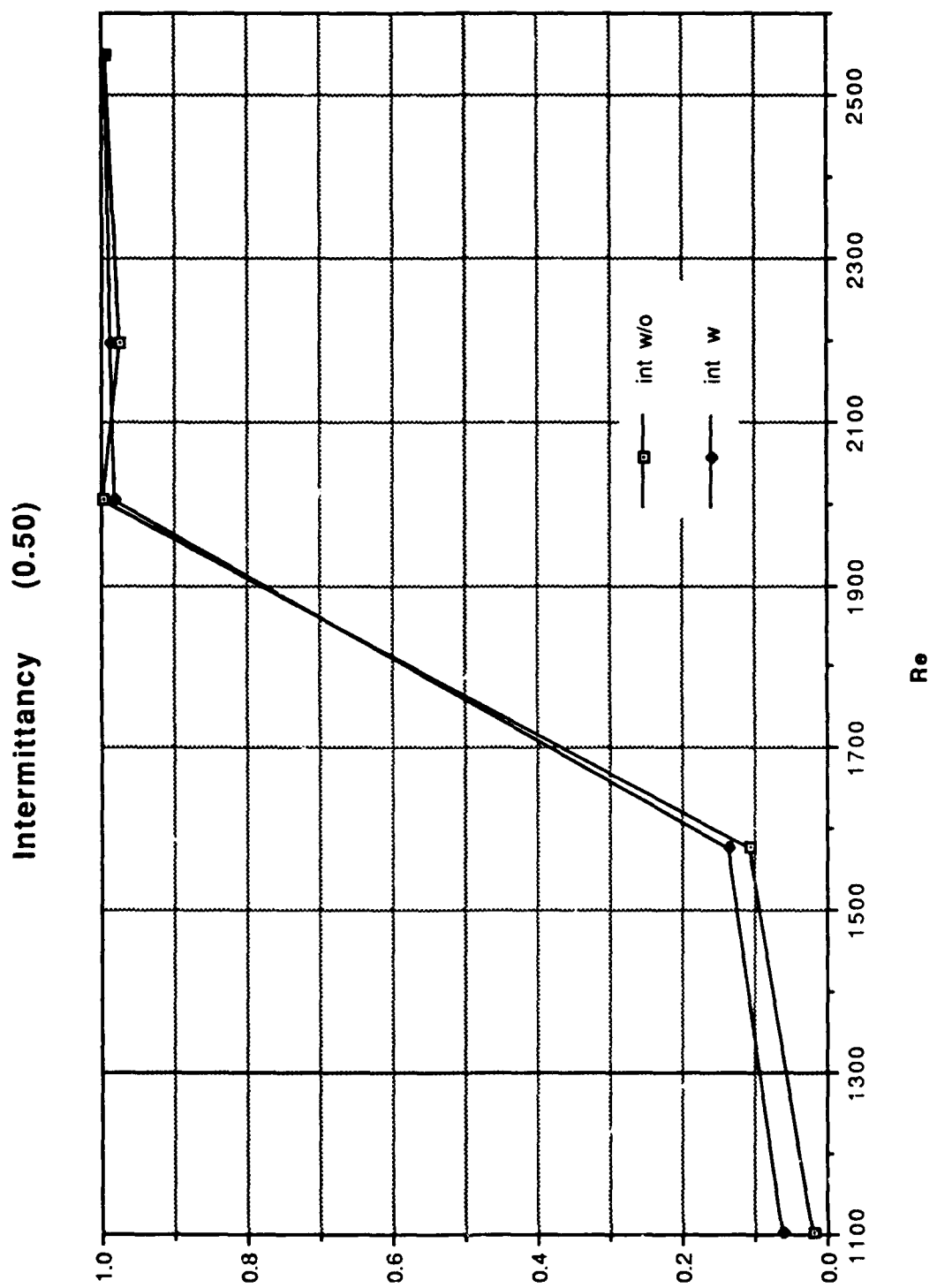
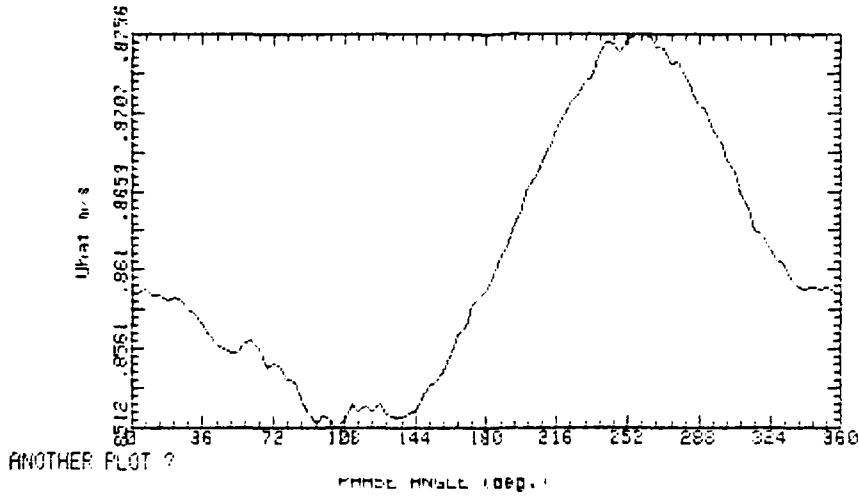


Figure 39.



RUND2 91189.2337  
 GAMMA - 1.724E-5  
 OSC. FREQ. 1Hz STR. # .05503  
 BULK VEL. 1.45m/s REY. # 1212



RUND2 91189.2337  
 GAMMA - 1.724E-5  
 OSC. FREQ. 1Hz STR. # .05503  
 BULK VEL. 1.45m/s REY. # 1212

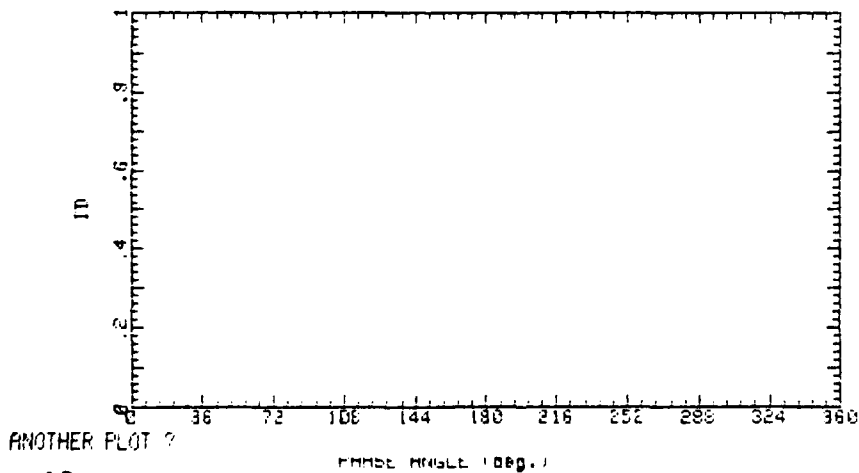
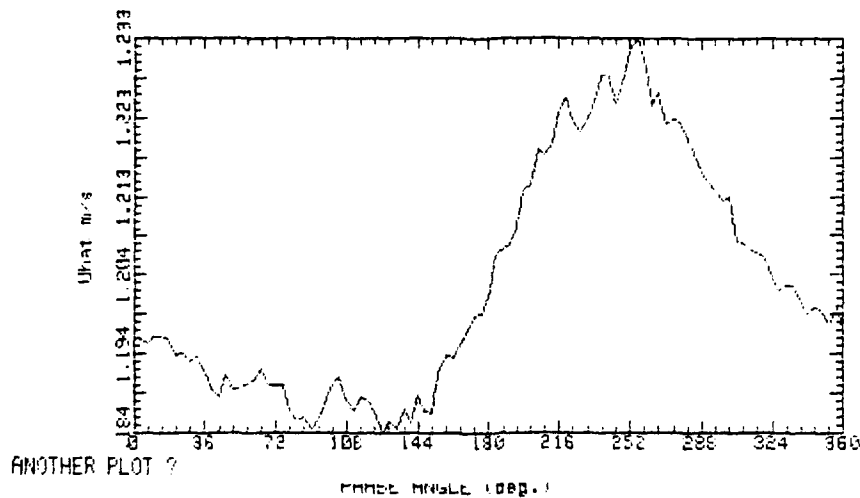


Figure 40.

RUNF16 191189.0236  
GAMMA - .105  
OSC. FREQ. 1Hz STR. # .04222  
BULK VEL. 1.89m/s REY. # 1578



RUNF16 191189.0236  
GAMMA - .105  
OSC. FREQ. 1Hz STR. # .04222  
BULK VEL. 1.89m/s REY. # 1578

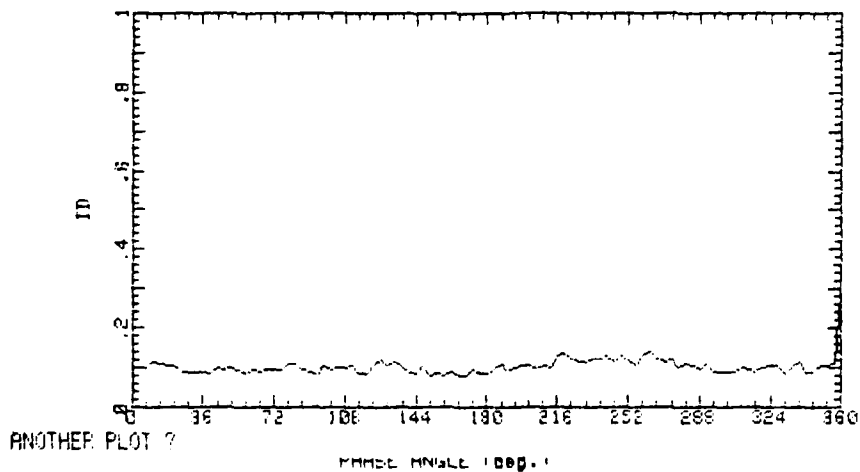
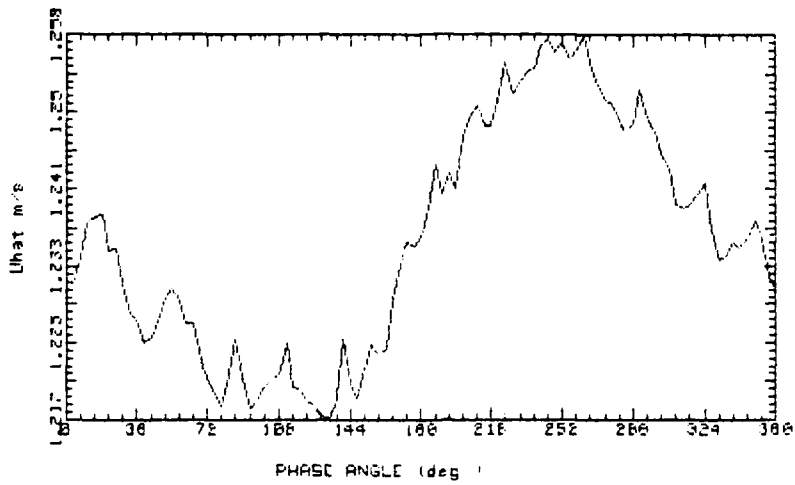


Figure 41.

RUND12 101189.0431  
GAMMA = .1505  
OSC. FREQ. 1Hz STR. # .0415E  
BULK VEL. 1.92m/s PEY. # 1604



RUND12 101189.0431  
GAMMA = .1505  
OSC. FREQ. 1Hz STR. # .0415E  
BULK VEL. 1.92m/s PEY. # 1604

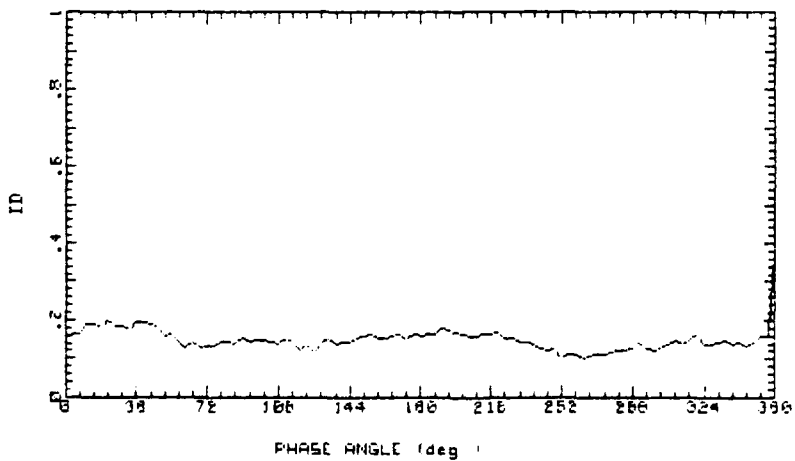
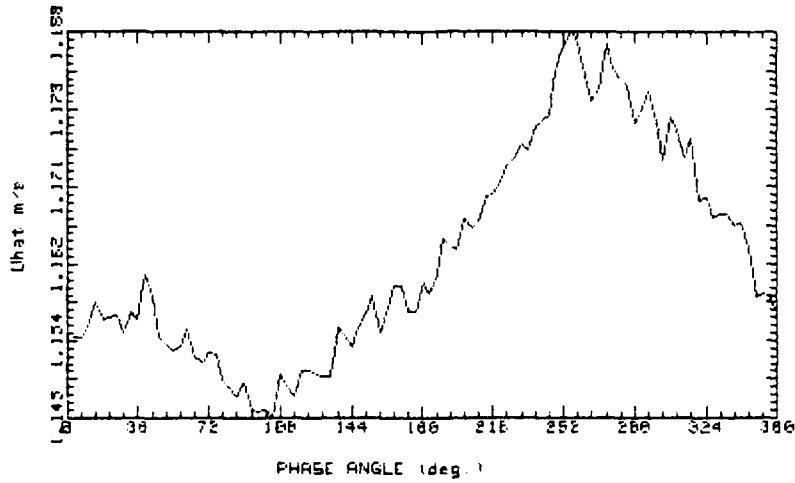


Figure 42.

RUNH55 170390.0204  
GAMMA = .2036  
OSC. FREQ. 1Hz STR. # .03939  
BULK VEL. 2.026m/s REY. # 1693



RUNH55 170390.0204  
GAMMA = .2036  
OSC. FREQ. 1Hz STR. # .03939  
BULK VEL. 2.026m/s REY. # 1693

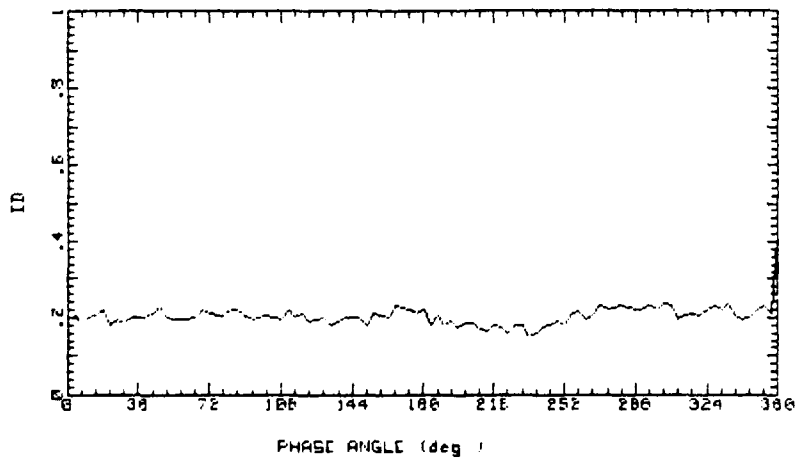
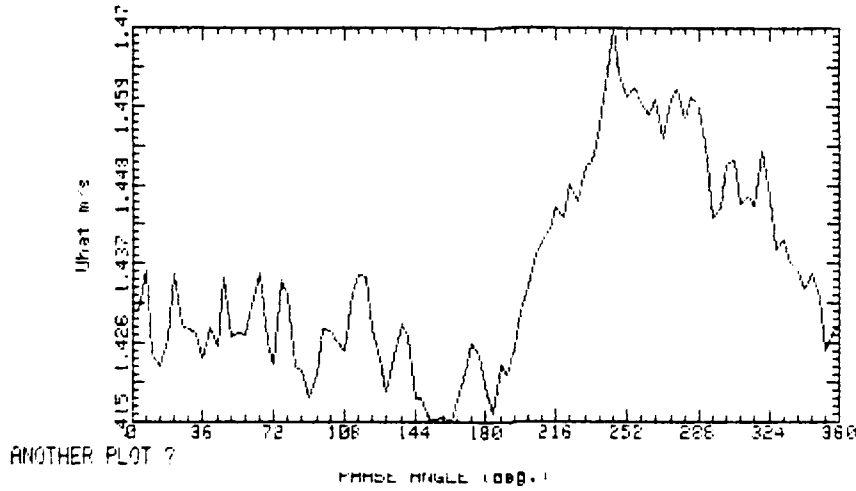


Figure 43.

RUN03 101109.0022  
GAMMA = .4685  
OSC. FREQ. 1Hz STR. # .03711  
BULK VEL. 2.15m/s REY. # 1796



RUN03 101109.0022  
GAMMA = .4685  
OSC. FREQ. 1Hz STR. # .03711  
BULK VEL. 2.15m/s REY. # 1796

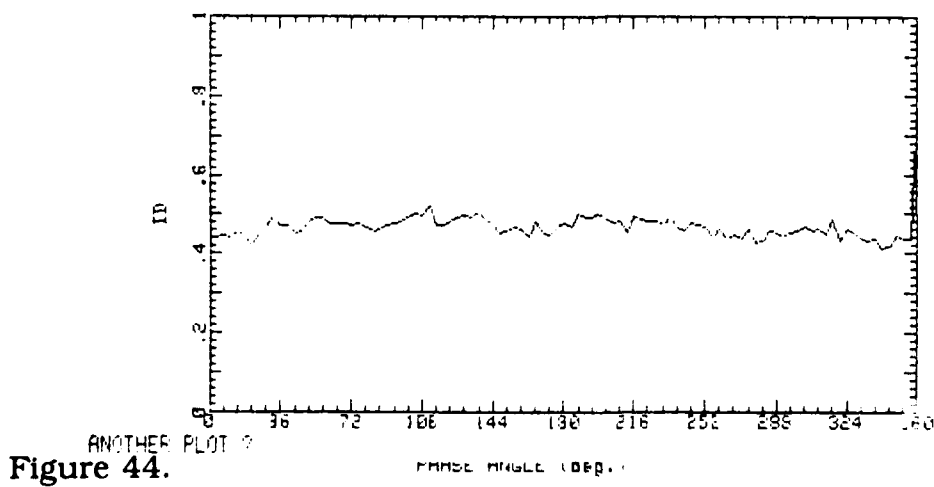
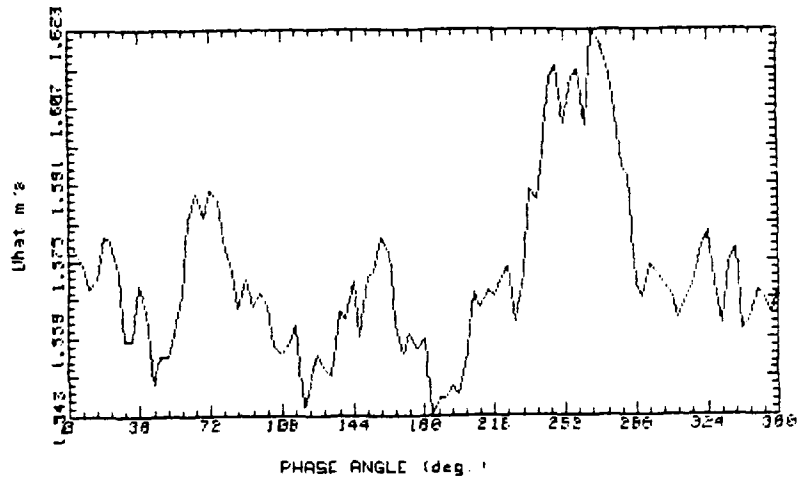


Figure 44.

RUND10 101109.0337  
GAMMA = .7157  
OSC. FREQ. 1Hz STR. \* .035  
BULK VEL. 2.28m/s REY. \* 1905



RUND10 101109.0337  
GAMMA = .7157  
OSC. FREQ. 1Hz STR. \* .035  
BULK VEL. 2.28m/s REY. \* 1905

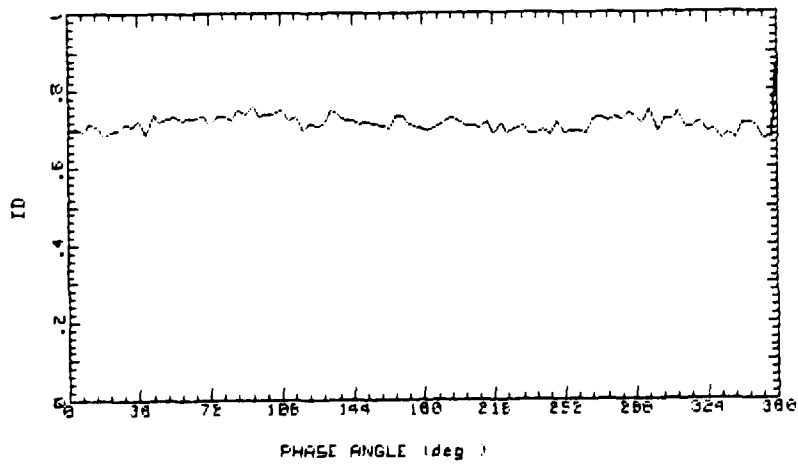
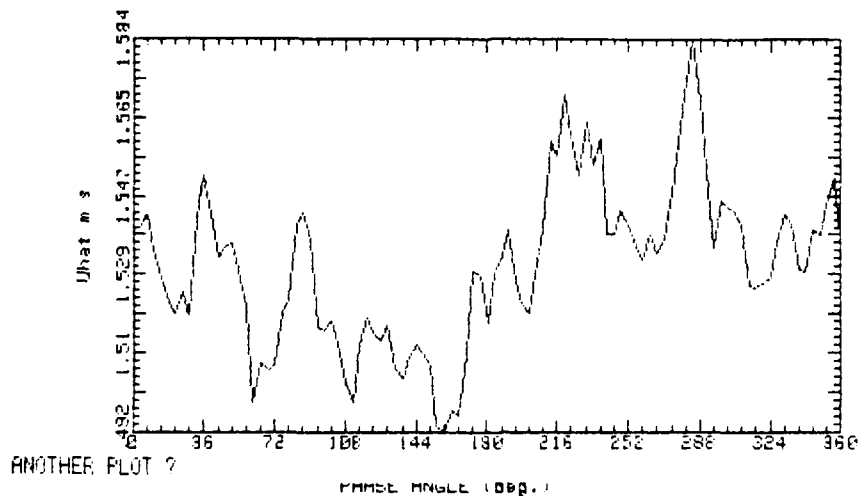


Figure 45.

RUNH19 30390.0720  
GAMMA = .0463  
OSC. FREQ. 1Hz STR. # .03325  
BULK VEL. 2.4m/s REY. # 2005



RUNH19 30390.0720  
GAMMA = .0463  
OSC. FREQ. 1Hz STR. # .03325  
BULK VEL. 2.4m/s REY. # 2005

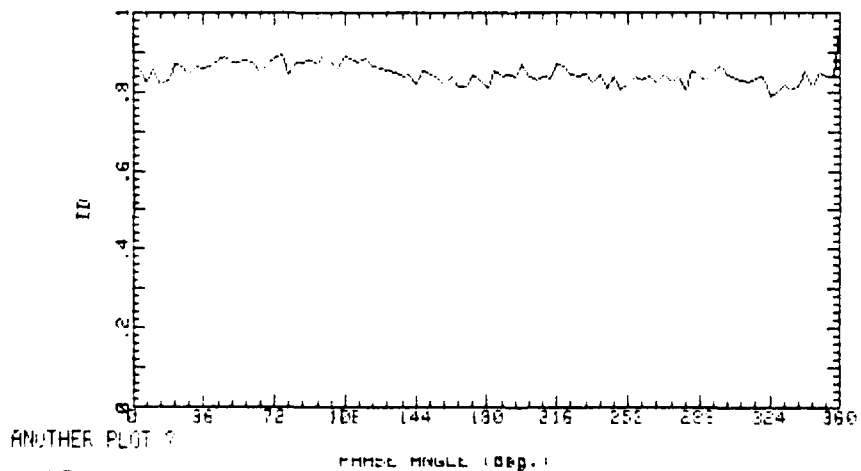
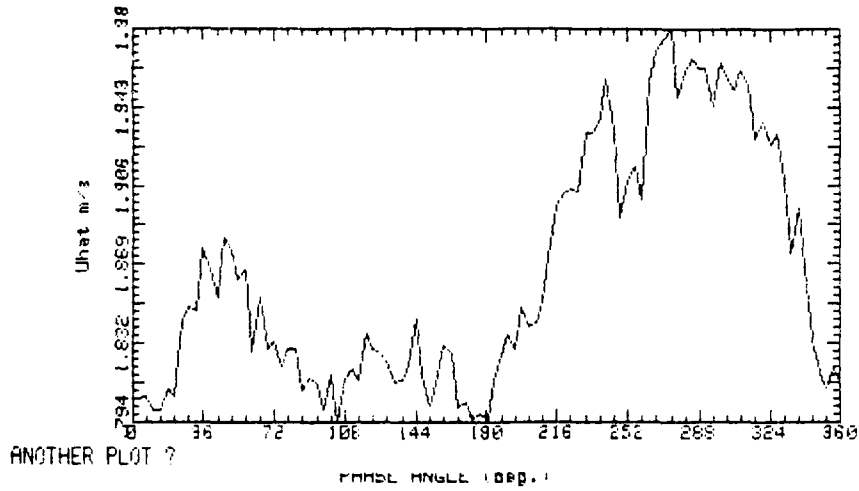


Figure 46.

RUND13 101109.0456  
GAMMA = .9865  
OSC. FREQ. 1Hz STR. # .03264  
BULK VEL. 2.445m/s REY. # 2043



RUND13 101109.0456  
GAMMA = .9865  
OSC. FREQ. 1Hz STR. # .03264  
BULK VEL. 2.445m/s REY. # 2043

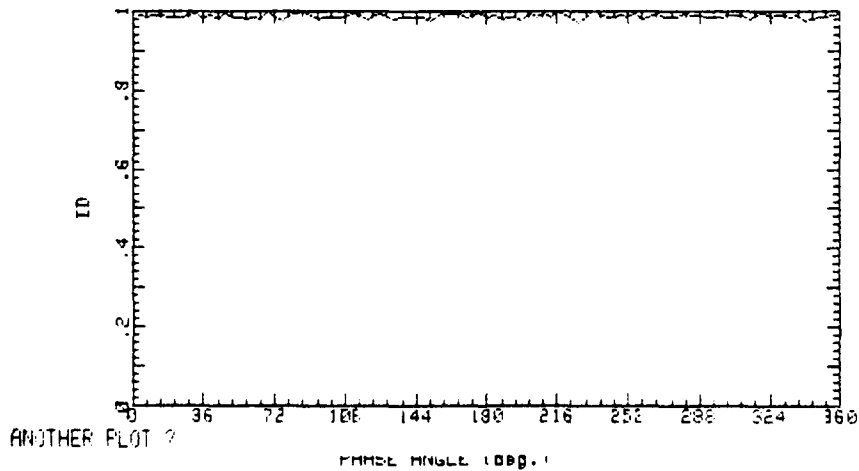
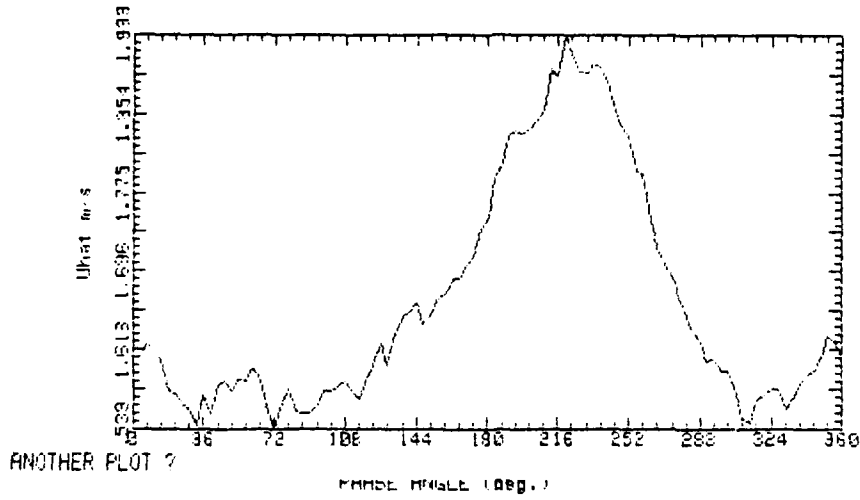


Figure 47.



RUNH55 110390.0427  
 GAMMA = .5736  
 OSC. FREQ. 1Hz STR. # .03166  
 BULK VEL. 2.52m/s REY. # 2106



RUNH55 110390.0427  
 GAMMA = .5736  
 OSC. FREQ. 1Hz STR. # .03166  
 BULK VEL. 2.52m/s REY. # 2106

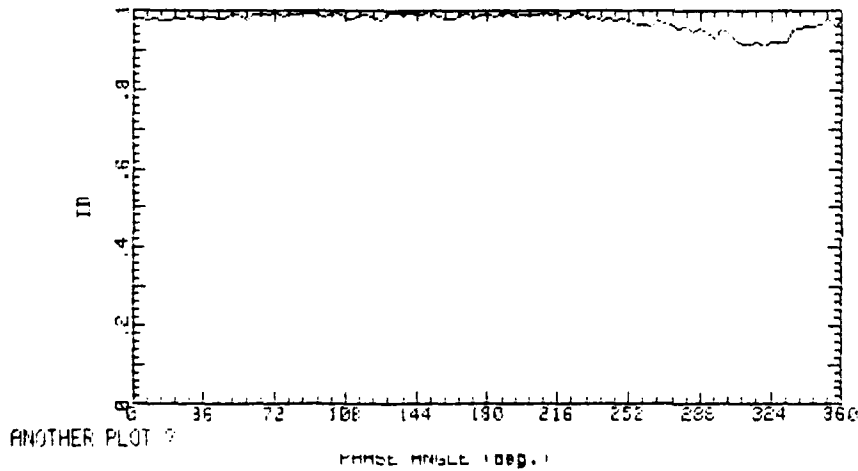
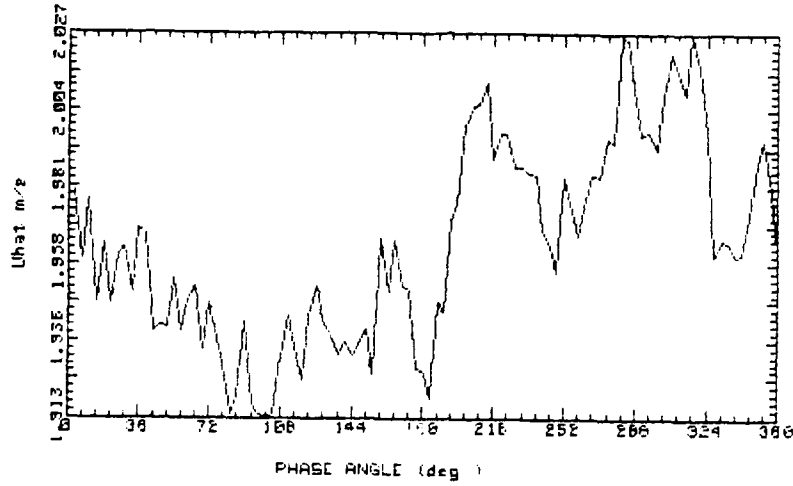


Figure 48.

RUND11 101109.0404  
GAMMA = .9901  
OSC. FREQ. 1Hz STR. # .03093  
BULK VEL. 2.50m/s REY. # 2156



RUND11 101109.0404  
GAMMA = .9901  
OSC. FREQ. 1Hz STR. # .03093  
BULK VEL. 2.50m/s REY. # 2156

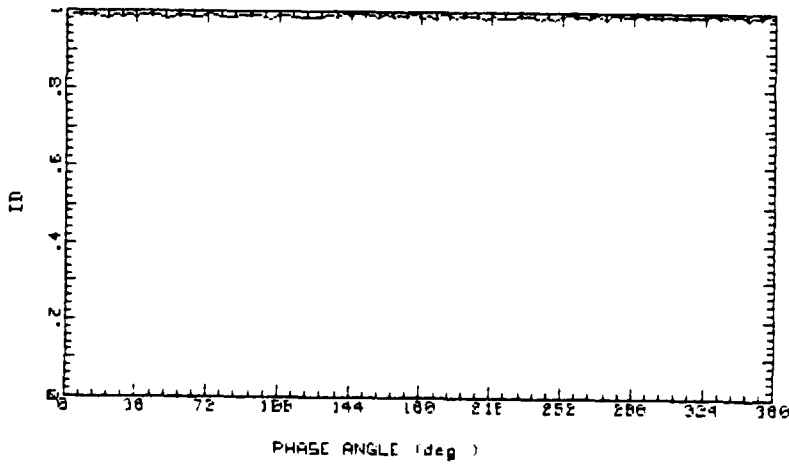
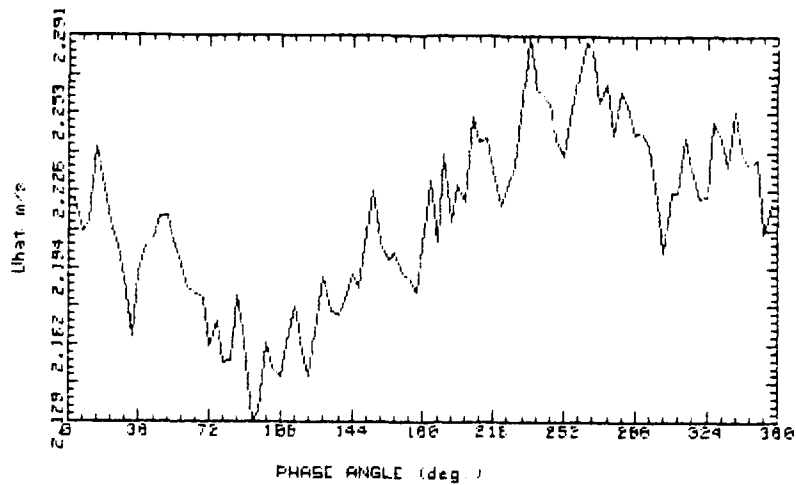


Figure 49.

RUNF32 21285.0334  
GAMMA = .9915  
OSC. FREQ. 1Hz STR. # .03034  
BULK VEL. 2.63m/s REY. # 2197



RUNF32 21289.0334  
GAMMA = .9915  
OSC. FREQ. 1Hz STR. # .03034  
BULK VEL. 2.63m/s REY. # 2197

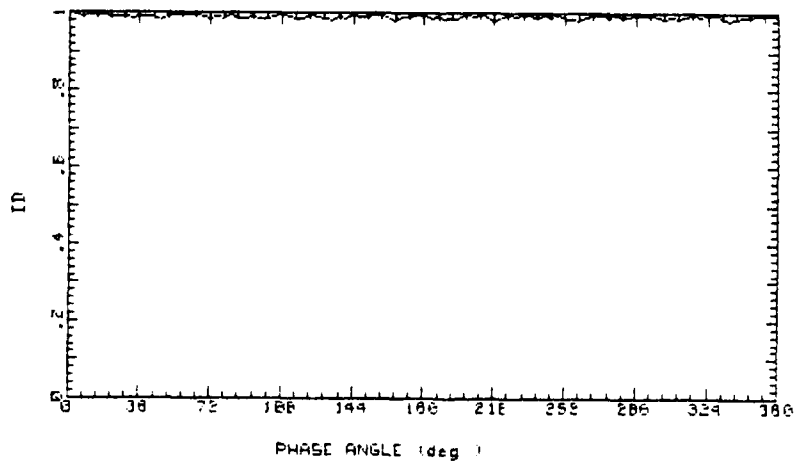
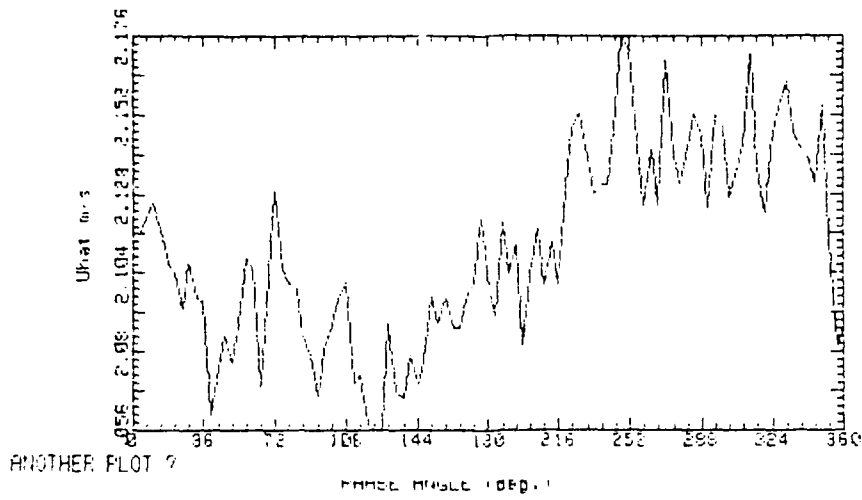


Figure 50.

RUND14 101109.0524  
GAMMA = .9923  
OSC. FREQ. 1Hz STP. # .02961  
BULK VEL. 2.695m/s PEY. # 2252



RUND14 101109.0524  
GAMMA = .9923  
OSC. FREQ. 1Hz STP. # .02961  
BULK VEL. 2.695m/s PEY. # 2252

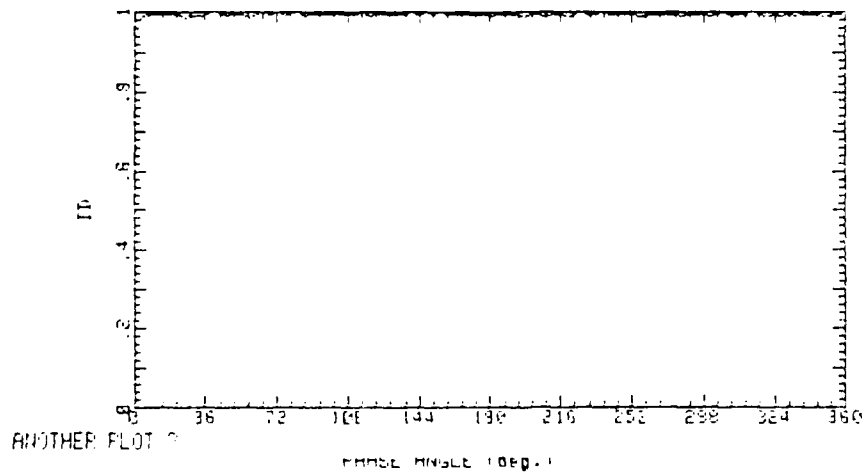


Figure 51.

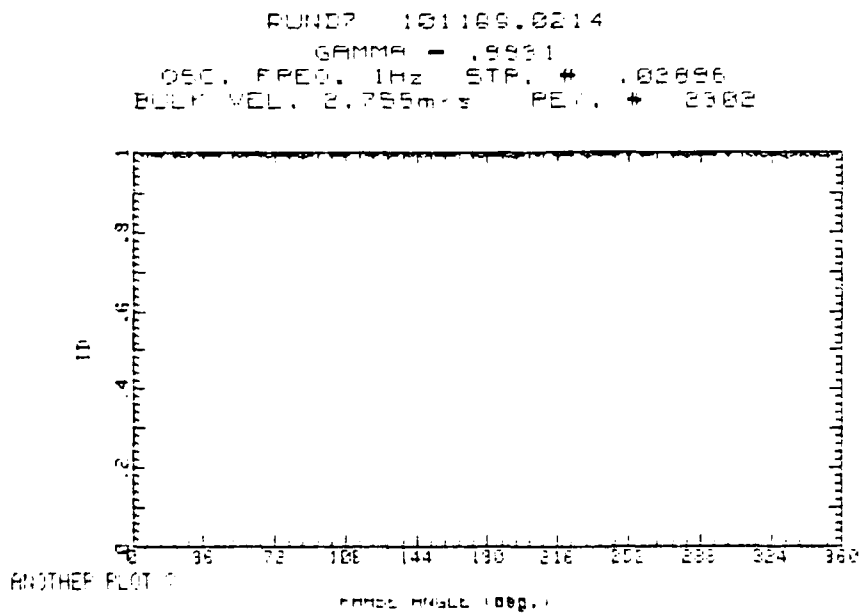
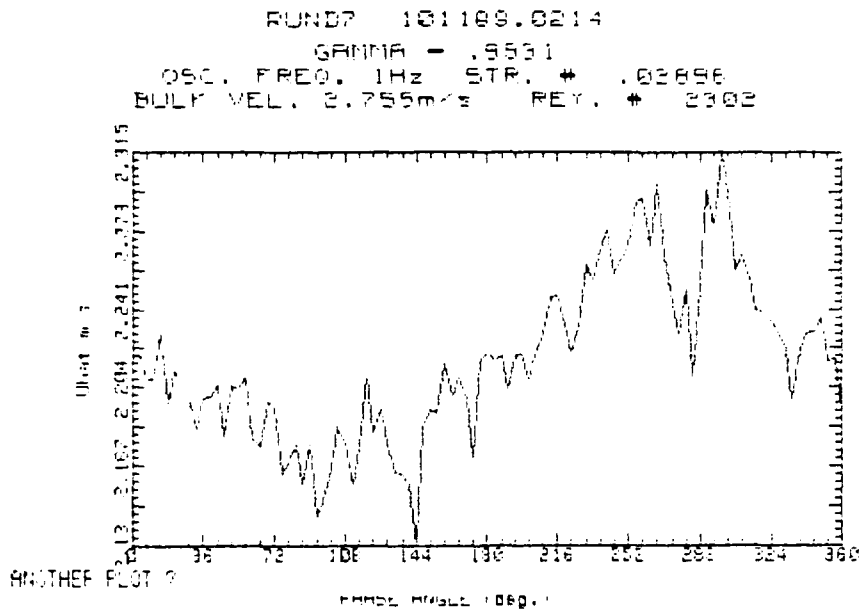
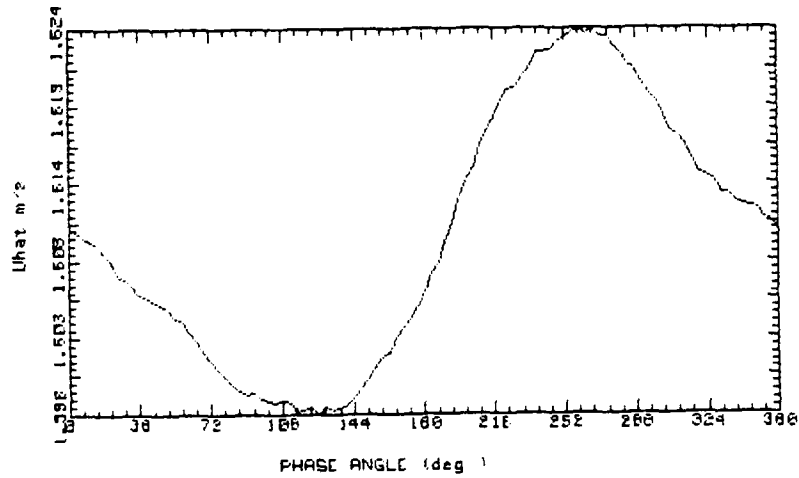


Figure 52.

RUNH09 30390.0224  
GAMMA = .0003276  
OSC. FREQ. 1Hz STR. # .06045  
BULK VEL. 1.32m/s REY. # 1103



RUNH09 30390.0224  
GAMMA = .0003276  
OSC. FREQ. 1Hz STR. # .06045  
BULK VEL. 1.32m/s REY. # 1103

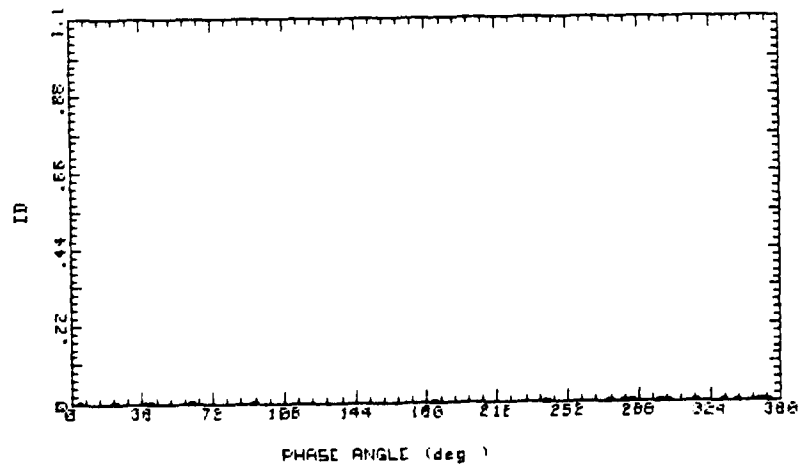


Figure 53.

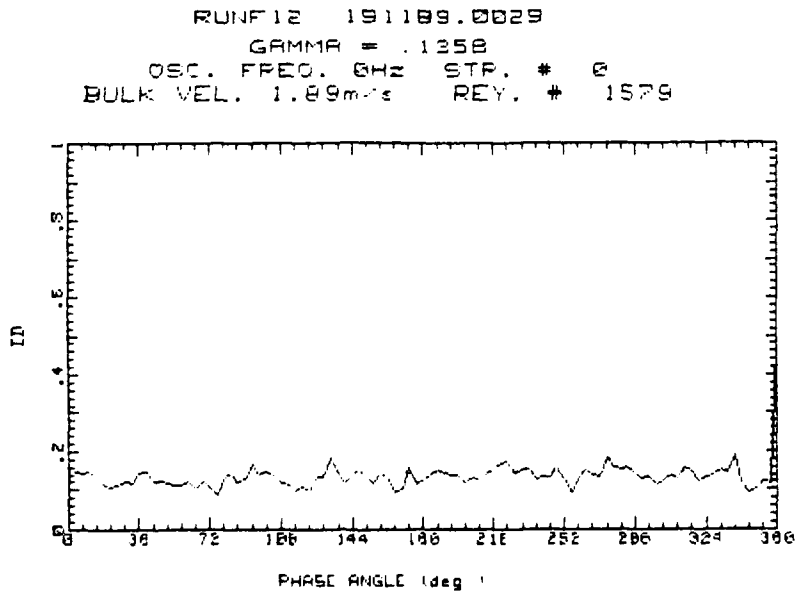
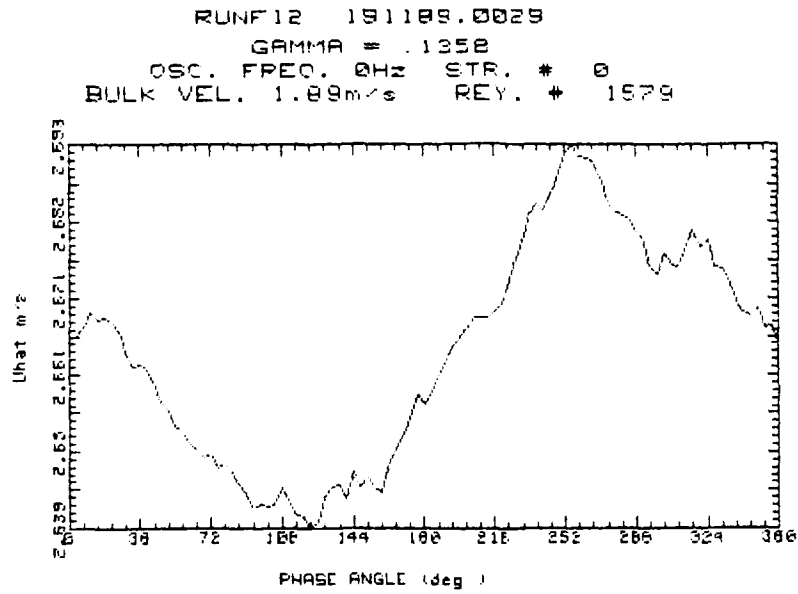
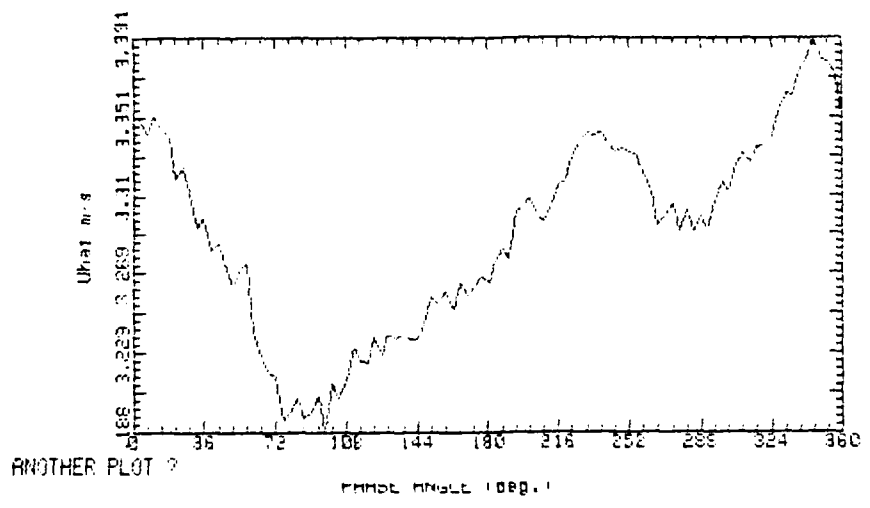


Figure 54.

RUN#21 11209.2149  
 GAMMA = .9822  
 OSC. FREQ. 1Hz STP. # .03325  
 BULK VEL. 2.4m/s REY. # 2005



RUN#21 11209.2149  
 GAMMA = .9822  
 OSC. FREQ. 1Hz STP. # .03325  
 BULK VEL. 2.4m/s REY. # 2005

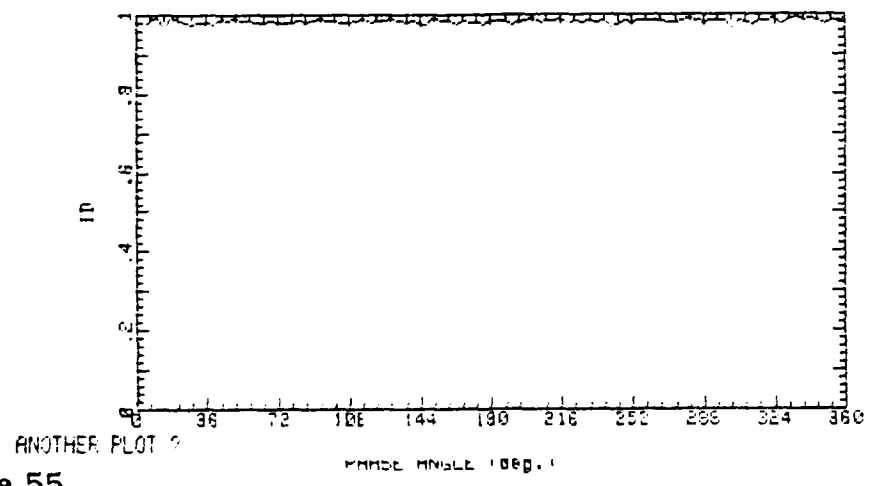
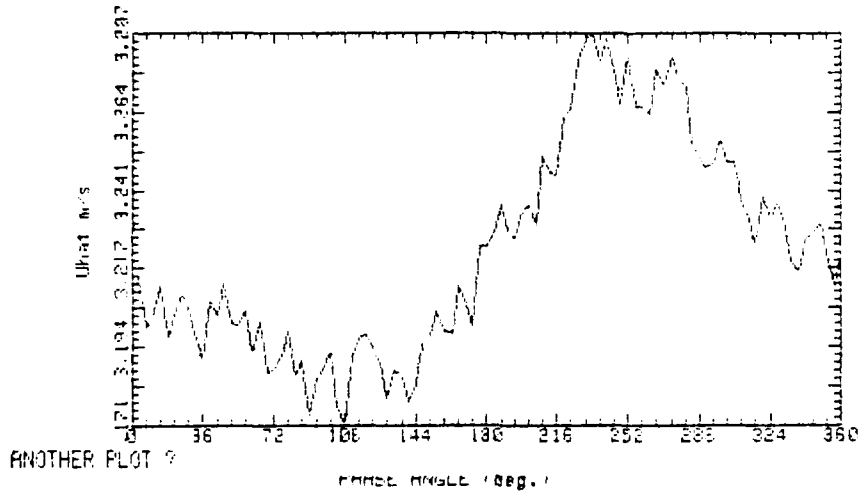


Figure 55.



RUNF28 21288.0146  
 GAMMA = .9867  
 OSC. FREQ. 1Hz STR. # .03034  
 BULK VEL. 2.69m/s PET. # 2157



RUNF28 21288.0146  
 GAMMA = .9867  
 OSC. FREQ. 1Hz STR. # .03034  
 BULK VEL. 2.69m/s PET. # 2157

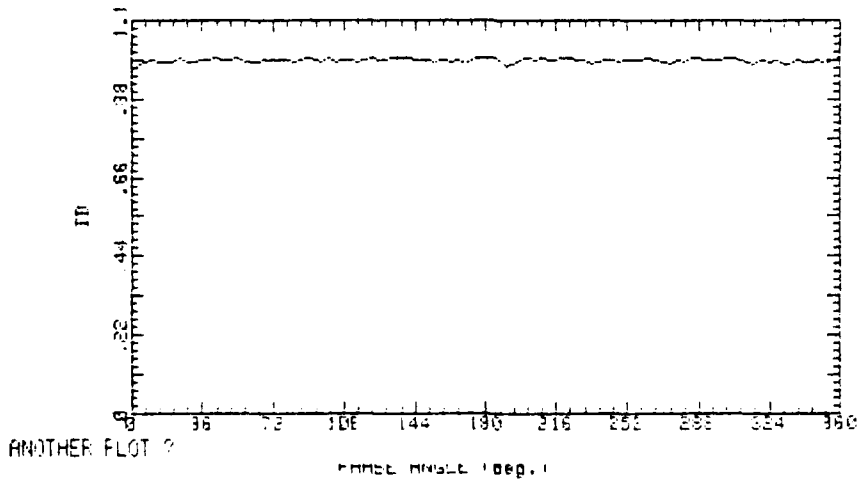
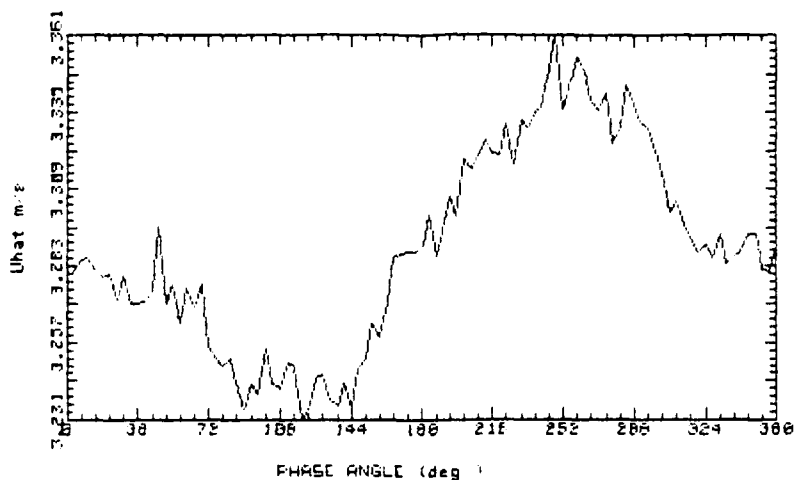


Figure 56.

RUNF37 21289.0602  
GAMMA = .9941  
OSC. FREQ. 1Hz STR. # .0261E  
BULK VEL. 3.05m/s REY. # 2548



RUNF37 21289.0602  
GAMMA = .9941  
OSC. FREQ. 1Hz STR. # .0261E  
BULK VEL. 3.05m/s REY. # 2548

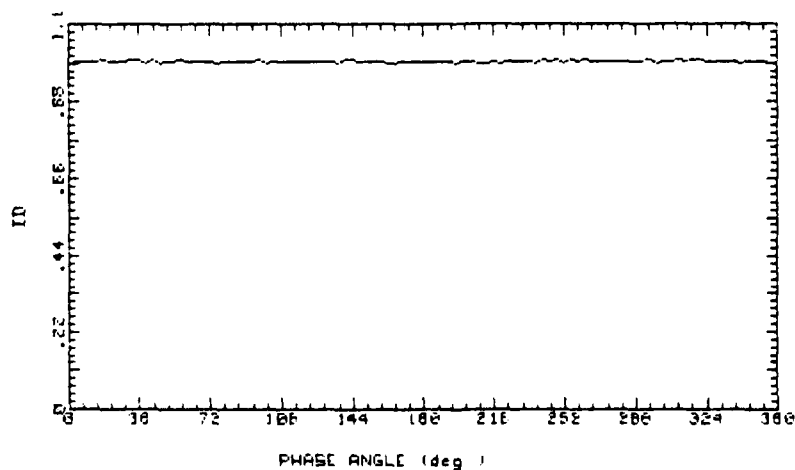


Figure 57.

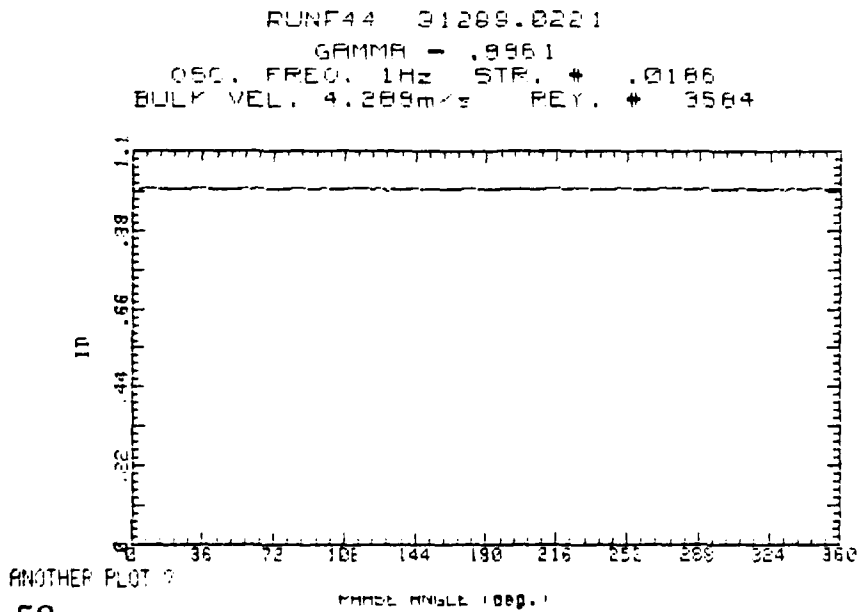
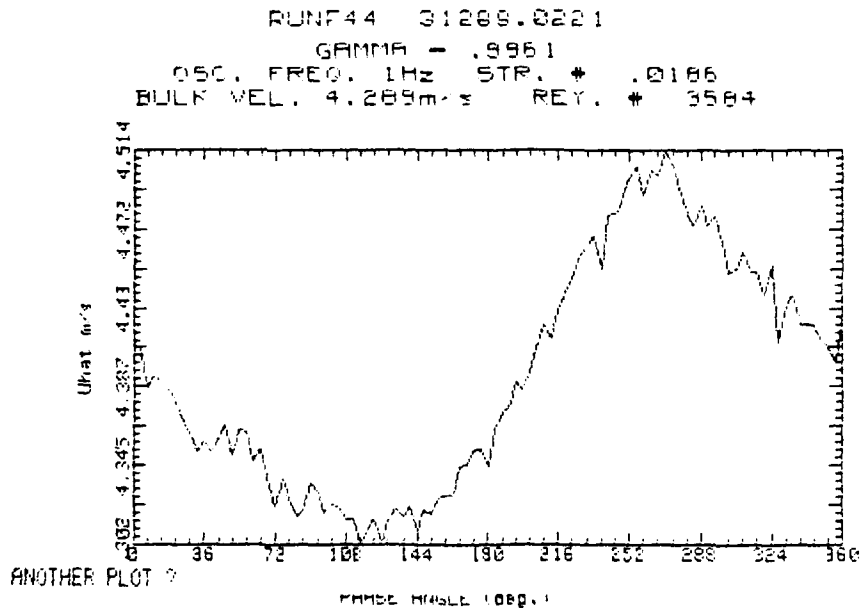


Figure 58.





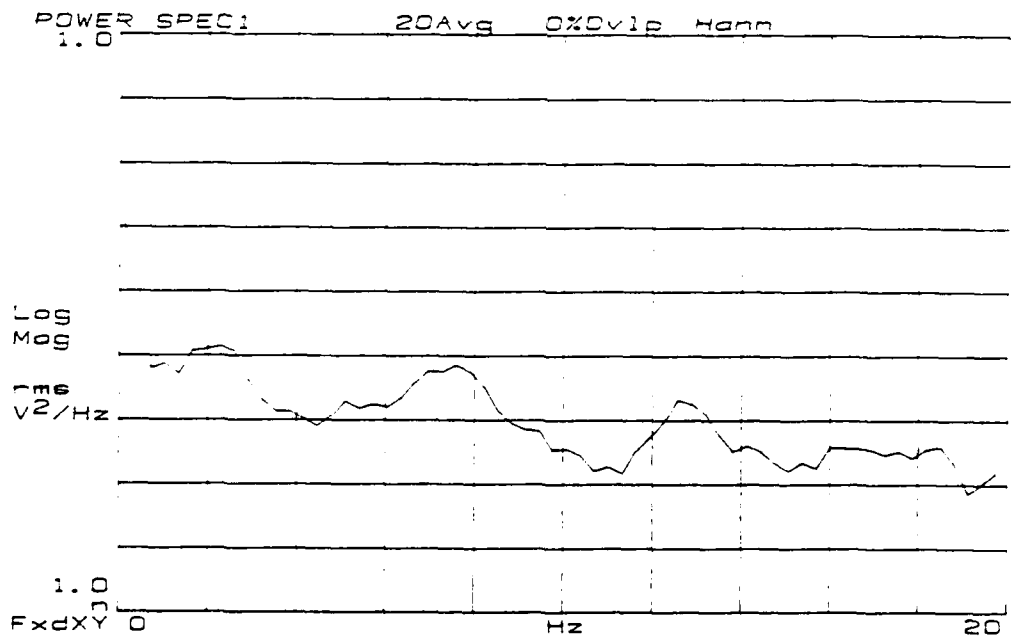
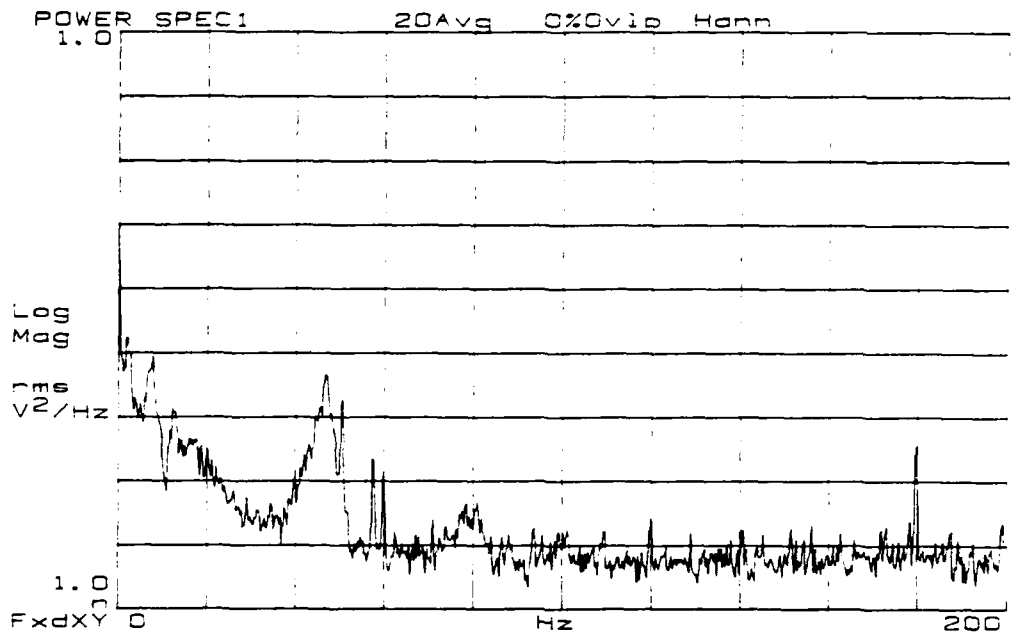


Figure 61. Re = 1308.







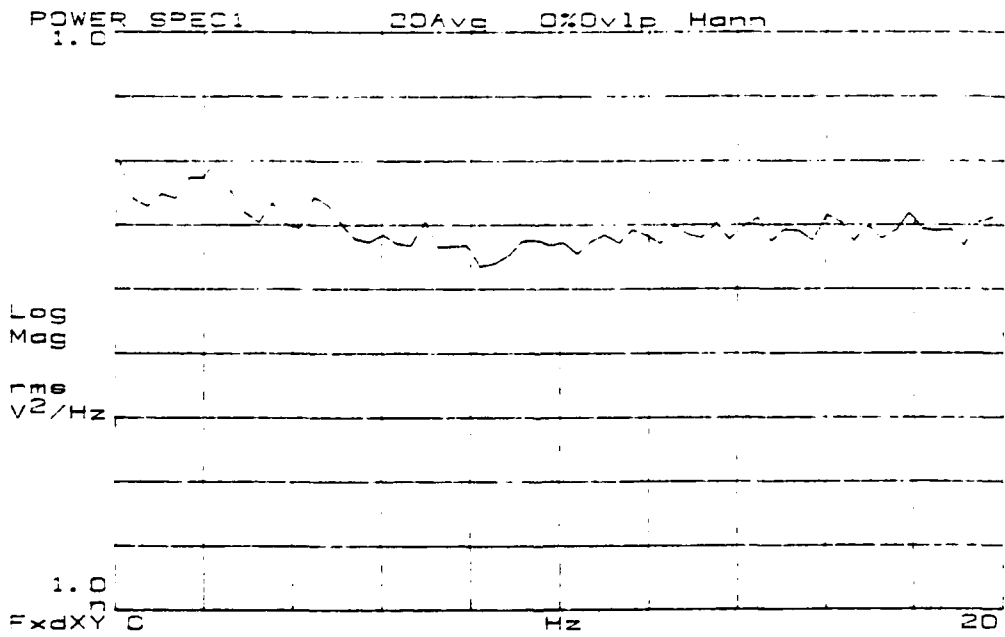
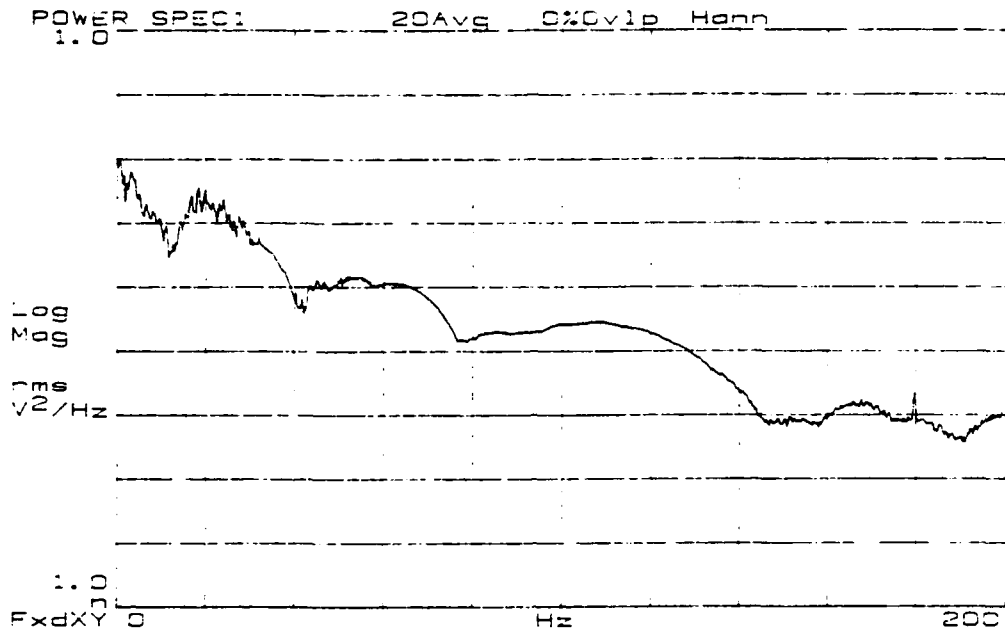


Figure 64. Re = 1542.

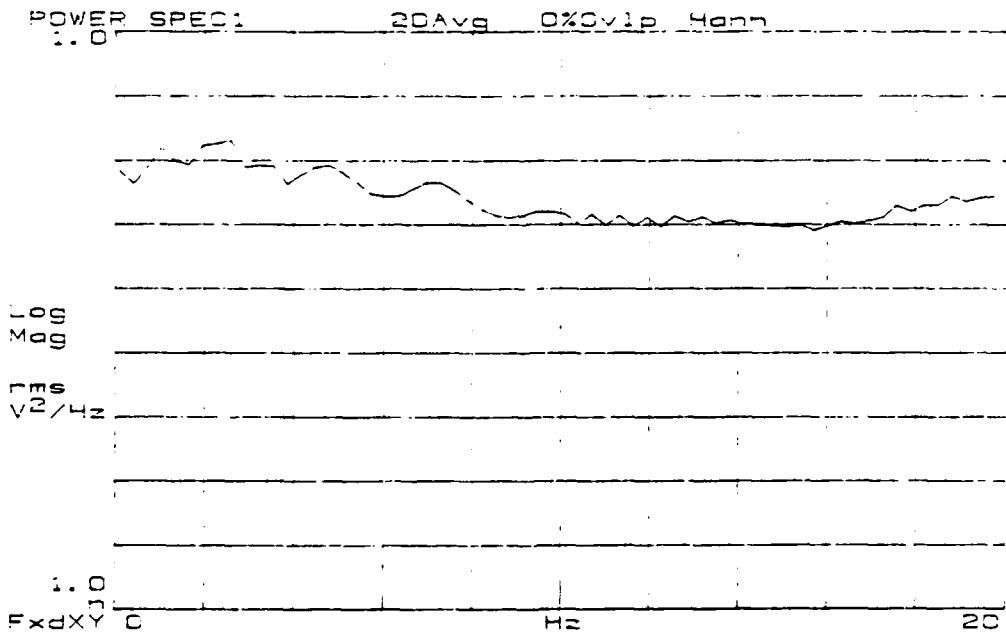
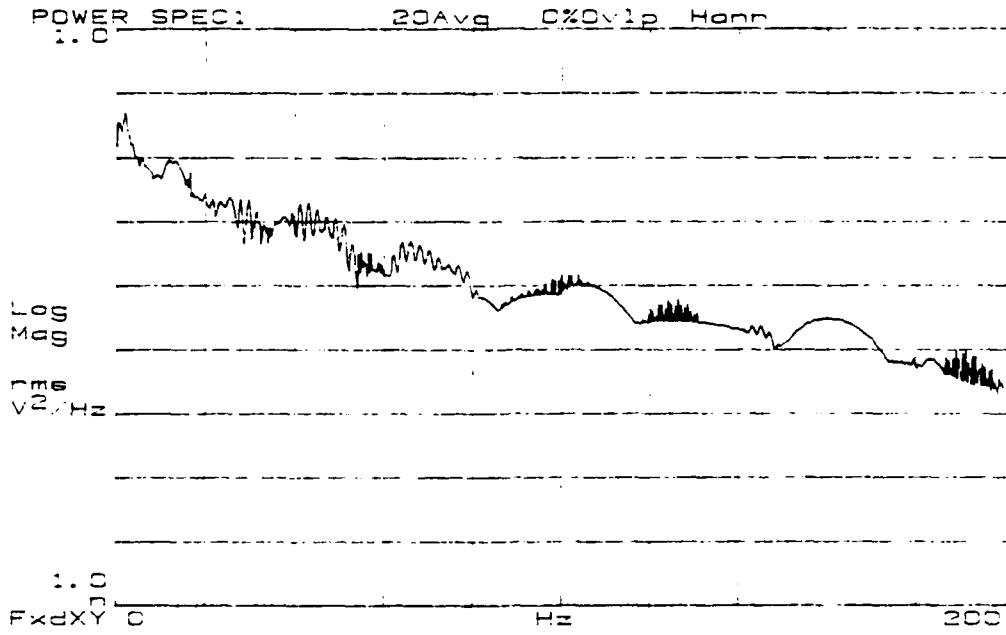


Figure 65. Re = 1604.

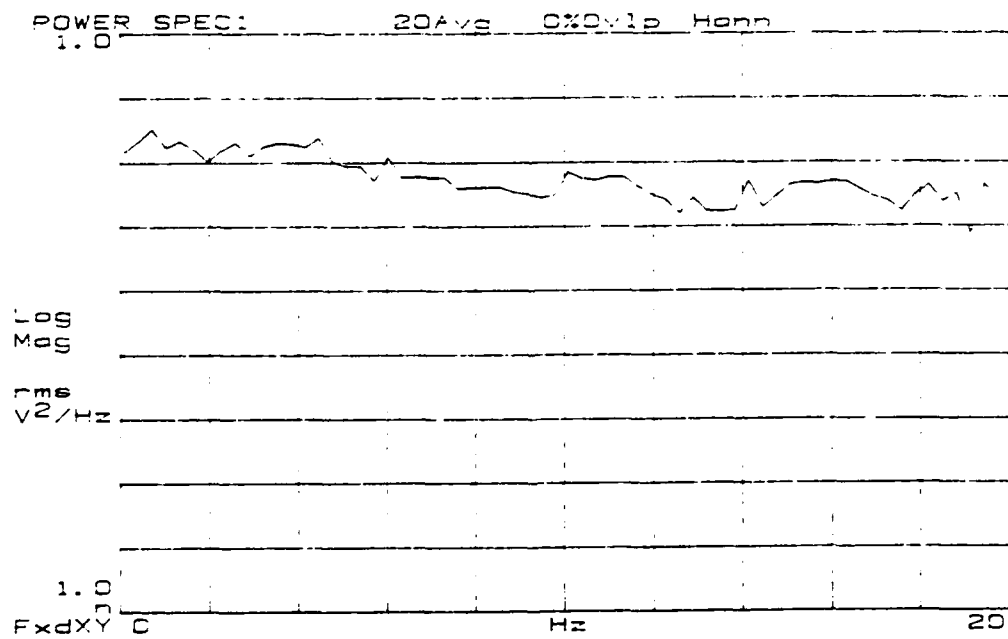
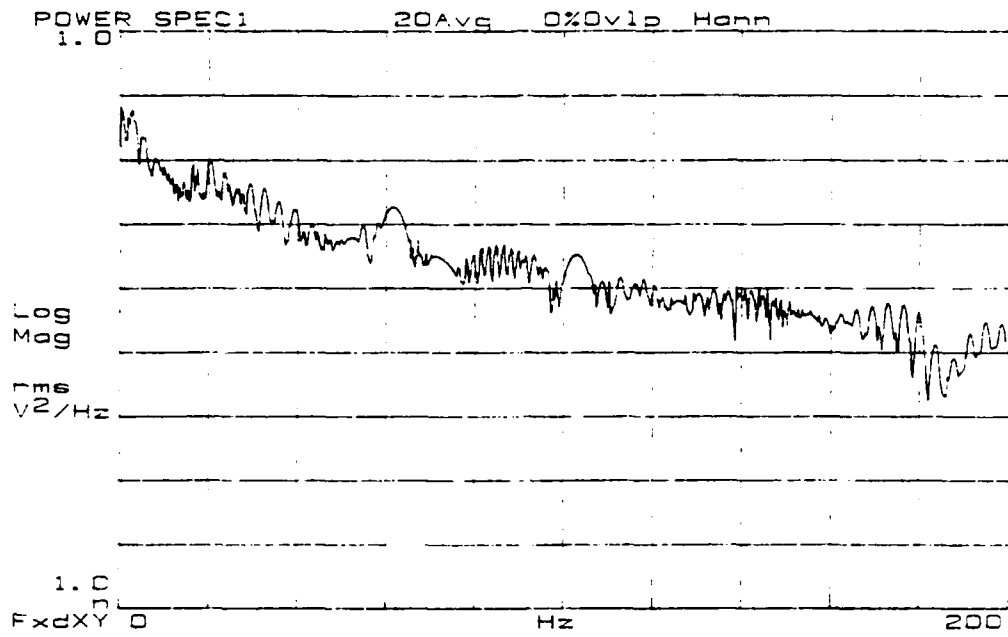


Figure 66. Re = 1650.

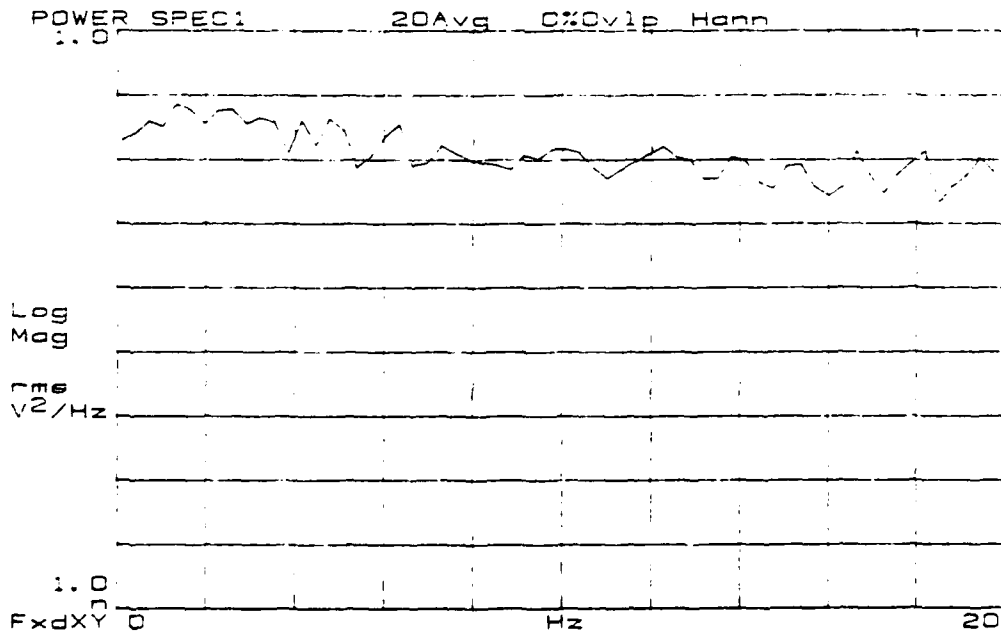
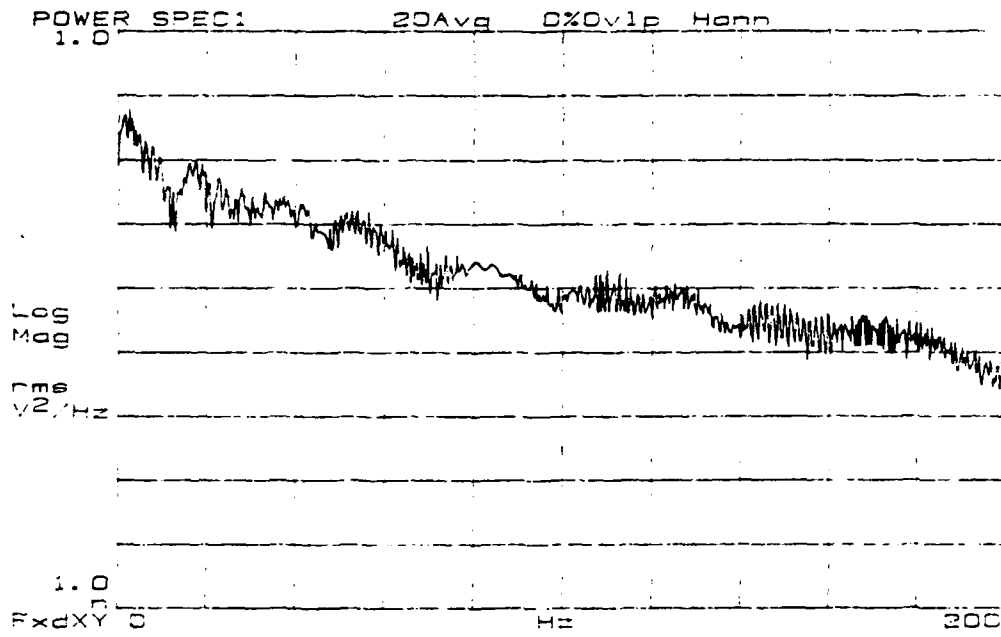


Figure 67. Re = 1697.

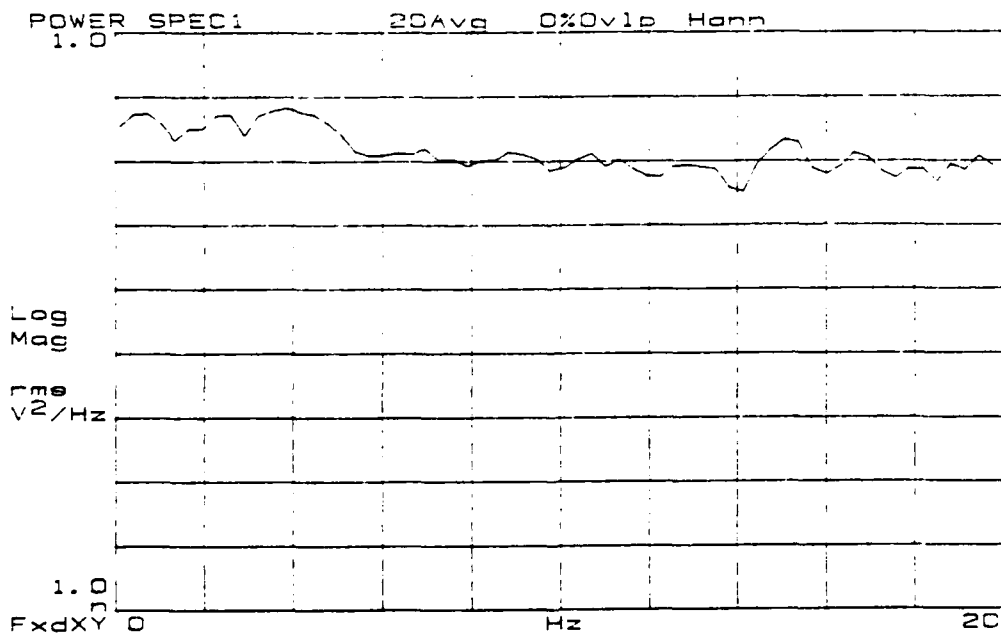
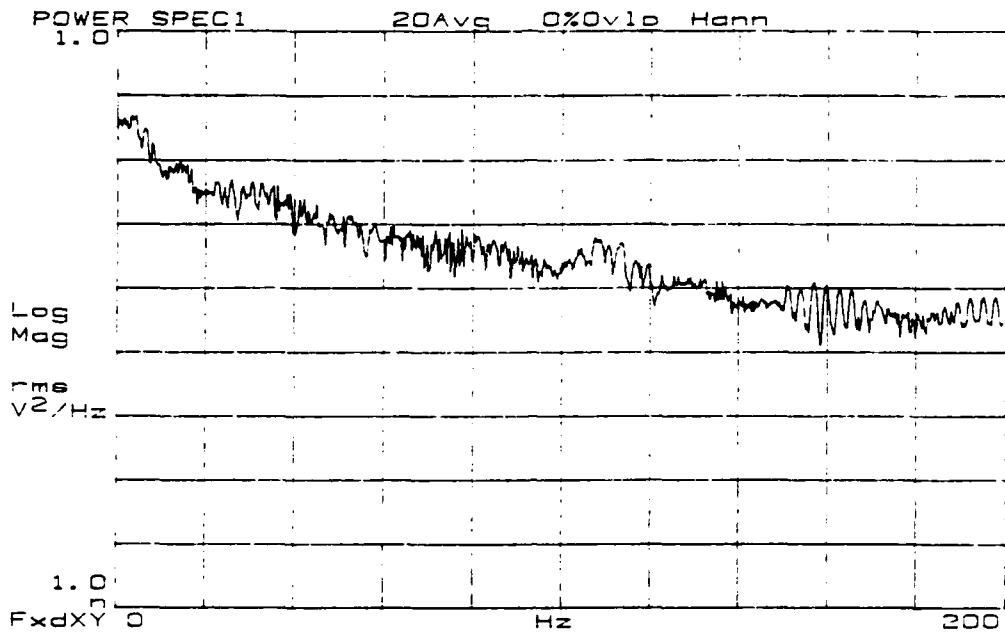


Figure 68. Re = 1742.

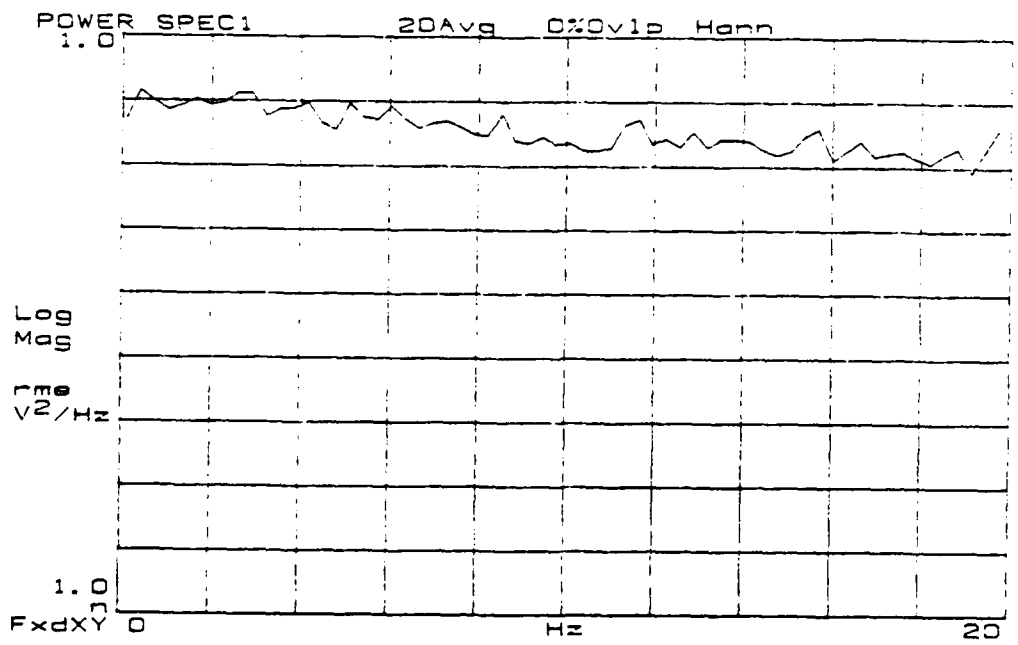
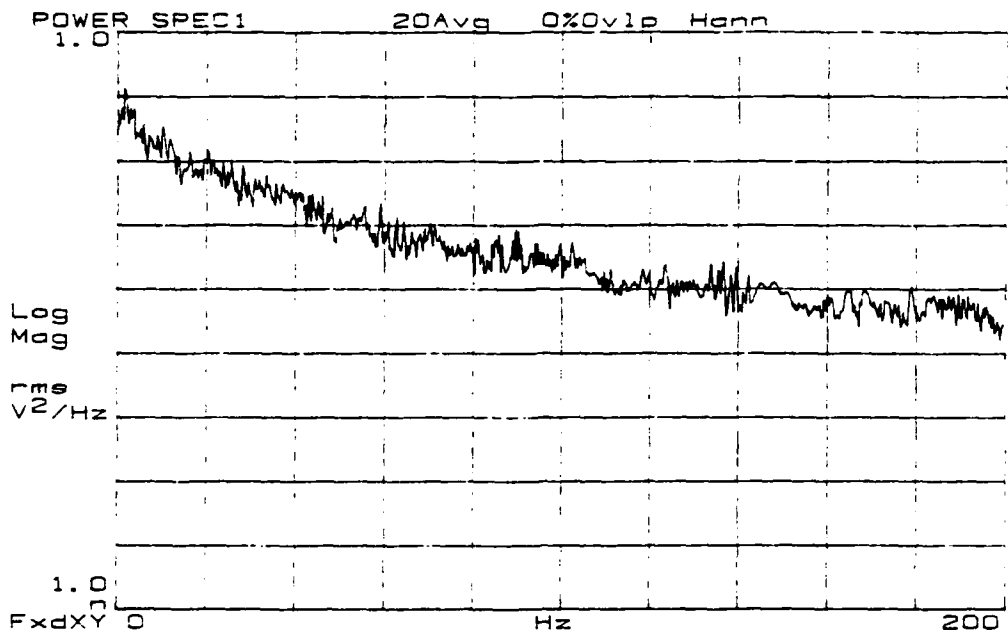


Figure 69. Re = 1796.

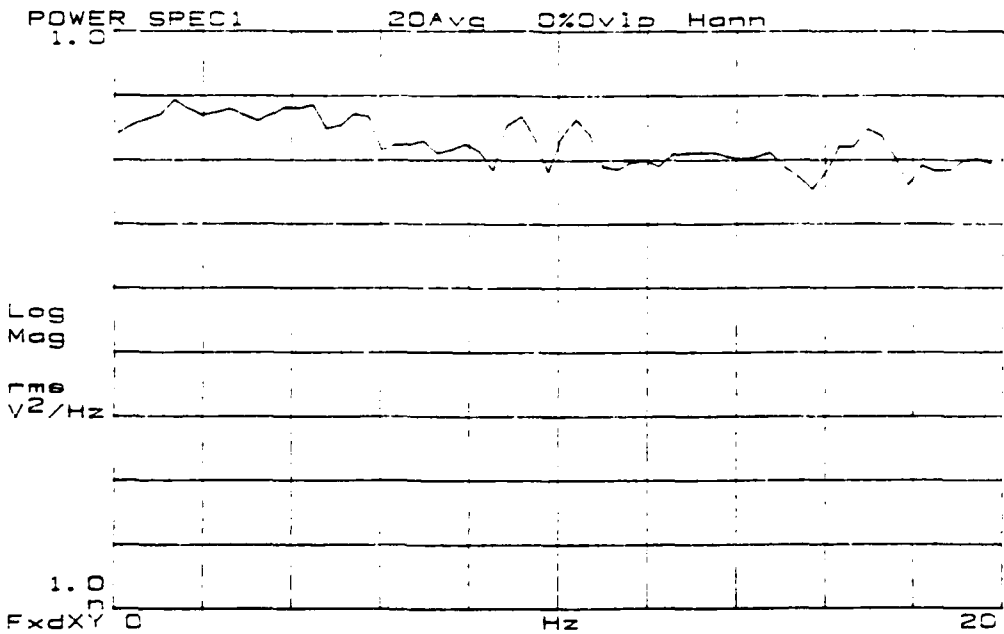
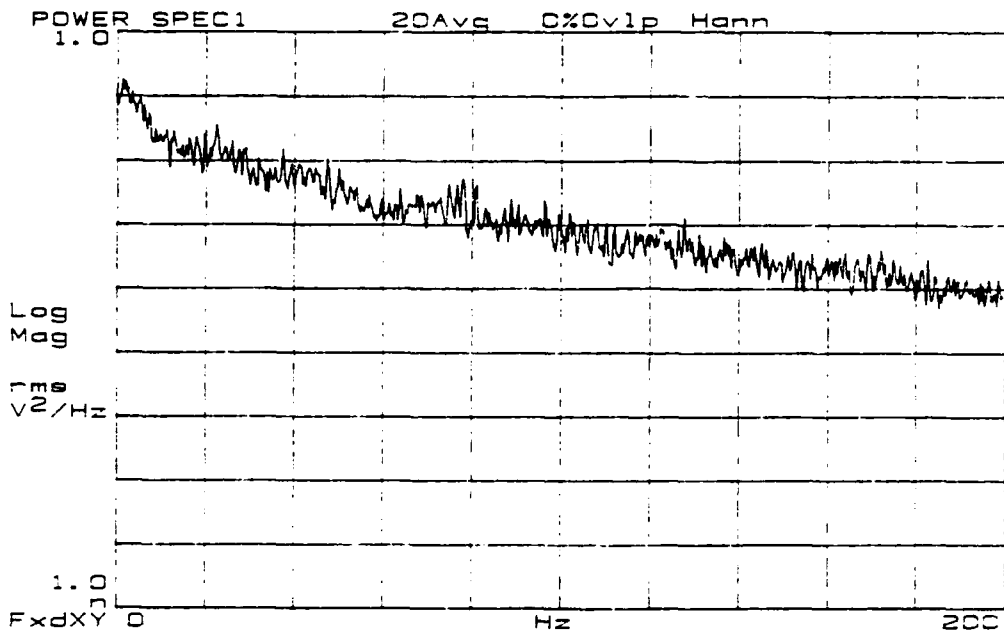


Figure 70. Re = 1905.

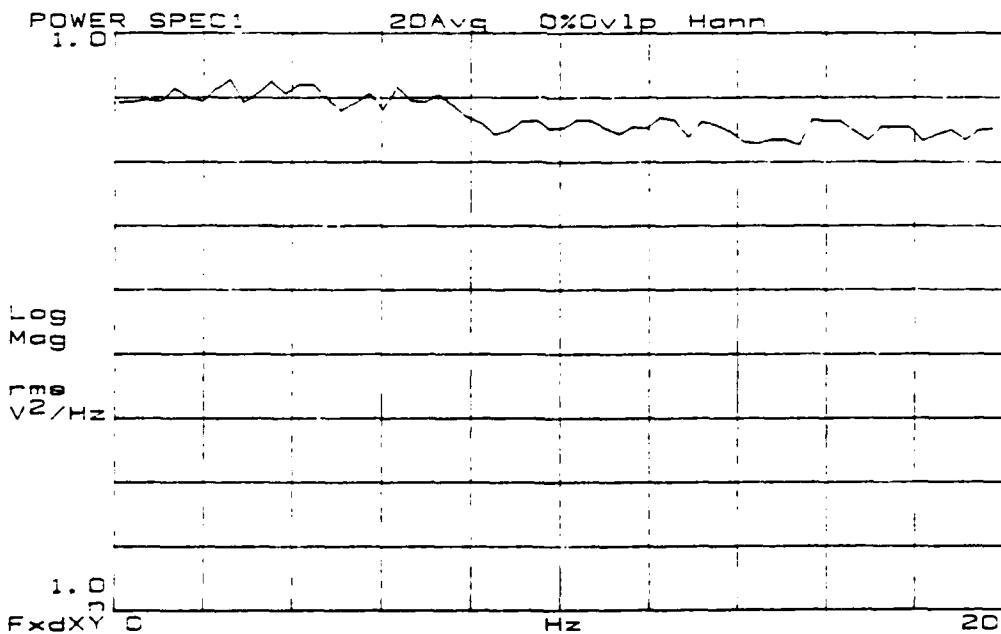
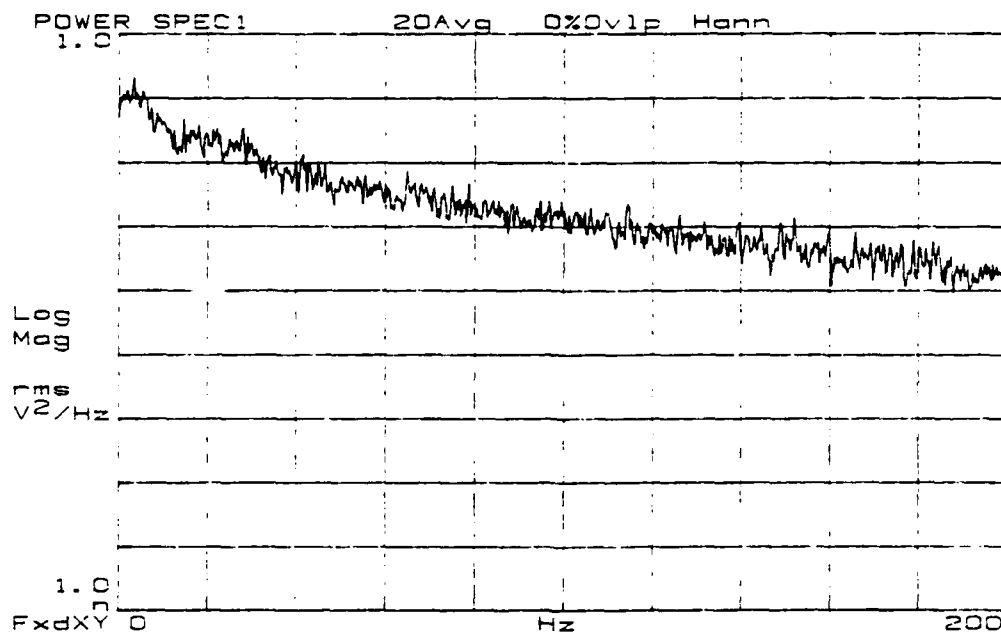


Figure 71. Re = 2005.



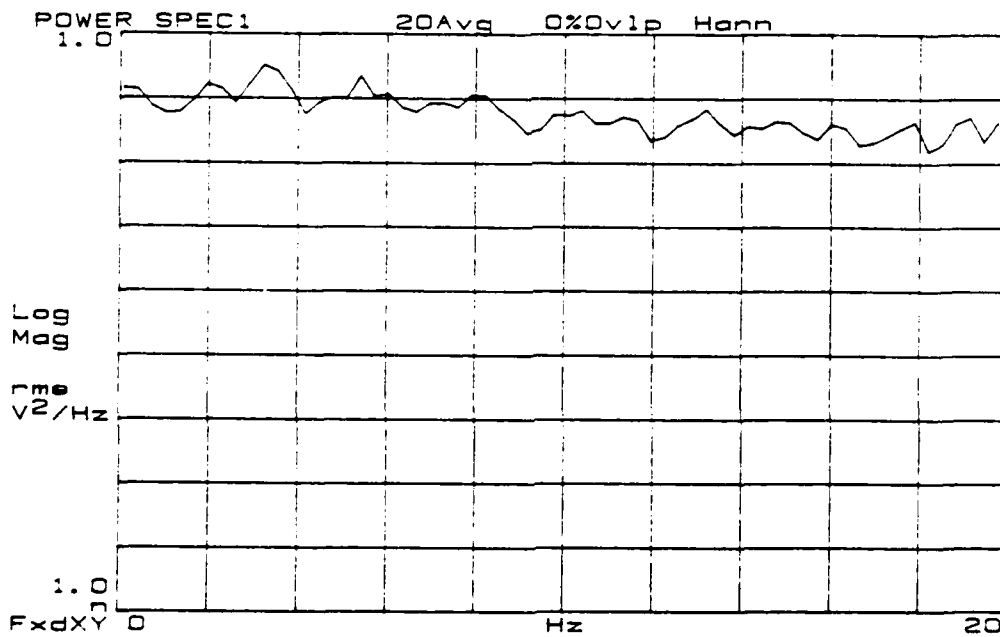
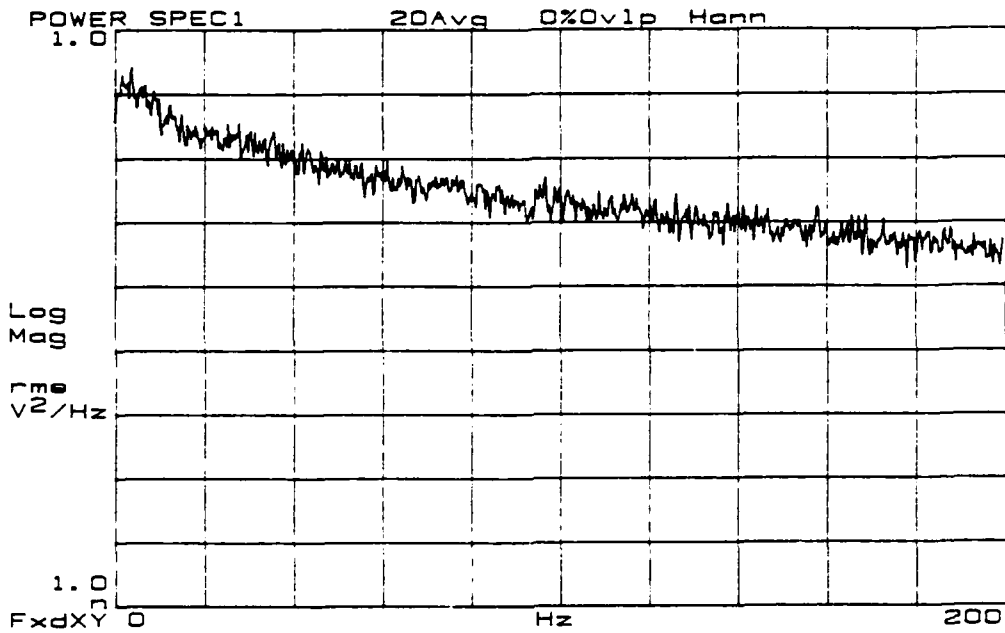


Figure 72. Re = 2097.

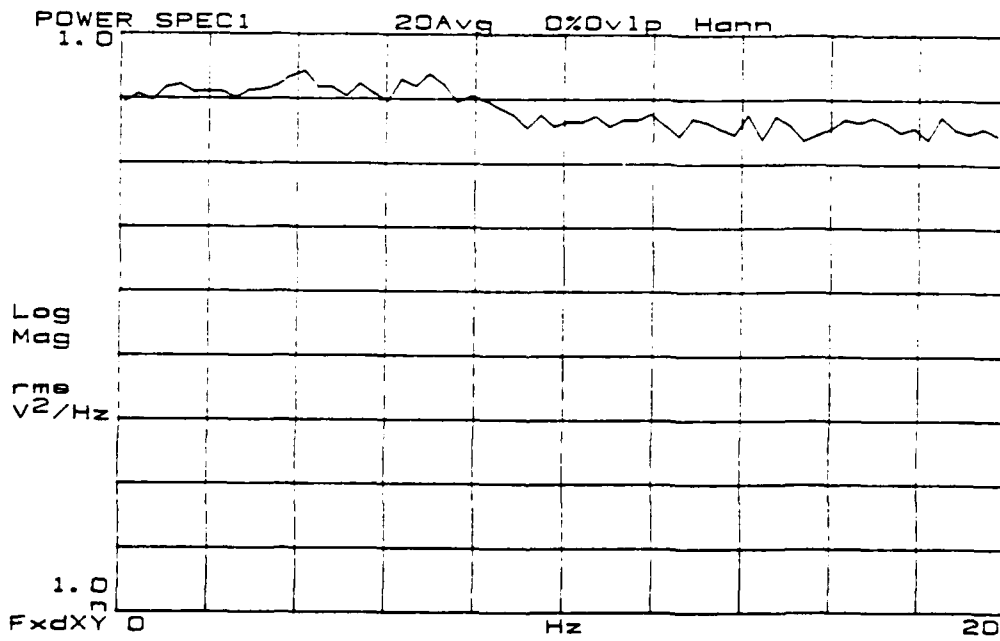
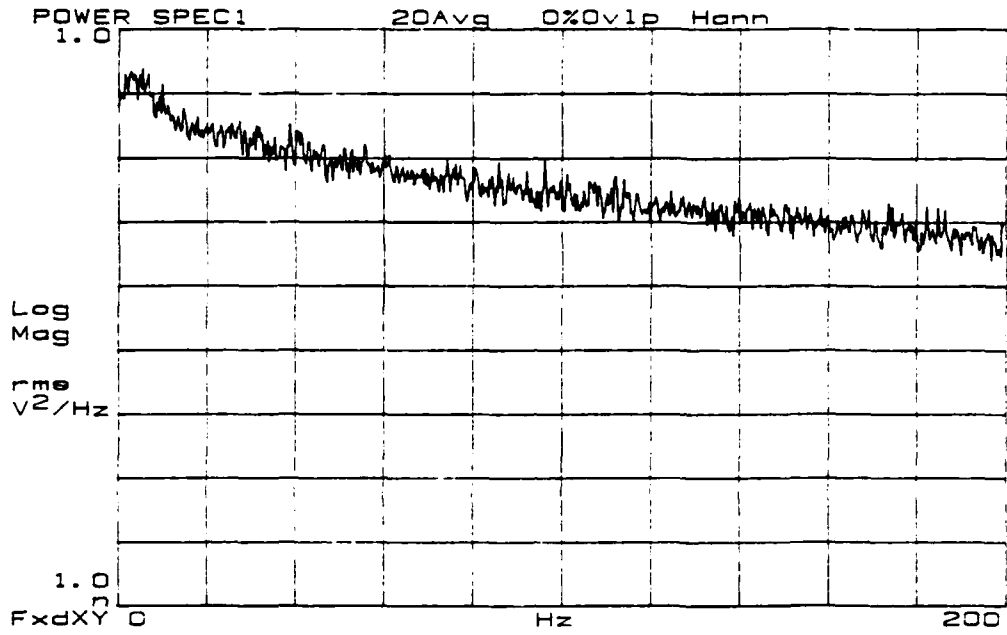


Figure 73. Re = 2198.

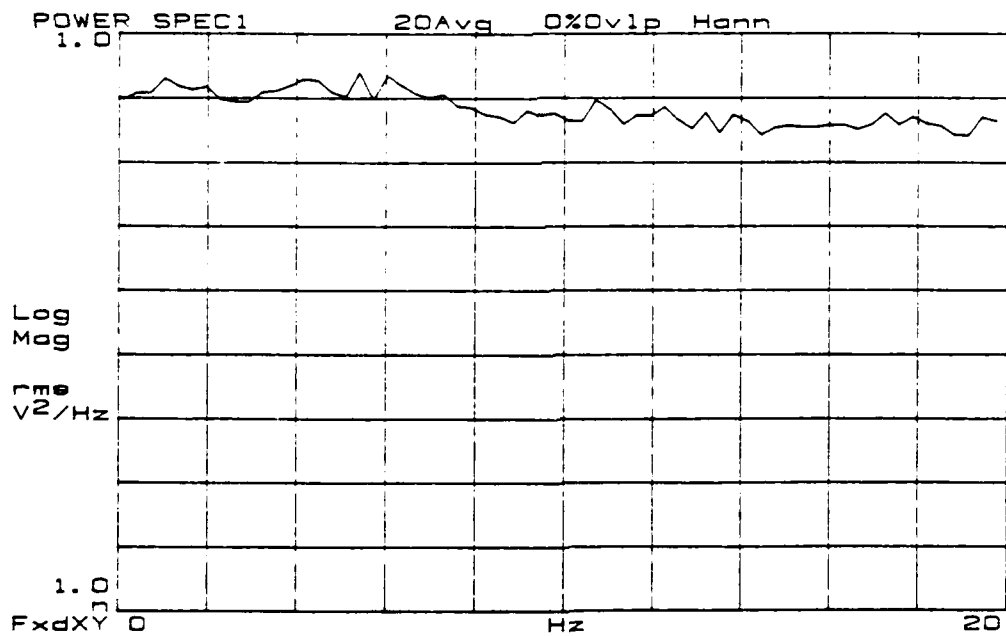
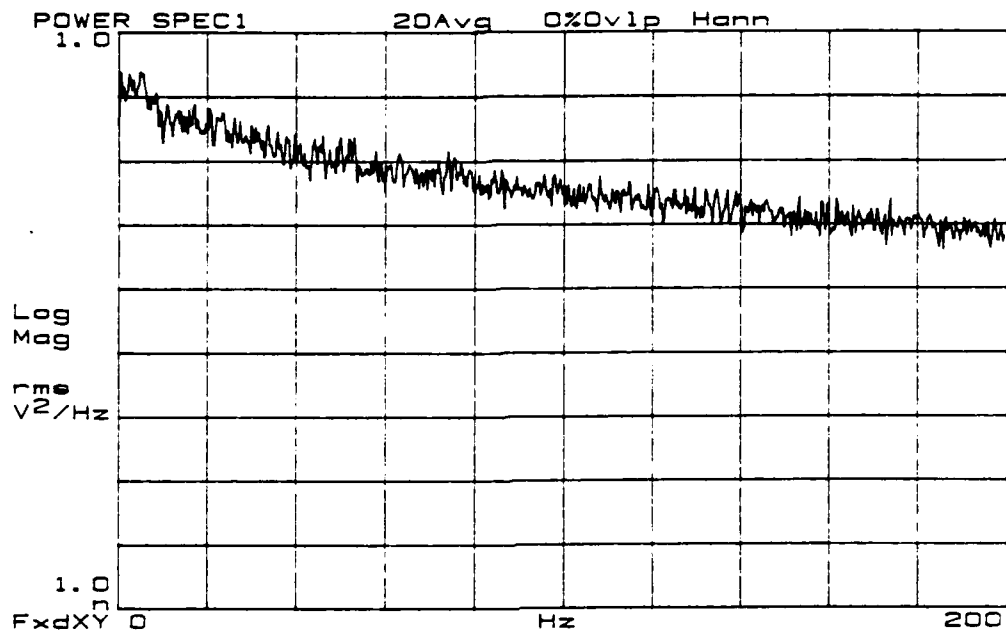


Figure 74. Re = 2298.

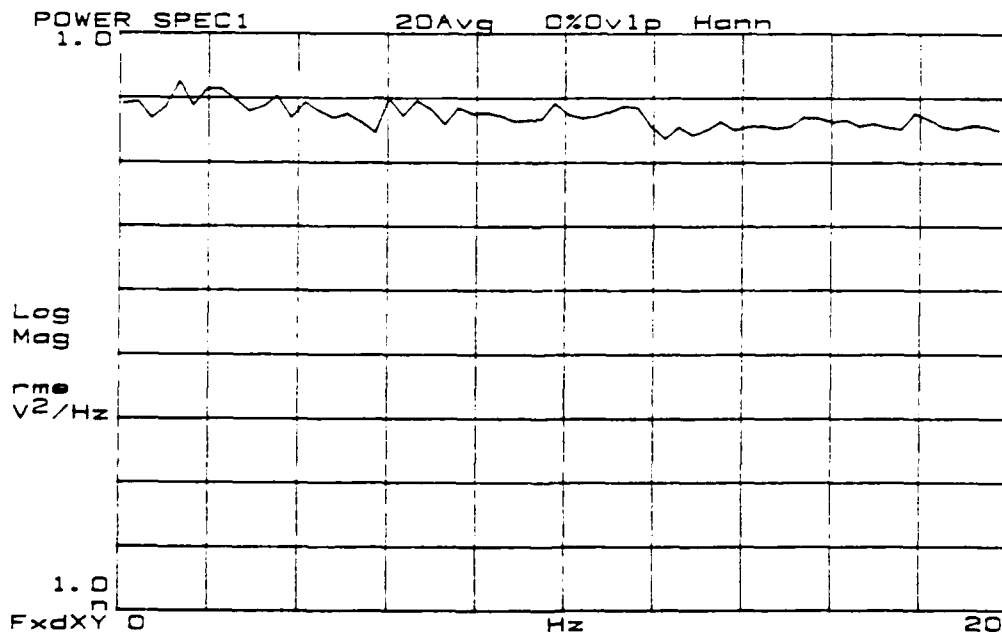
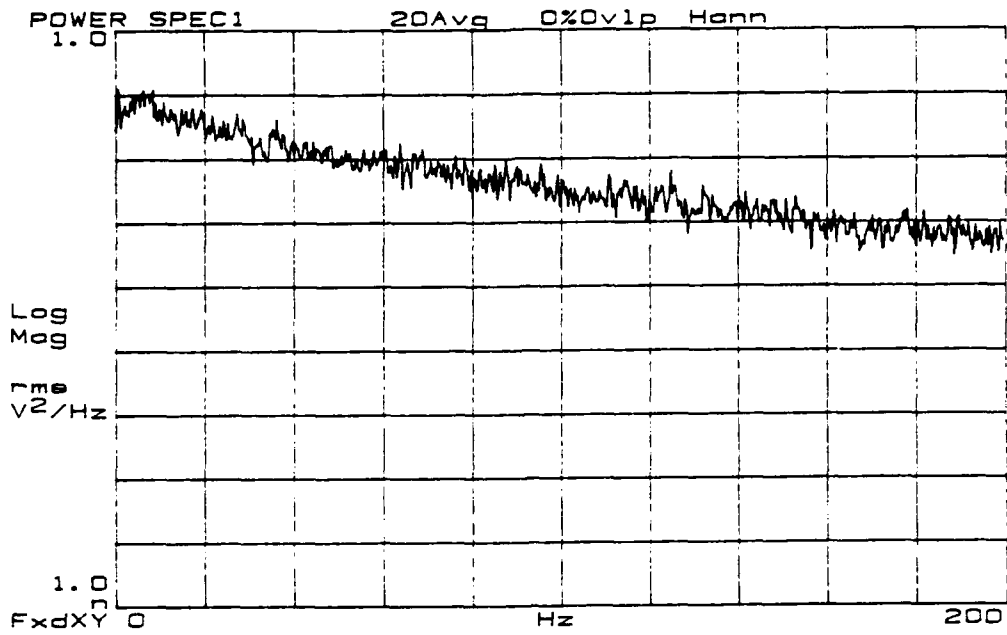


Figure 75. Re = 2402.



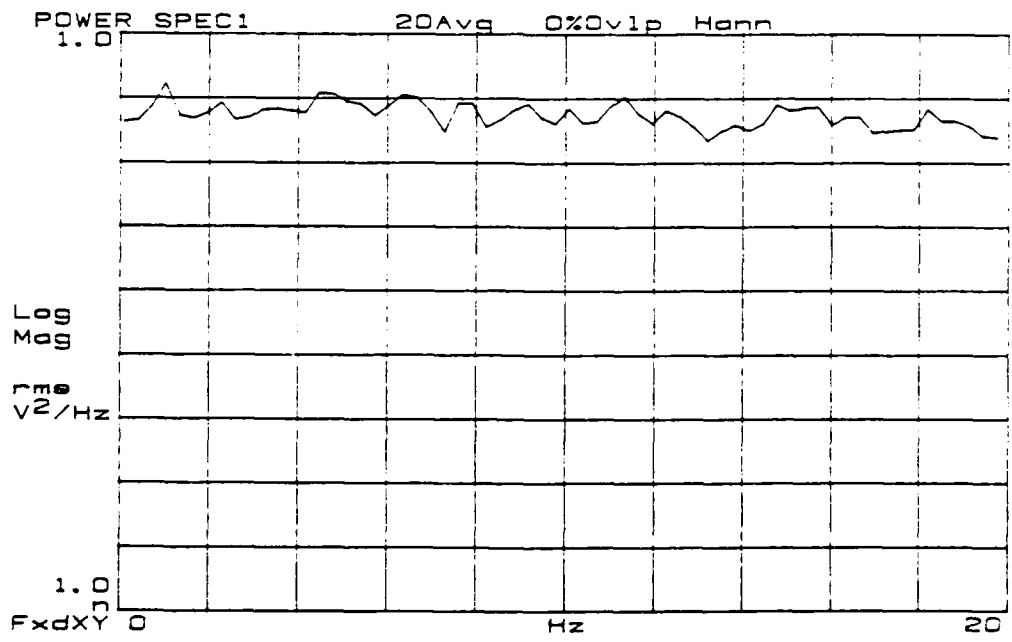
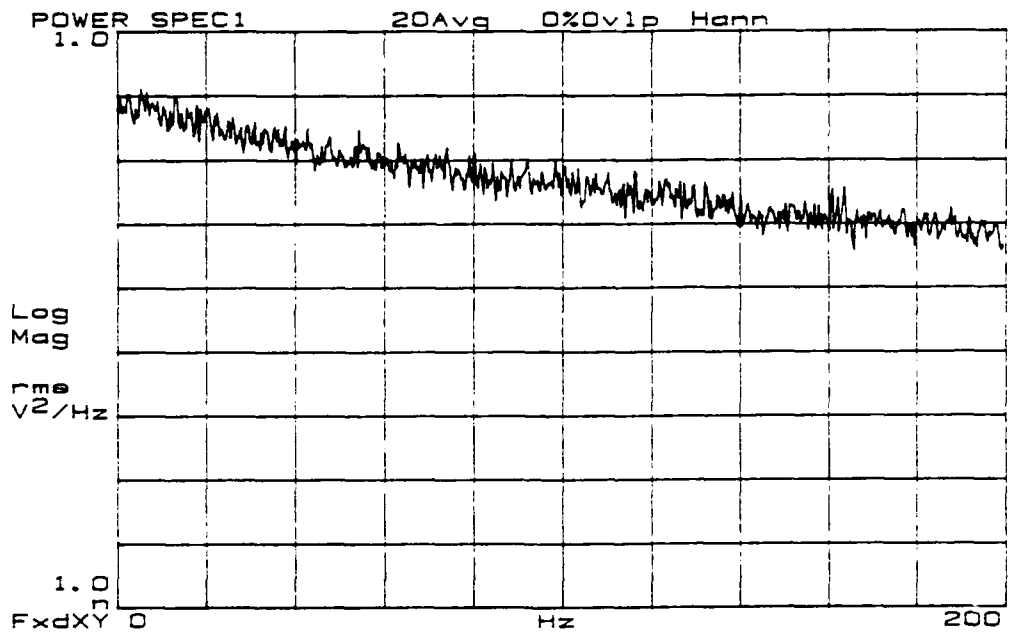


Figure 77. Re = 2599.

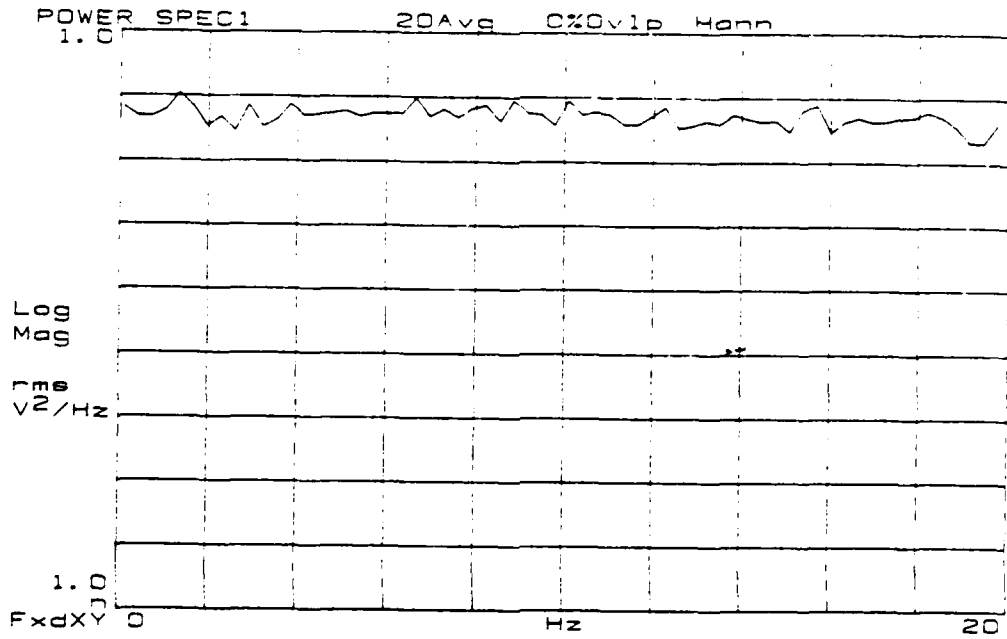
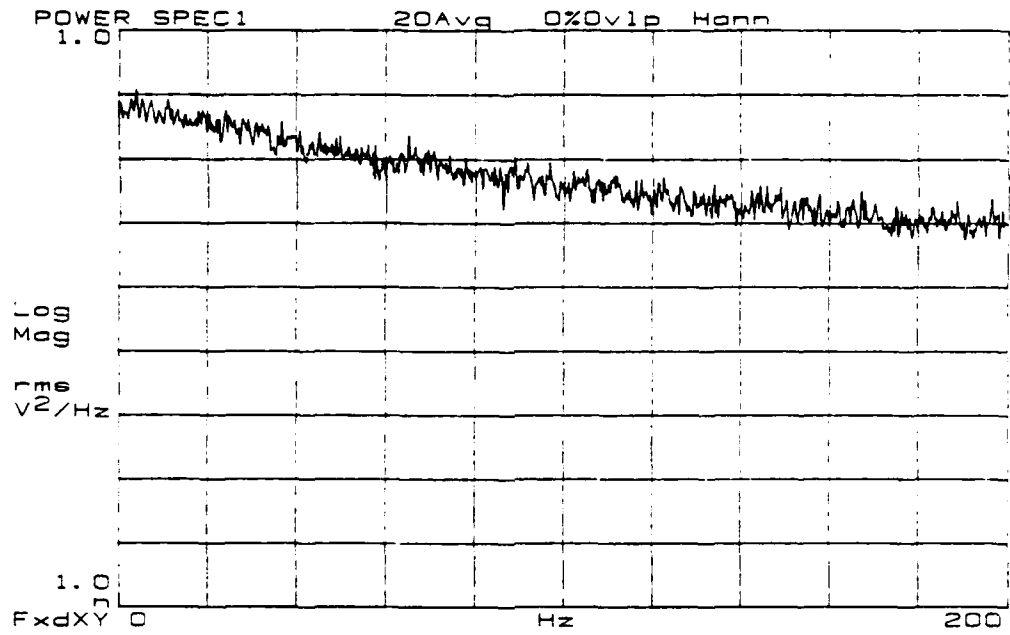


Figure 78. Re = 2699.

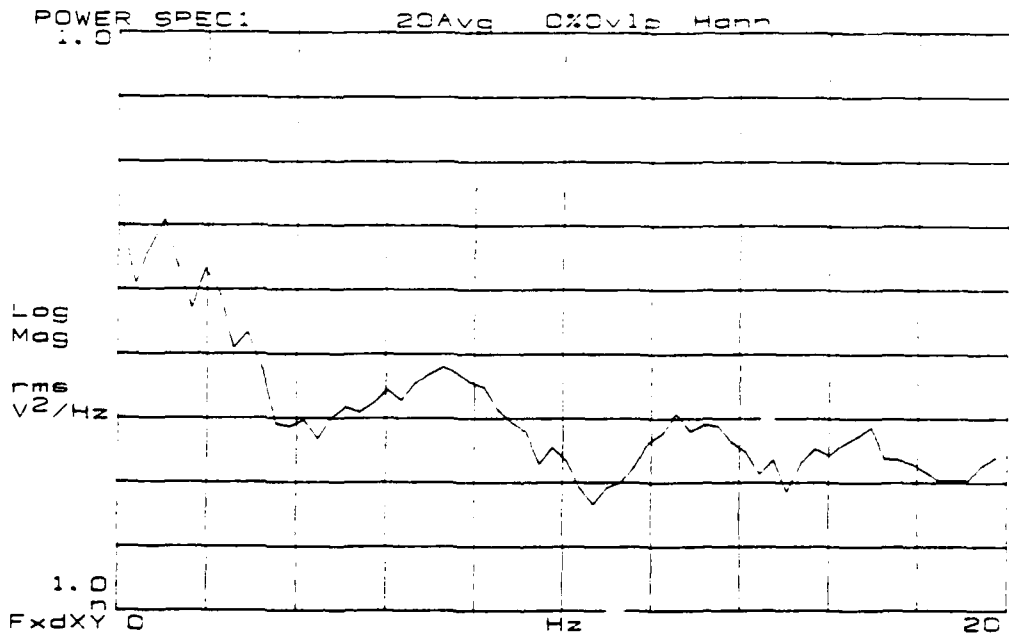
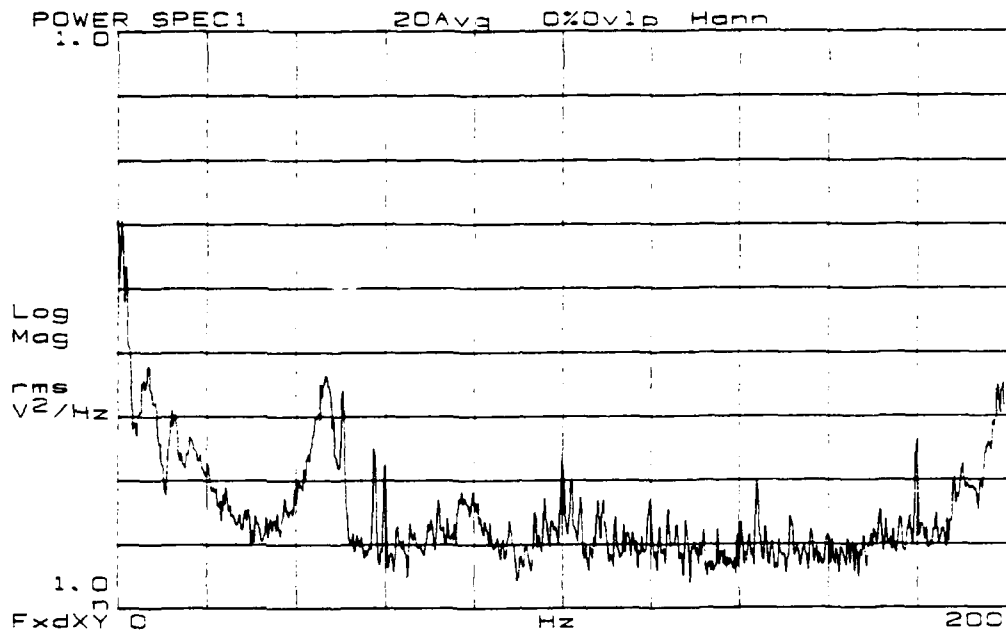


Figure 79.  $Re = 1103$ ,  $f_{osc} = 1$  Hz.



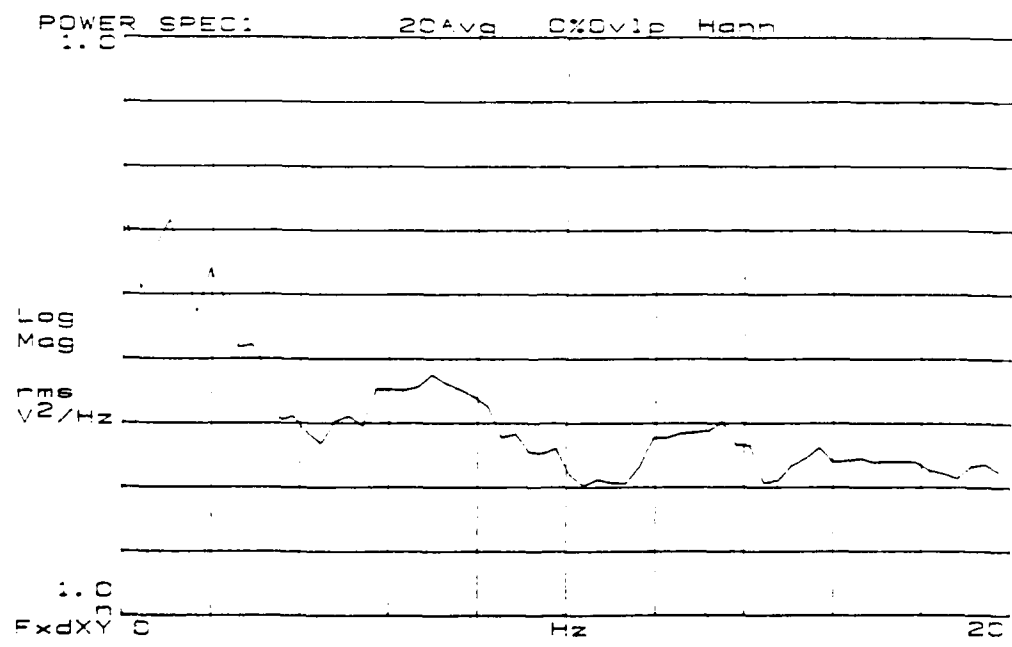
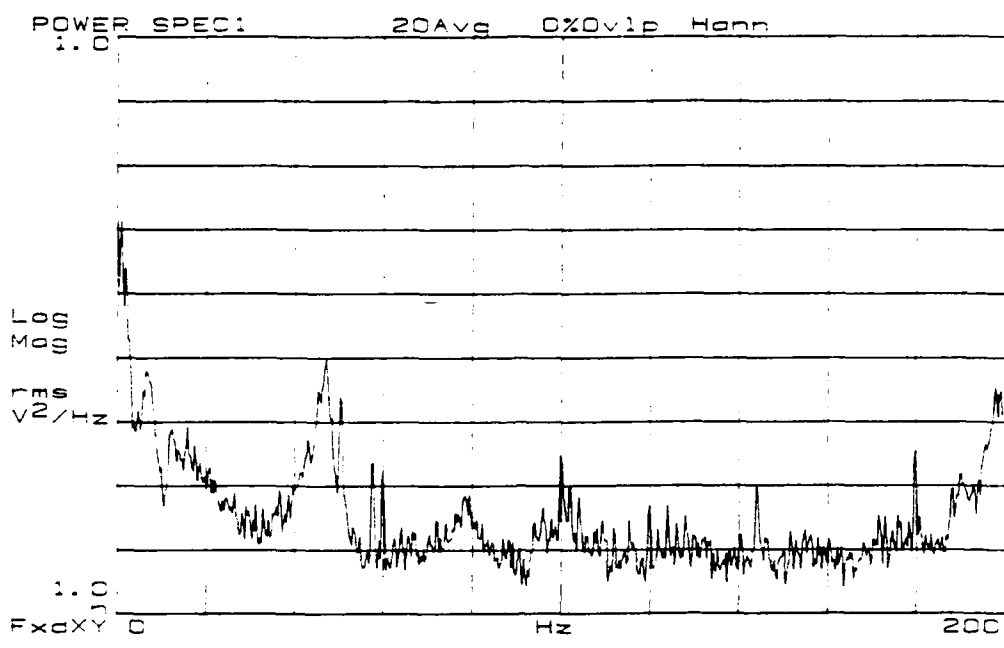


Figure 80.  $R_e = 1212$ ,  $f_{osc} = 1$  Hz.





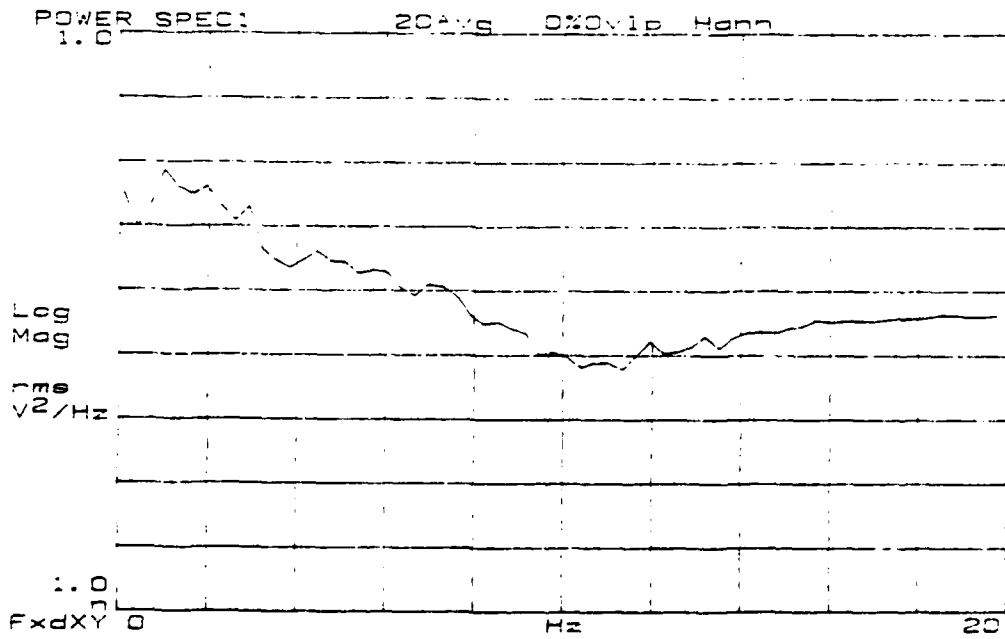
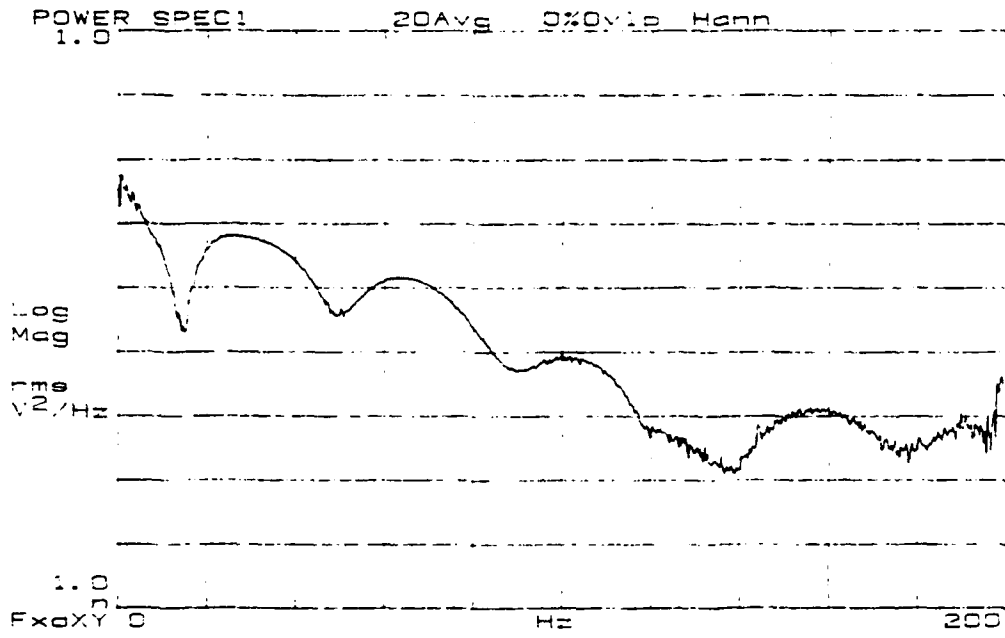


Figure 83.  $Re = 1496$ ,  $f_{osc} = 1$  Hz.



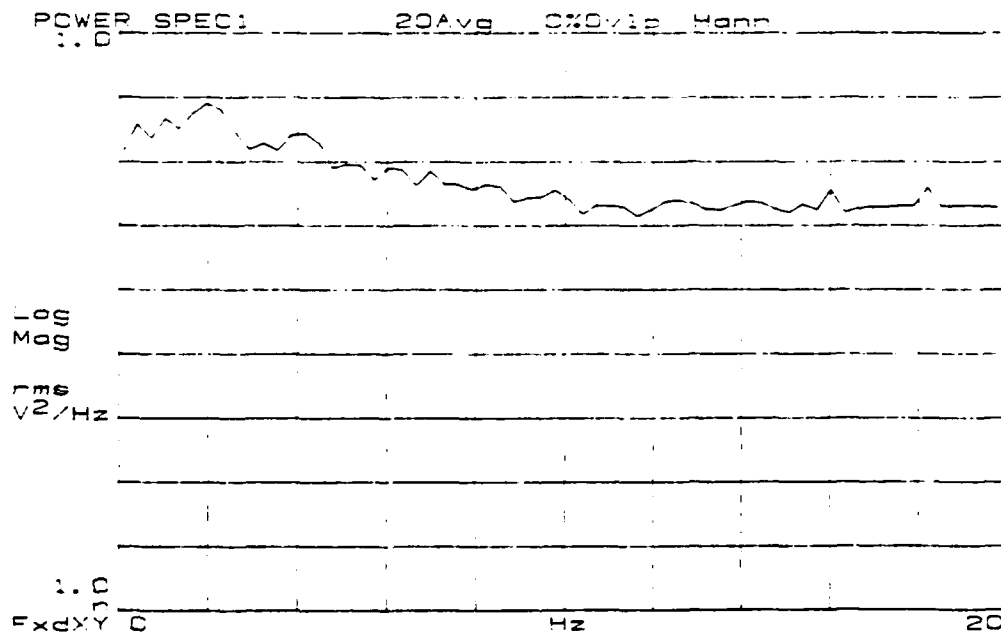
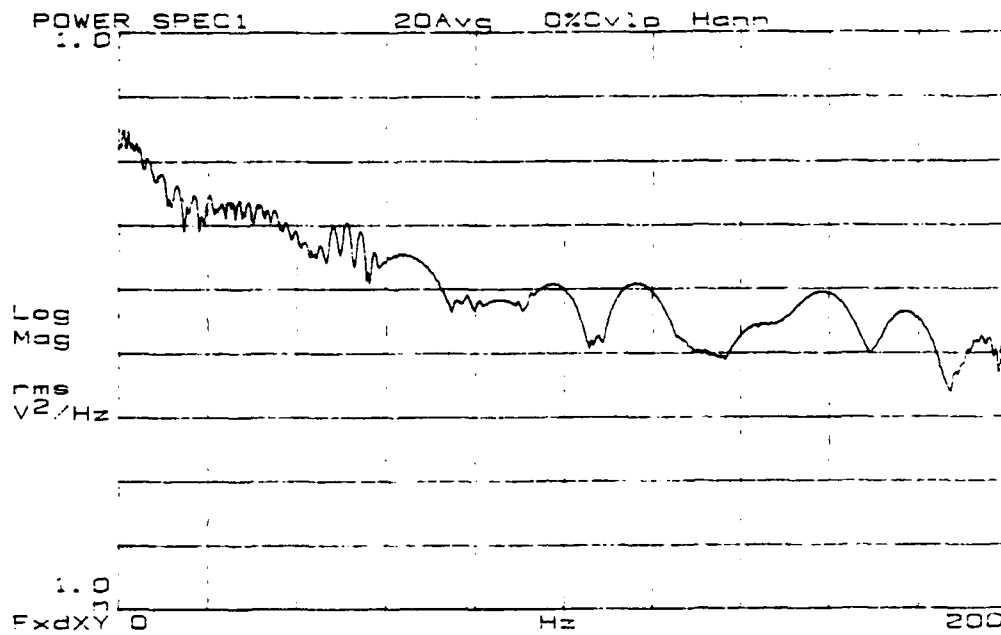


Figure 85.  $Re = 1604$ ,  $f_{osc} = 1$  Hz.

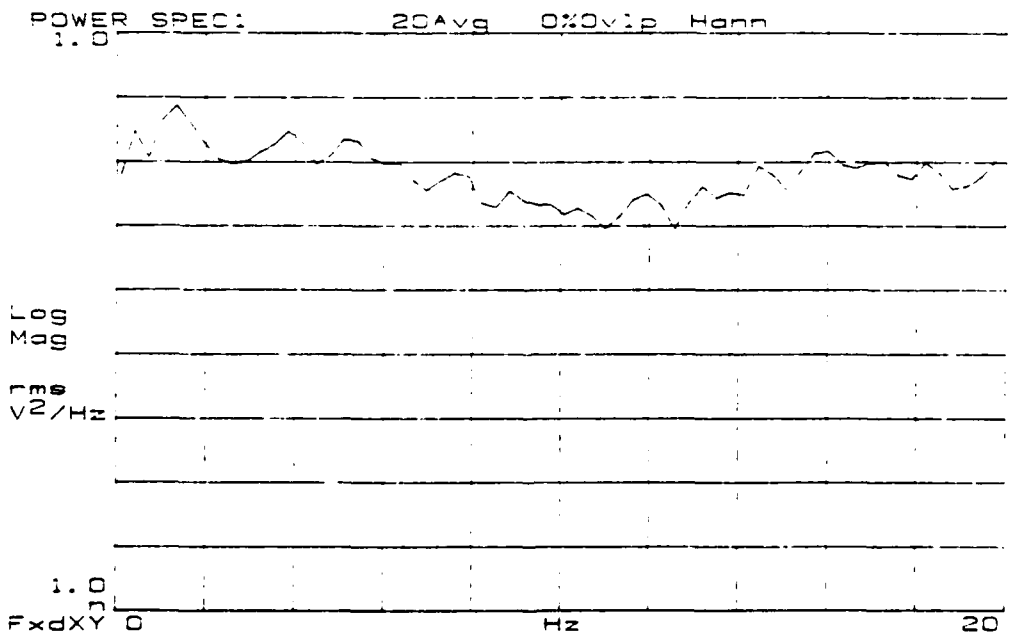
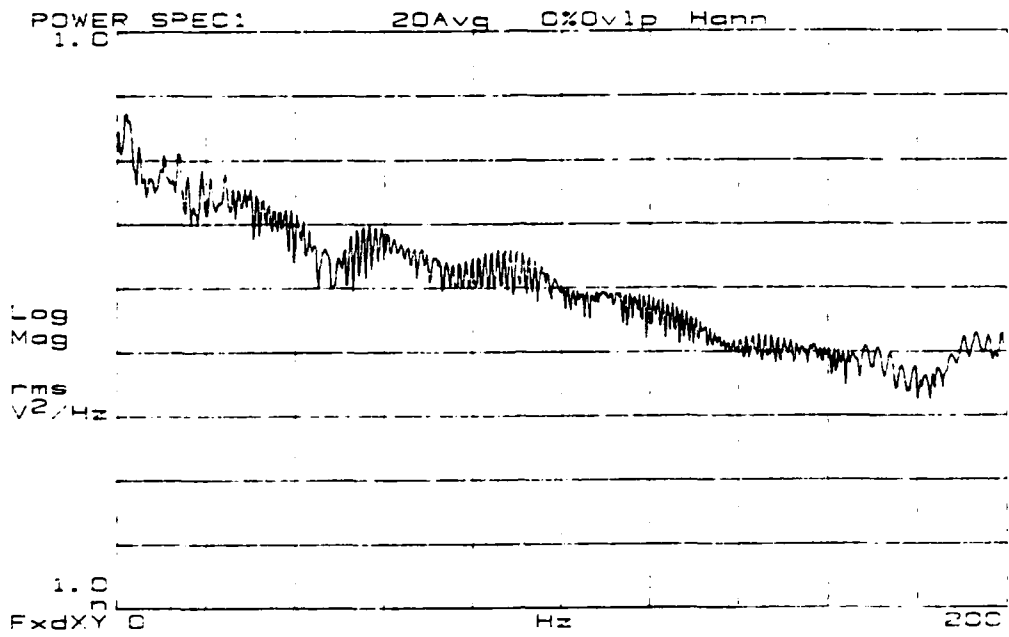


Figure 86.  $Re = 1650$ ,  $f_{osc} = 1$  Hz.





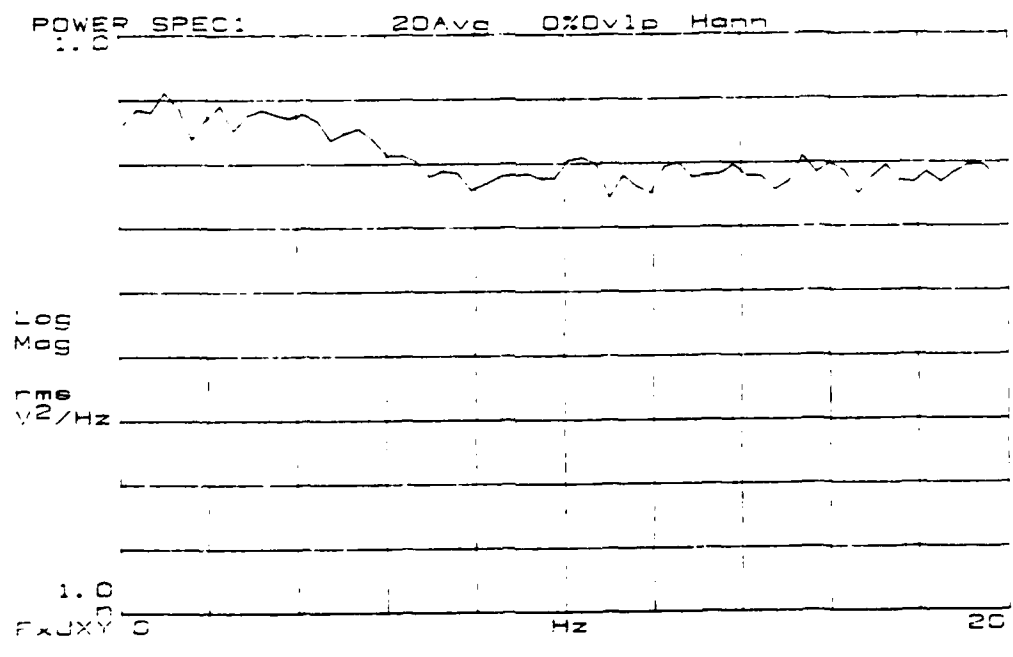
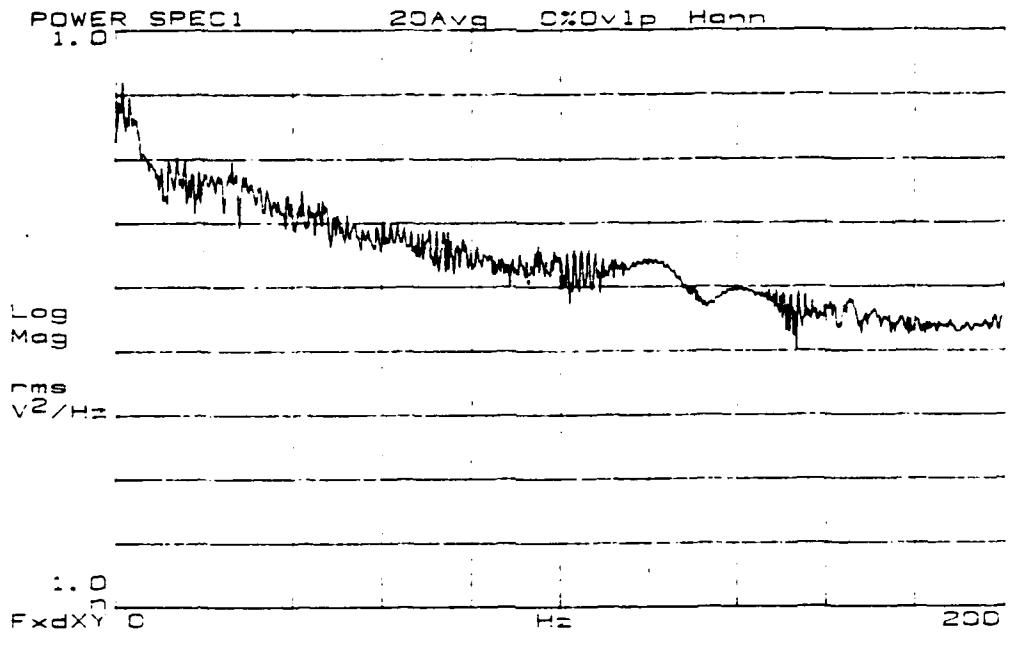


Figure 88.  $Re = 1742$ ,  $f_{osc} = 1$  Hz.

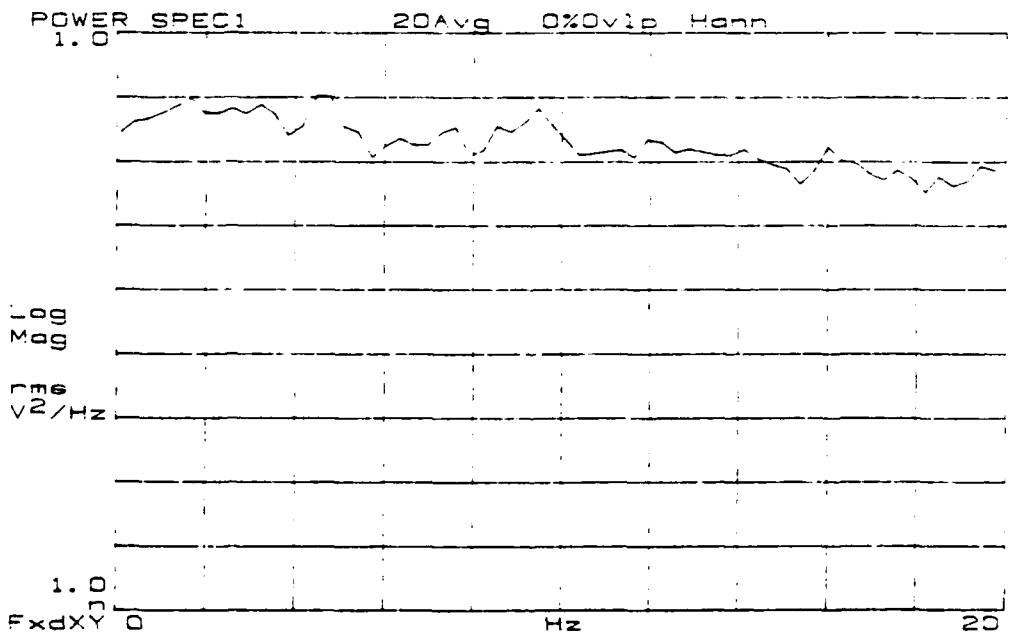
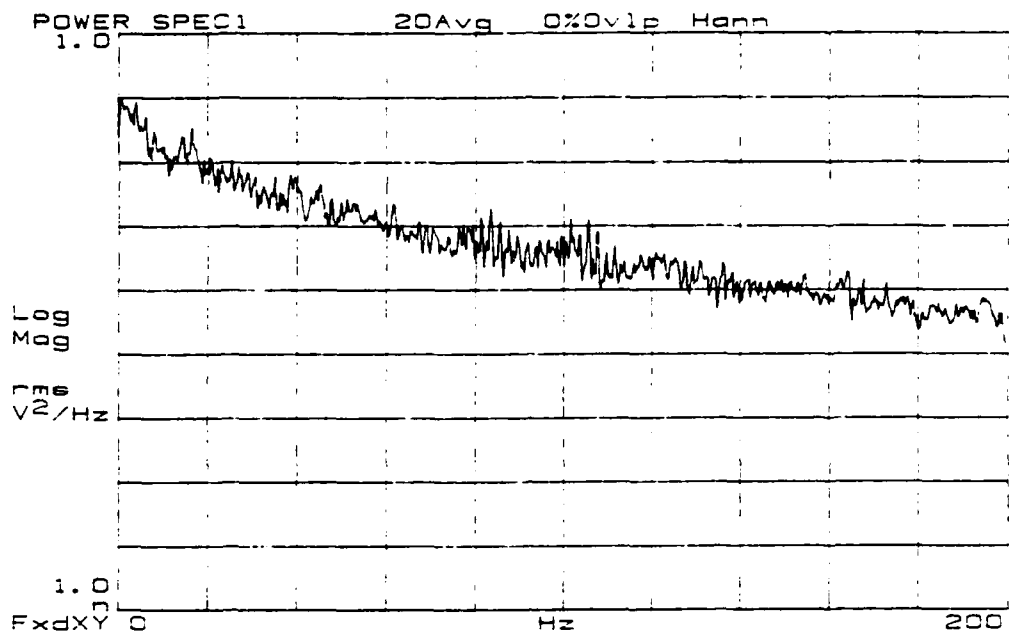


Figure 89.  $Re = 1796$ ,  $f_{osc} = 1$  Hz.

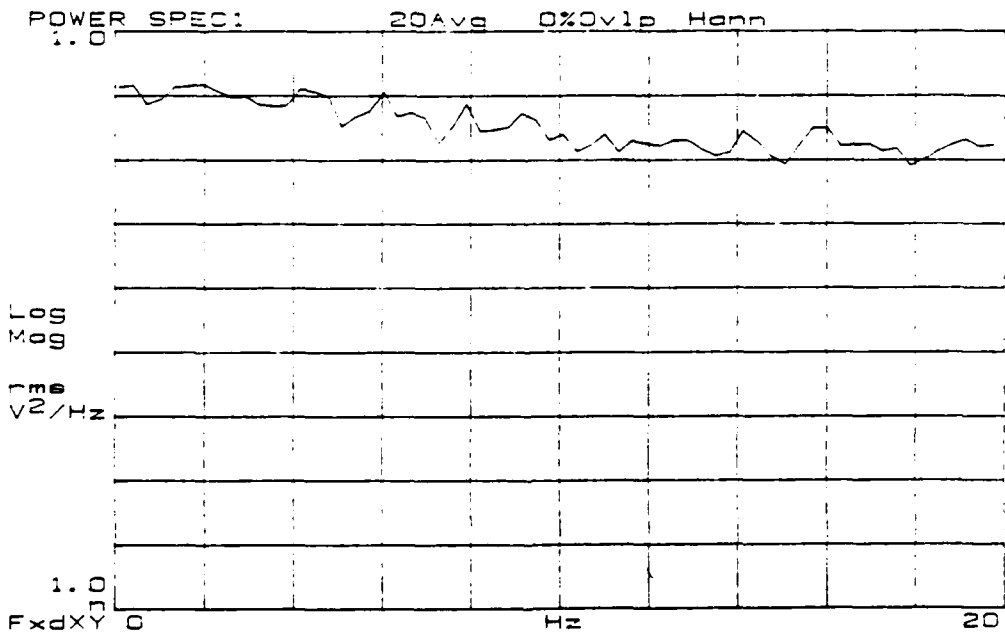
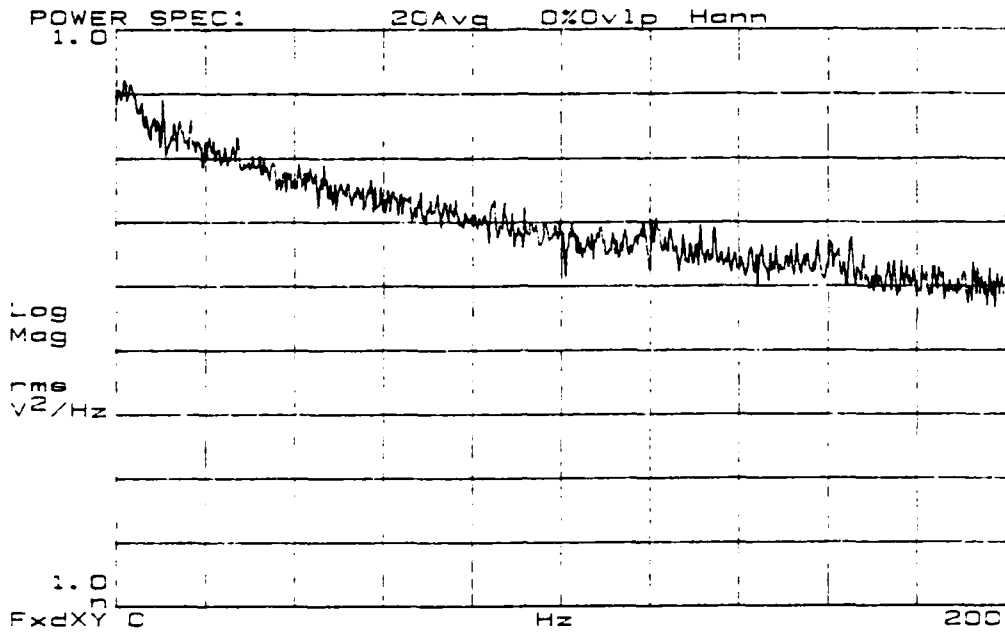


Figure 90.  $Re = 1905$ ,  $f_{osc} = 1$  Hz.

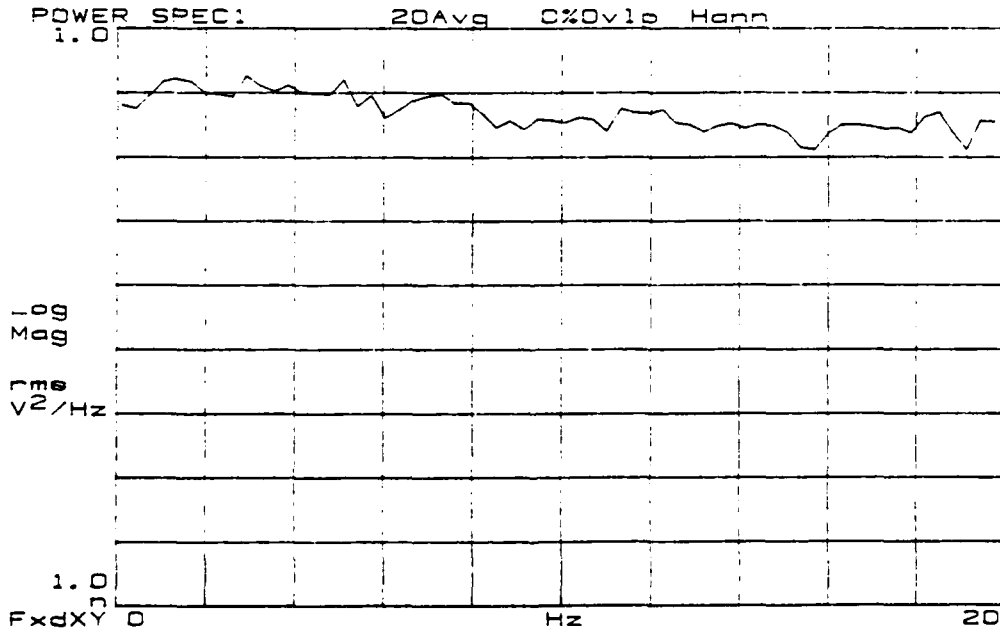
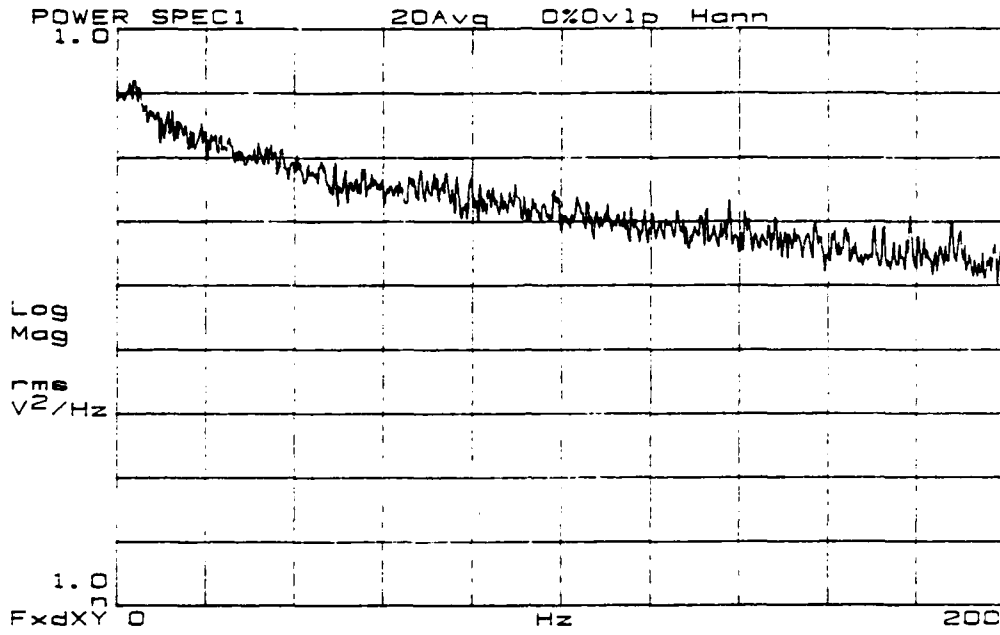


Figure 91. Re = 2005,  $f_{osc} = 1$  Hz.

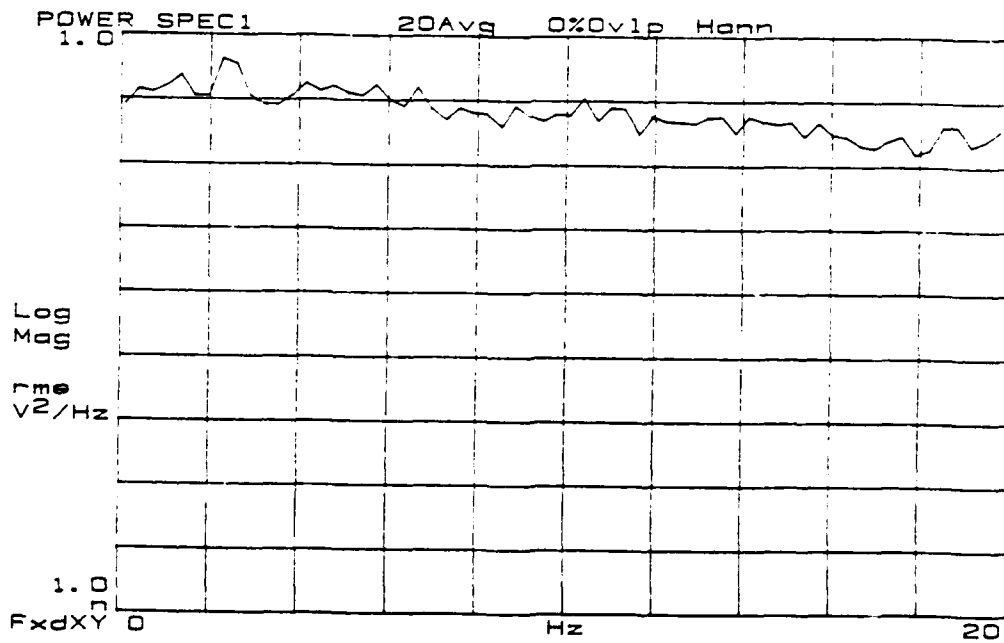
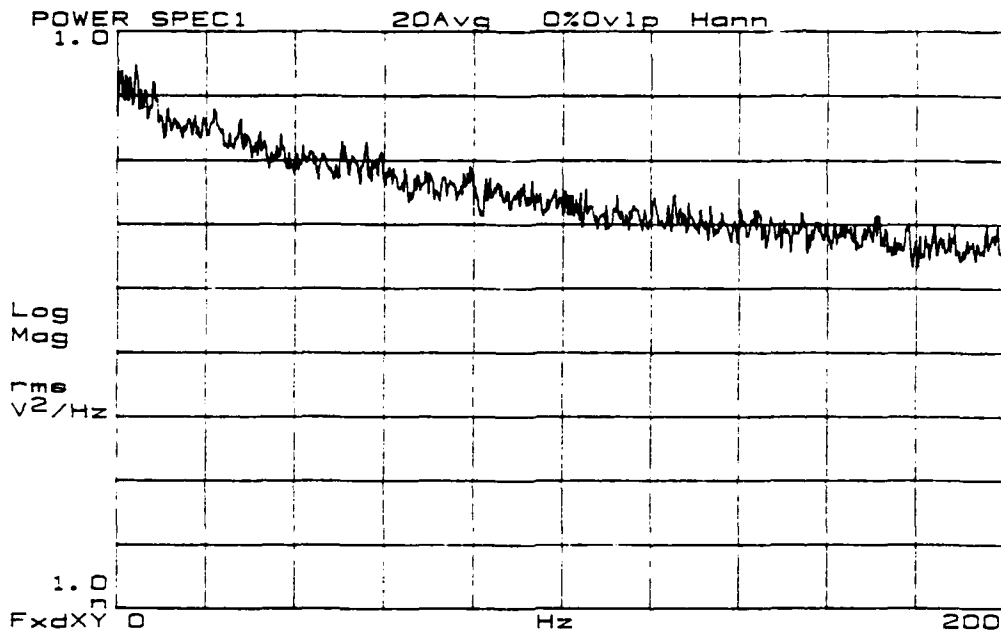


Figure 92.  $Re = 2097$ ,  $f_{osc} = 1$  Hz.

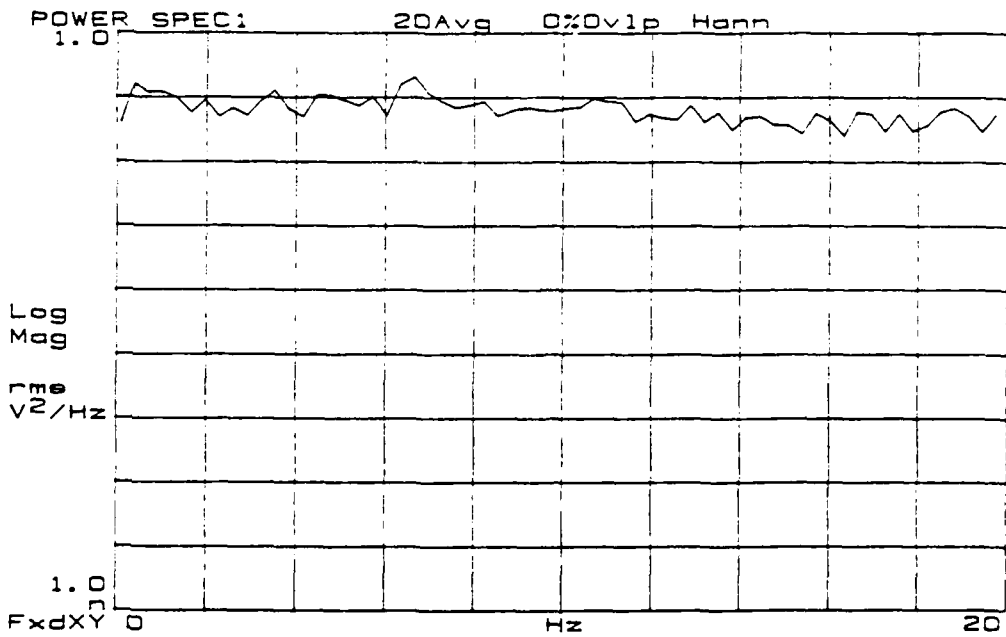
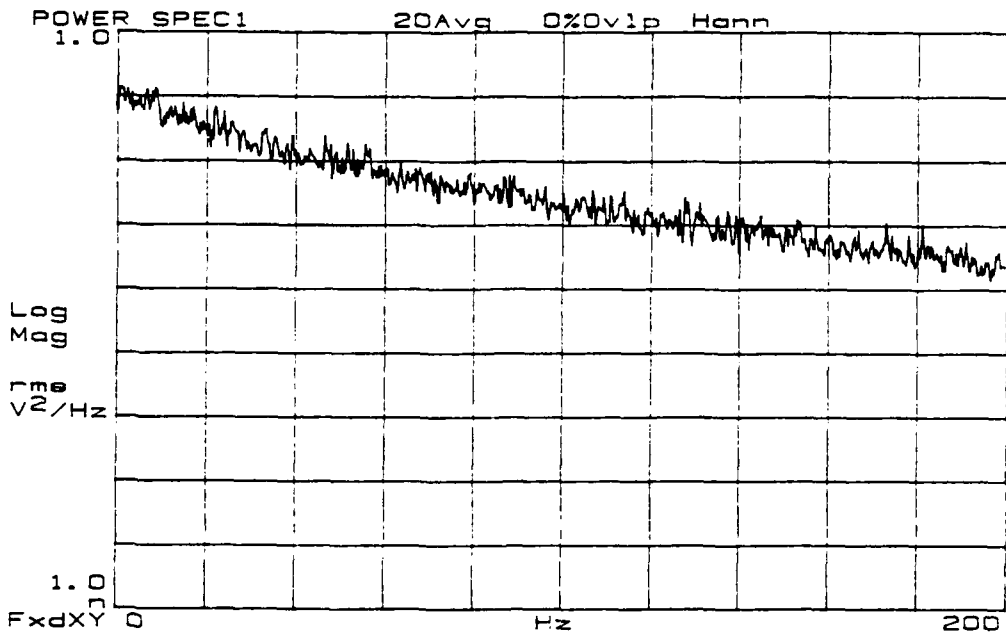


Figure 93.  $Re = 2197$ ,  $f_{osc} = 1$  Hz.

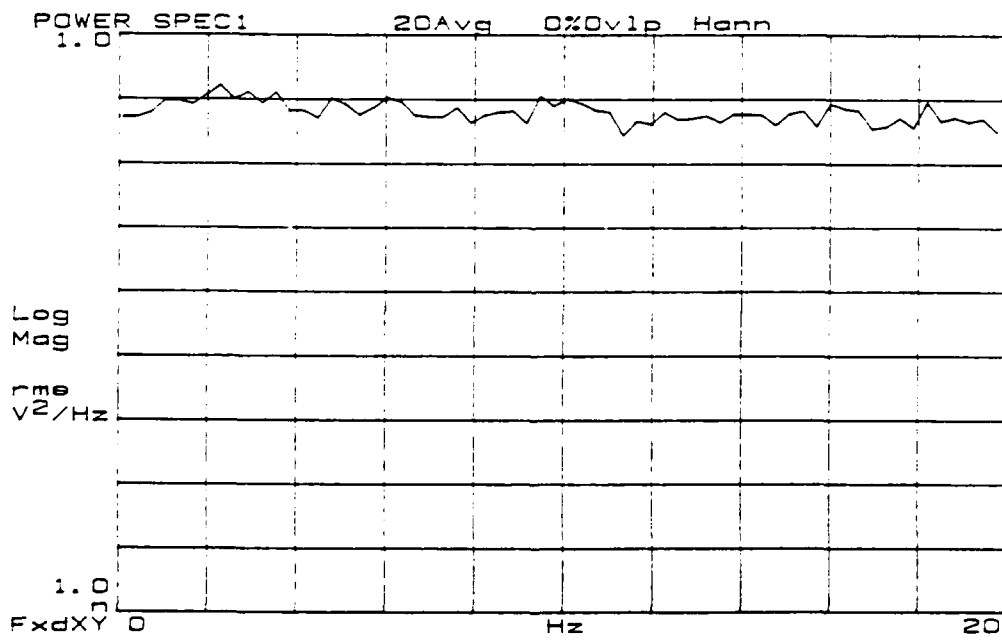
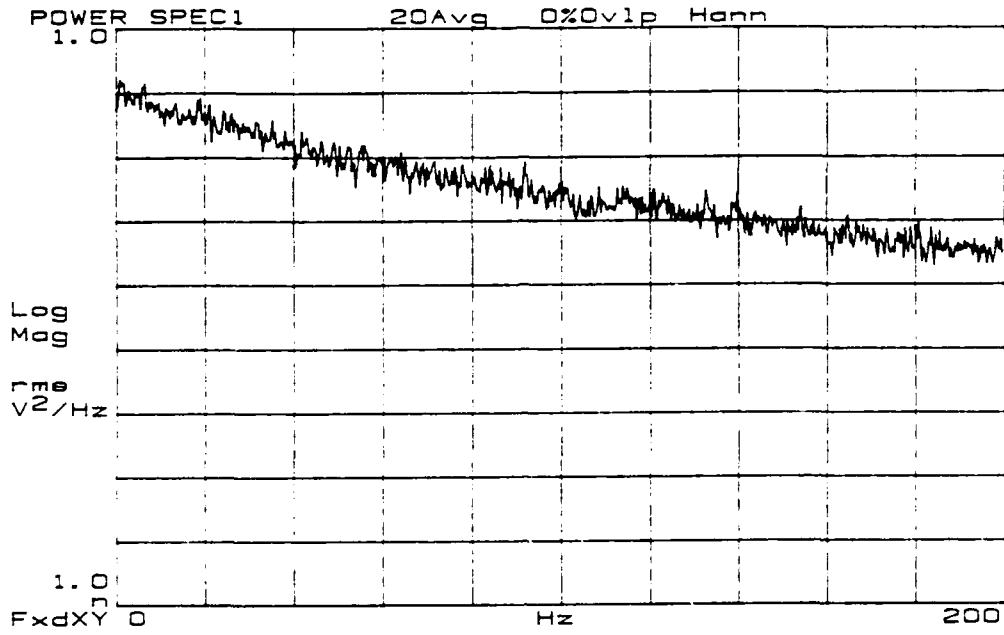


Figure 94.  $R_e = 2298$ ,  $f_{osc} = 1$  Hz.

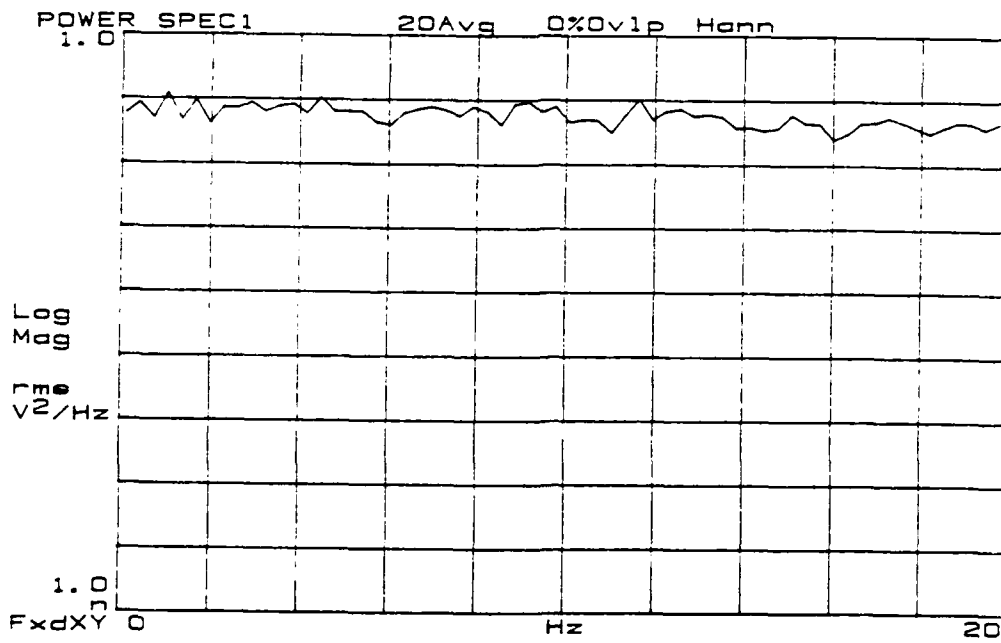
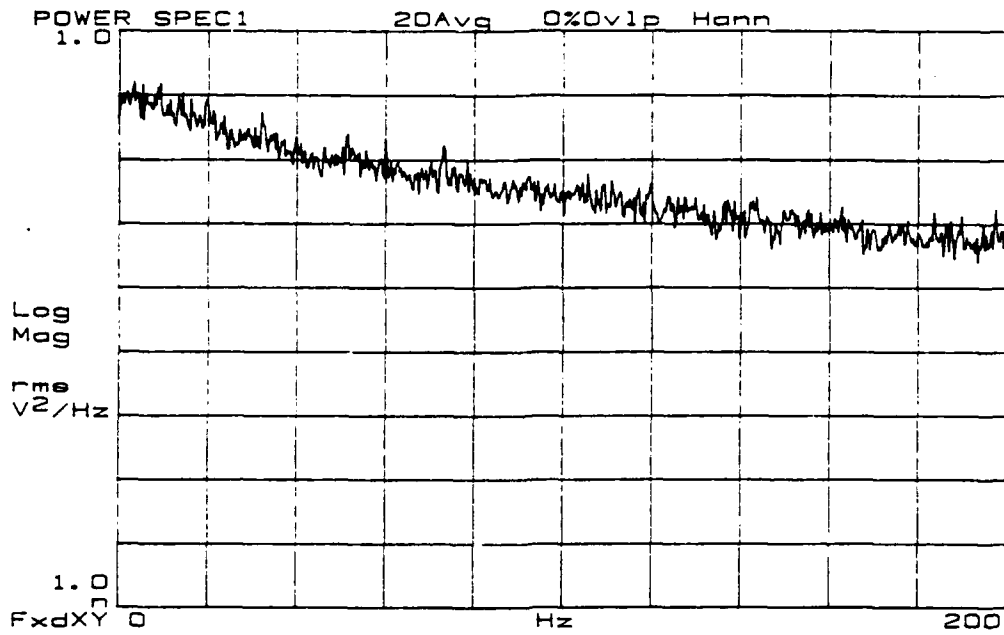


Figure 95.  $R_e = 2402$ ,  $f_{osc} = 1$  Hz.



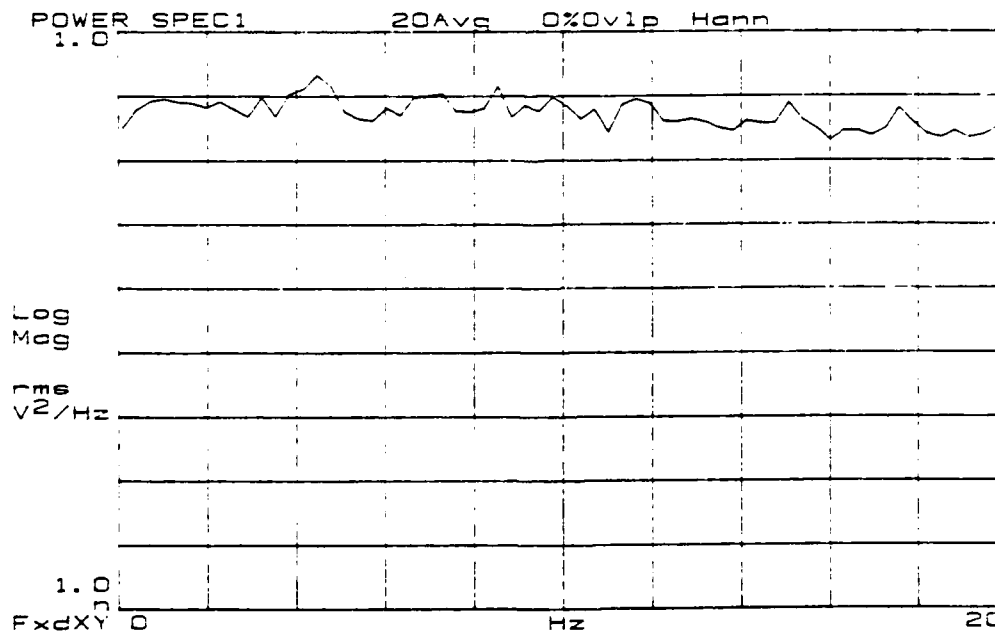
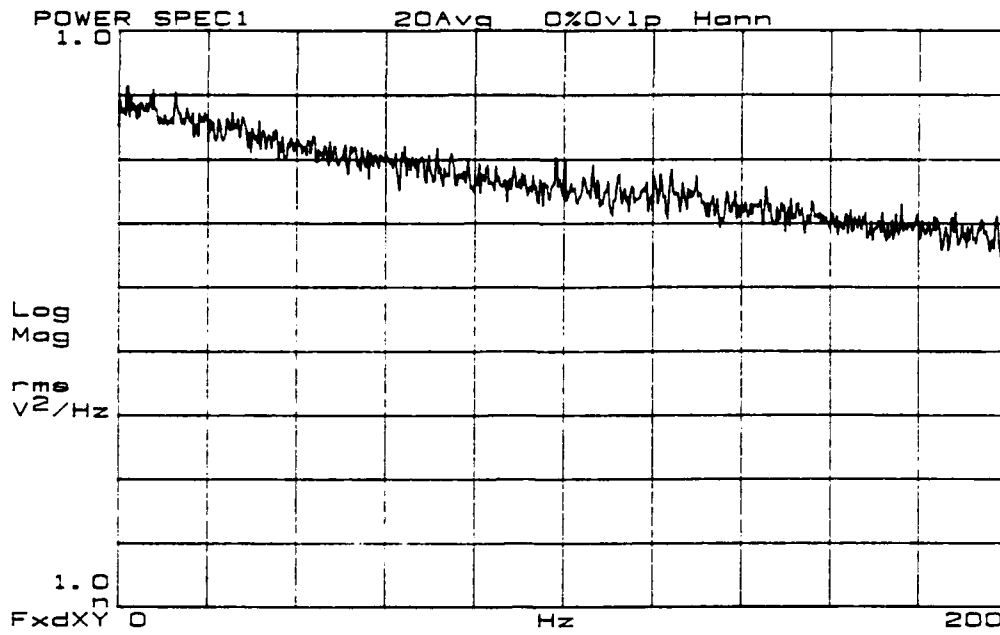


Figure 96.  $Re = 2498$ ,  $f_{osc} = 1$  Hz.

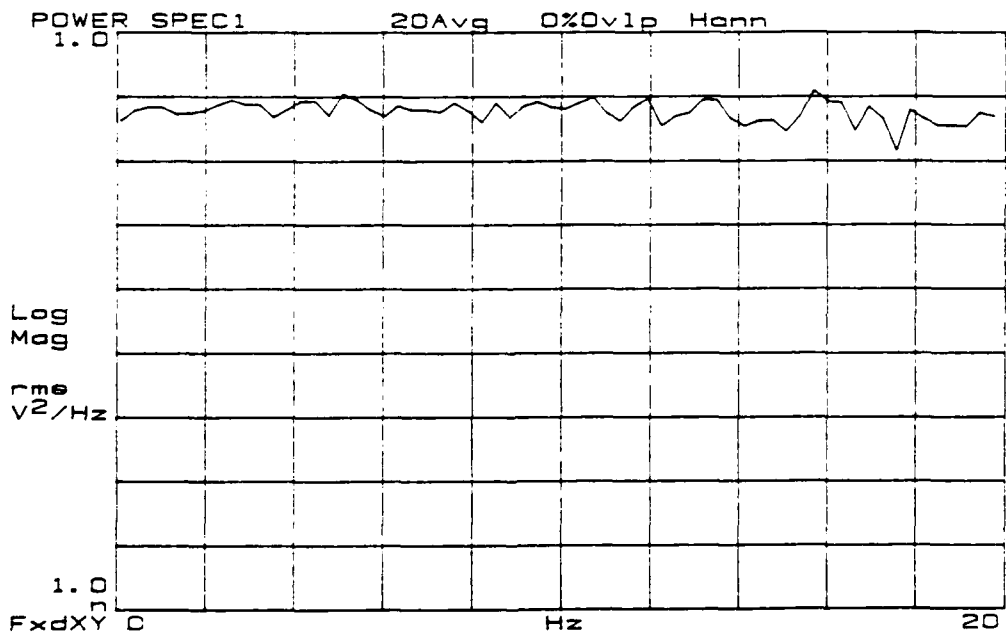
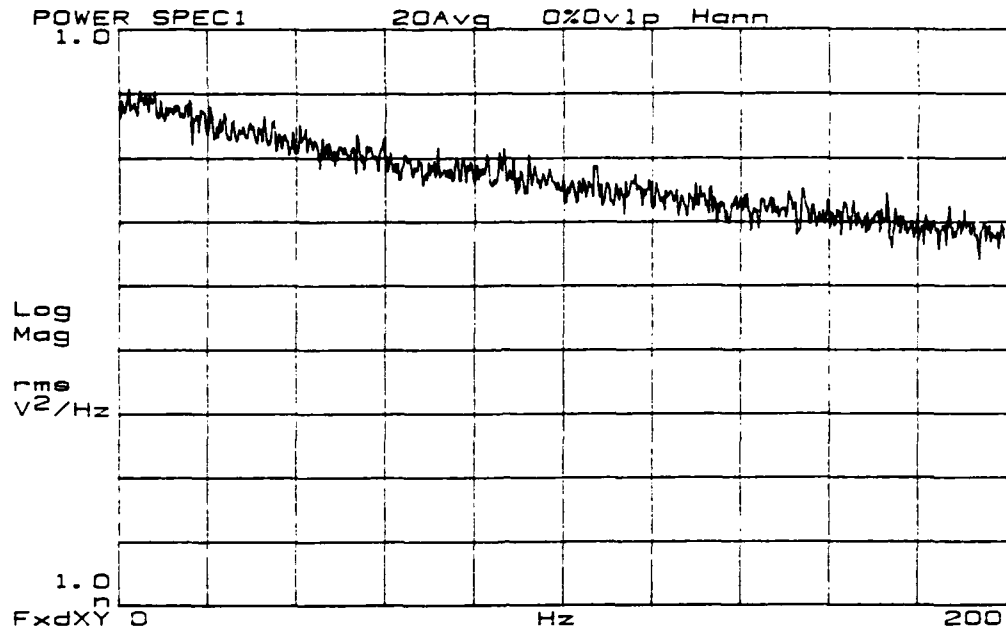


Figure 97.  $Re = 2599$ ,  $f_{osc} = 1$  Hz.

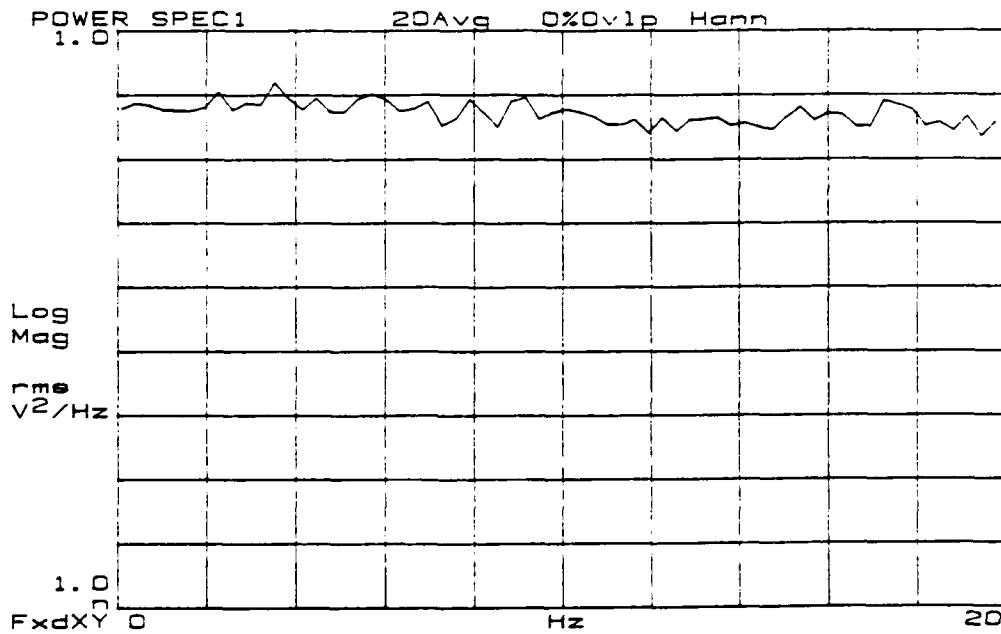
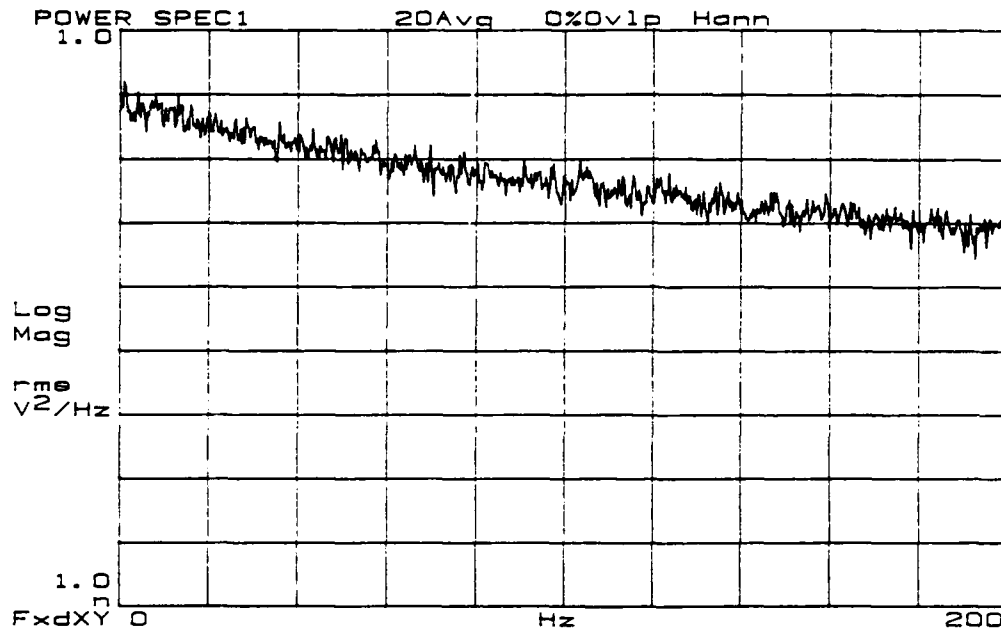


Figure 98.  $Re = 2699$ ,  $f_{osc} = 1$  Hz.

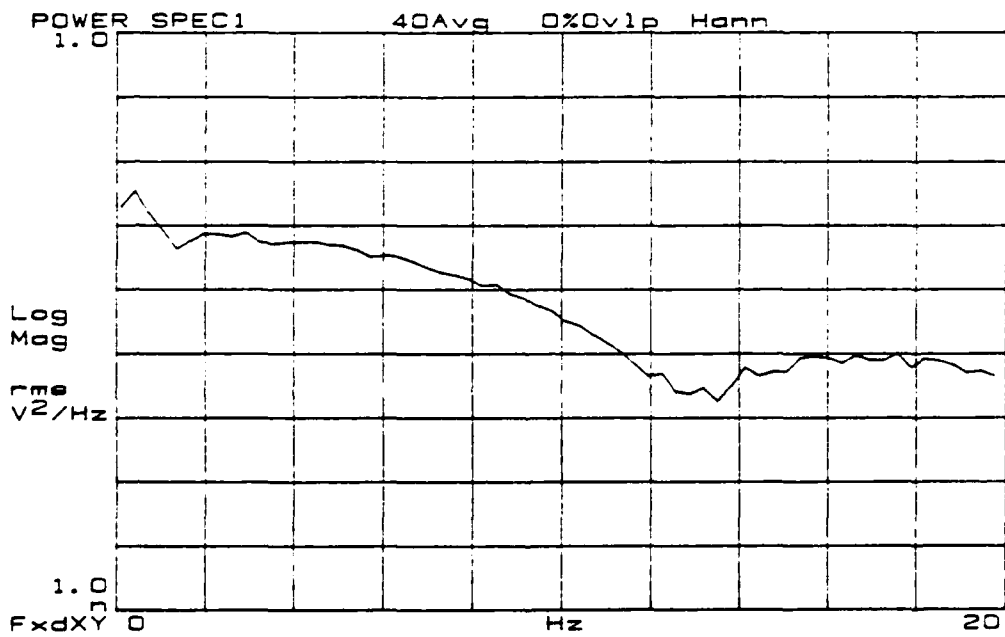
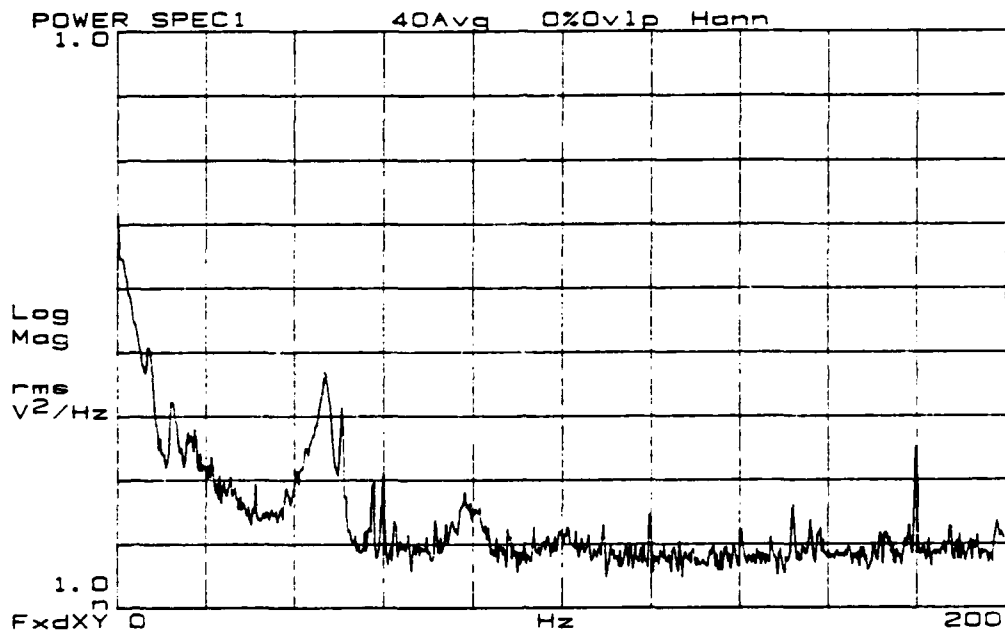


Figure 99. Re = 1396.

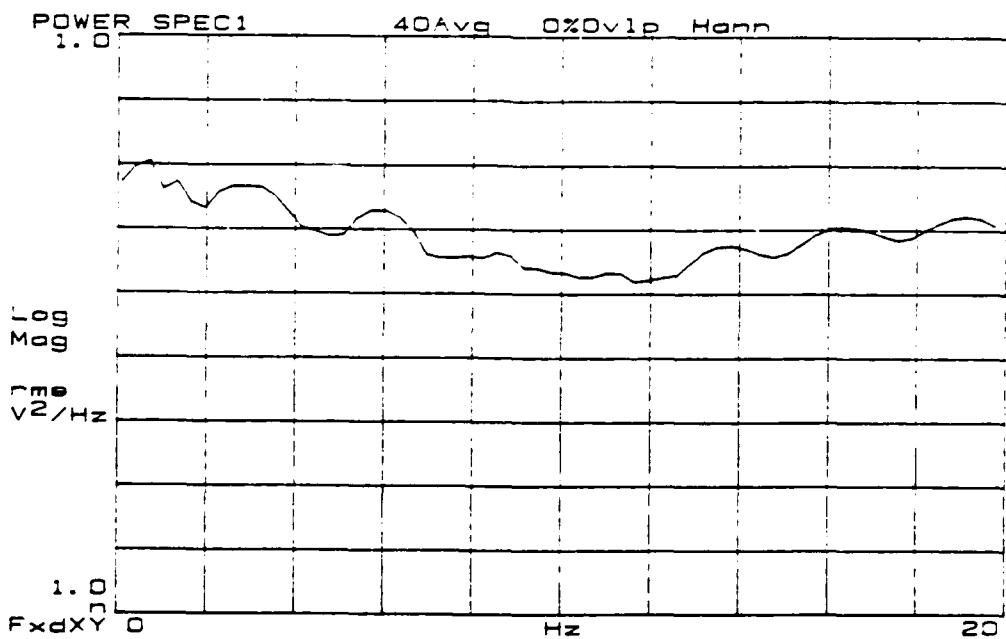
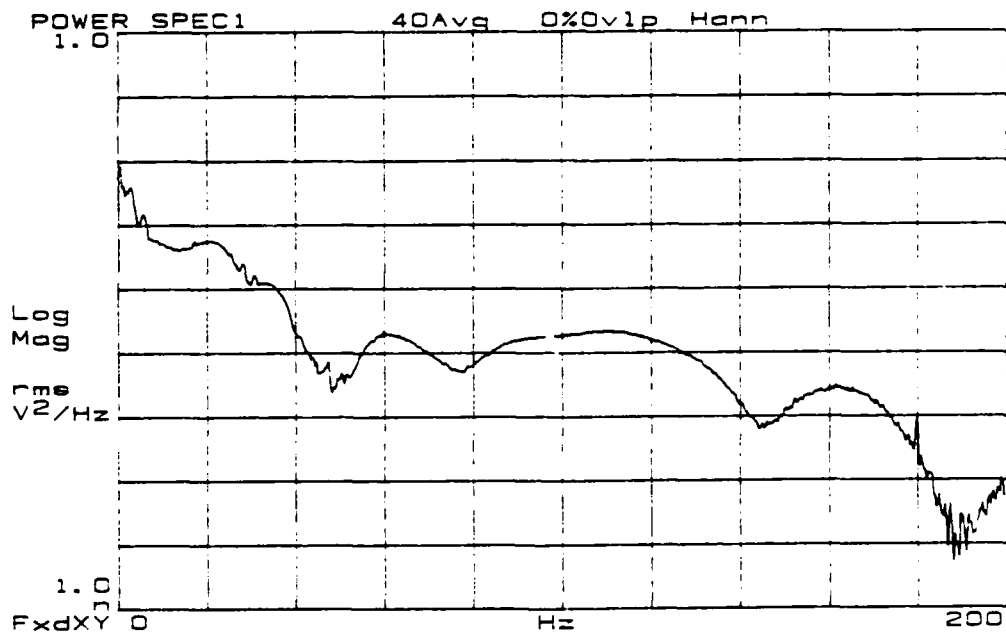


Figure 100. Re = 1454.

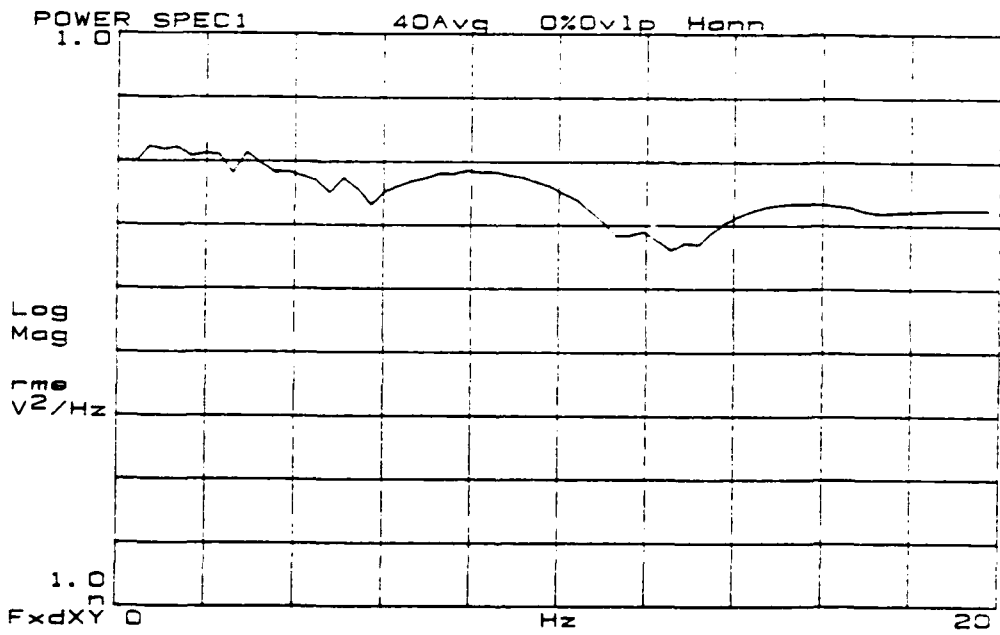
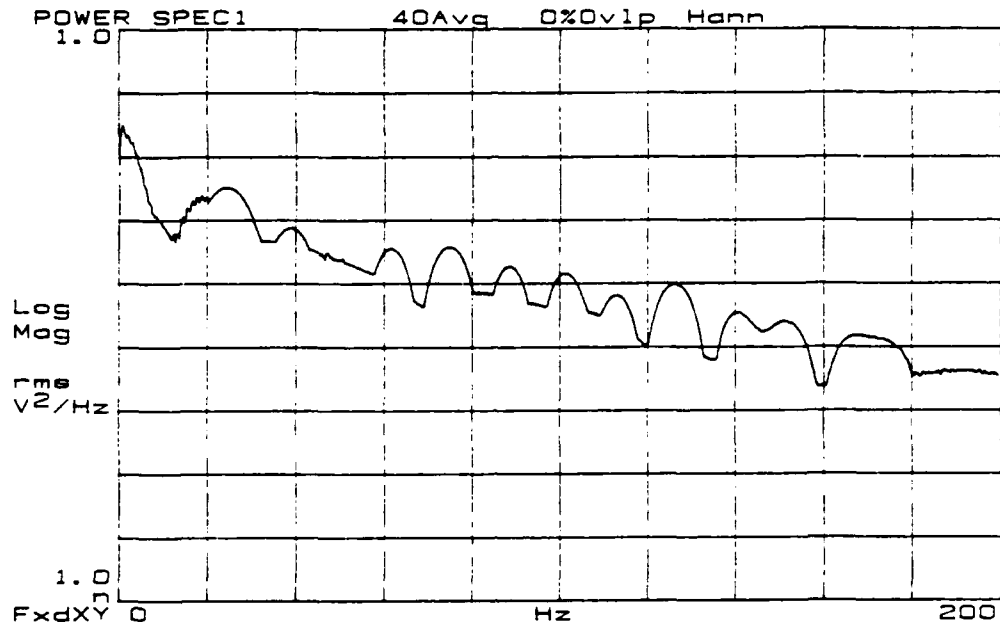


Figure 101. Re = 1496.

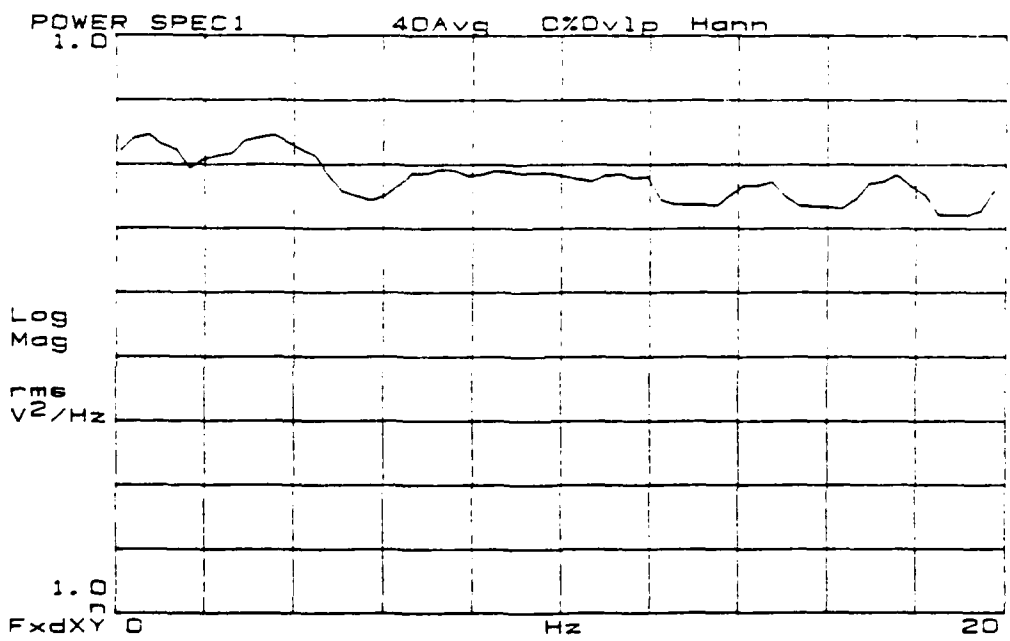
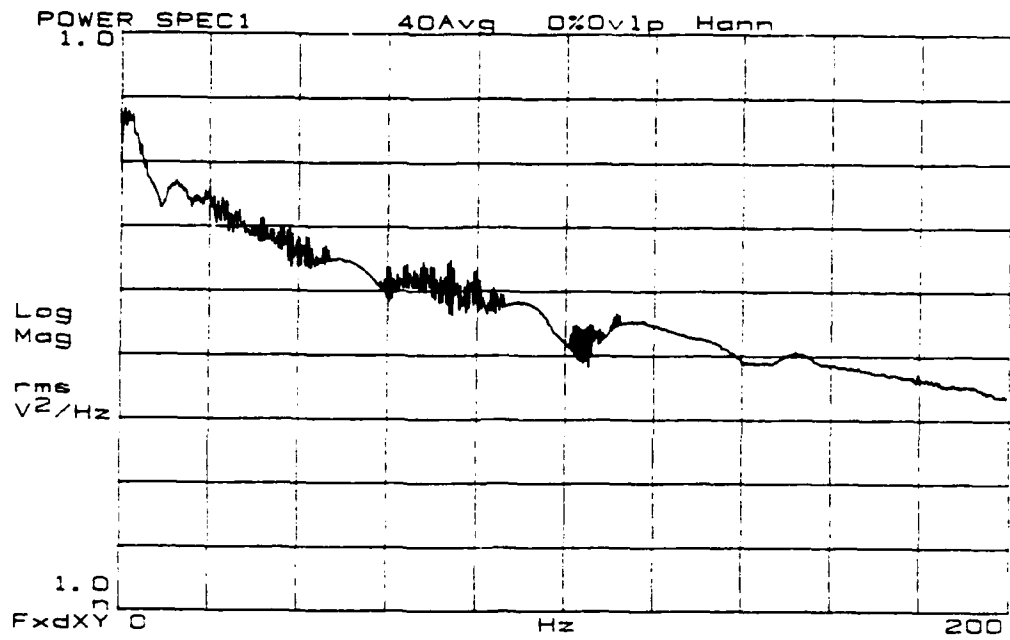


Figure 102. Re = 1542.

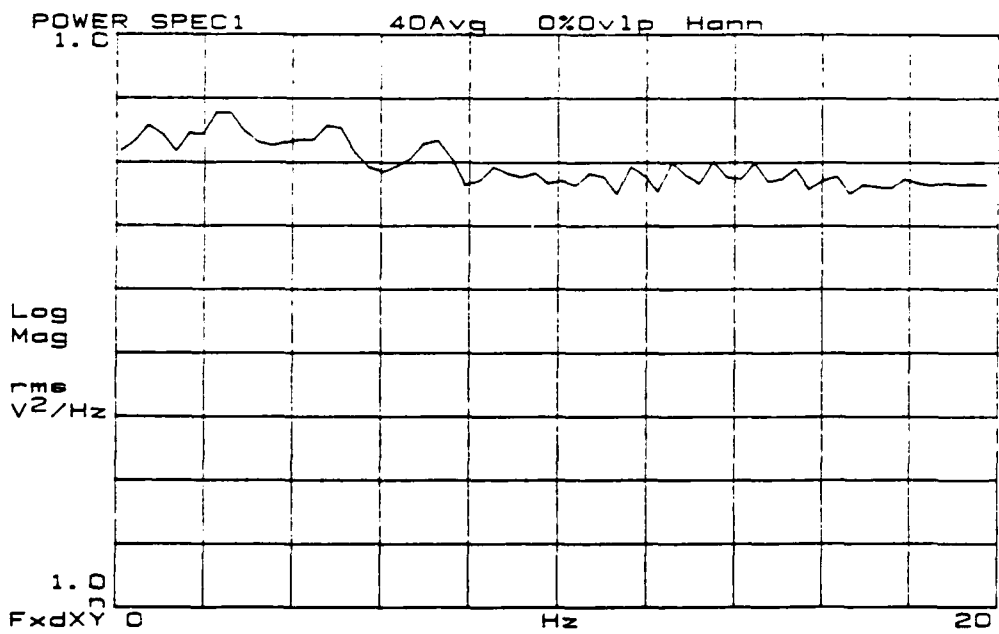
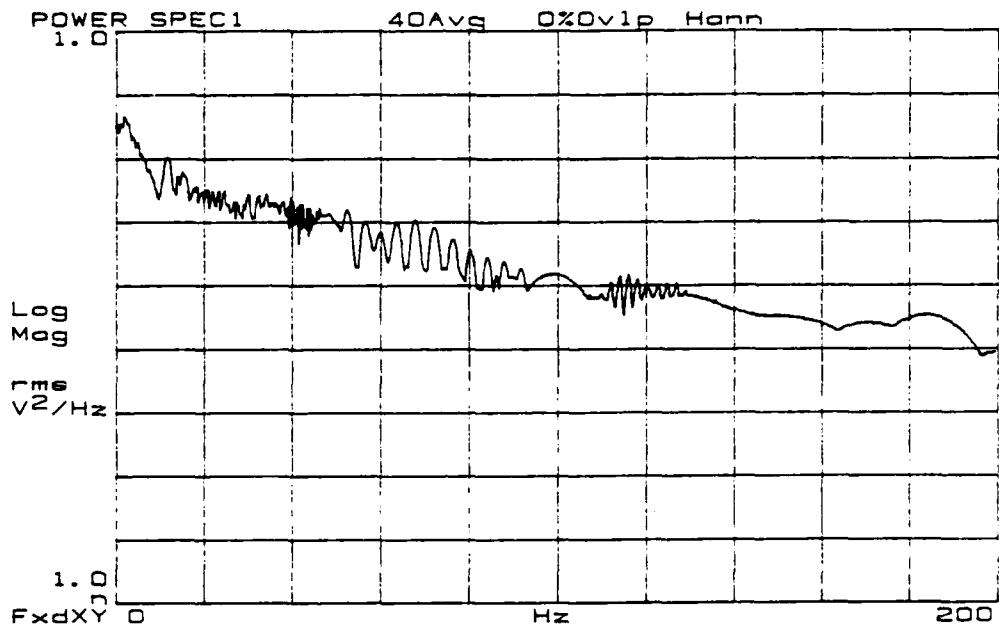


Figure 103. Re = 1604.



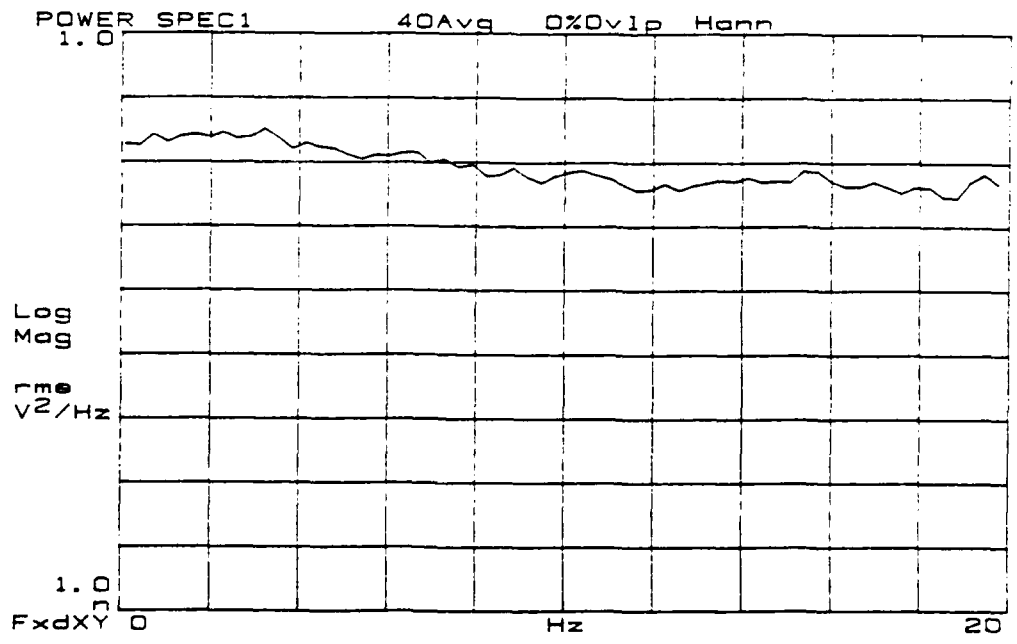
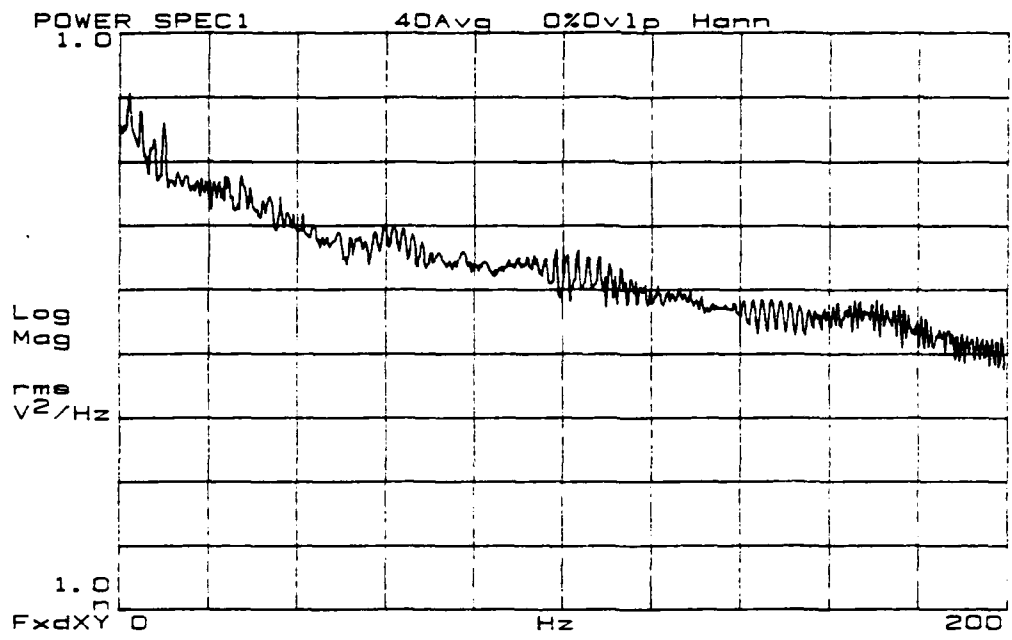


Figure 104. Re = 1650.

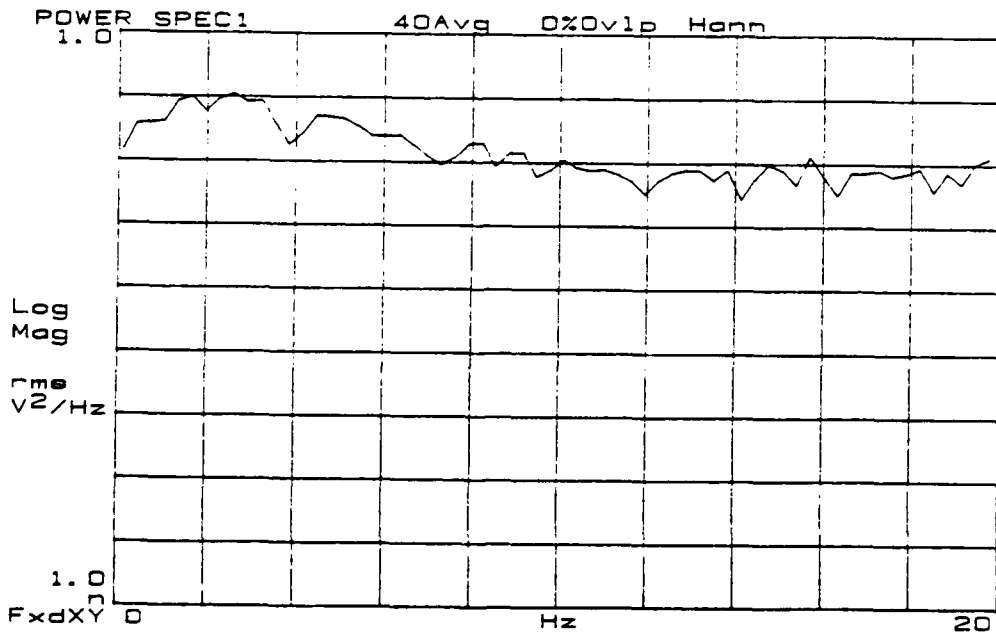
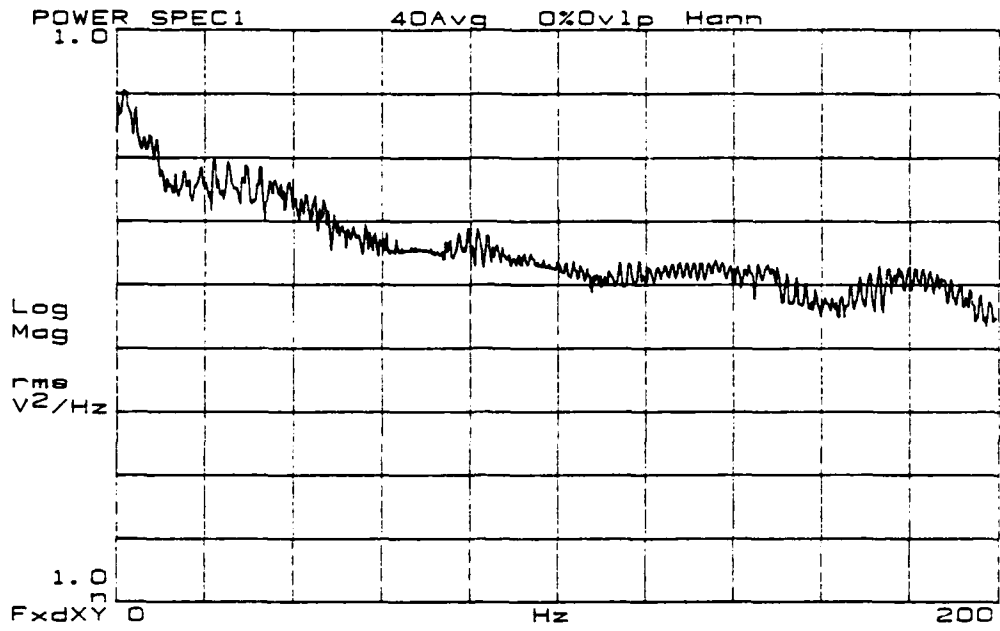


Figure 105. Re = 1697.

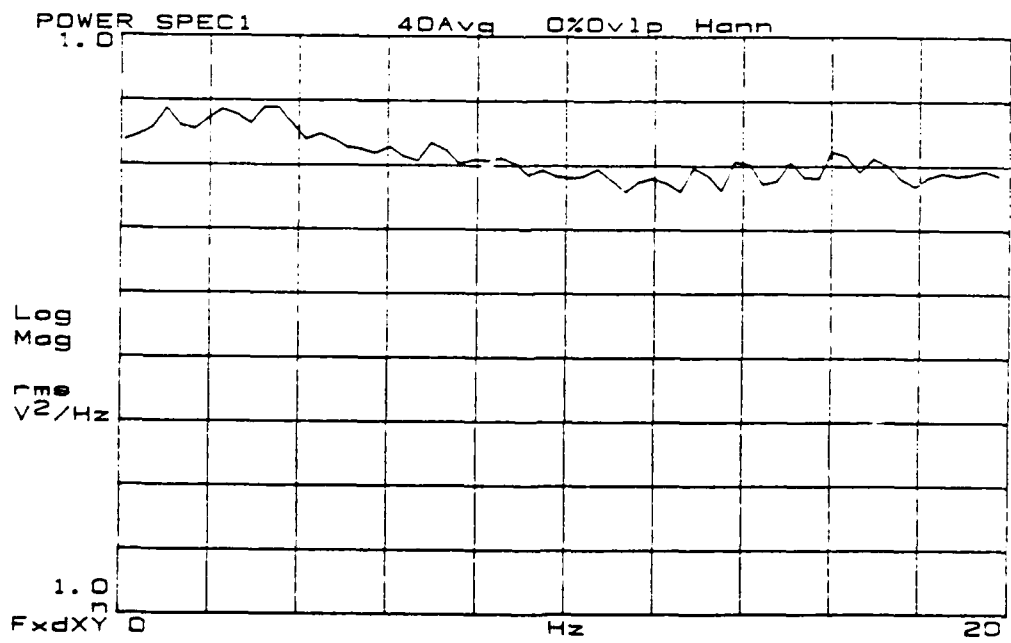
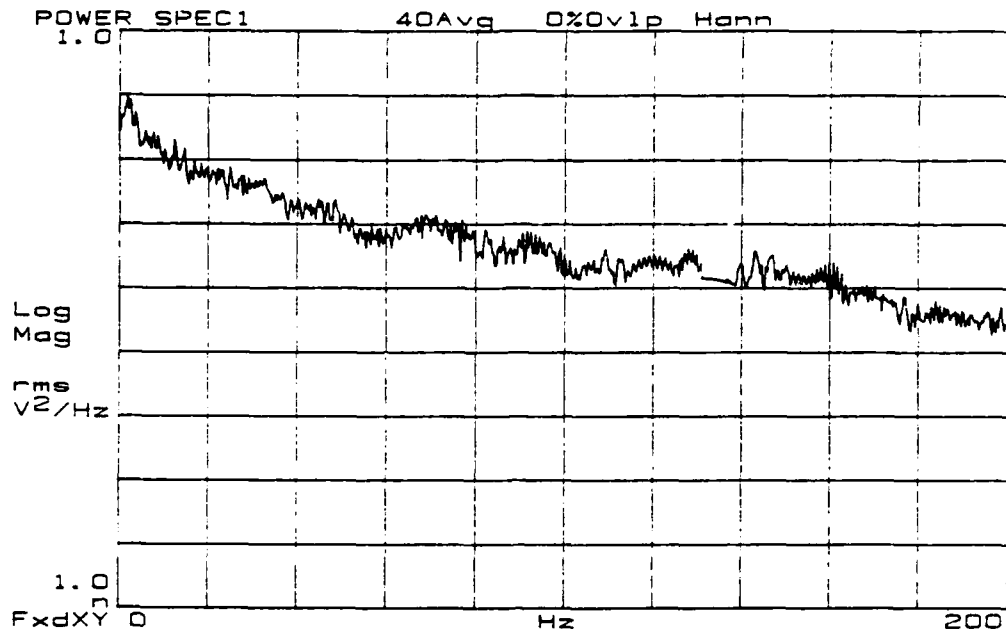


Figure 106. Re = 1742.

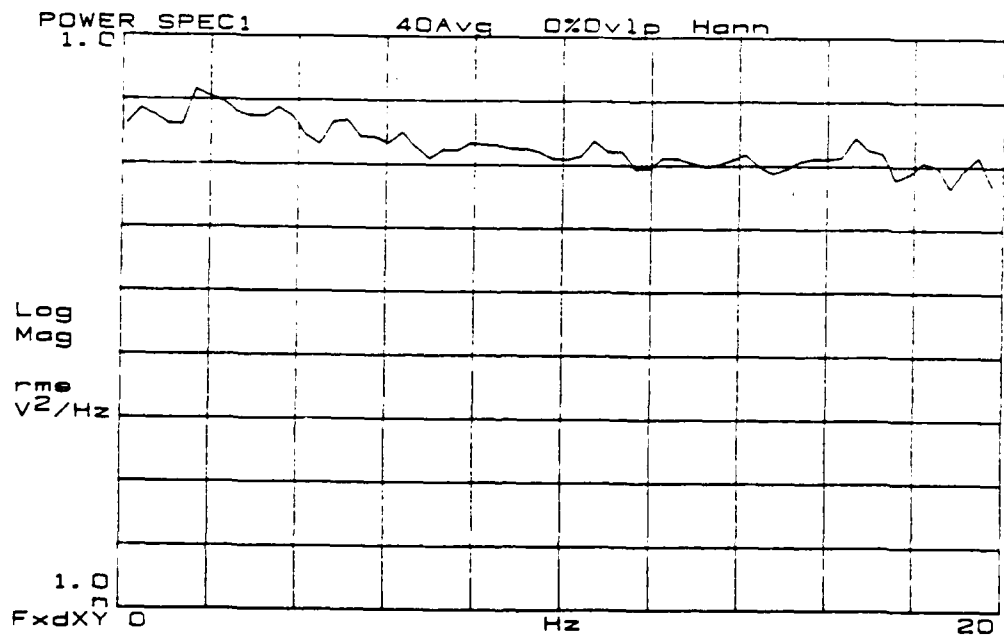
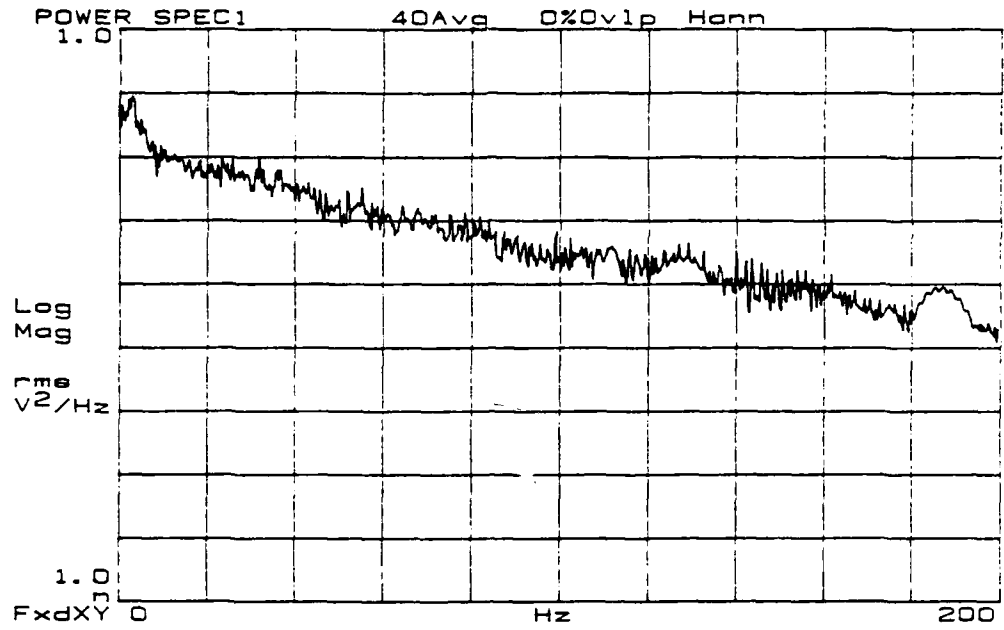


Figure 107. Re = 1796.

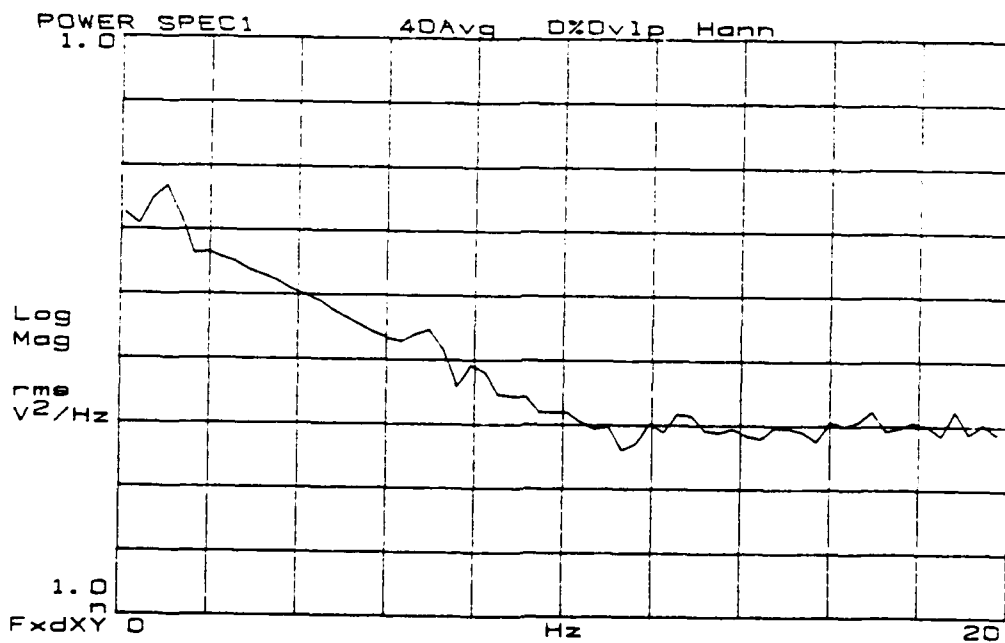
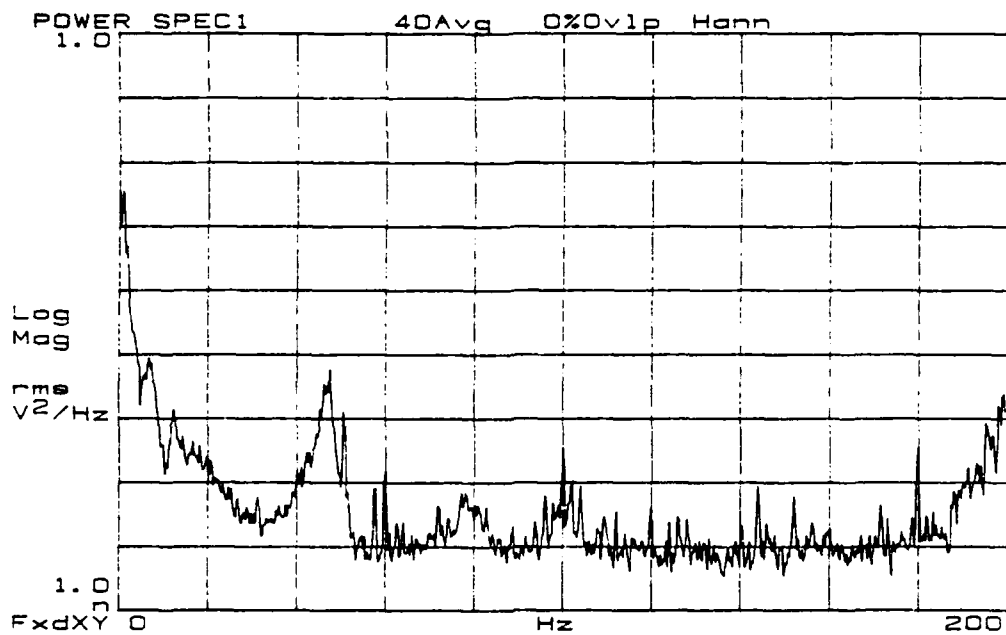


Figure 108.  $Re = 1396$ ,  $f_{osc} = 1$  Hz.



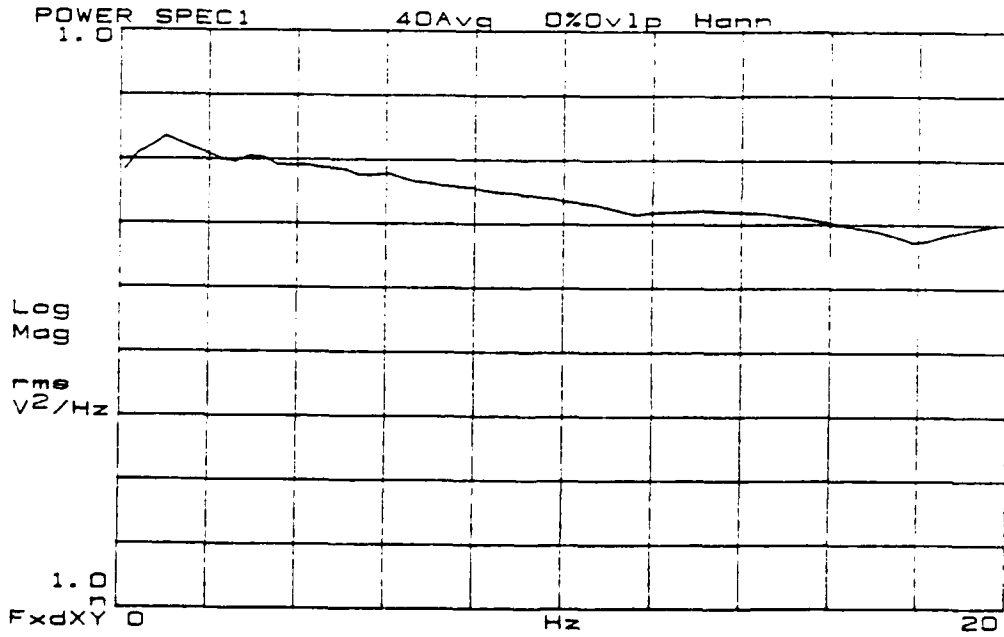
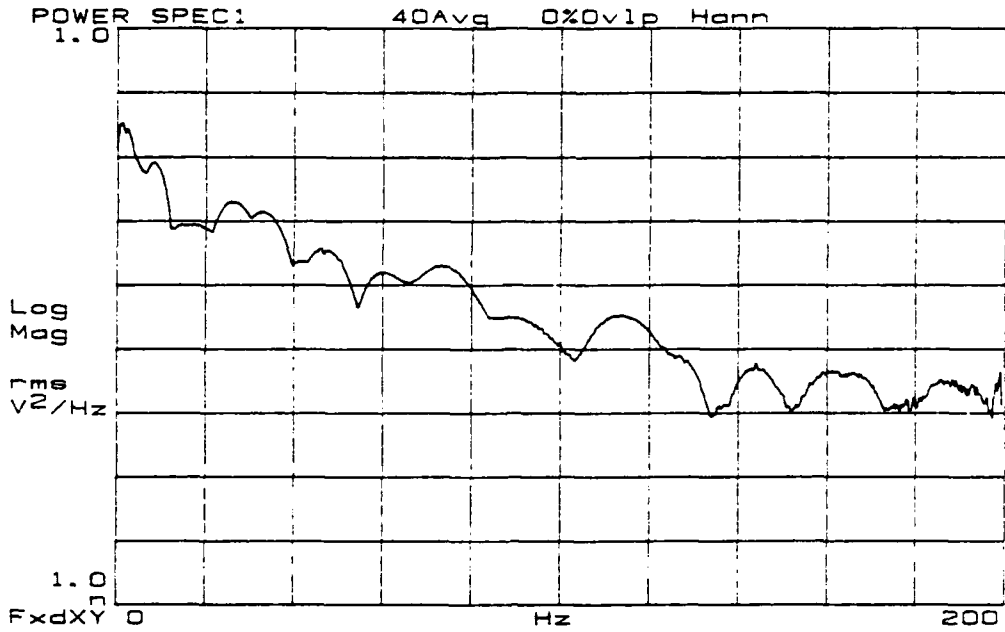


Figure 110.  $Re = 1496$ ,  $f_{osc} = 1$  Hz.

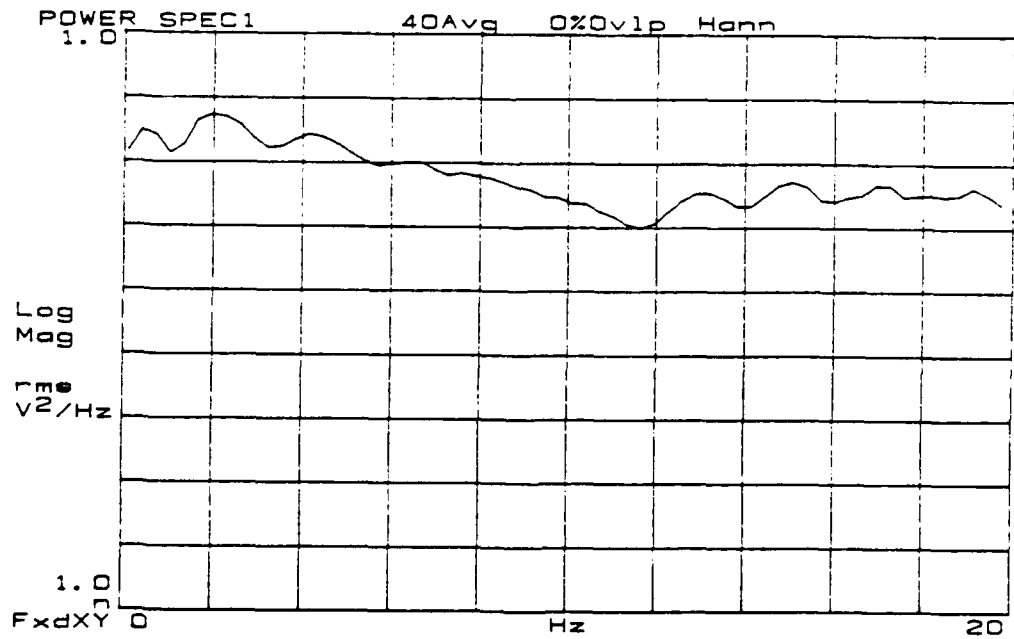
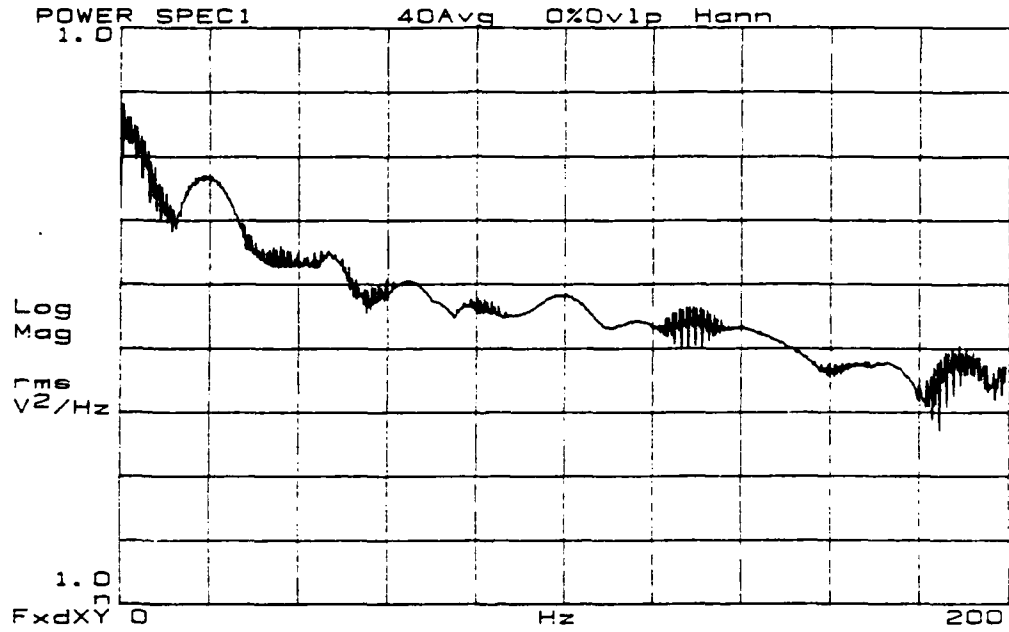


Figure 111.  $Re = 1542$ ,  $f_{osc} = 1$  Hz.



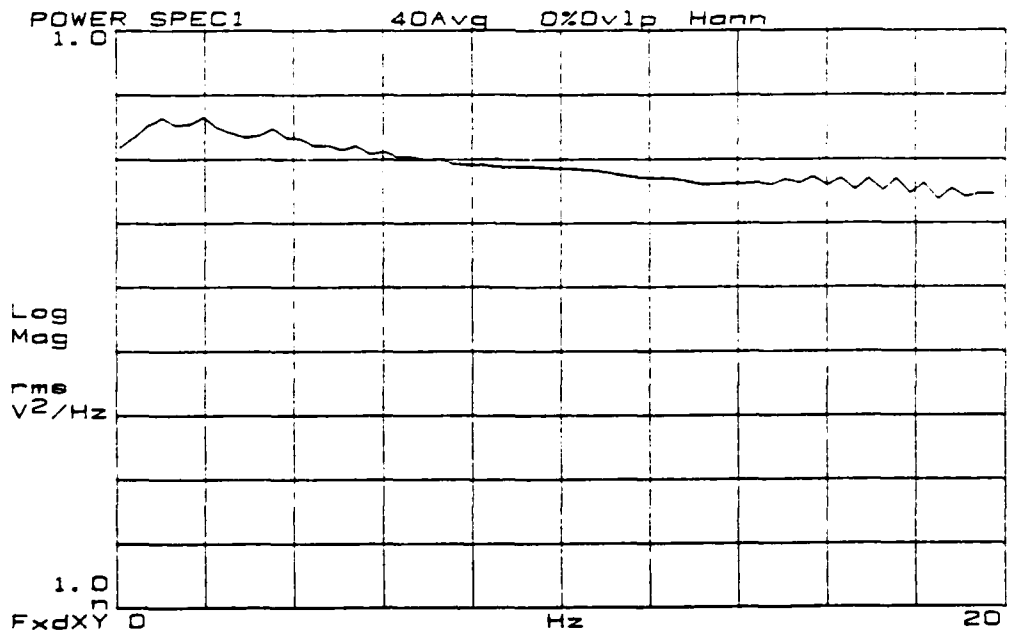
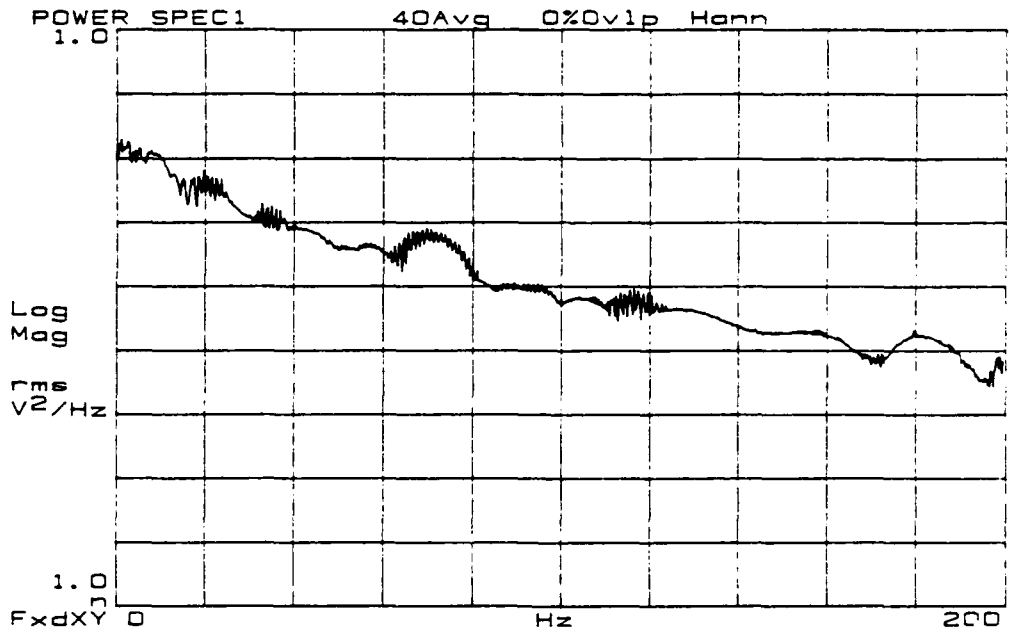


Figure 112.  $Re = 1604$ ,  $f_{osc} = 1$  Hz.



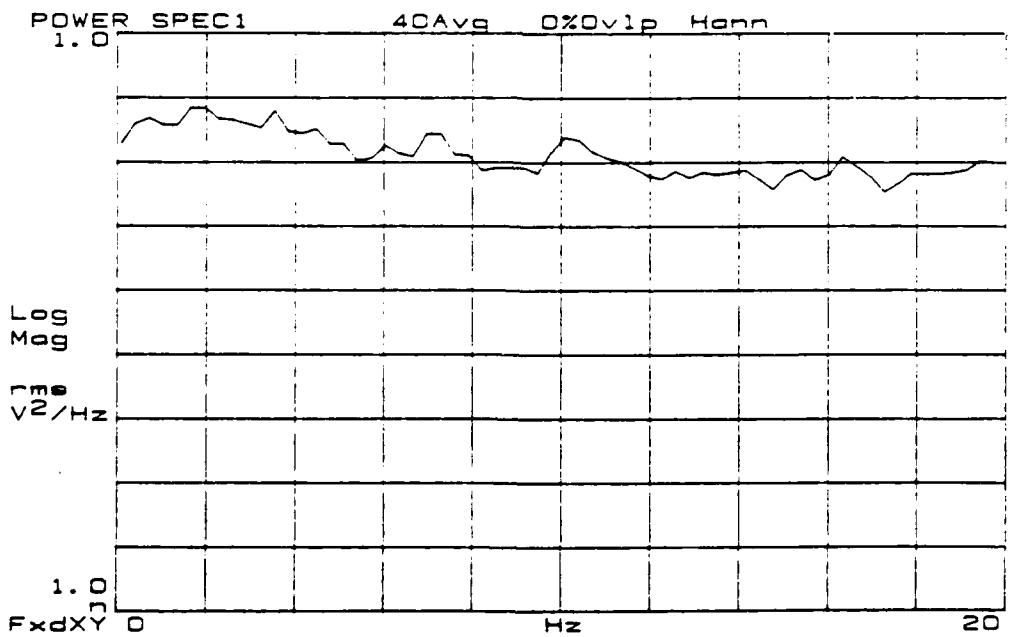
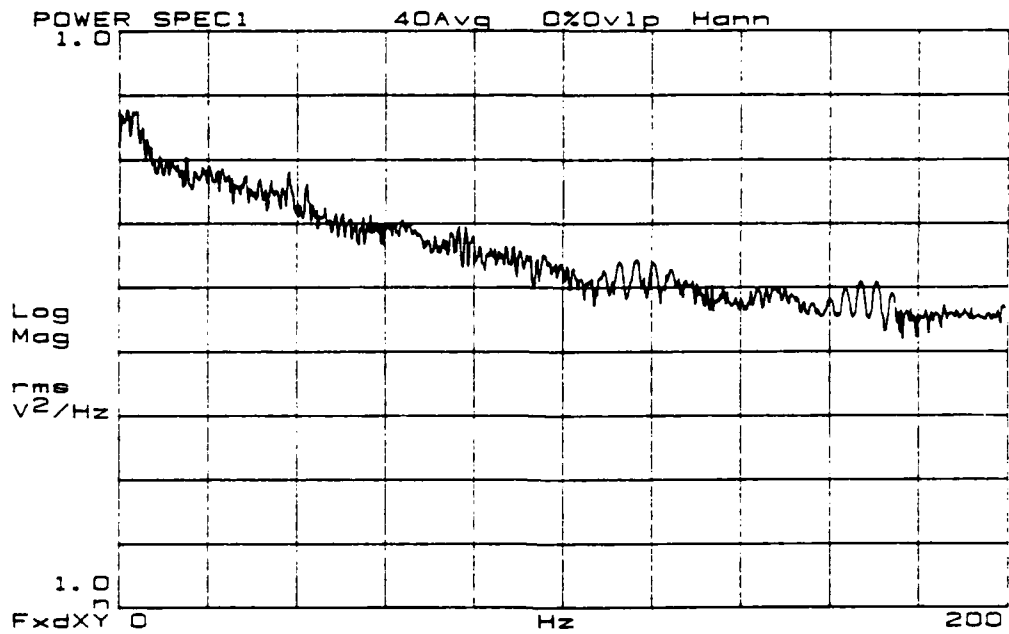


Figure 114.  $Re = 1696$ ,  $f_{osc} = 1$  Hz.

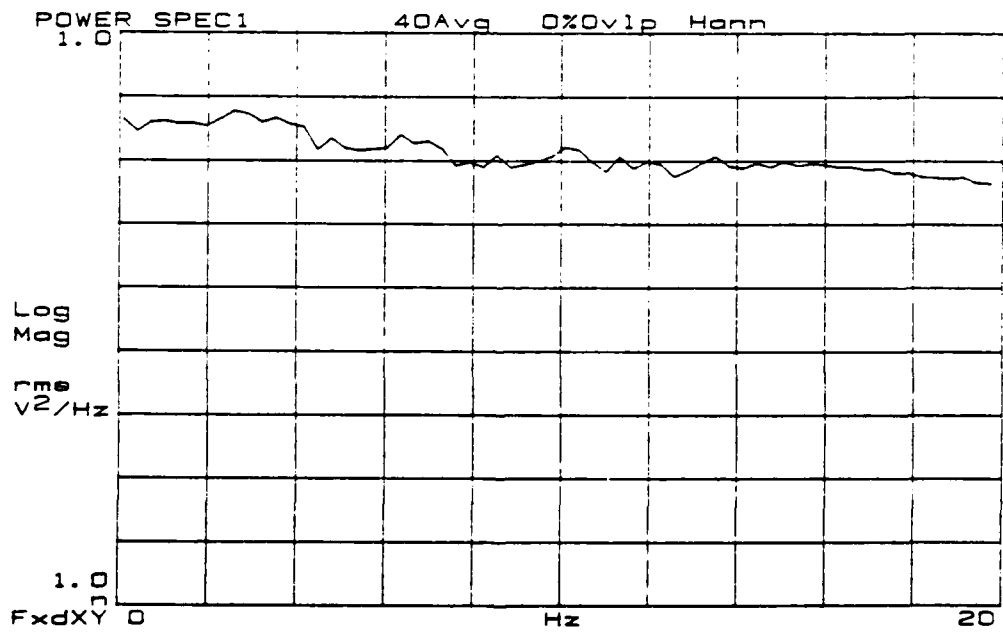
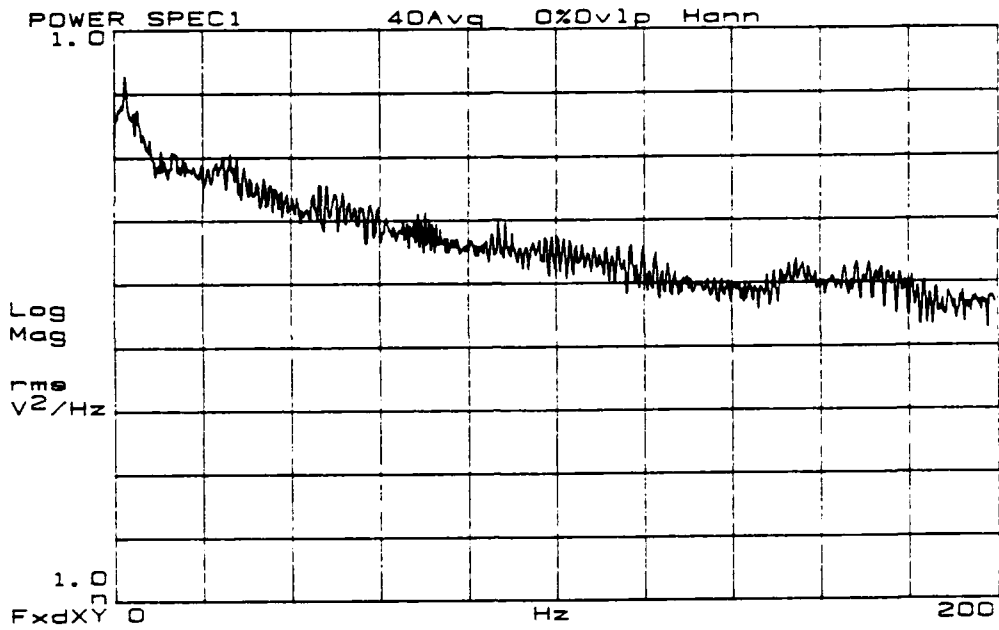


Figure 115.  $Re = 1742$ ,  $f_{osc} = 1$  Hz.

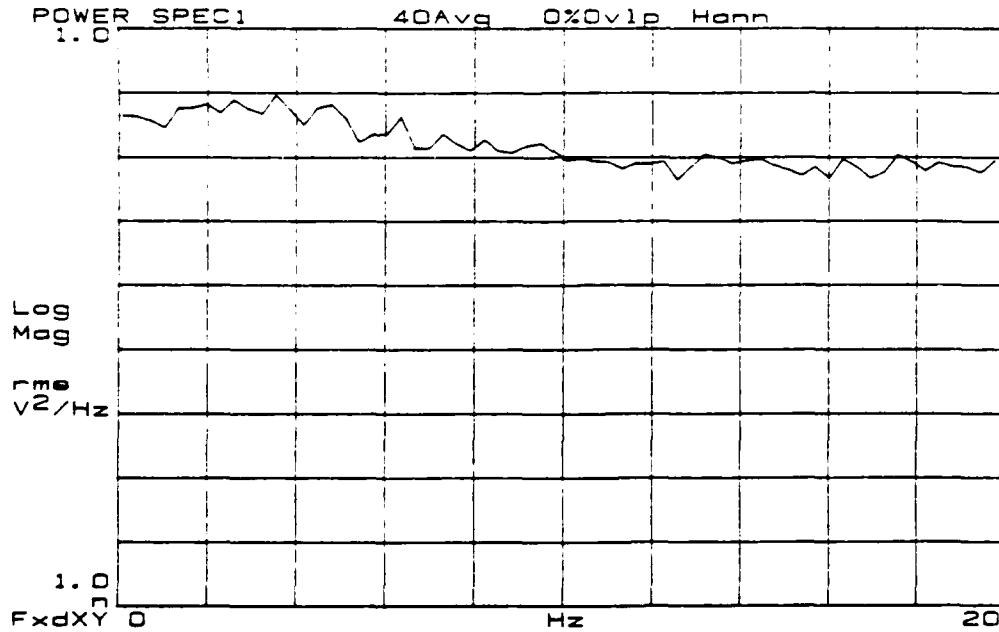
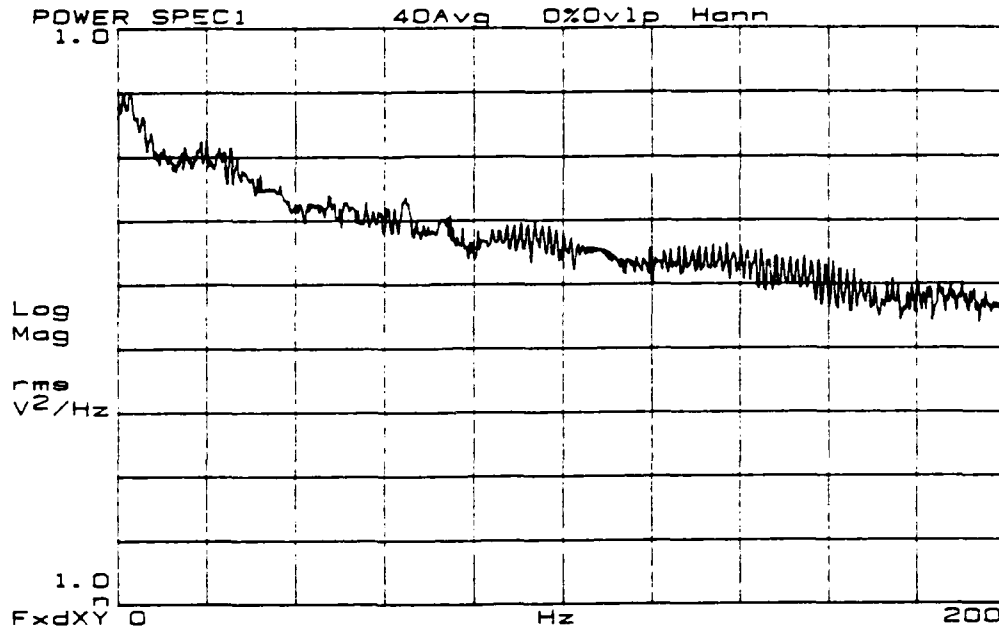


Figure 116.  $Re = 1796$ ,  $f_{osc} = 1$  Hz.

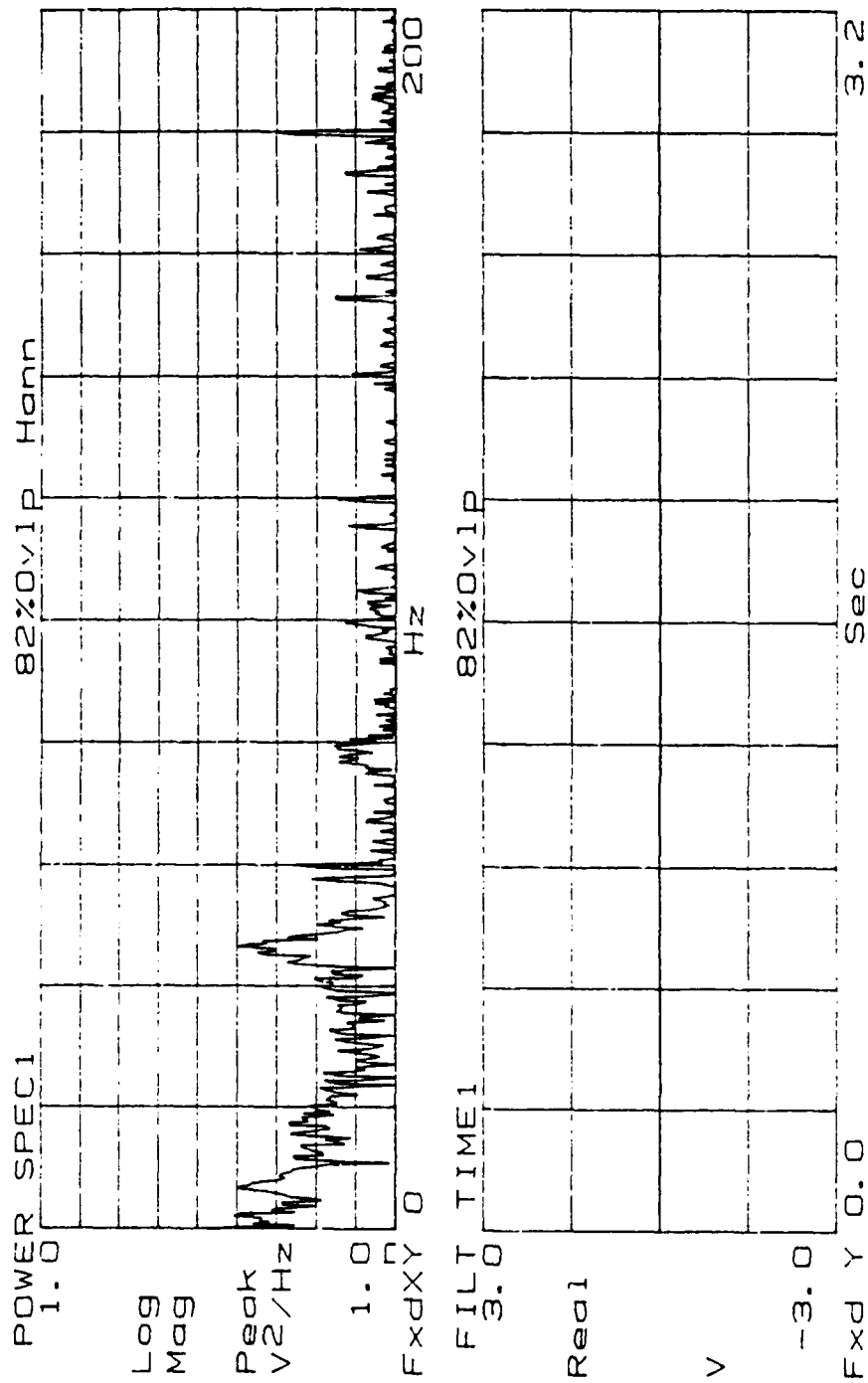


Figure 117. Re = 1396.

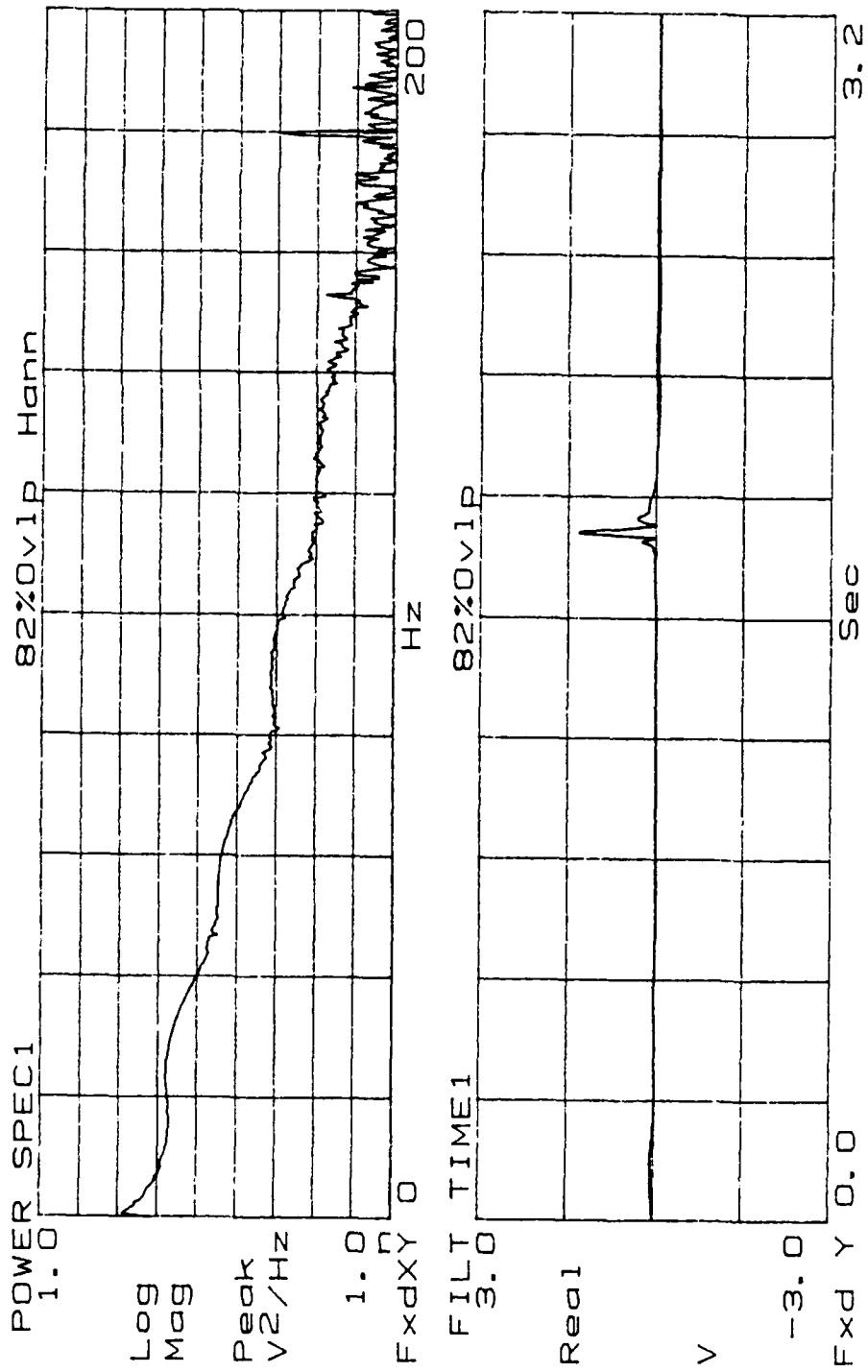


Figure 118. Re = 1454.

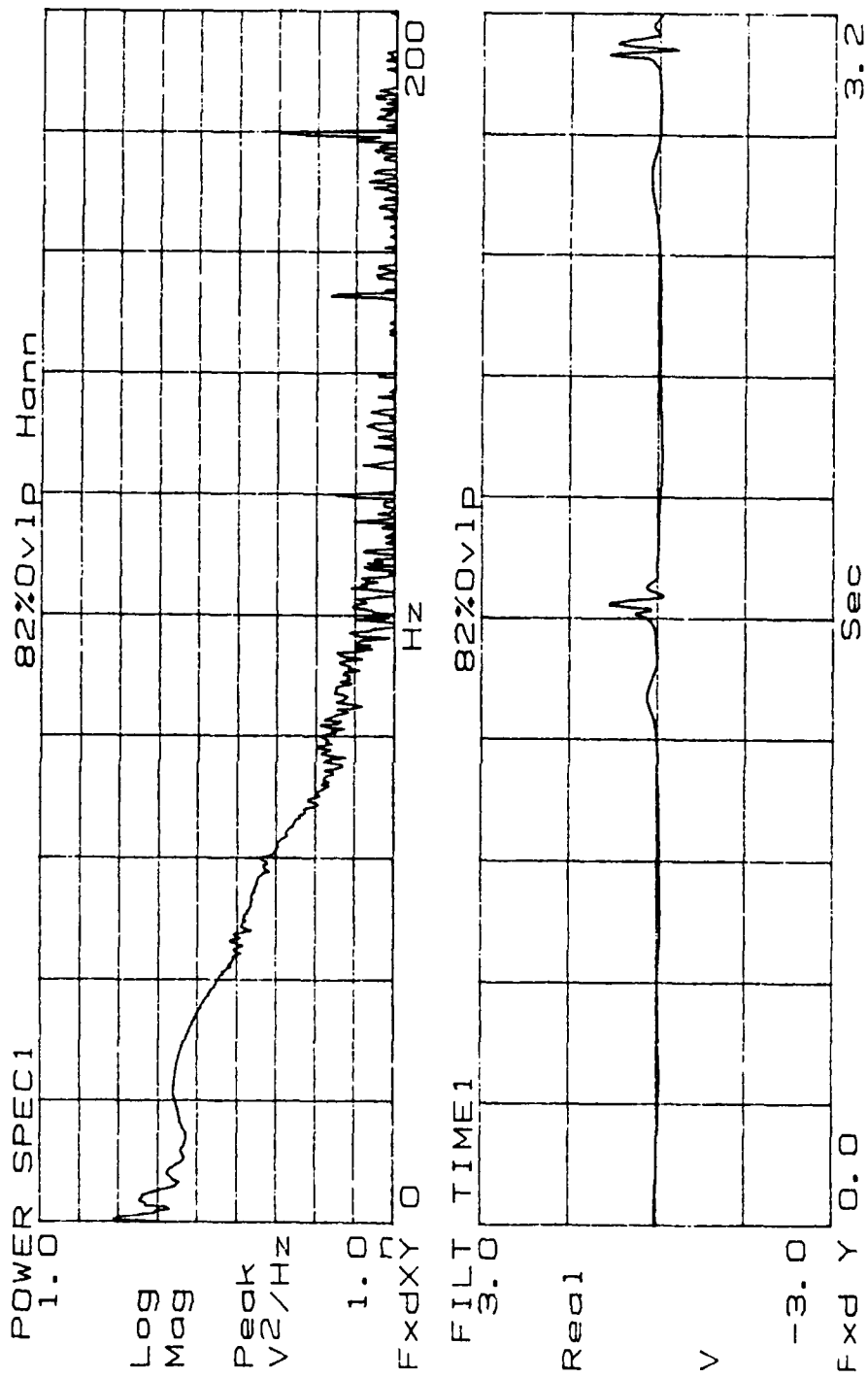


Figure 119. Re = 1496.



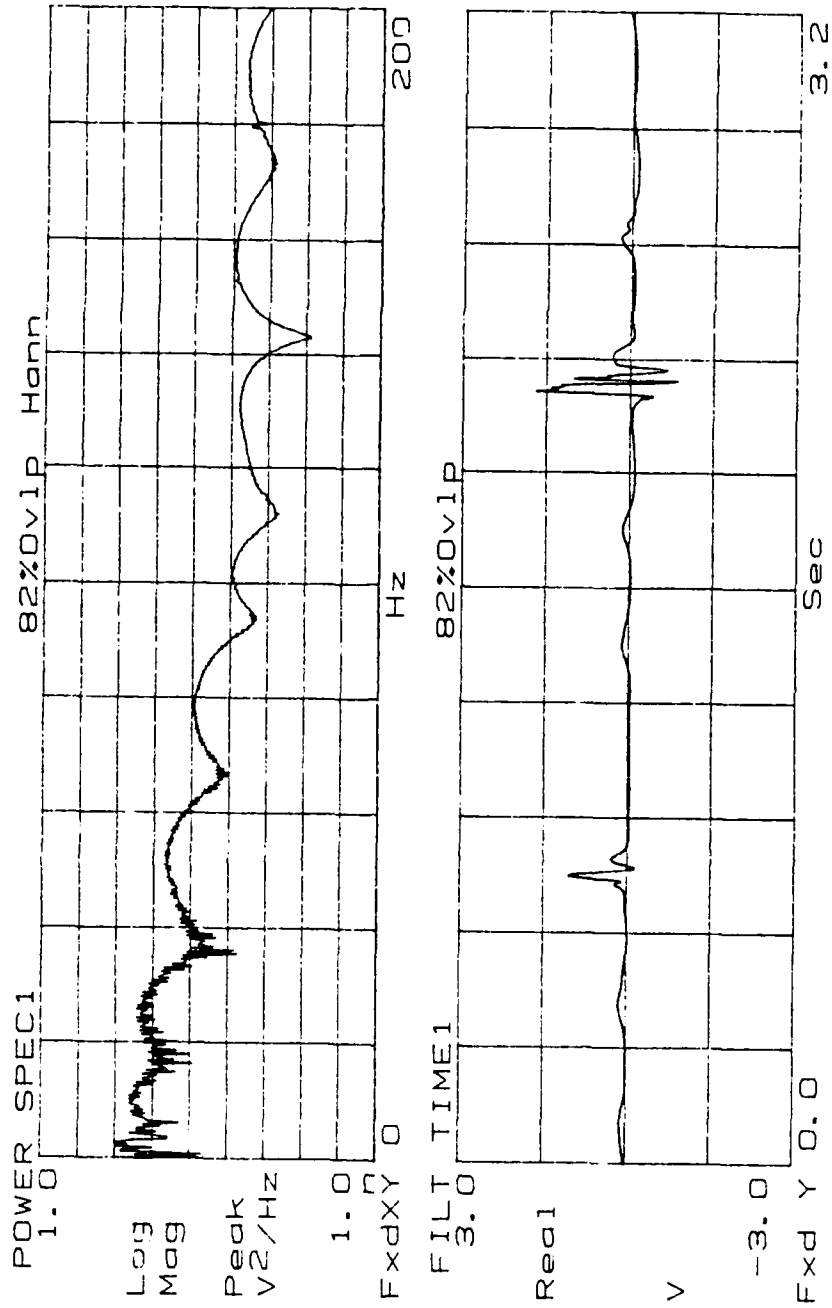


Figure 120. Re = 1542.

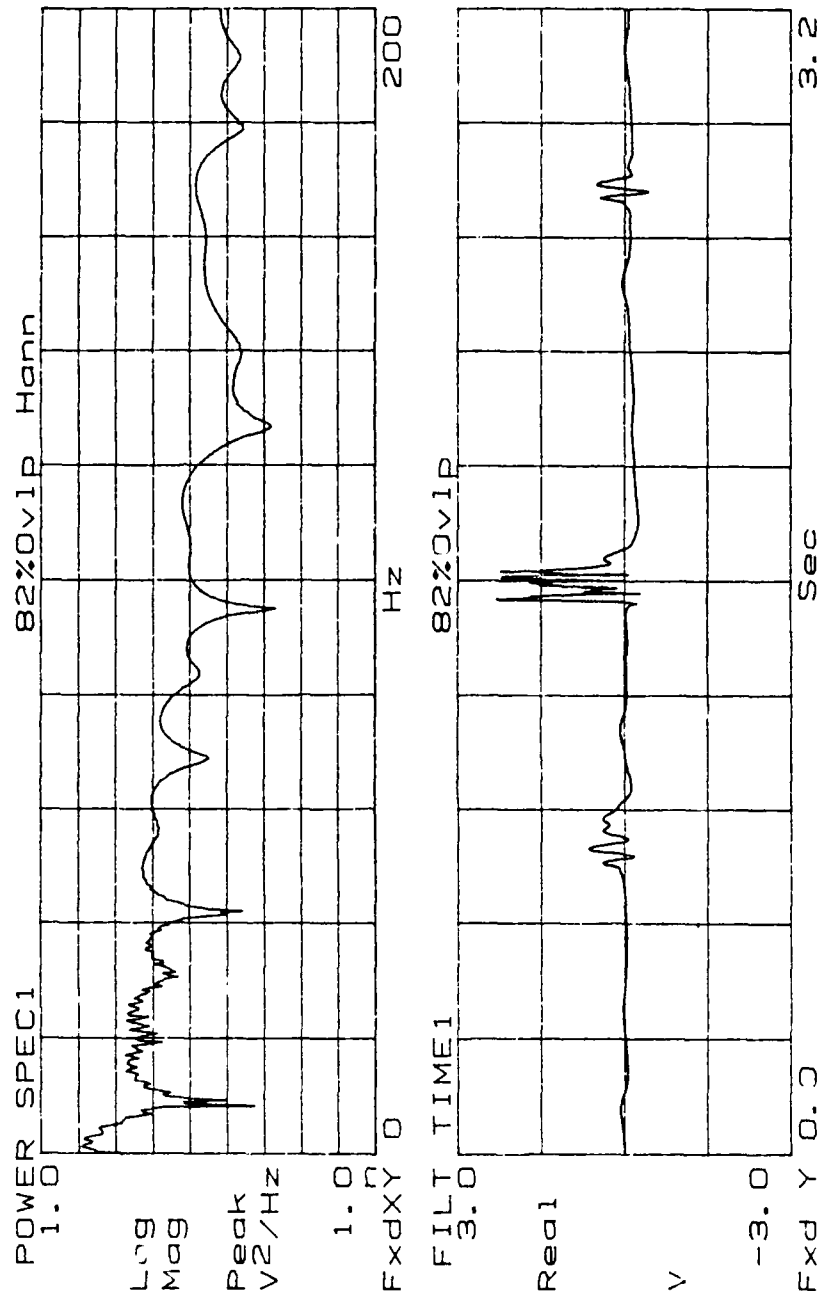


Figure 121. Re = 1604.

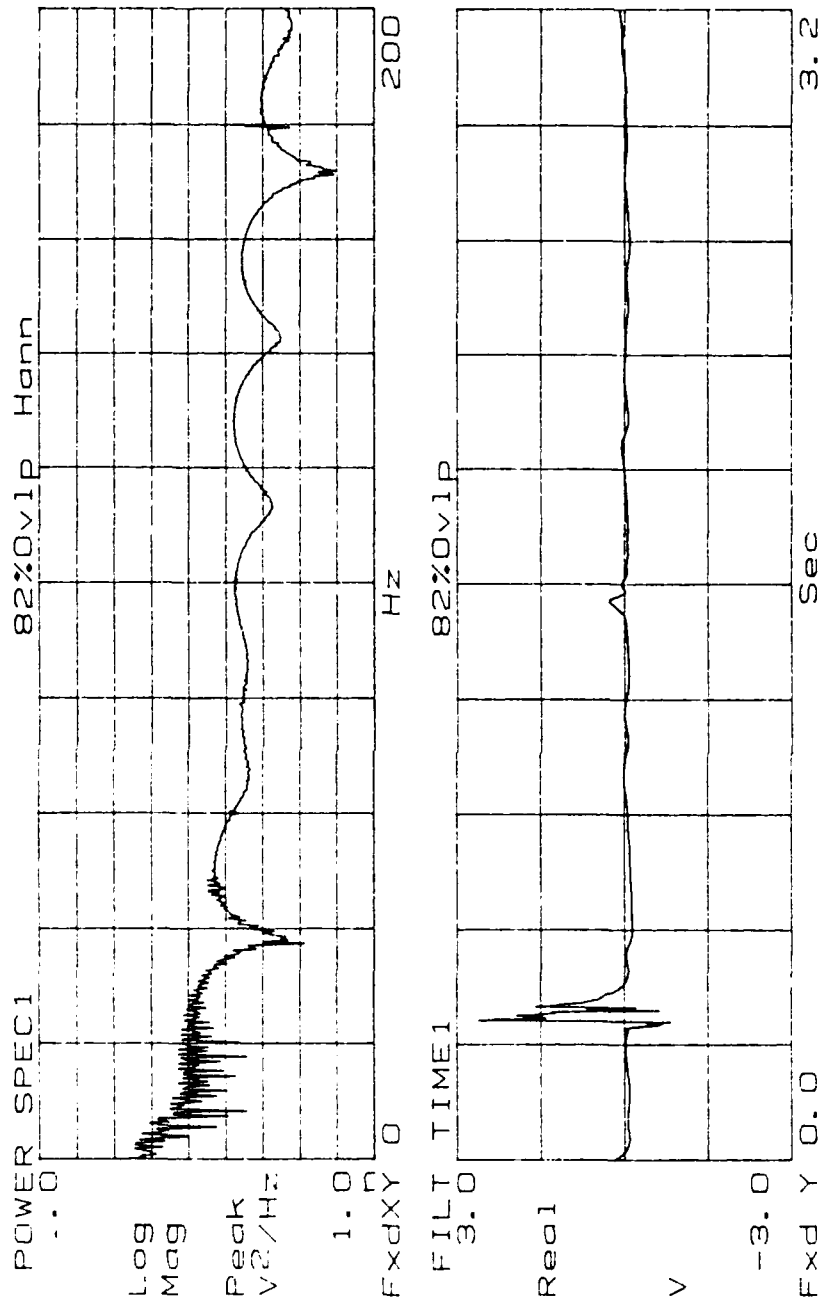


Figure 122. Re = 1650.

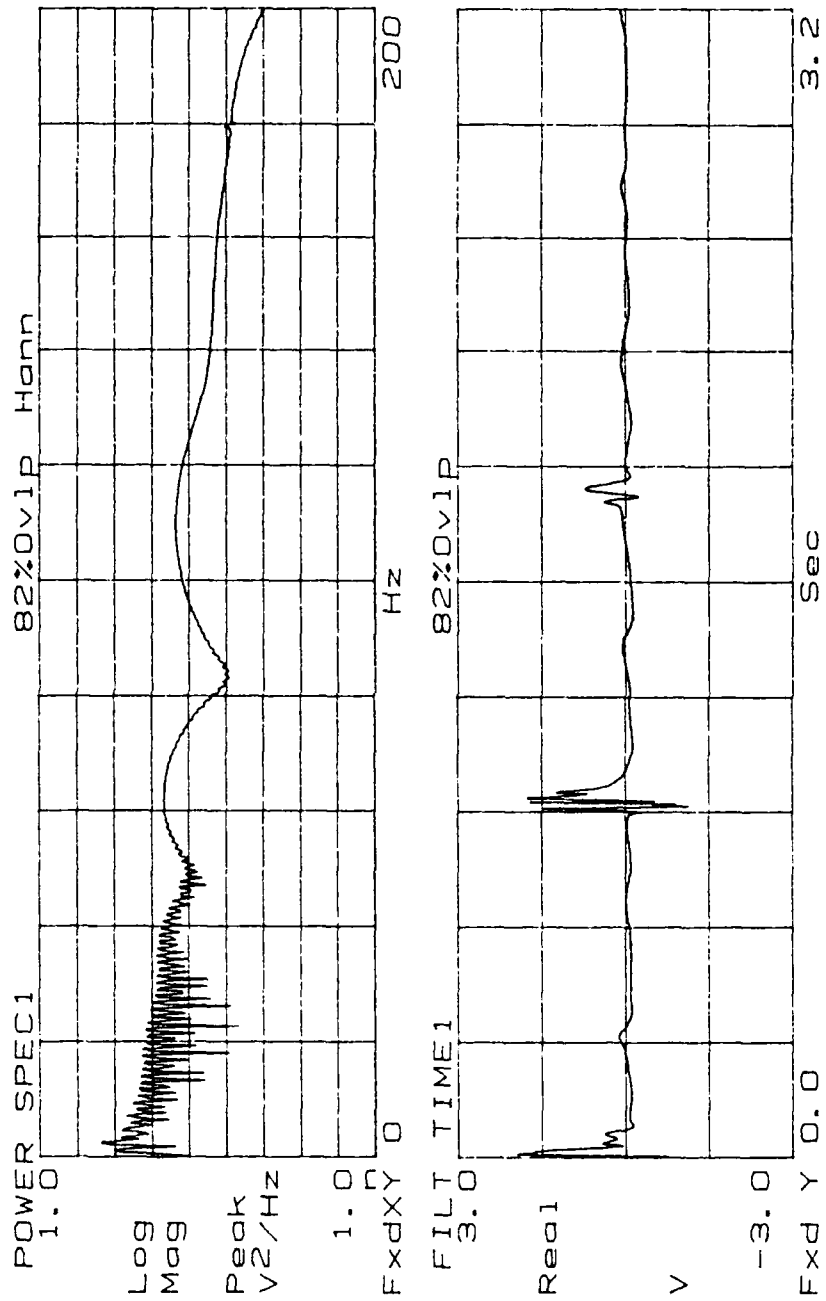


Figure 123. Re = 1697.

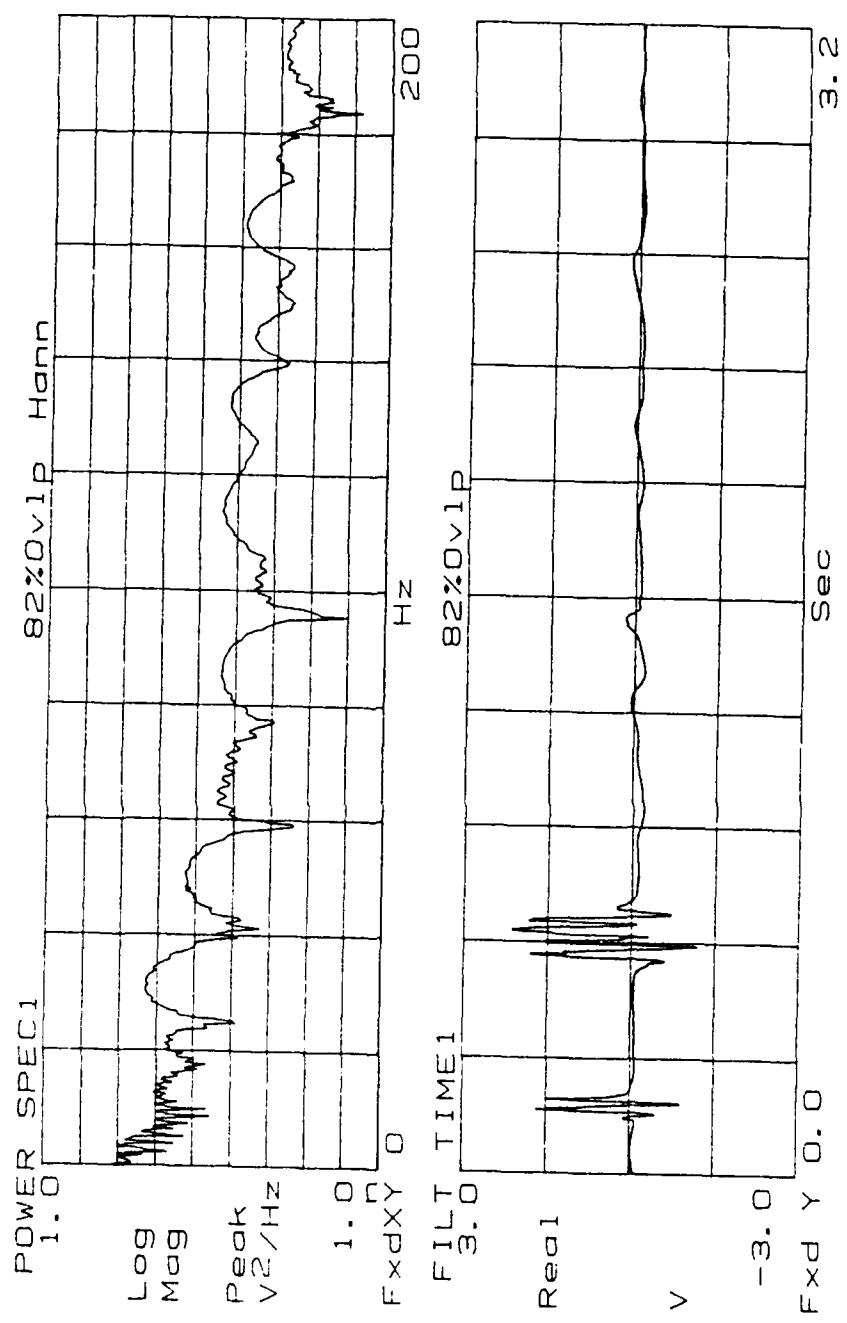


Figure 124. Re = 1742.

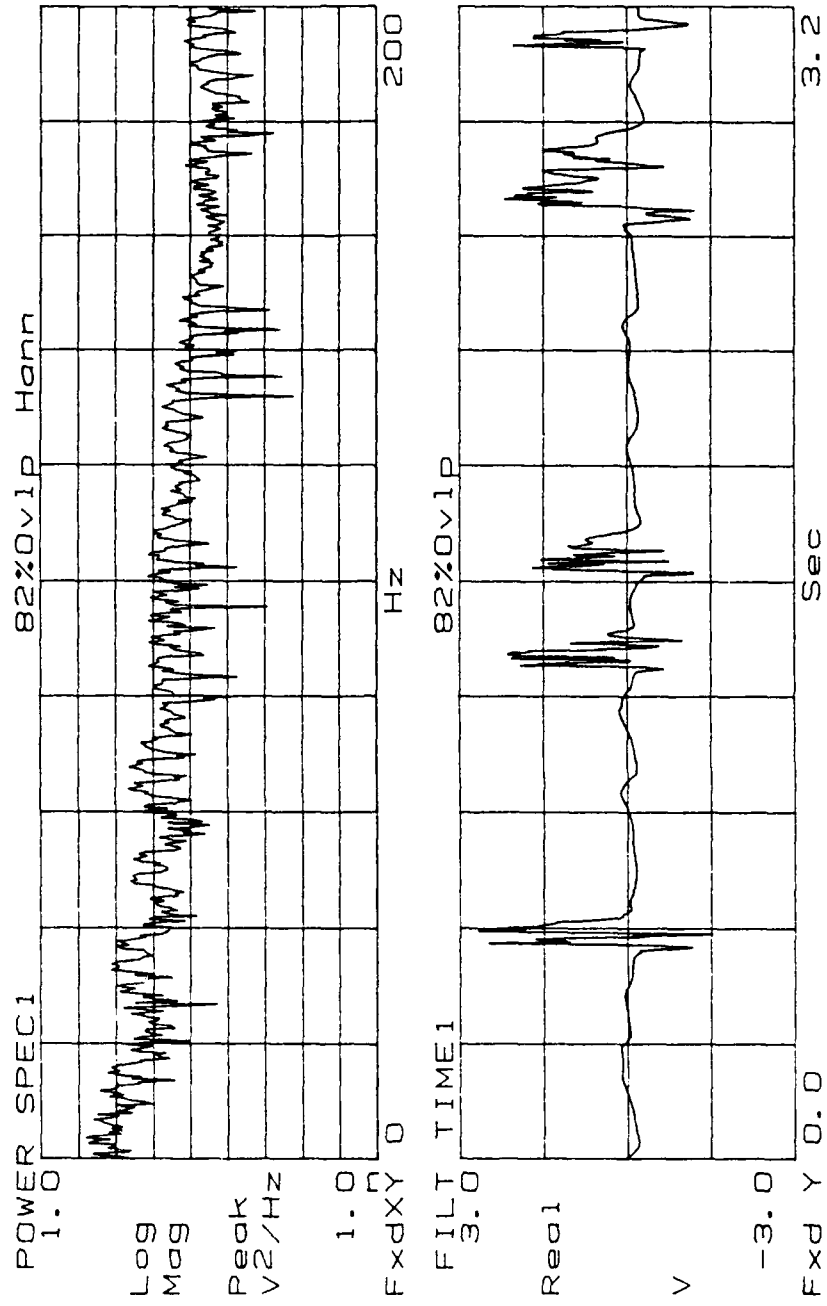


Figure 125. Re = 1796.

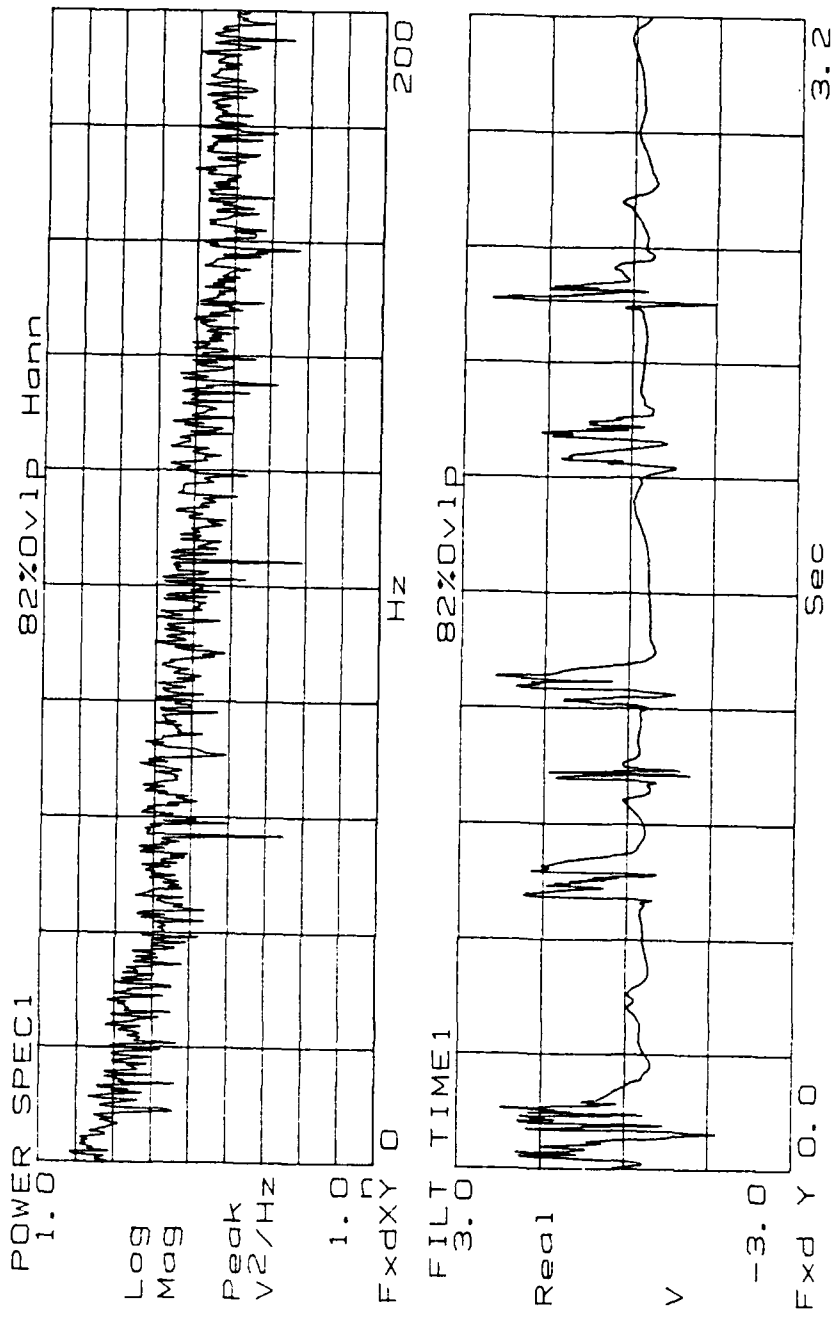


Figure 126. Re = 1905.

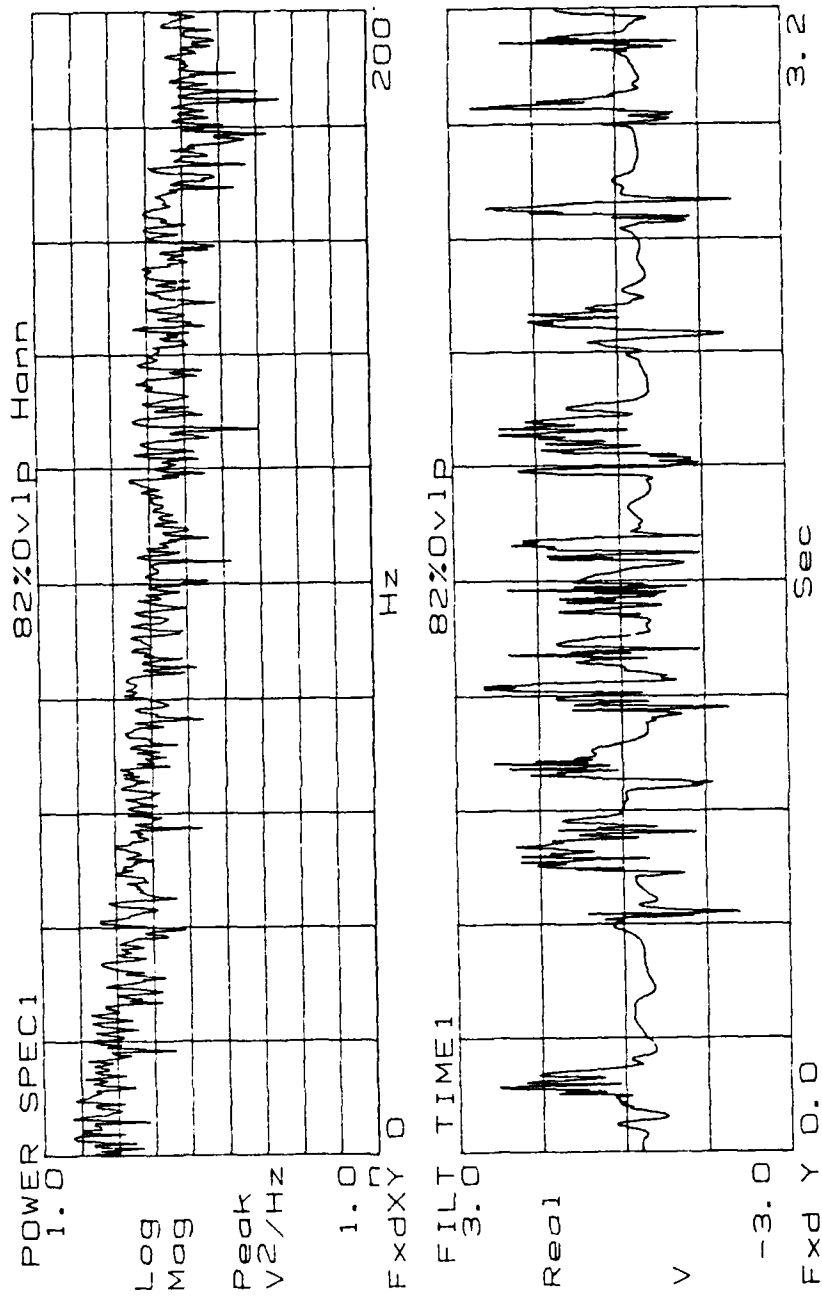


Figure 127. Re = 2005.



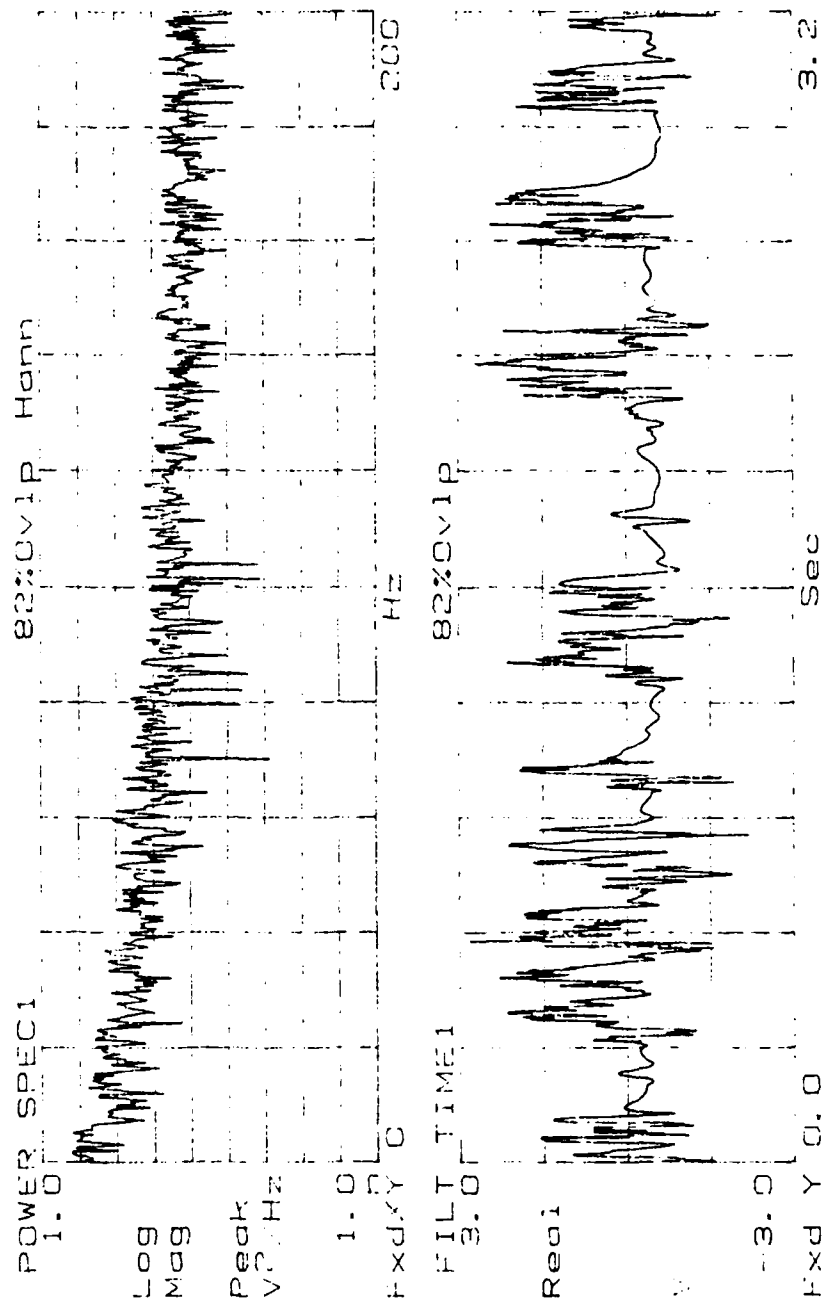


Figure 128. Re = 2097.

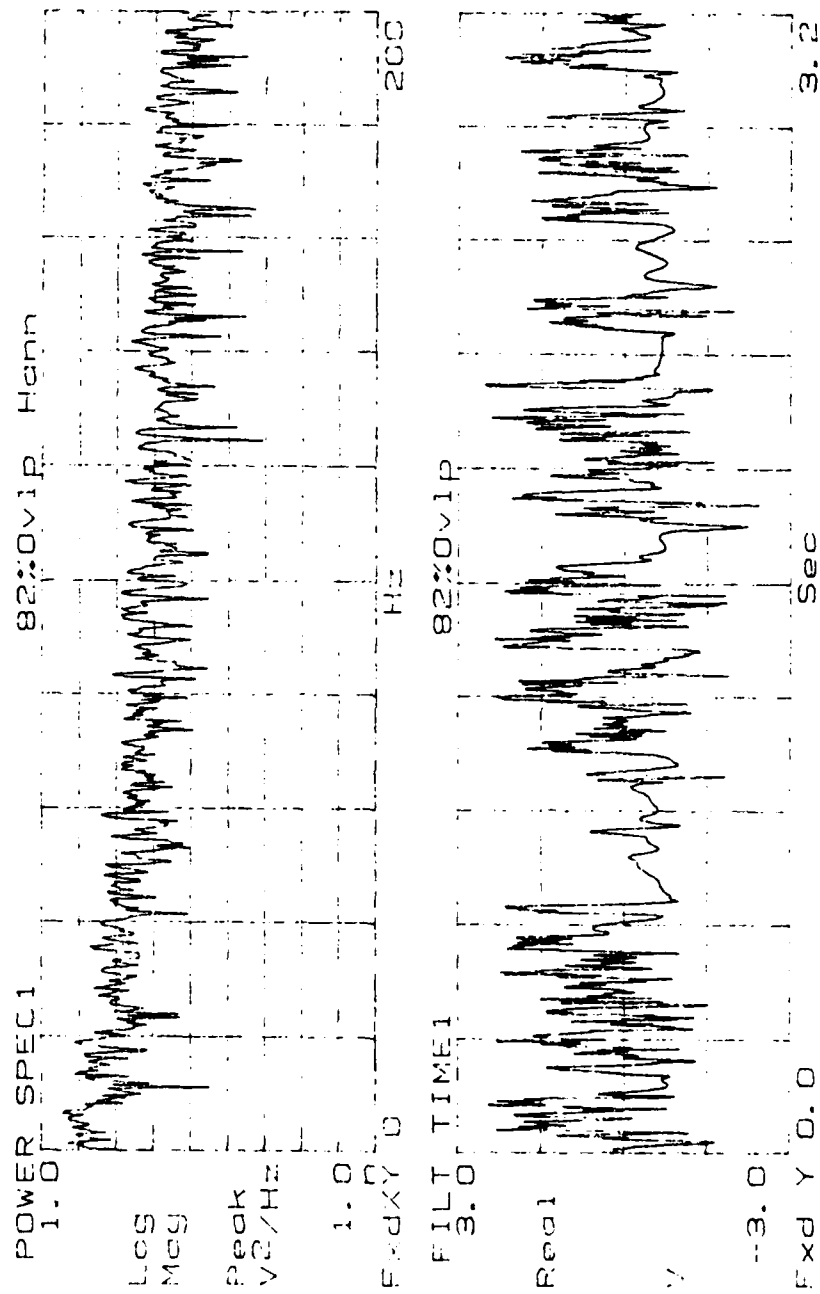


Figure 129. Re = 2198.

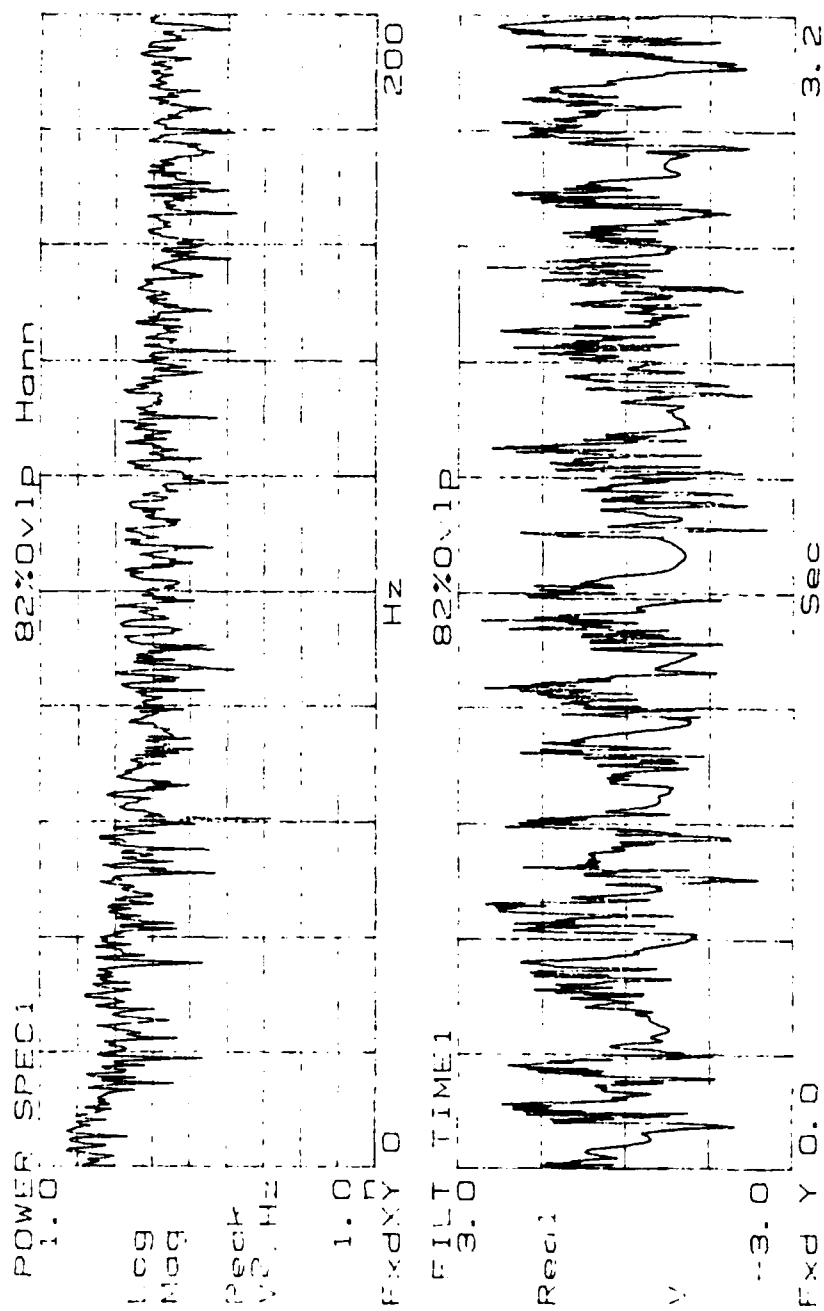


Figure 130. Re = 2298.

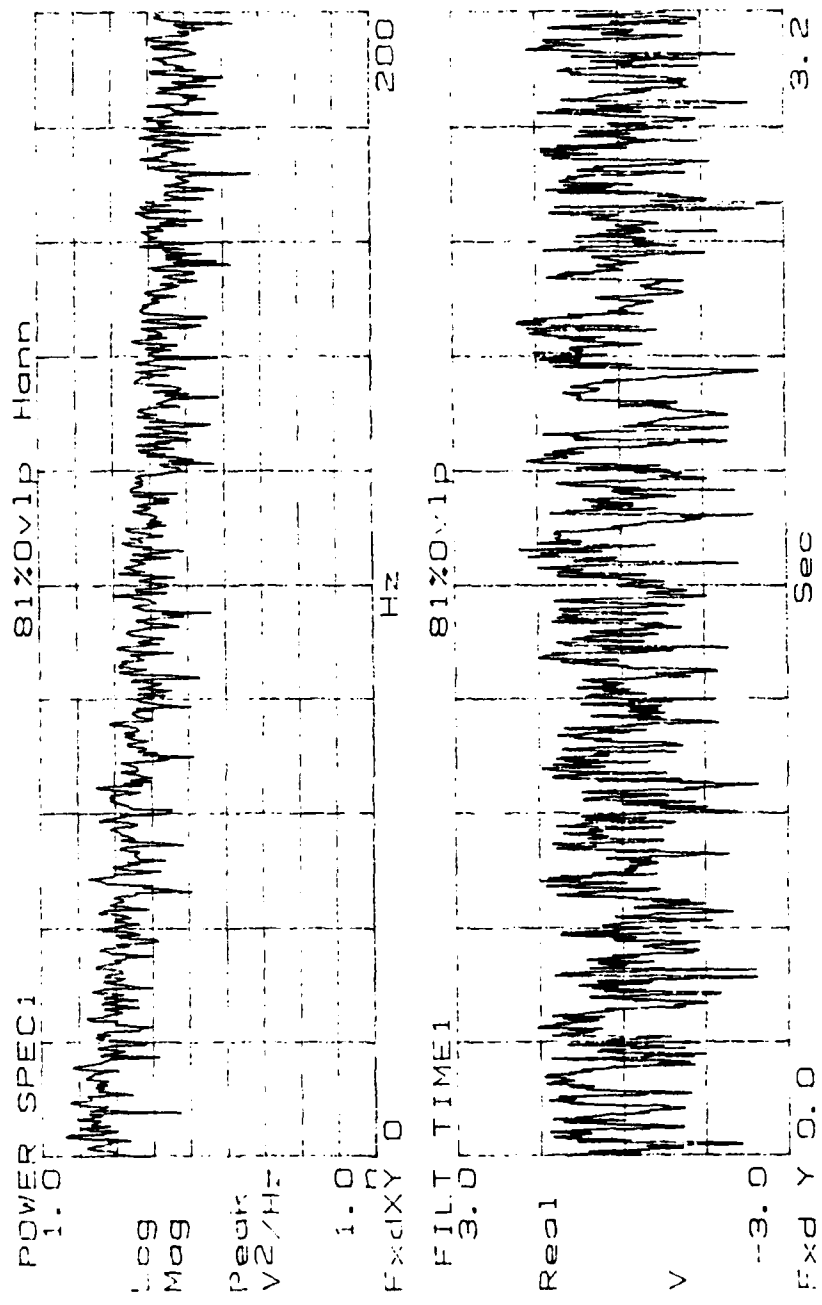


Figure 131. Re = 2402.

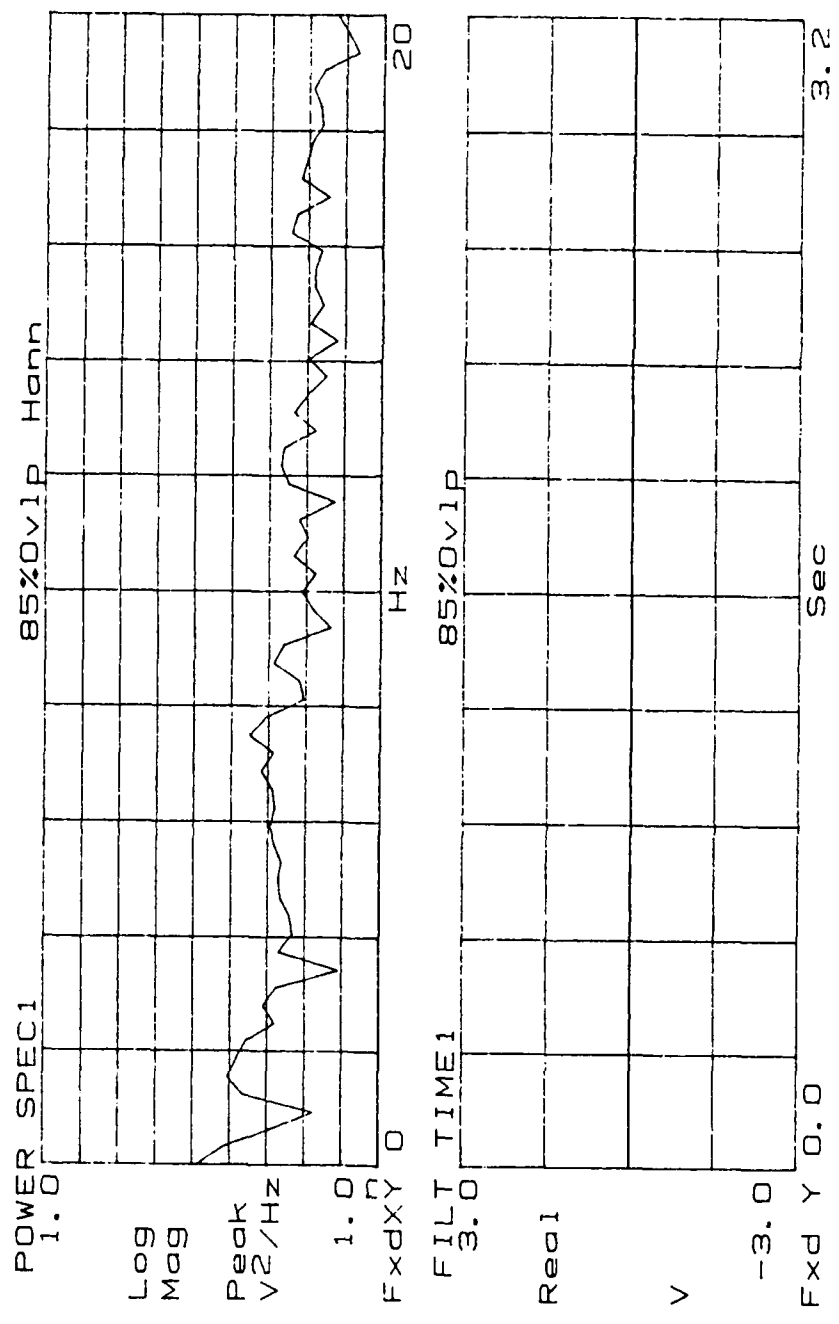


Figure 132. Re = 1396.

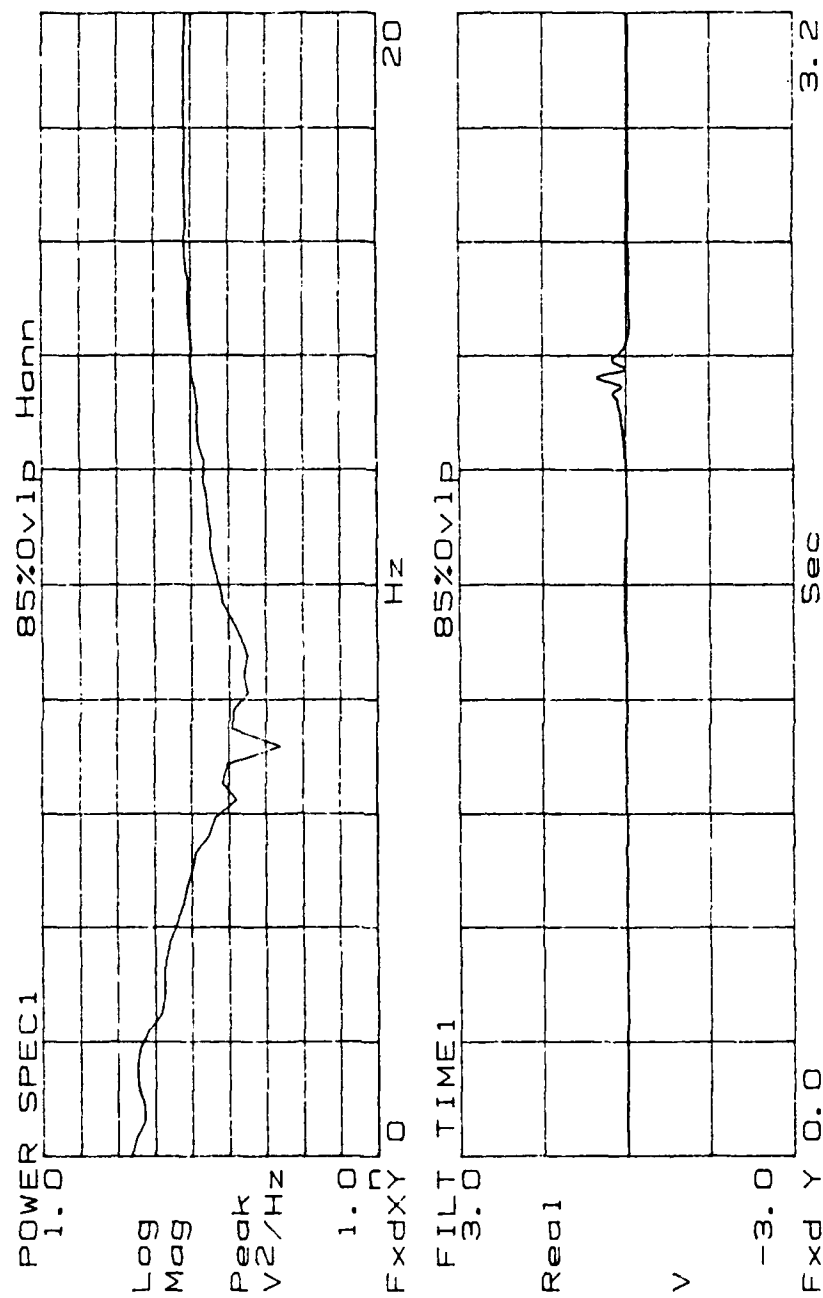


Figure 133. Re = 1454.

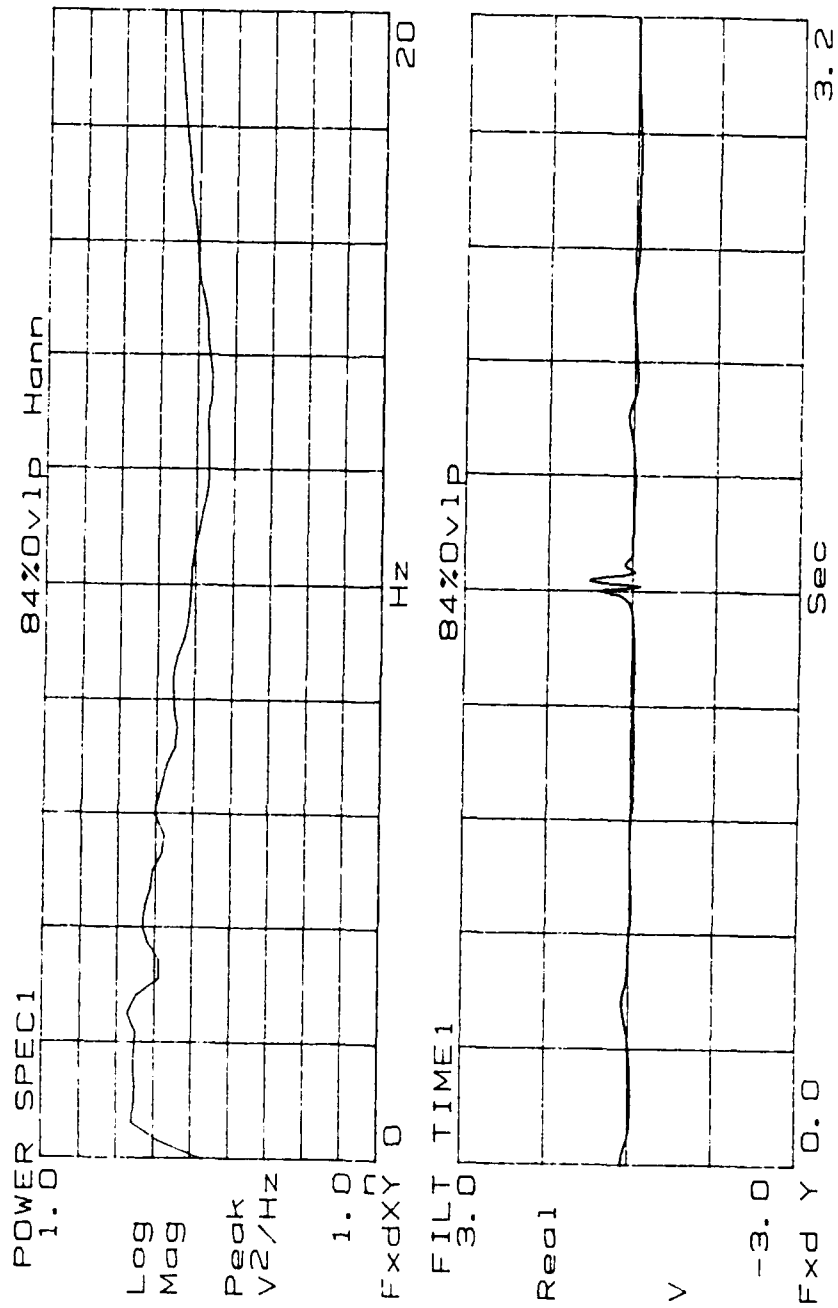


Figure 134. Re = 1496.

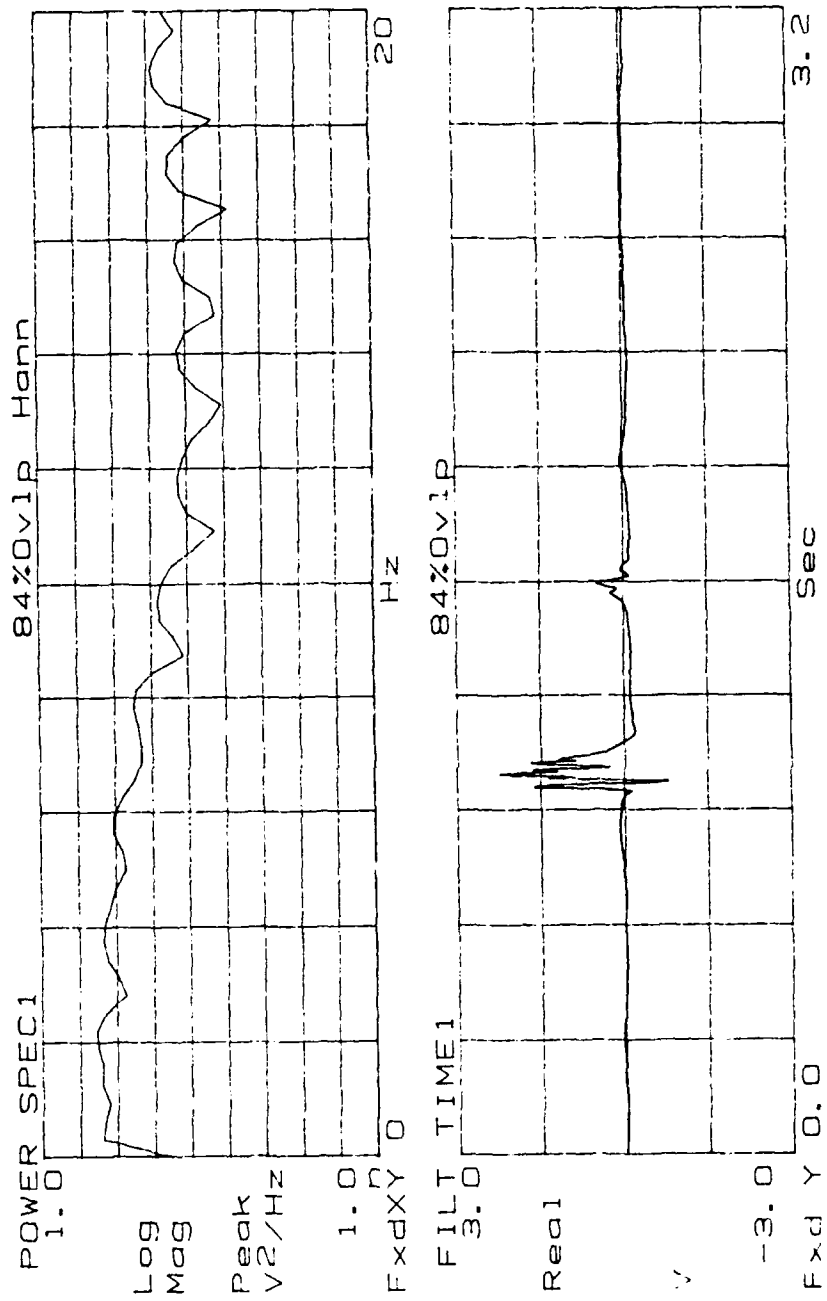


Figure 135. Re = 1542.



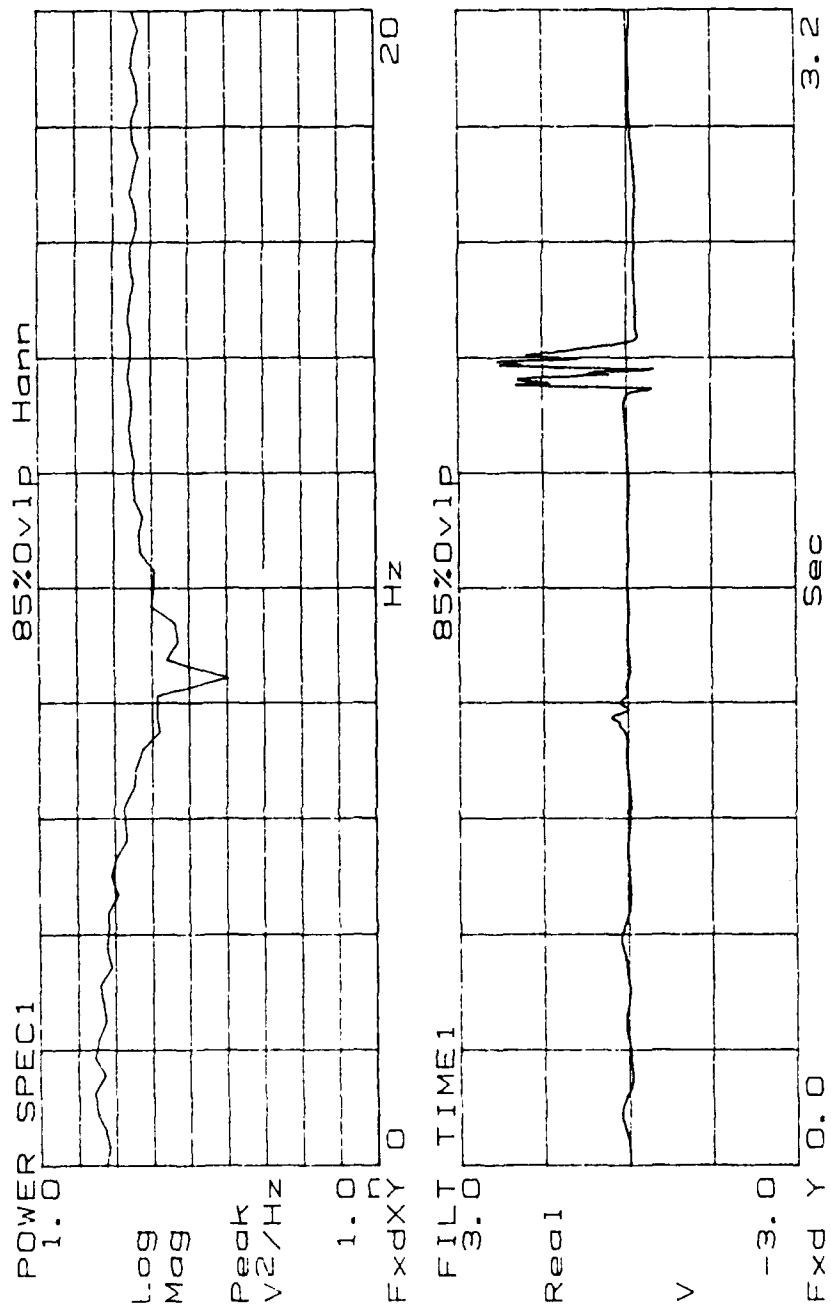


Figure 136. Re = 1604.

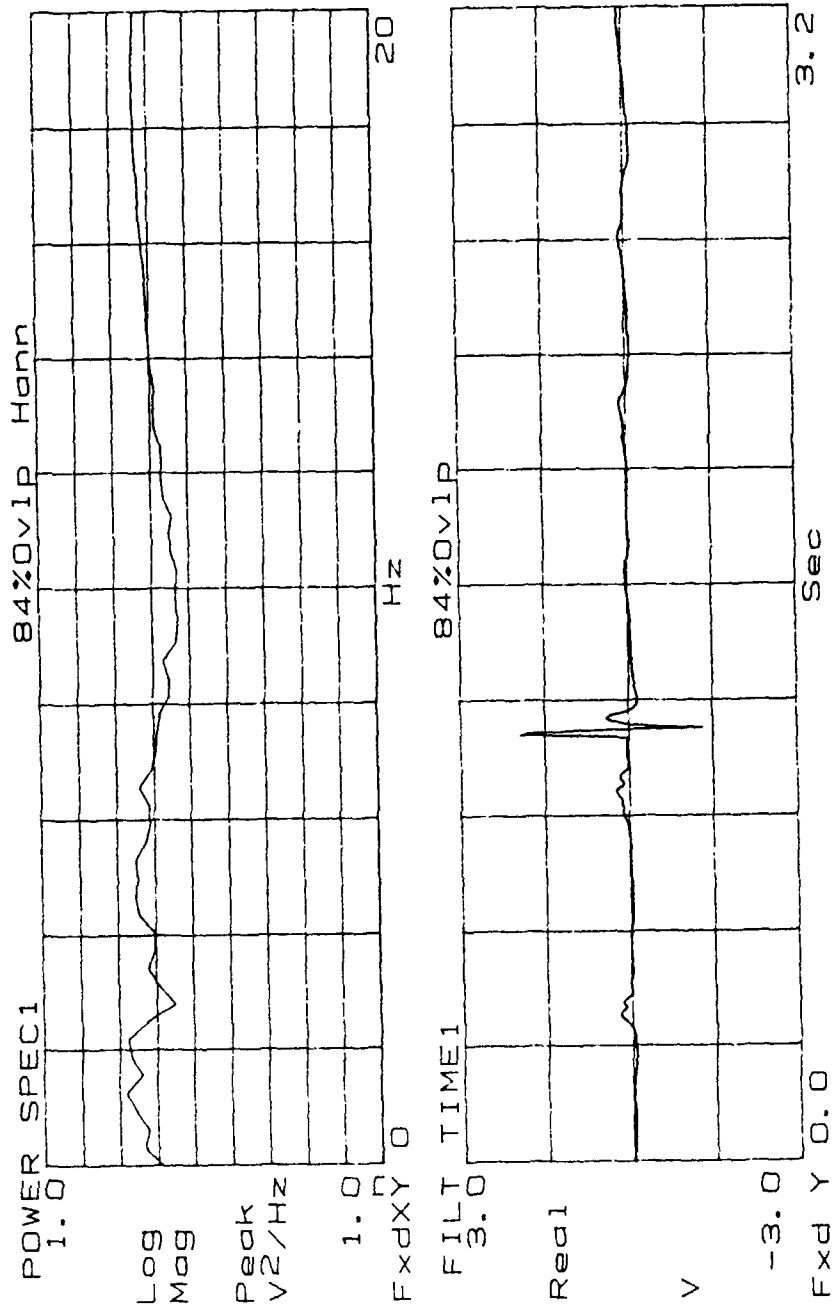


Figure 137. Re = 1650.

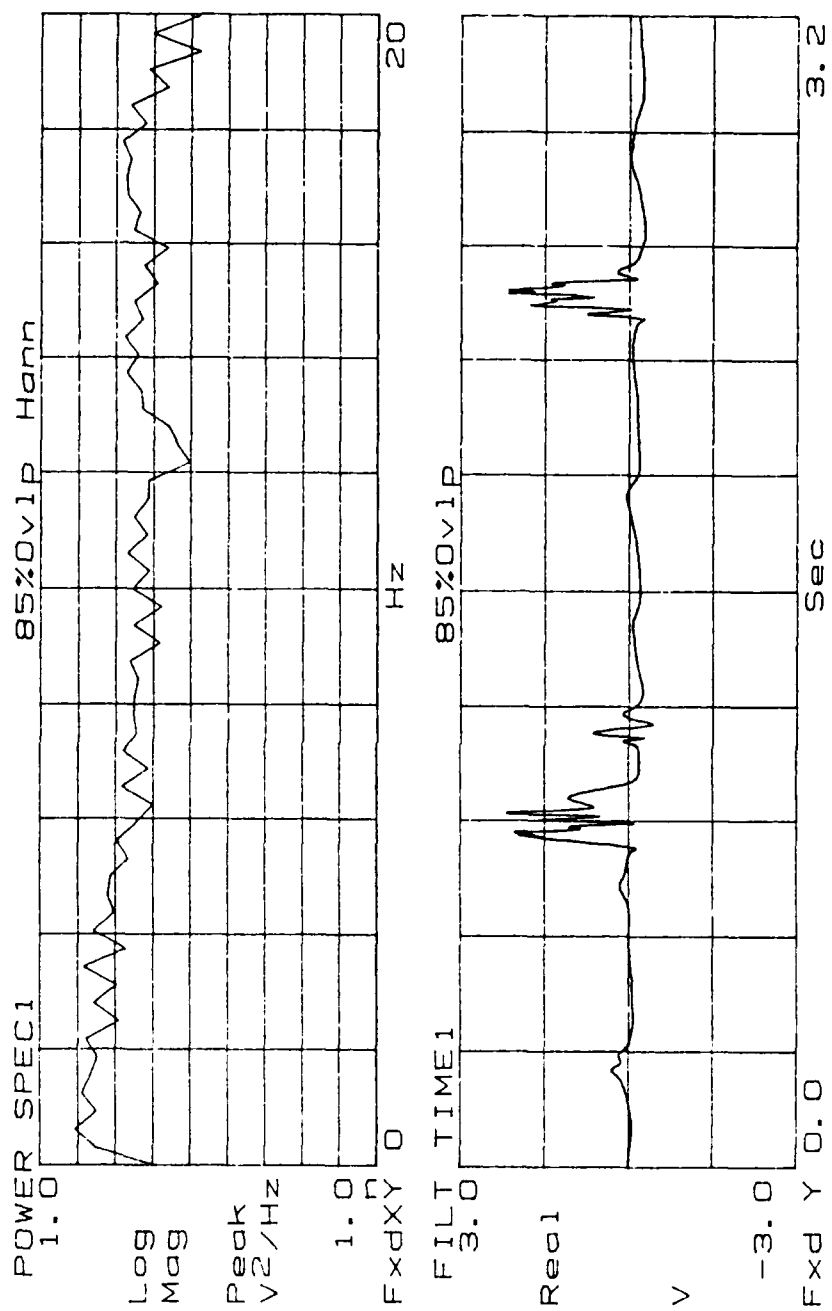


Figure 138. Re = 1697.

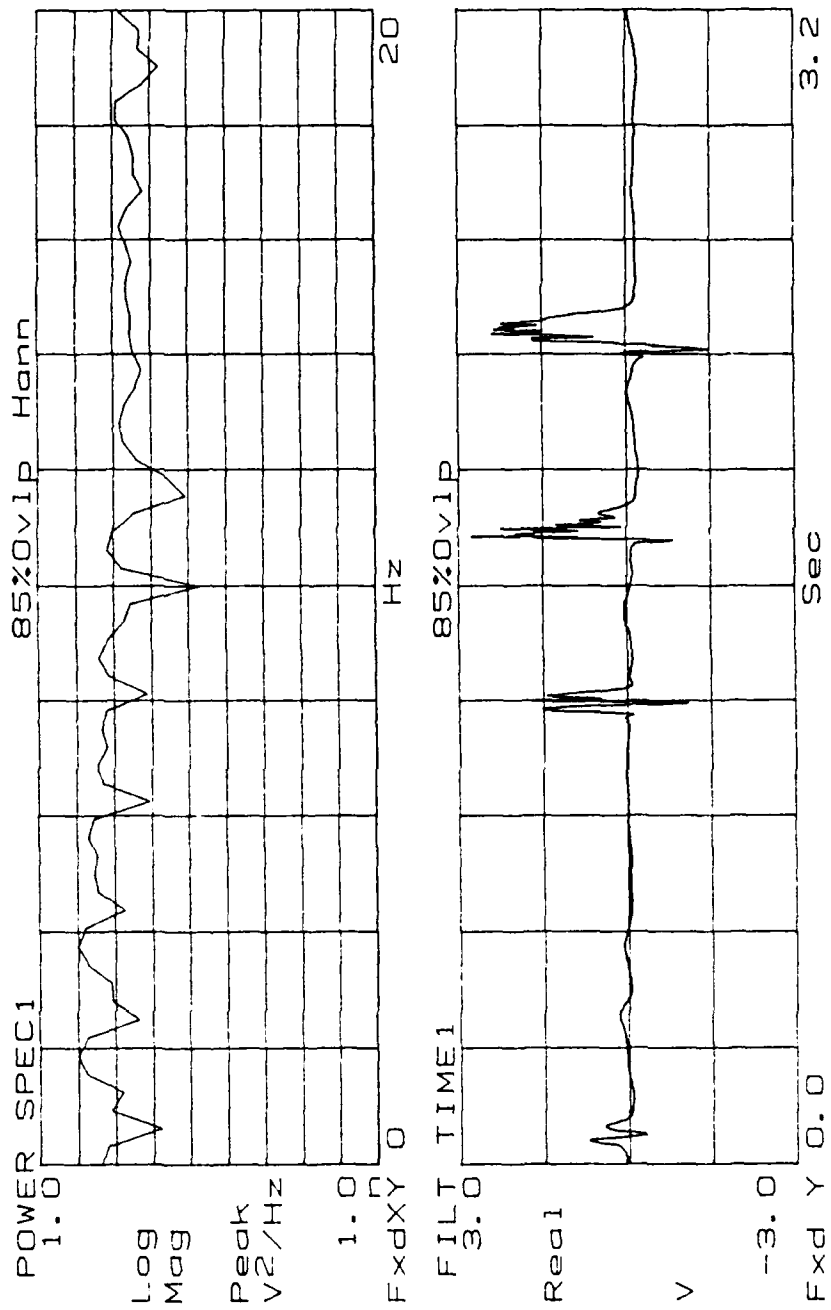


Figure 139. Re = 1742.

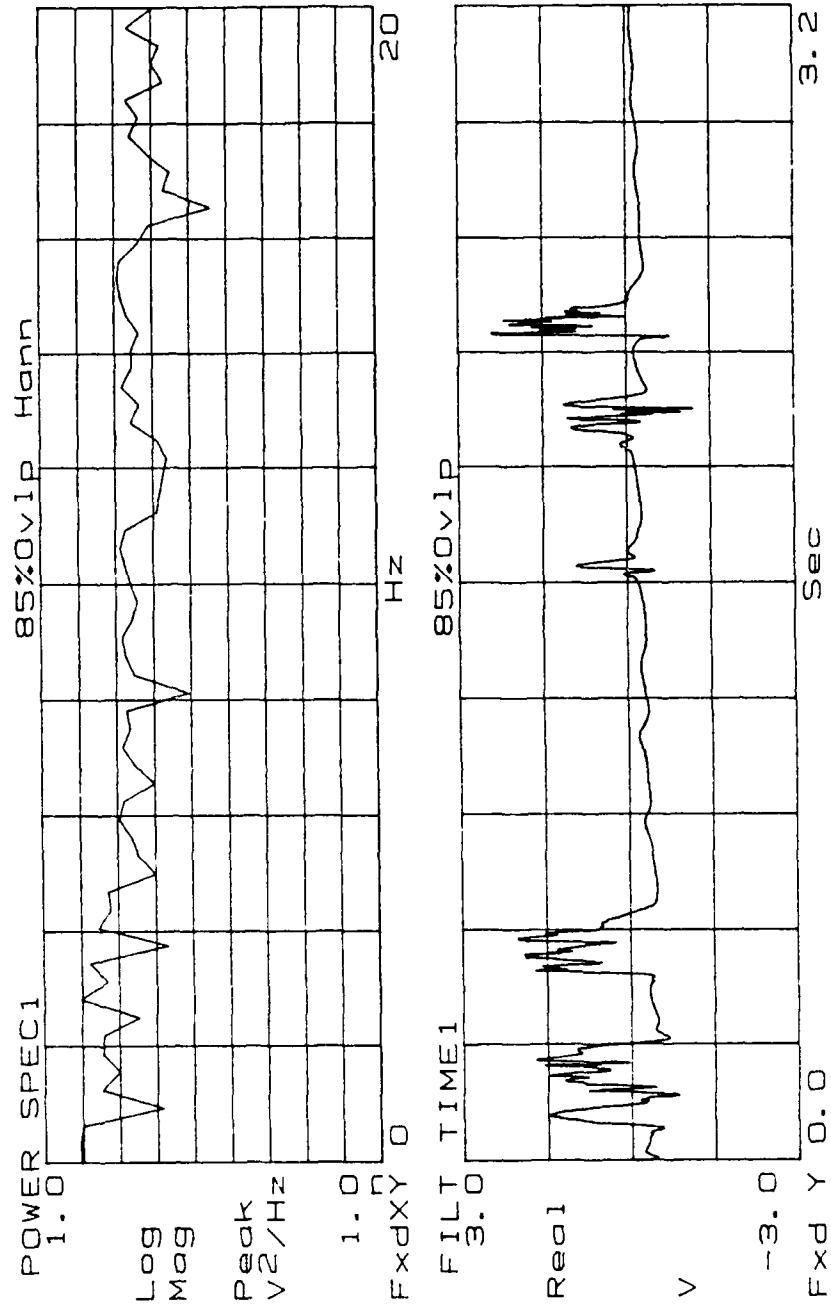


Figure 140. Re = 1796.

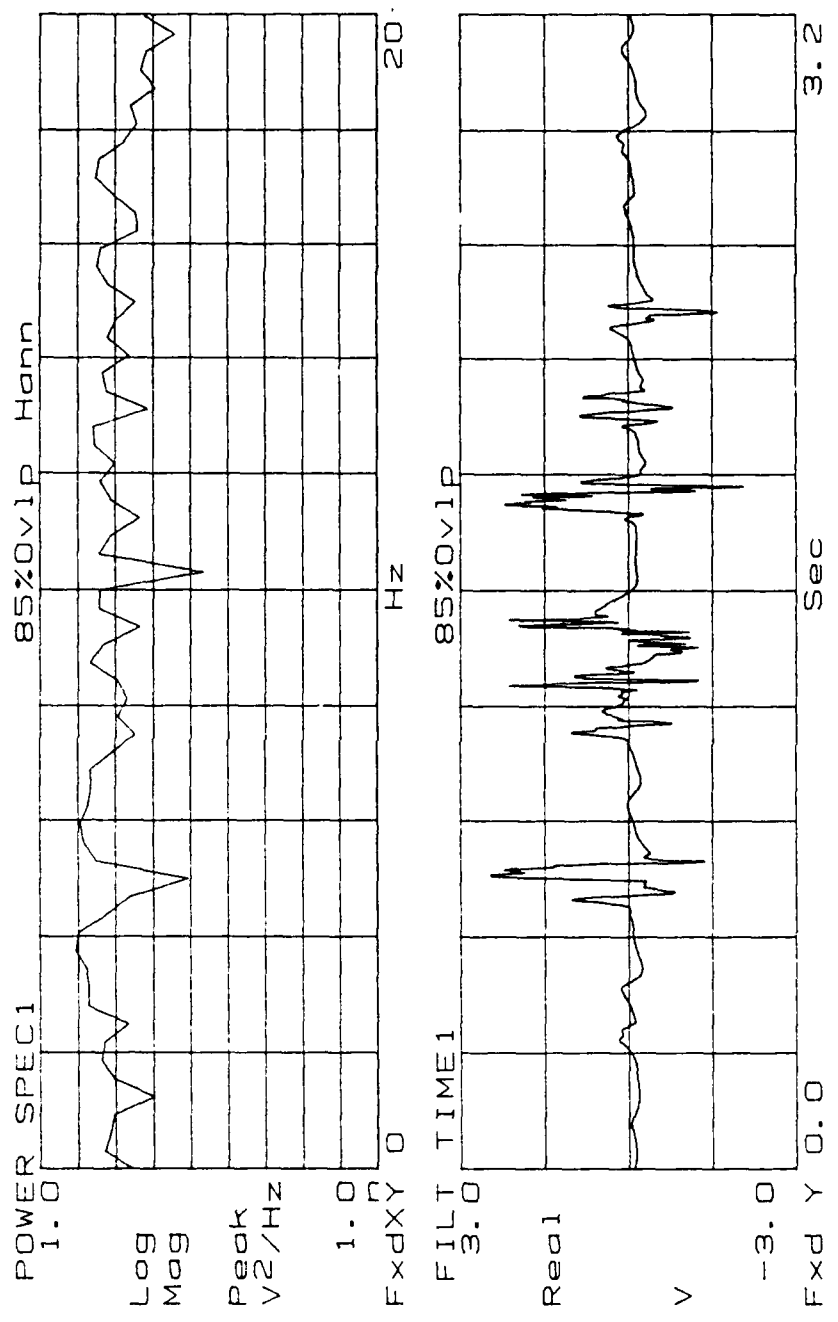


Figure 141. Re = 1905.

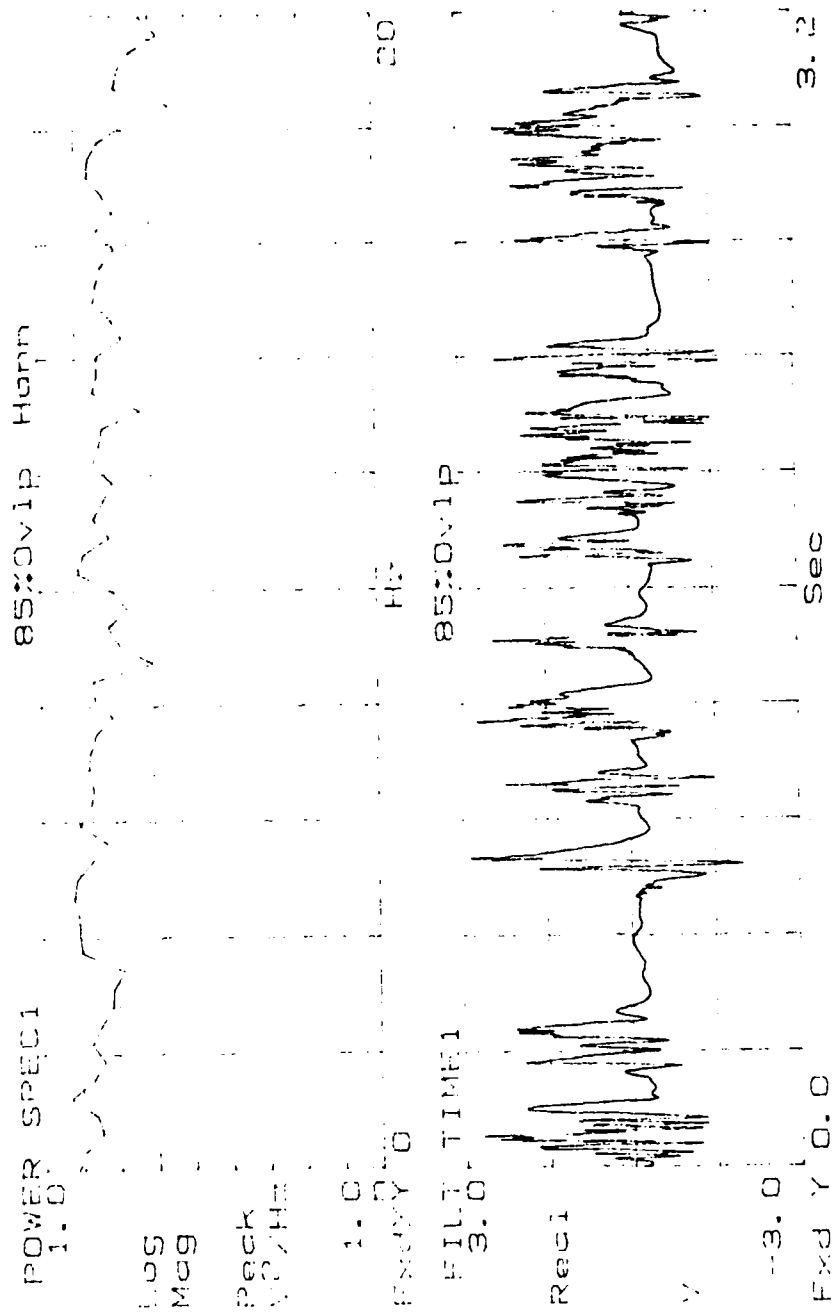


Figure 142. Re = 2005.

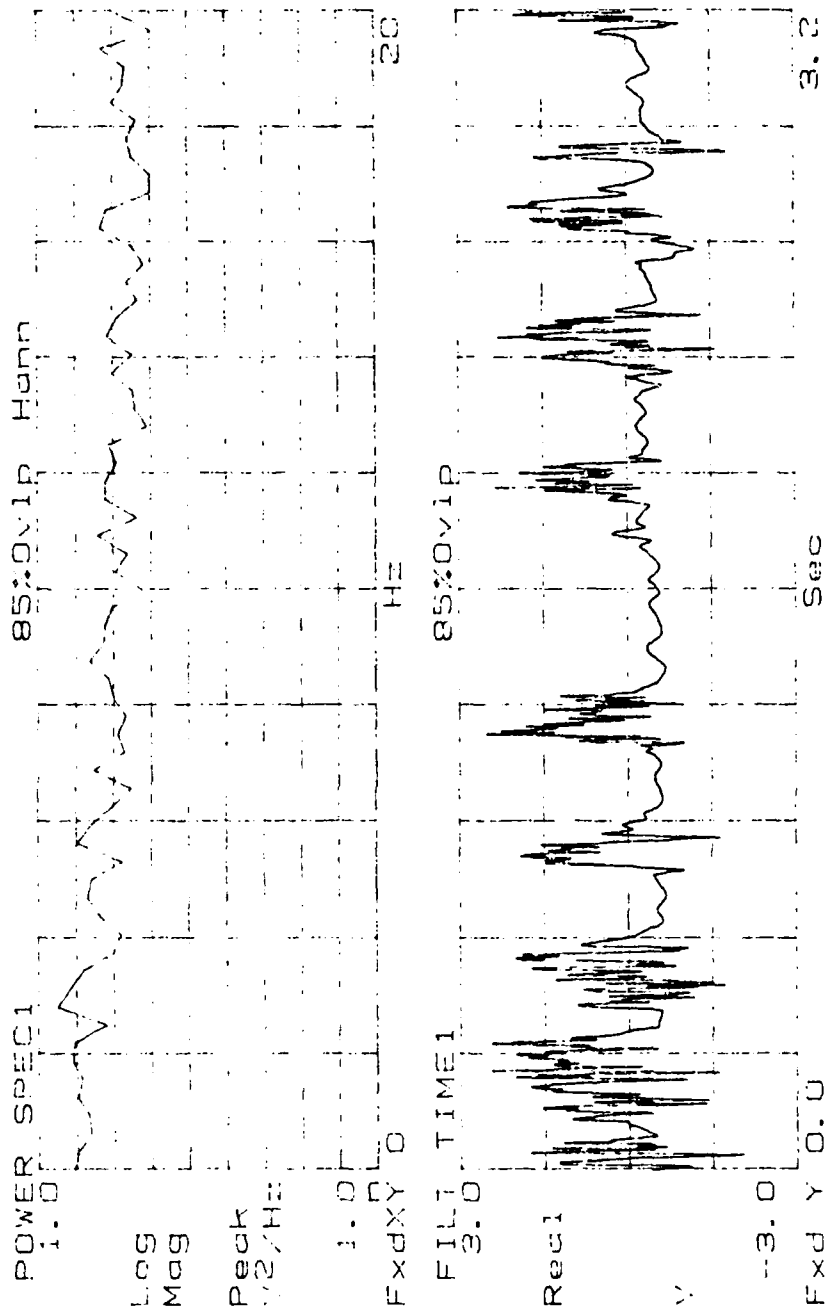


Figure 143. Re = 2097.



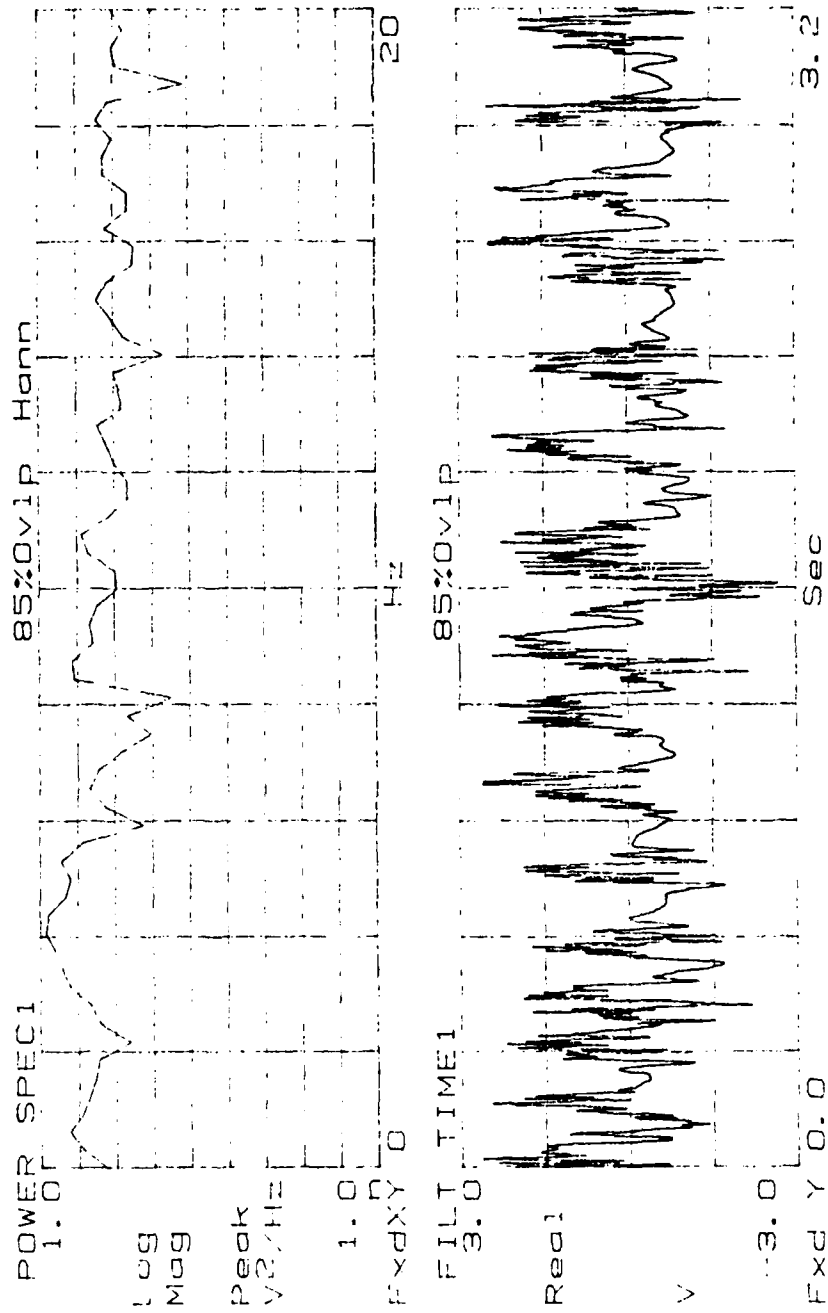


Figure 144. Re = 2198.

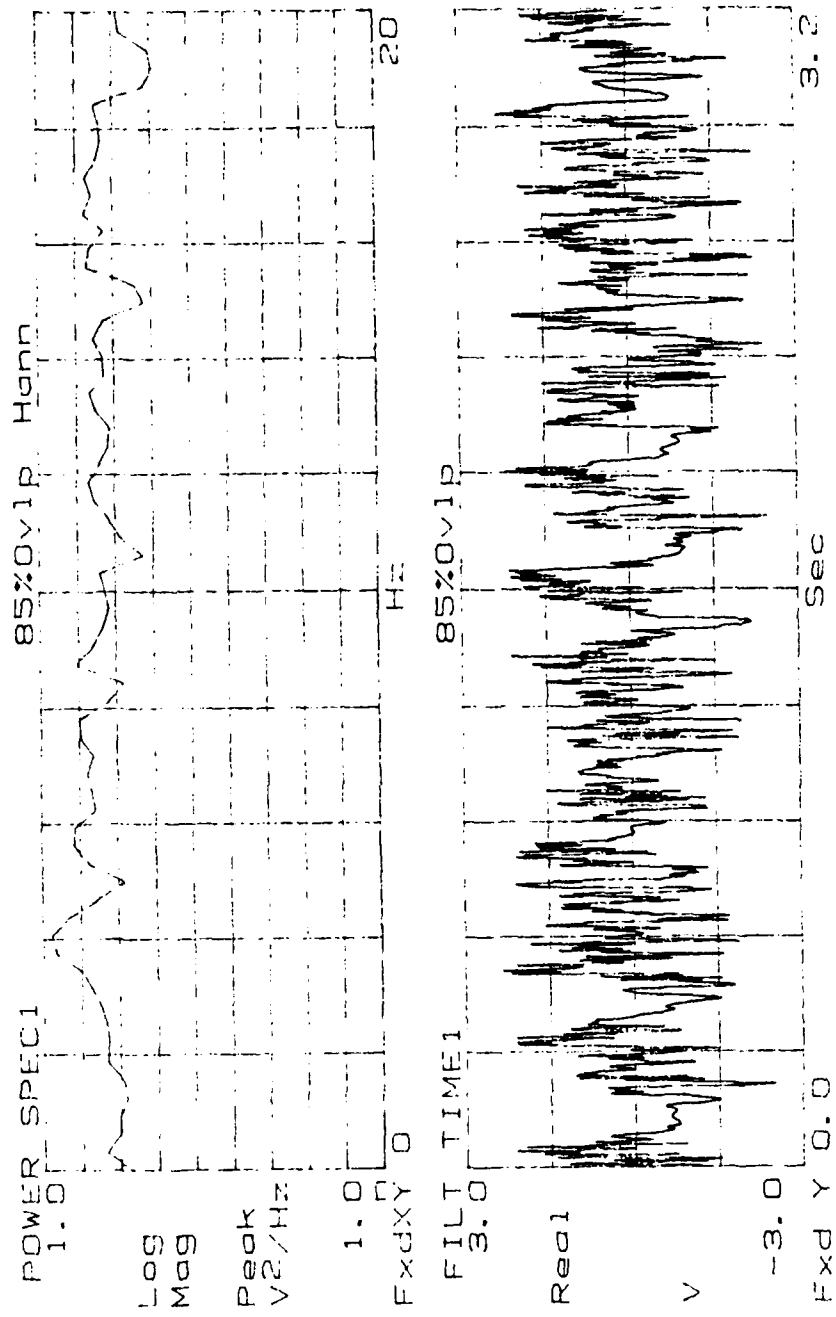


Figure 145. Re = 2298.

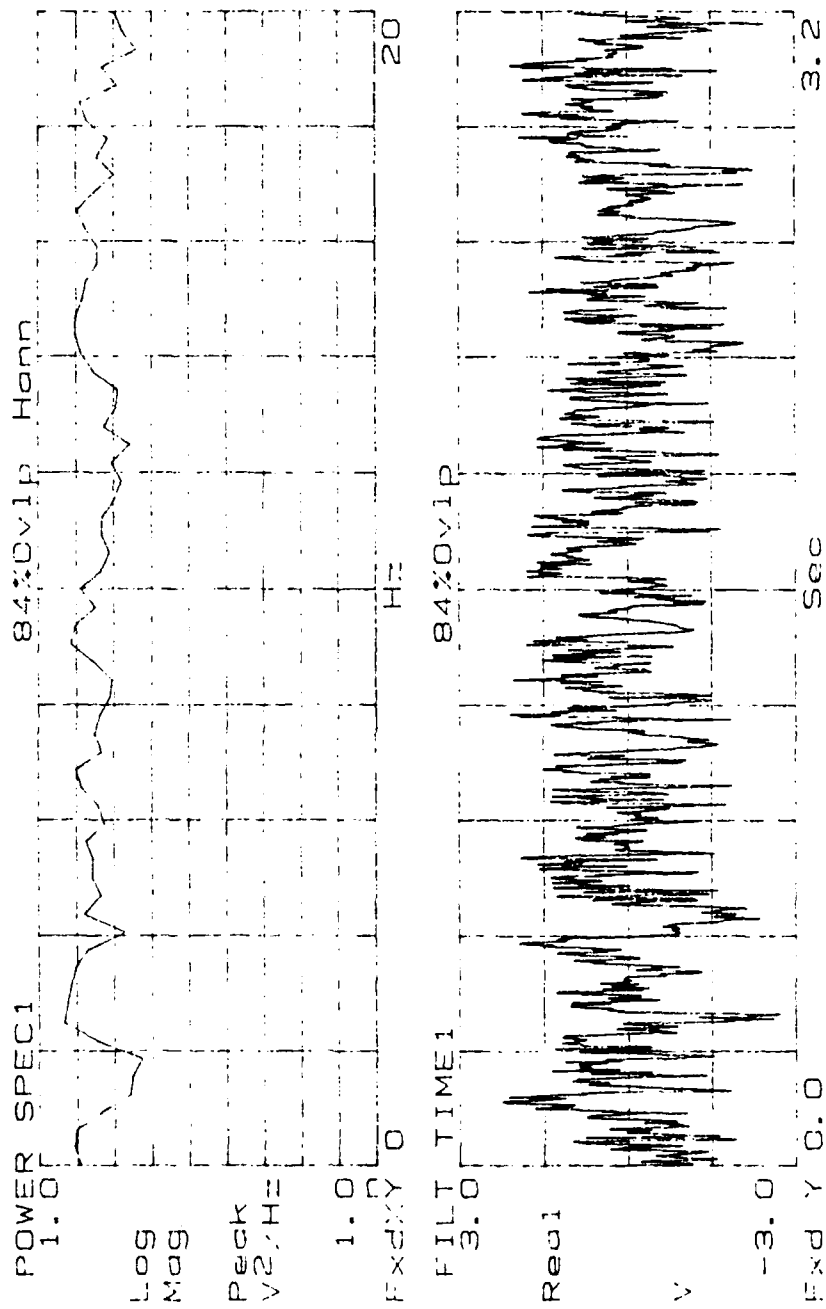


Figure 146. Re = 2402.

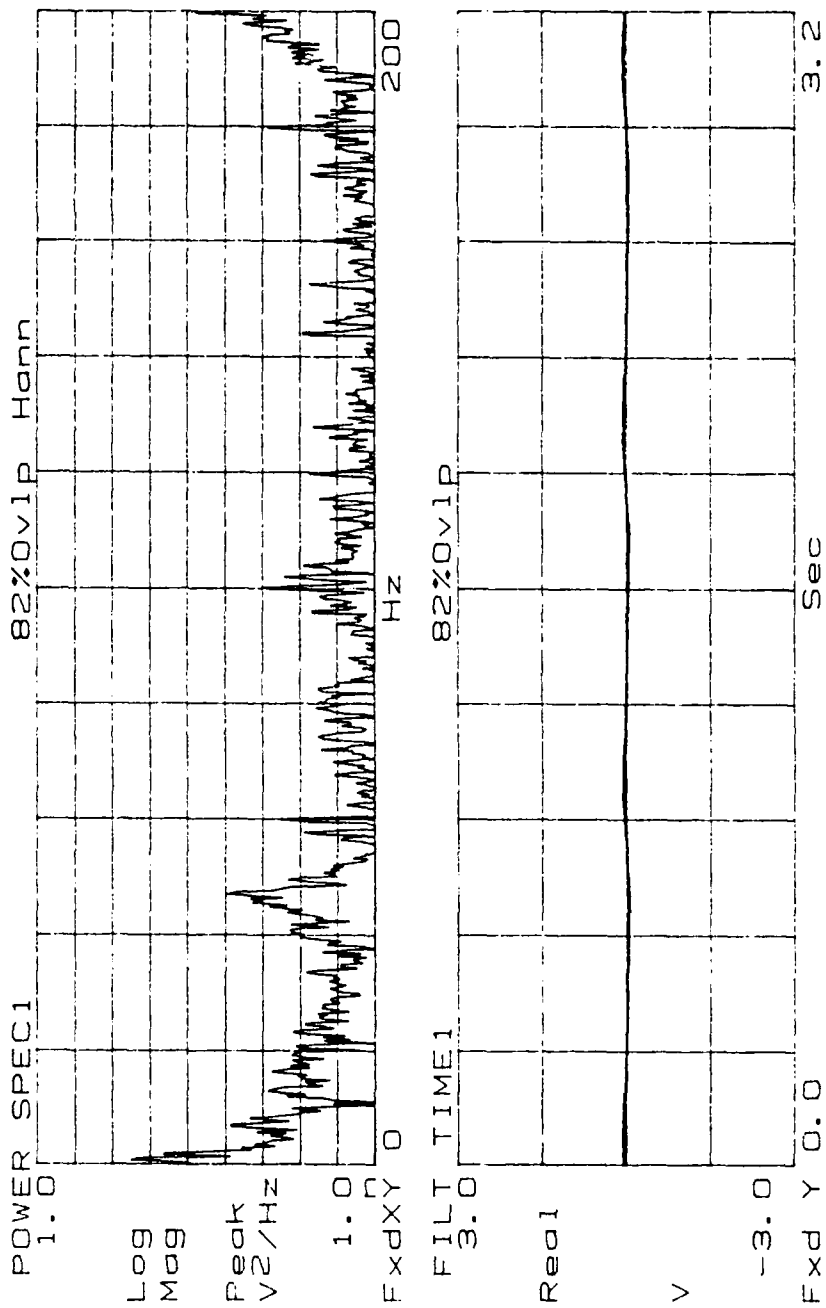


Figure 147.  $Re = 1396$ ,  $f_{osc} = 1$  Hz.

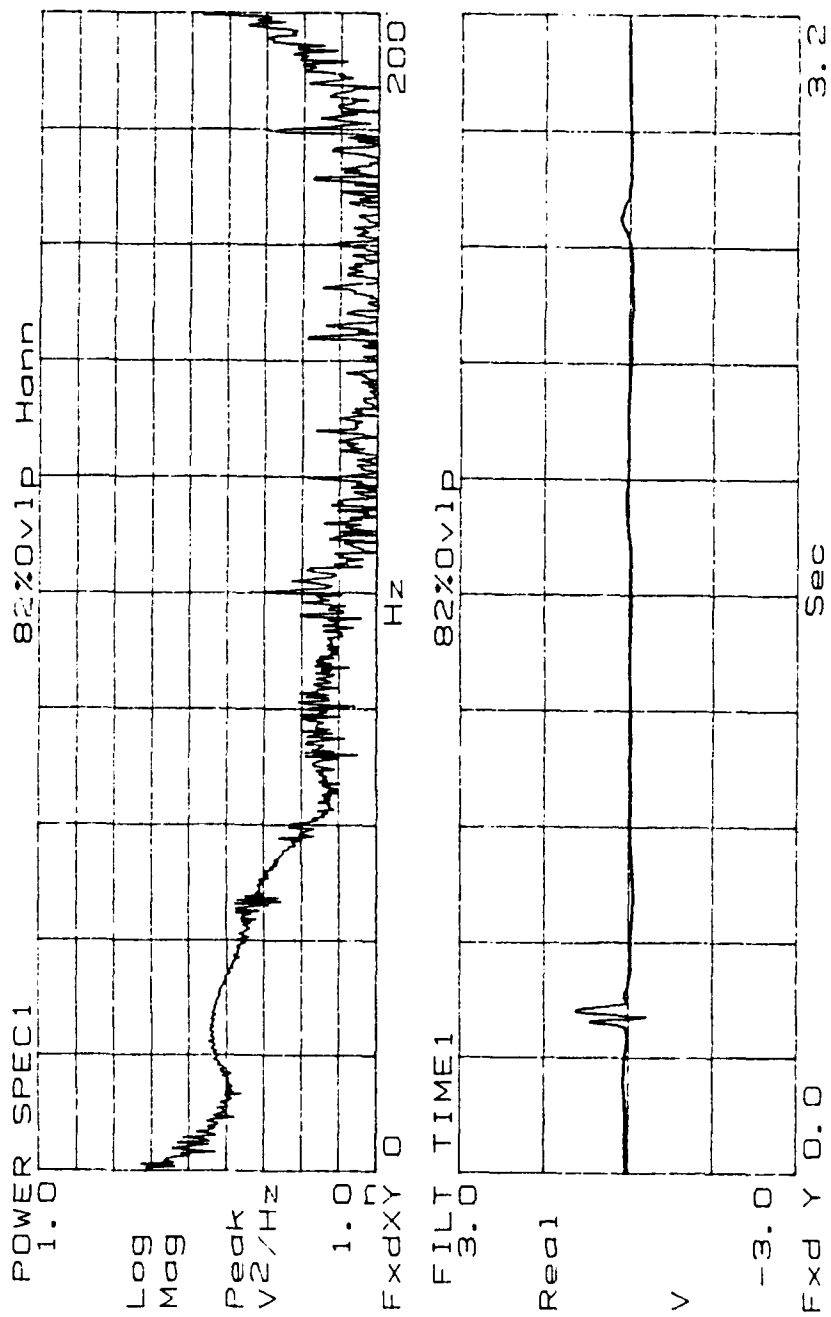


Figure 148.  $Re = 1454$ ,  $f_{osc} = 1$  Hz.

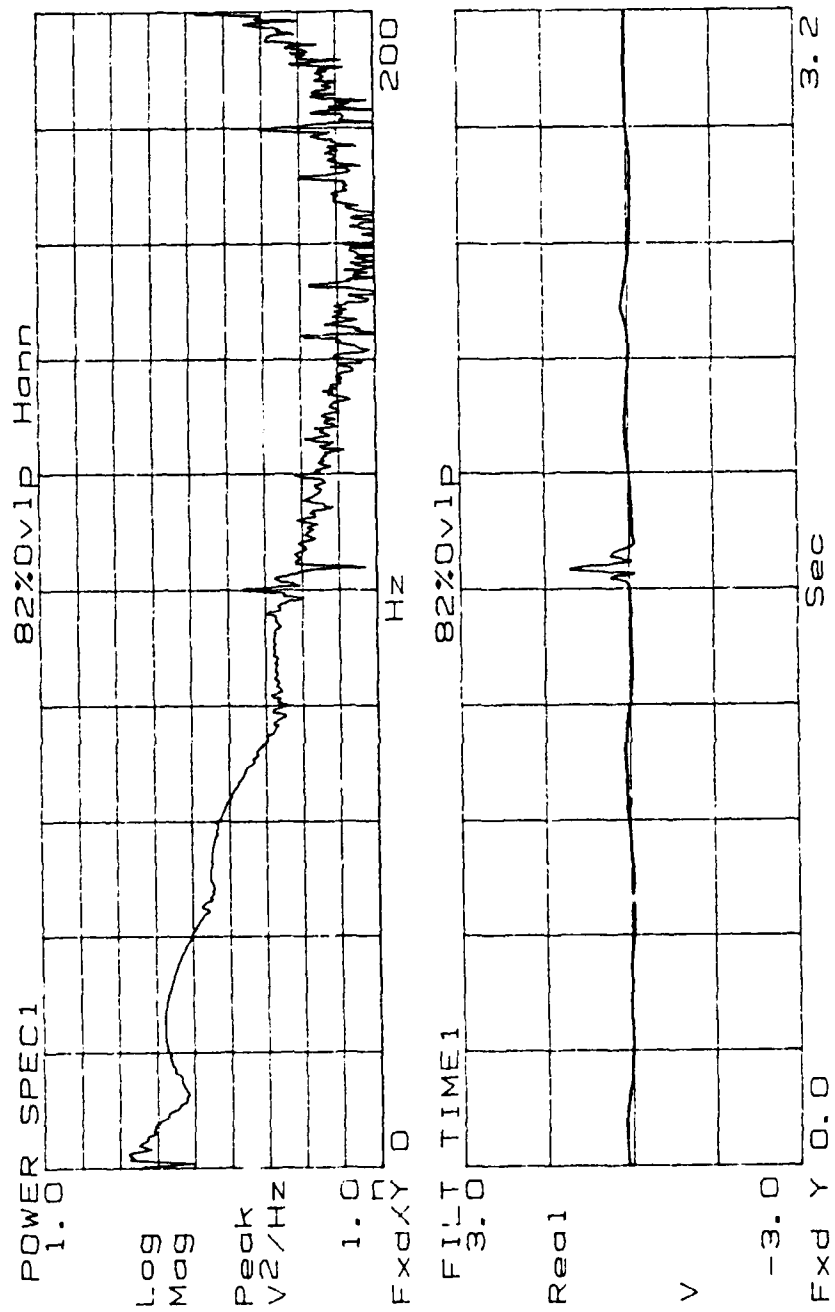


Figure 149.  $R_e = 1496$ ,  $f_{osc} = 1$  Hz.

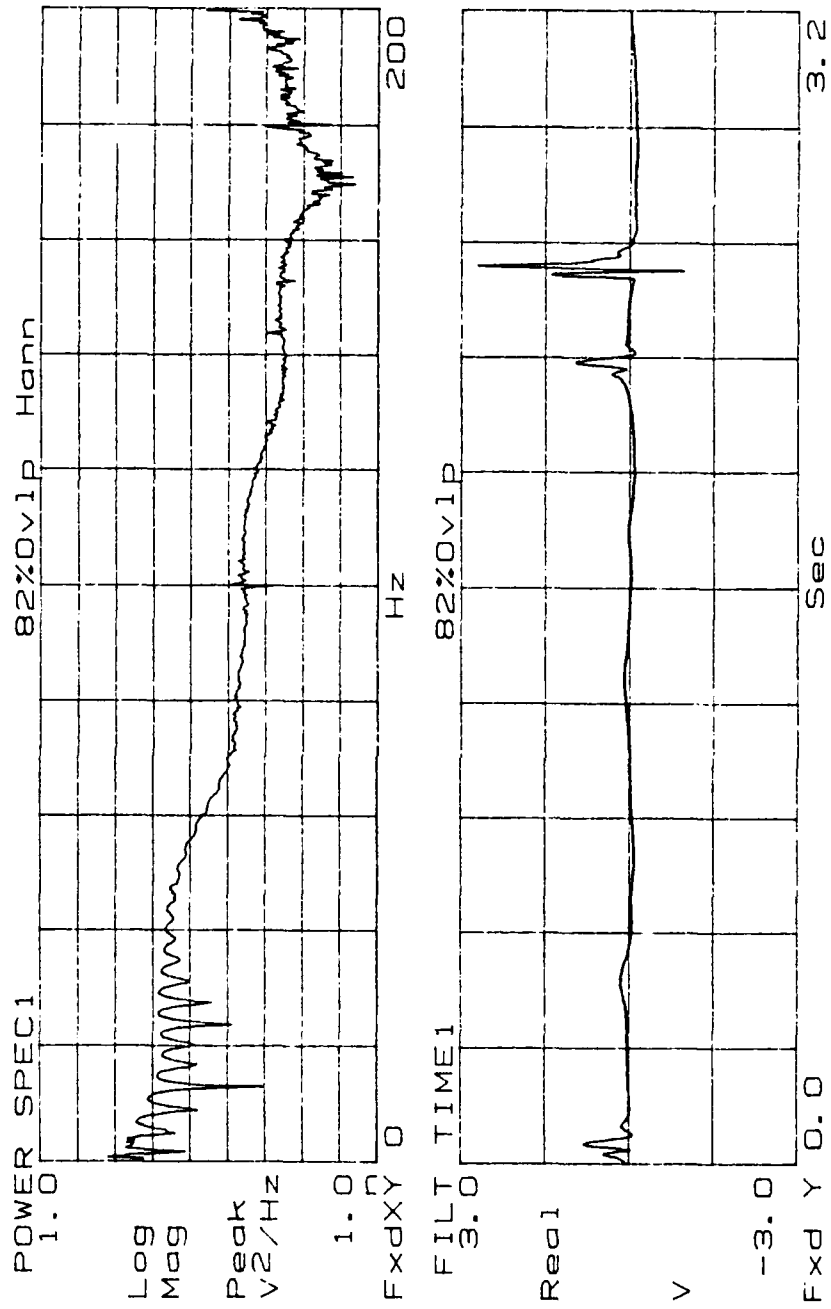


Figure 150.  $Re = 1542$ ,  $f_{osc} = 1$  Hz.

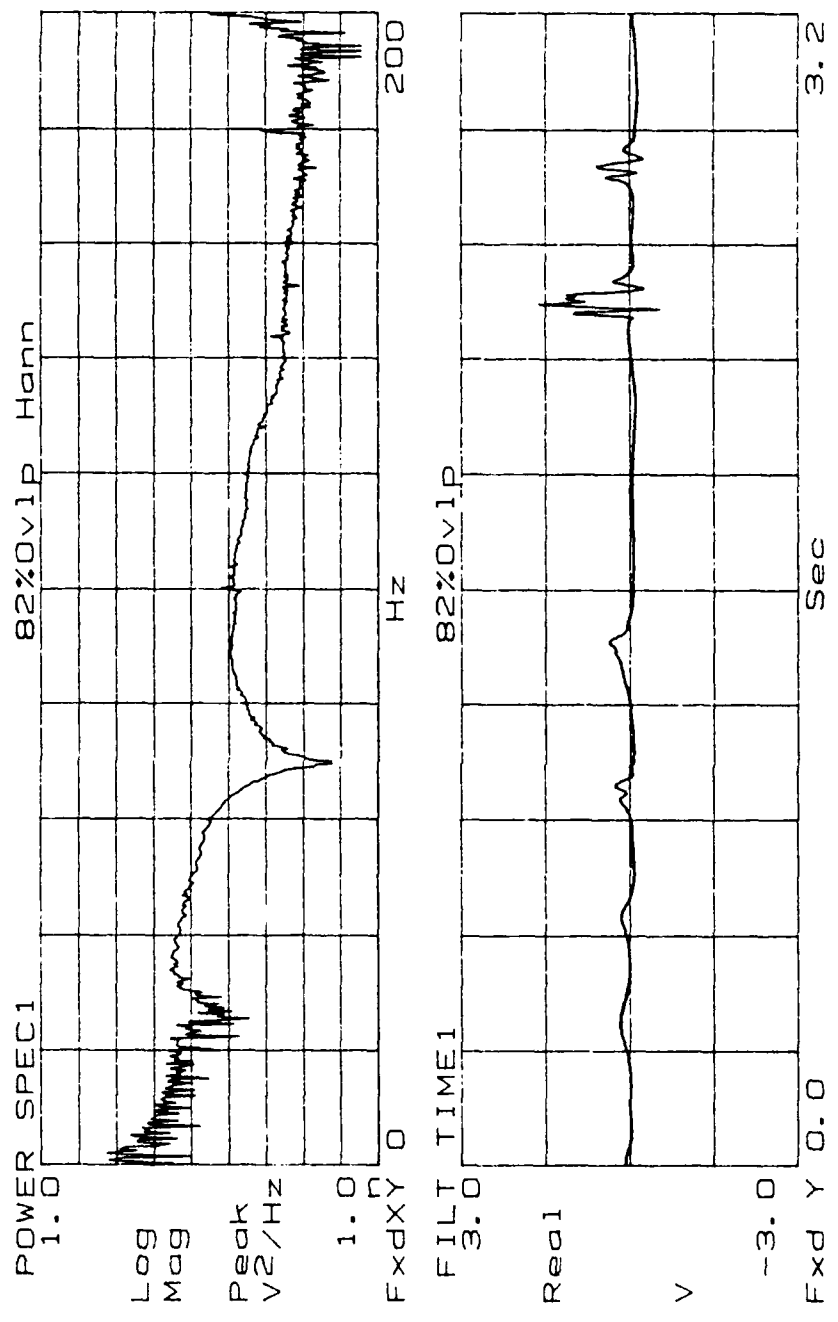


Figure 151.  $Re = 1604$ ,  $f_{osc} = 1$  Hz.



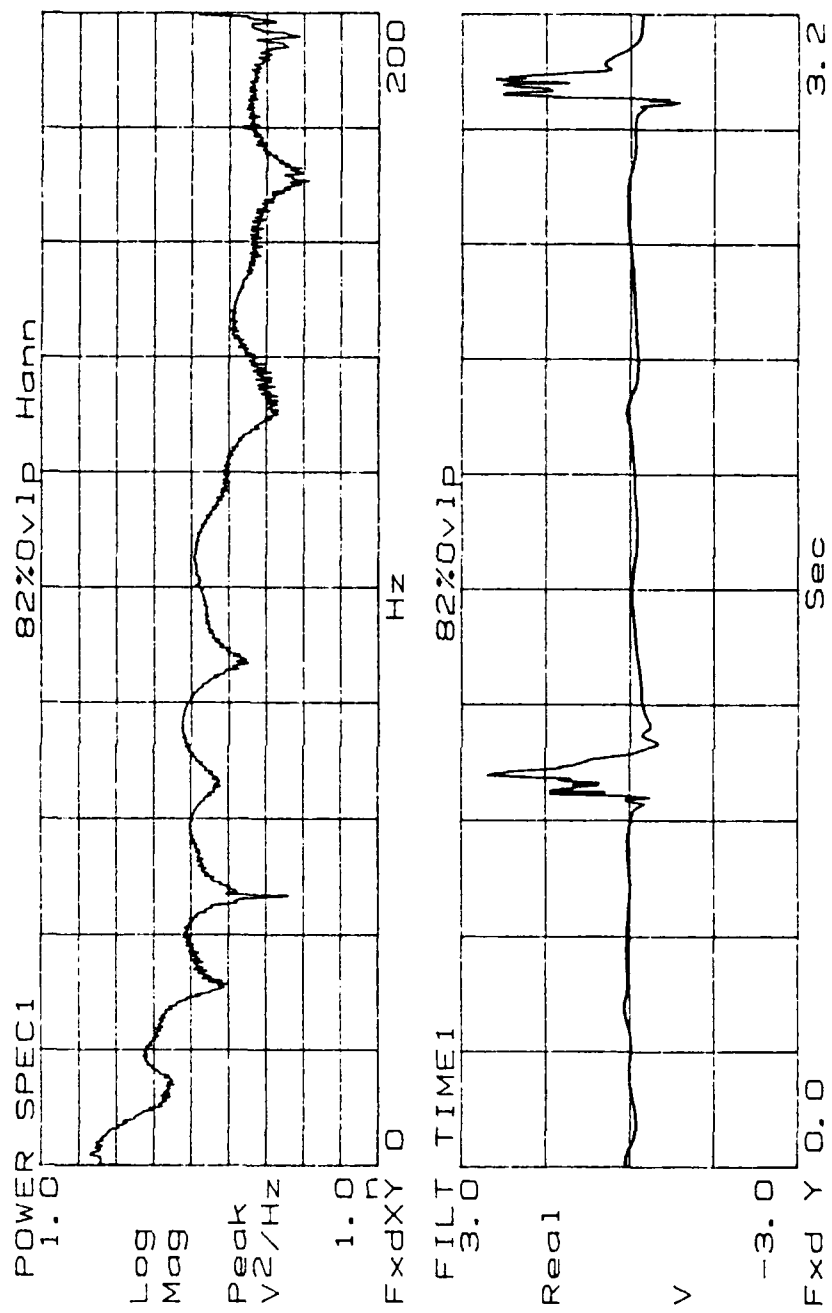


Figure 152.  $Re = 1650$ ,  $f_{osc} = 1$  Hz.

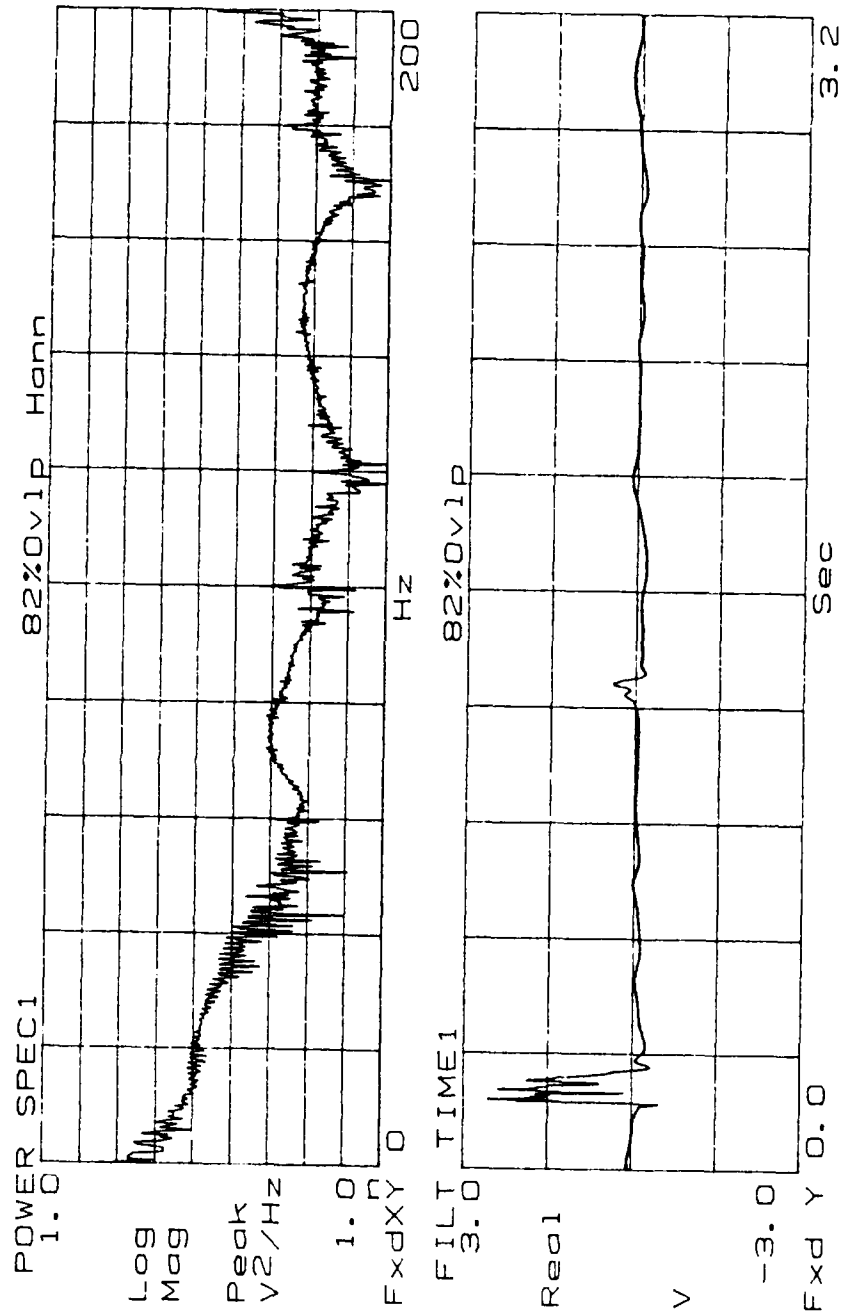


Figure 153.  $R_e = 1696$ ,  $f_{osc} = 1$  Hz.

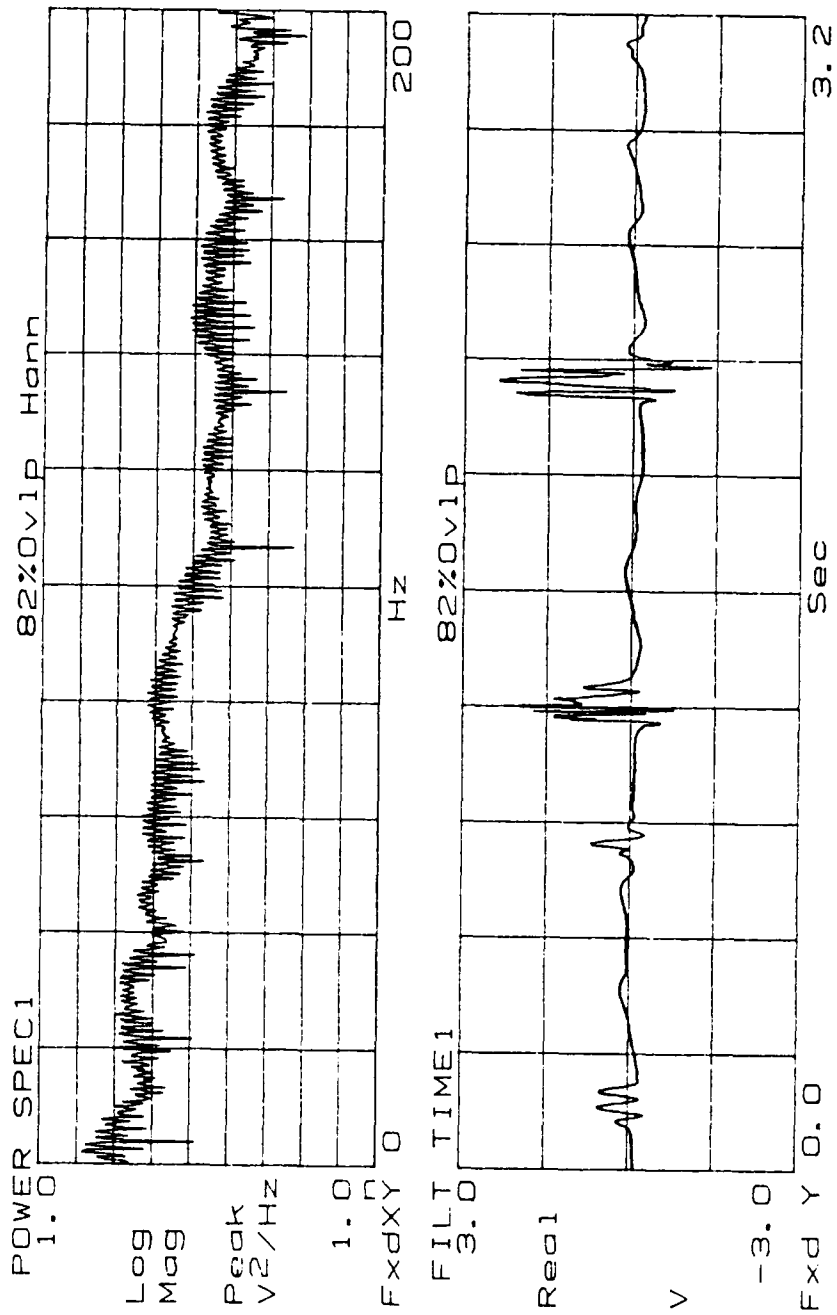


Figure 154.  $Re = 1742$ ,  $f_{osc} = 1$  Hz.

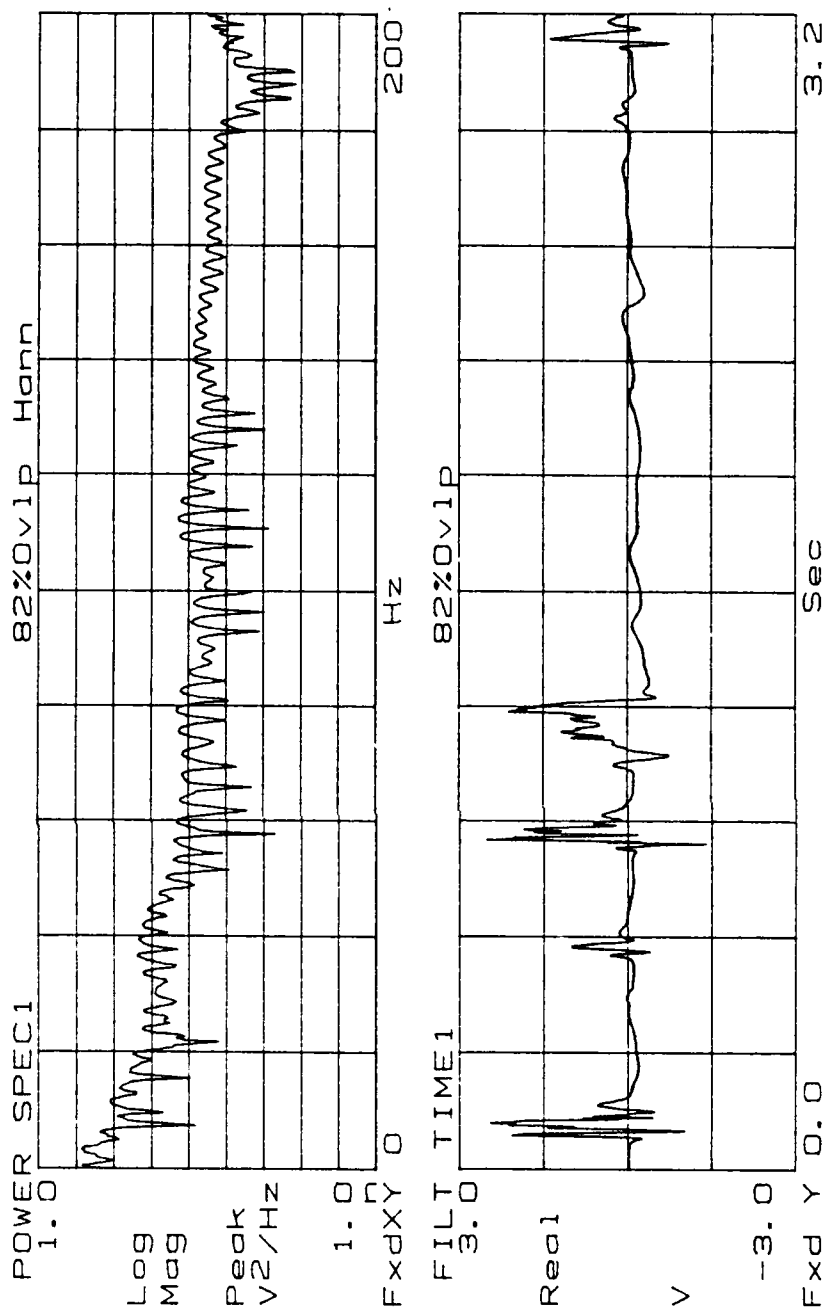


Figure 155.  $Re = 1796$ ,  $f_{osc} = 1$  Hz.

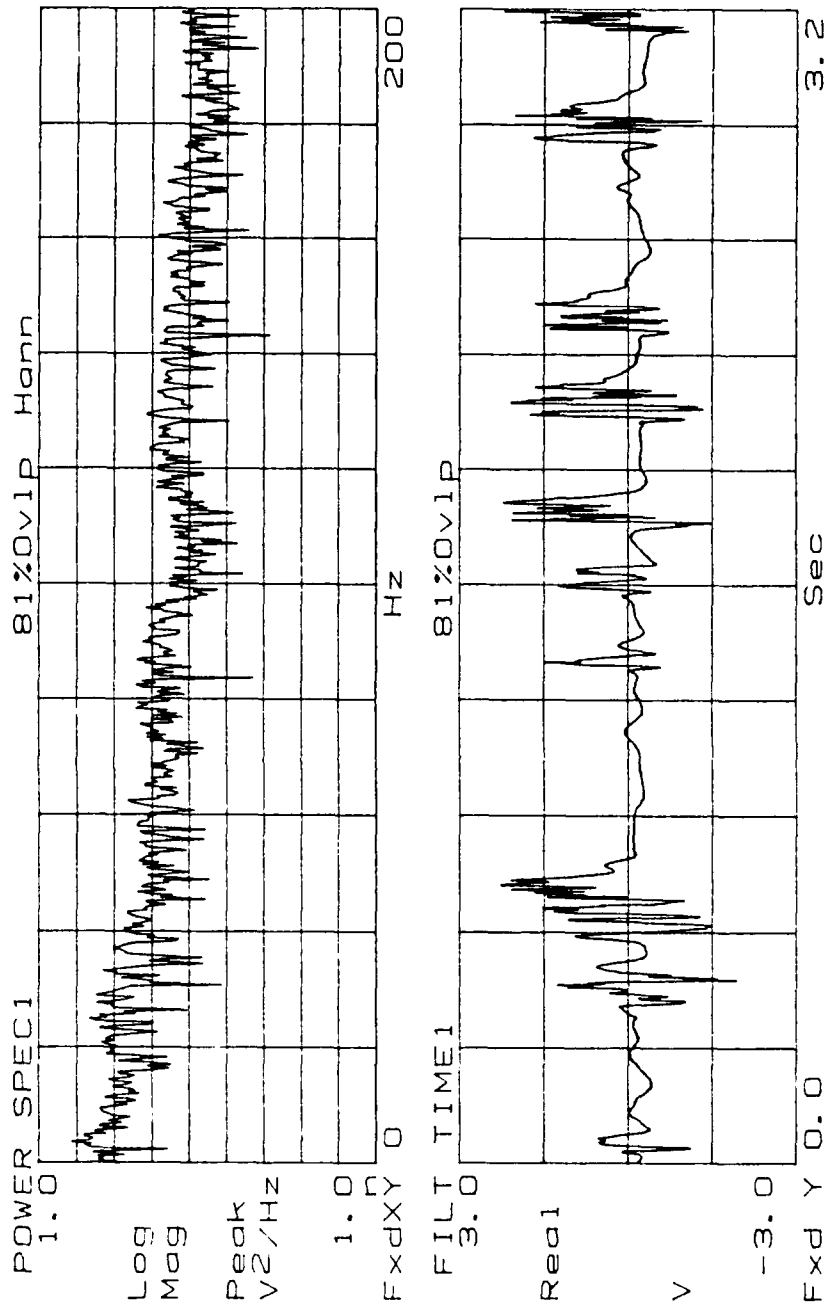


Figure 156. Re = 1905,  $f_{osc} = 1$  Hz.



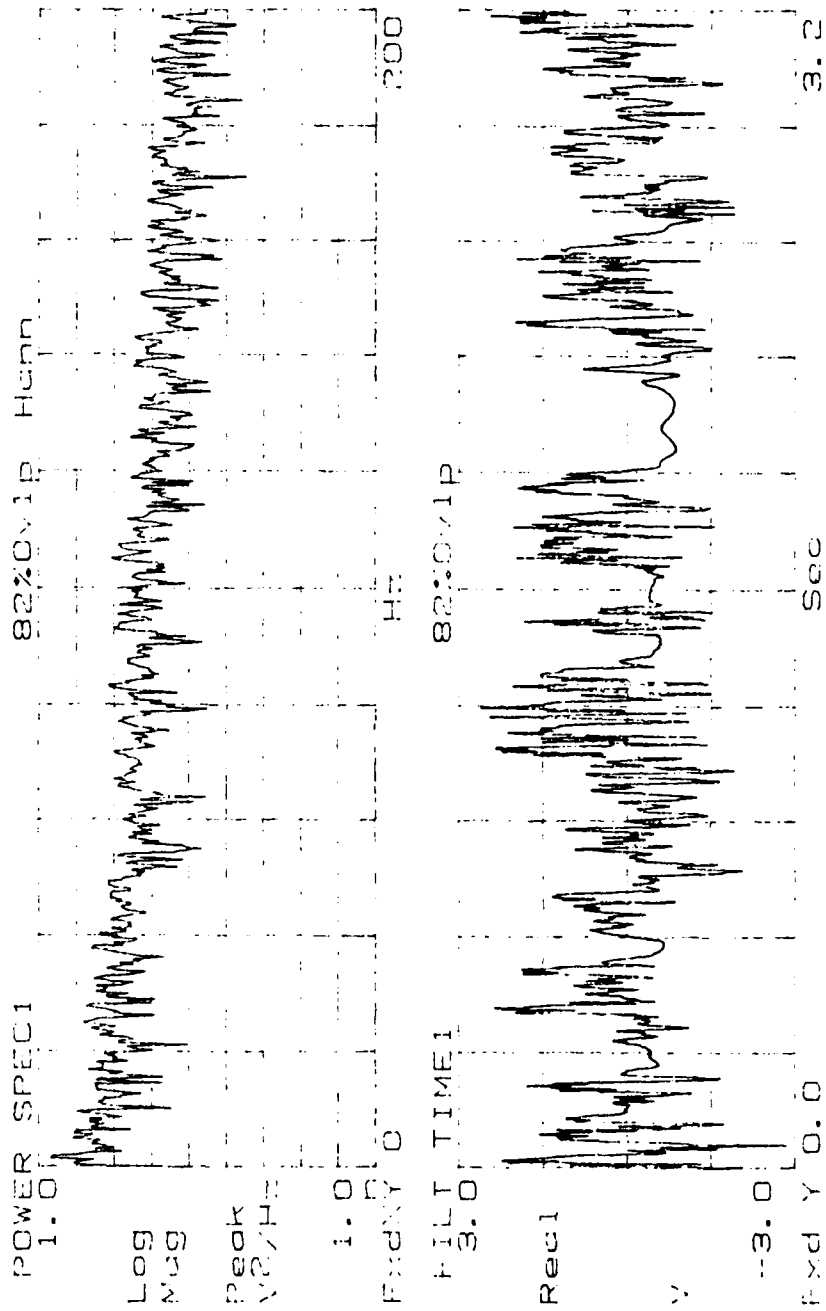


Figure 158.  $Re = 2097$ ,  $f_{osc} = 1$  Hz.

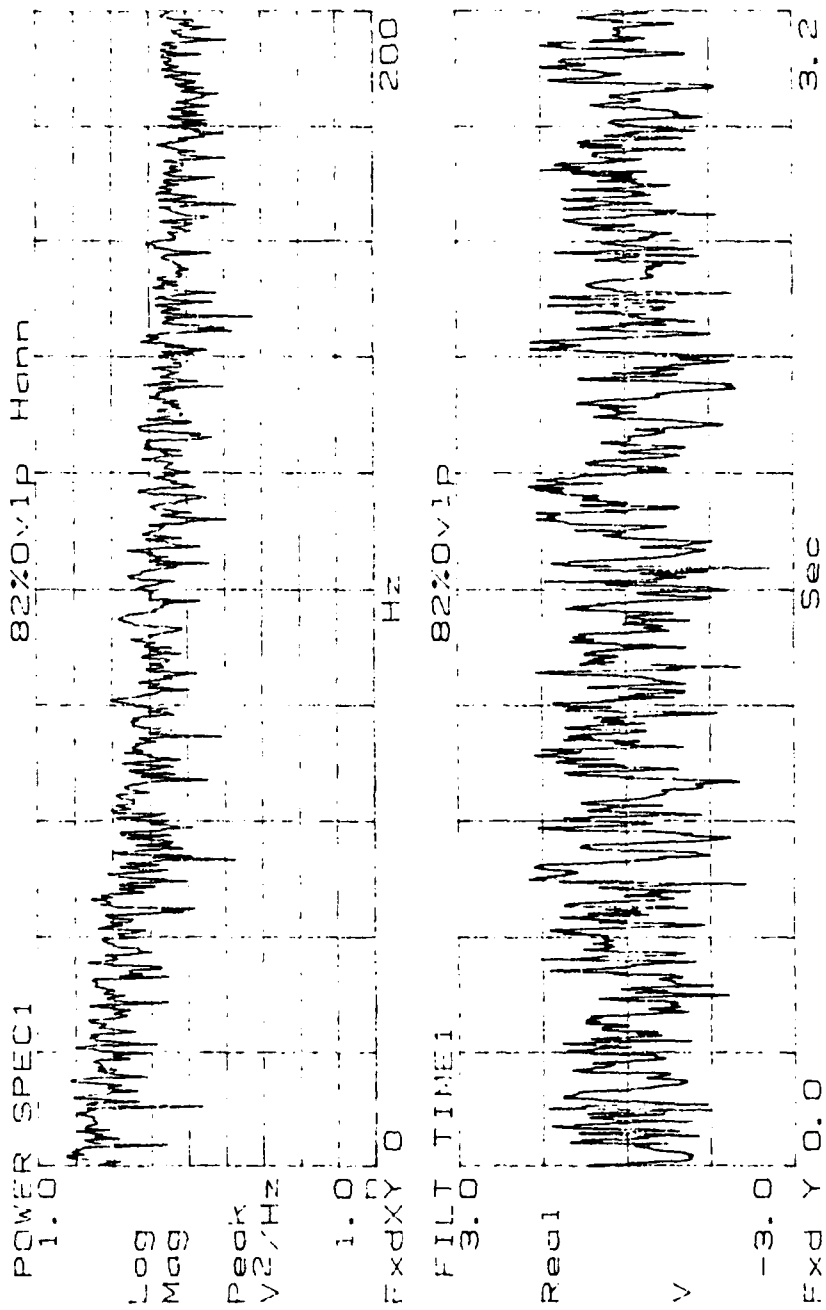


Figure 159.  $Re = 2197$ ,  $f_{osc} = 1$  Hz.



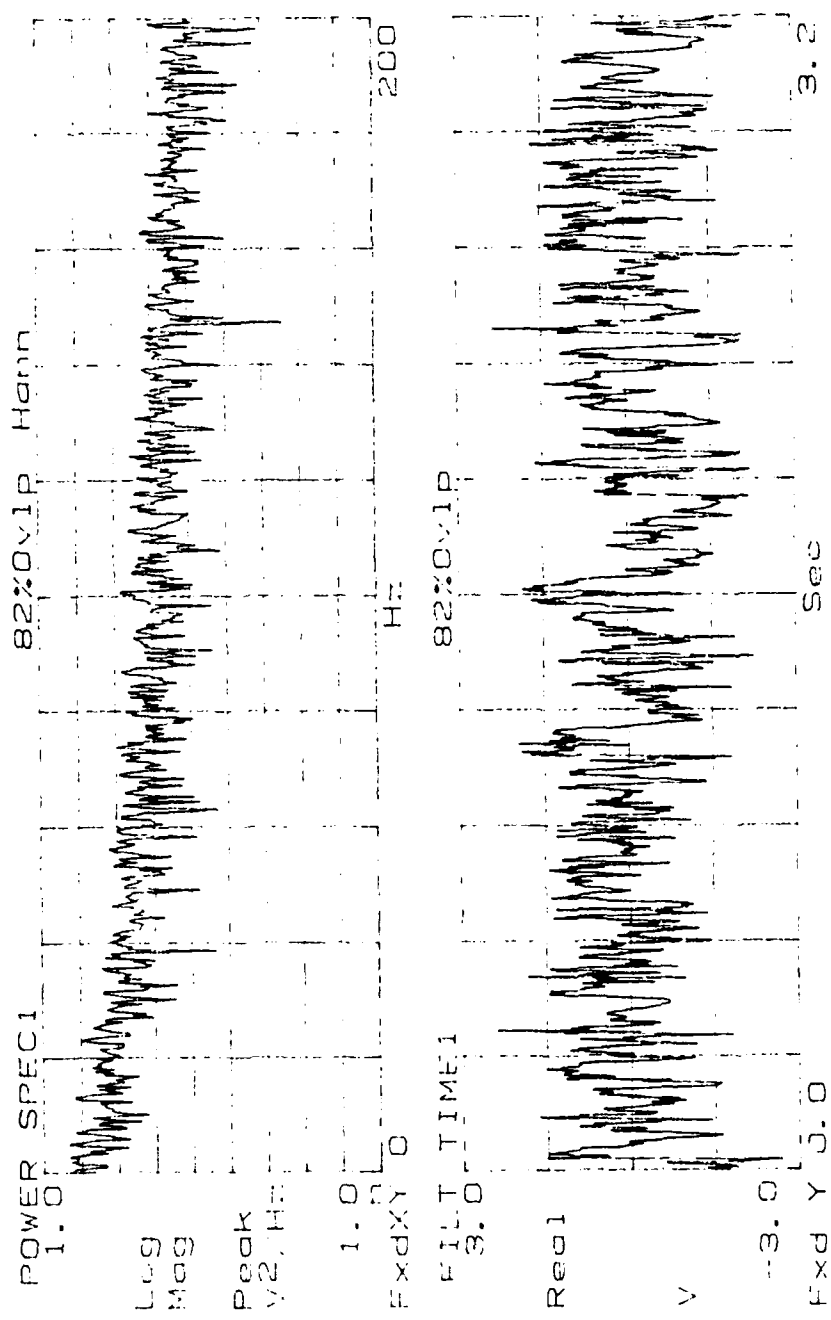


Figure 160.  $Re = 2298$ ,  $f_{osc} = 1$  Hz.

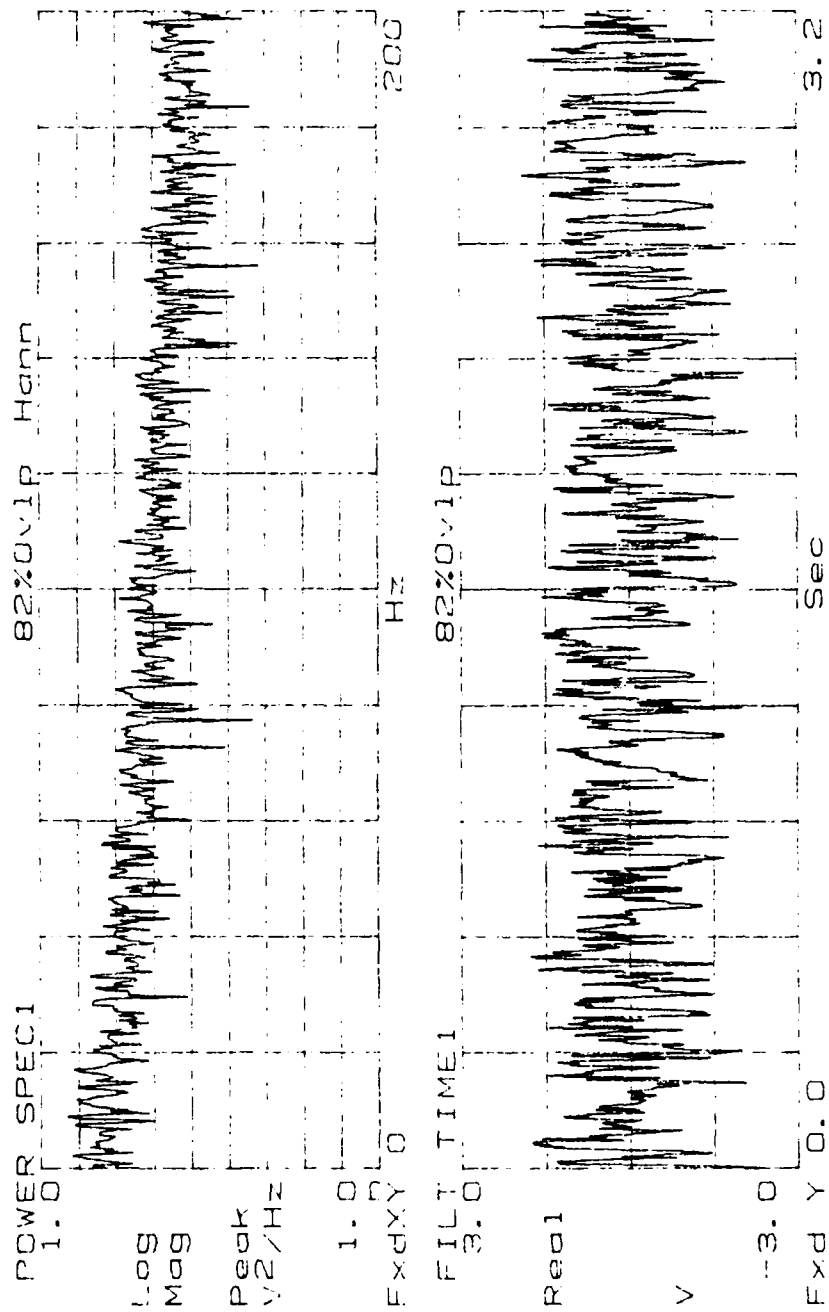


Figure 161.  $Re = 2402$ ,  $f_{osc} = 1$  Hz.

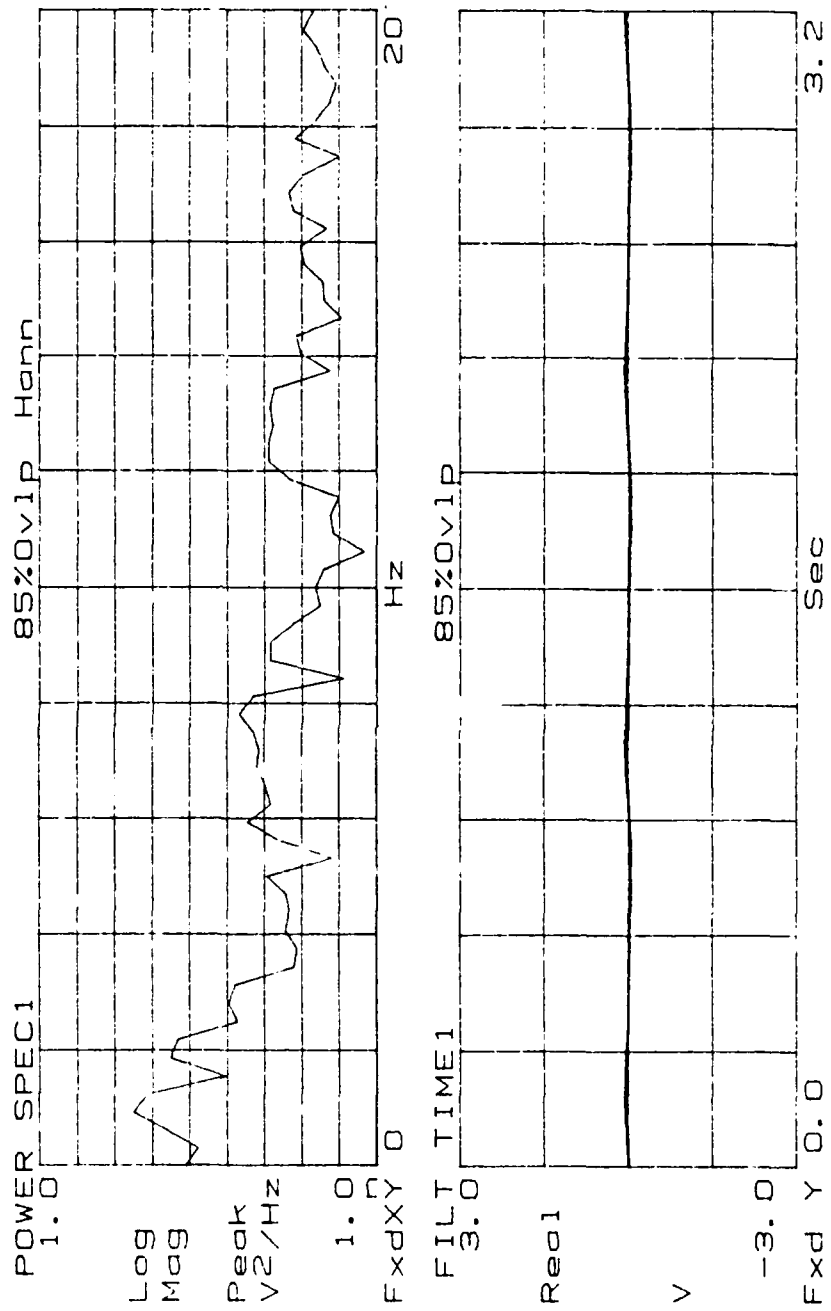


Figure 162.  $Re = 1396$ ,  $f_{osc} = 1$  Hz.

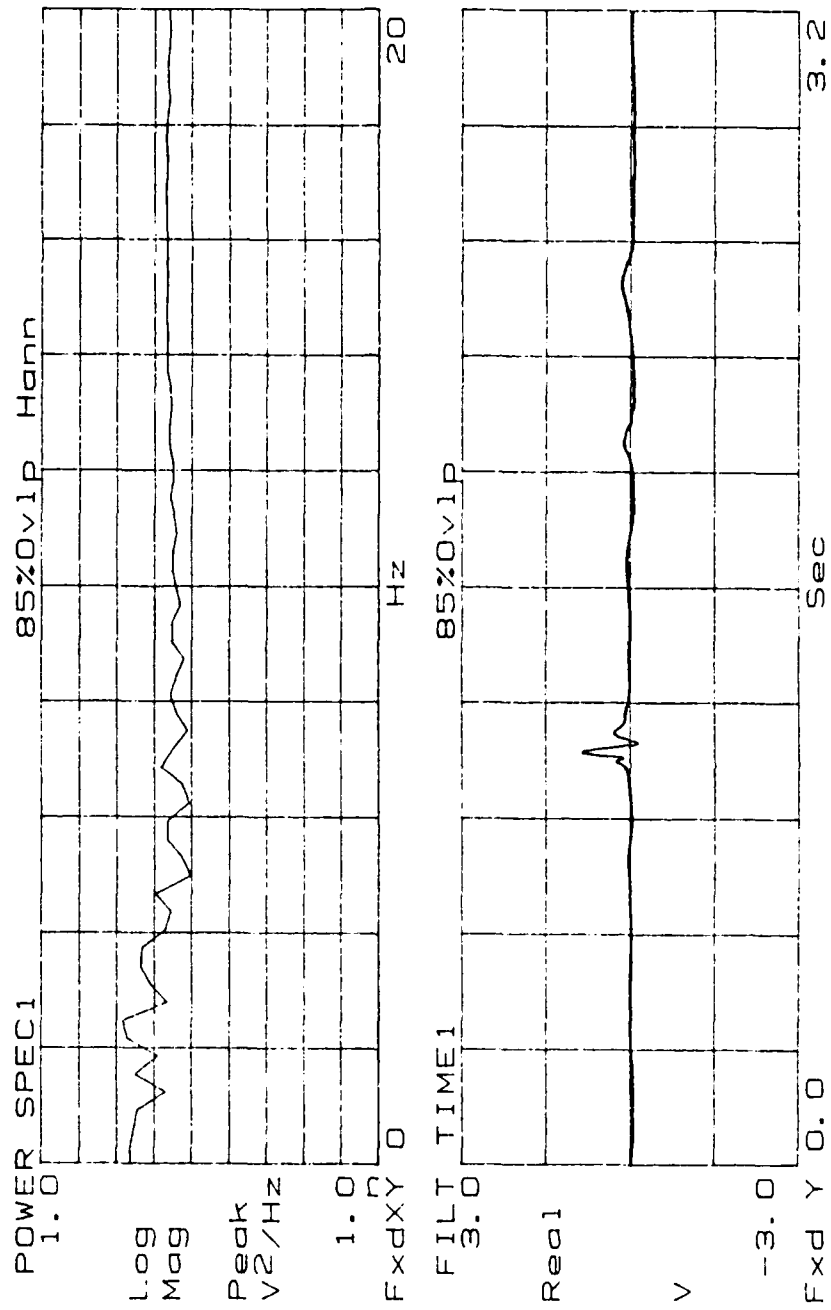


Figure 163.  $Re = 1454$ ,  $f_{osc} = 1$  Hz.

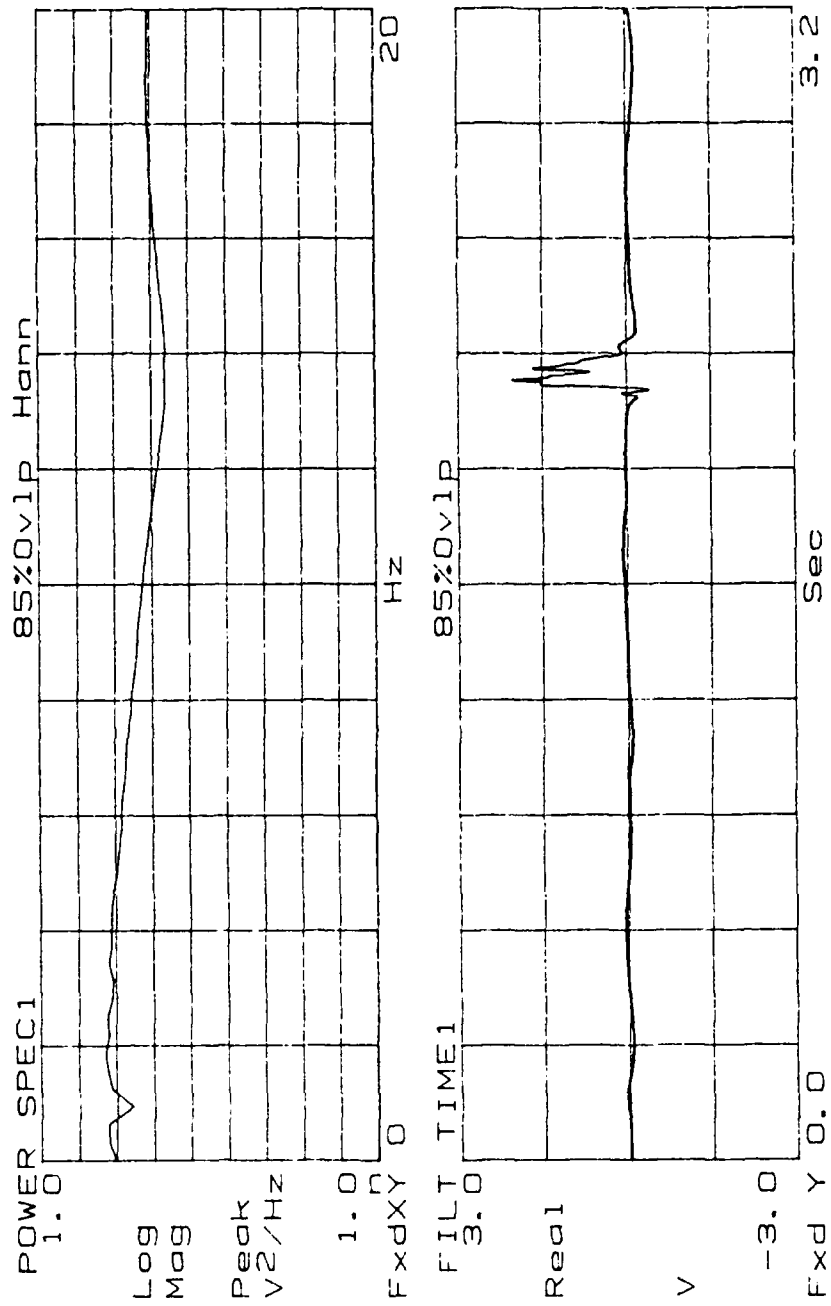


Figure 164.  $Re = 1496$ ,  $f_{osc} = 1$  Hz.

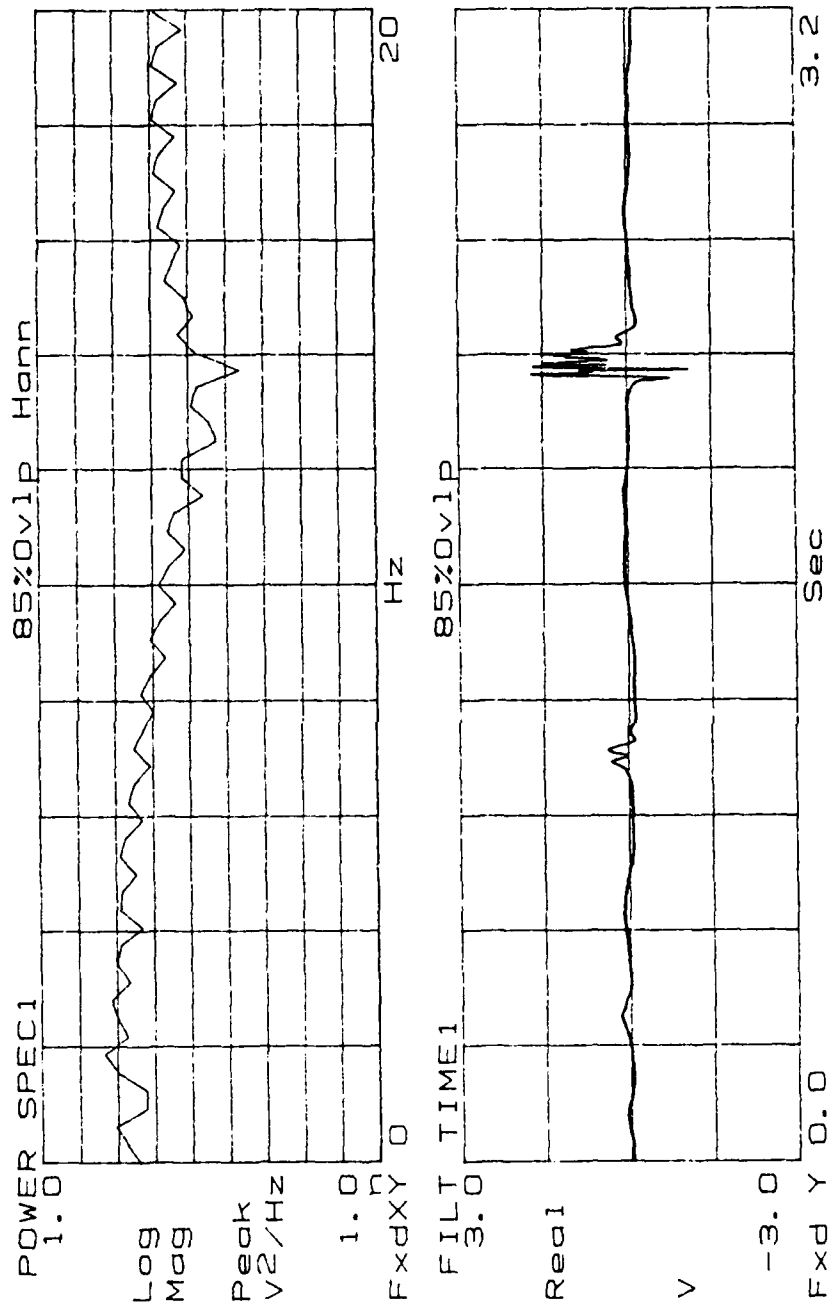


Figure 165.  $Re = 1542$ ,  $f_{osc} = 1$  Hz.

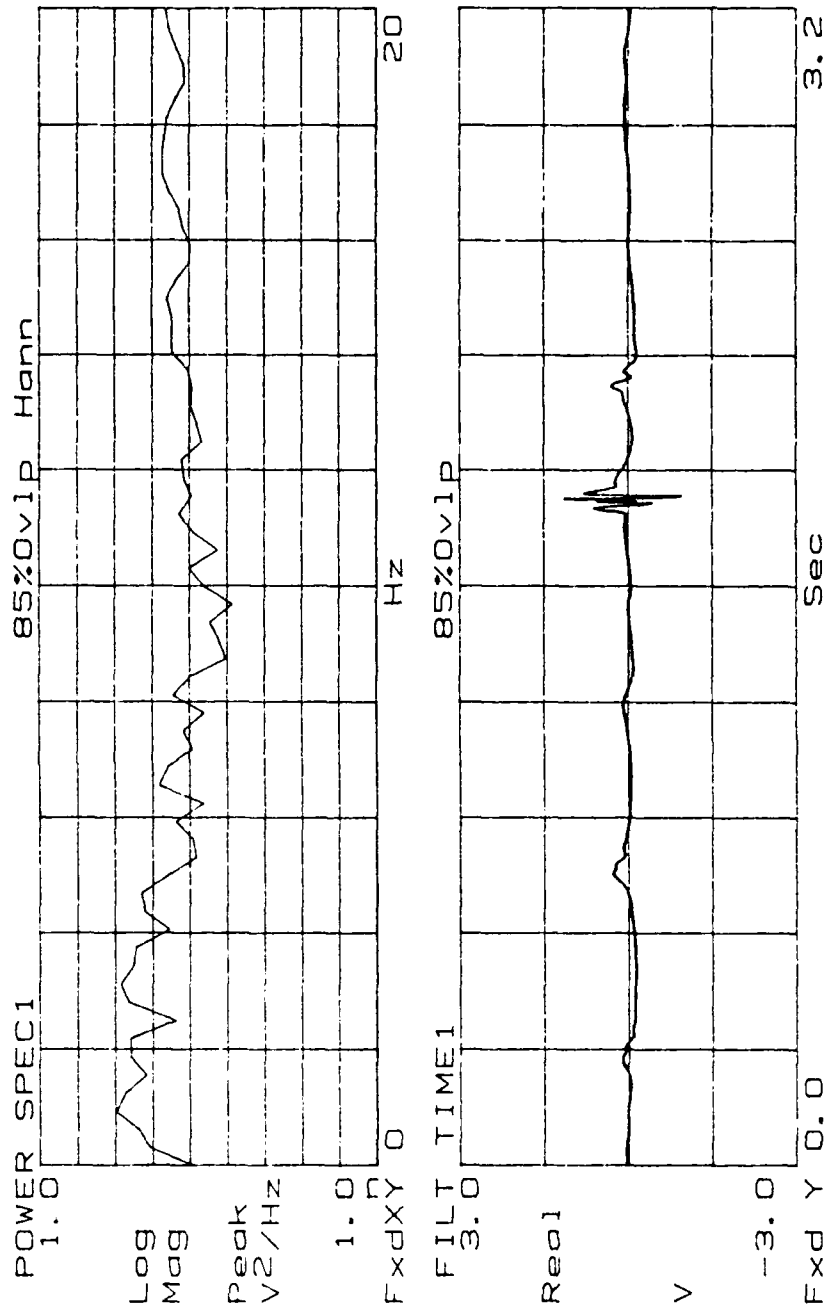


Figure 166.  $Re = 1604$ ,  $f_{osc} = 1$  Hz.

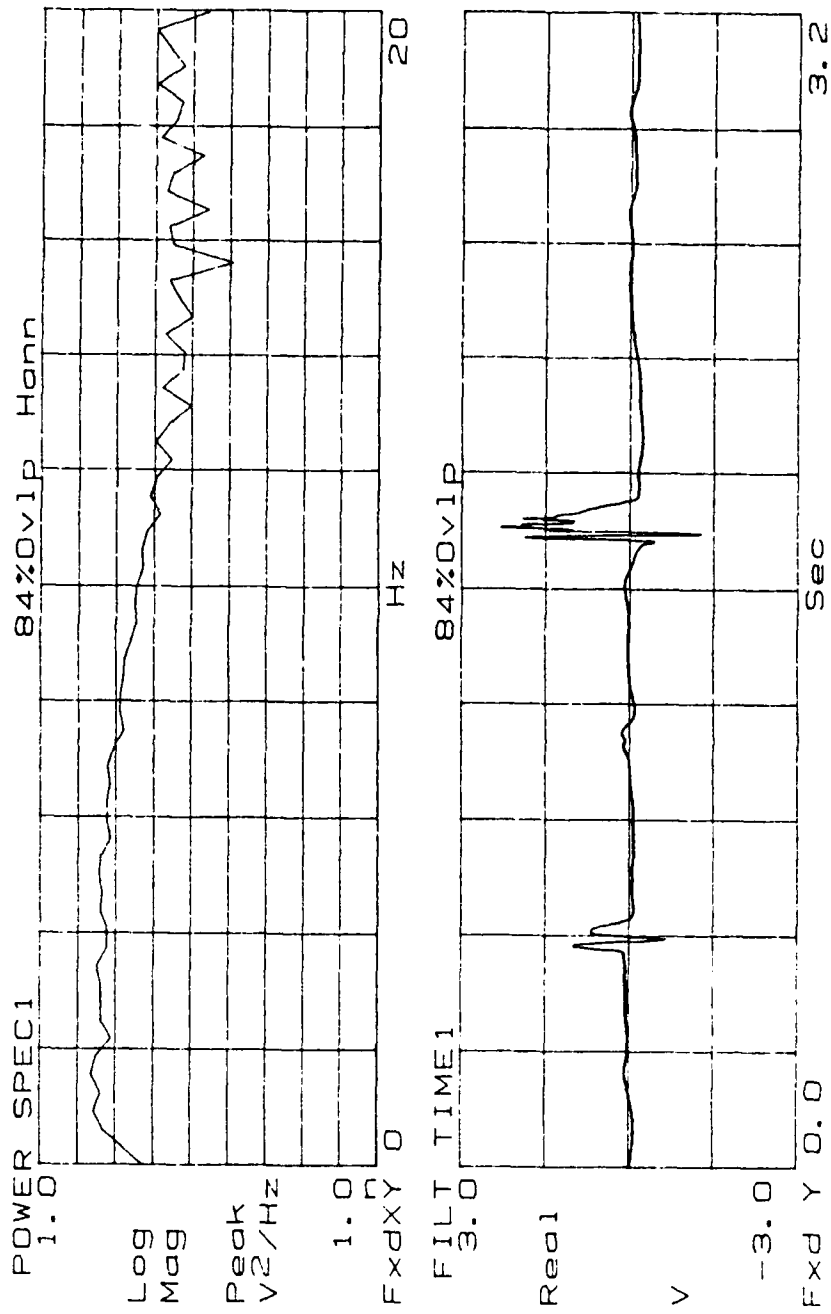


Figure 167.  $Re = 1650$ ,  $f_{osc} = 1$  Hz.



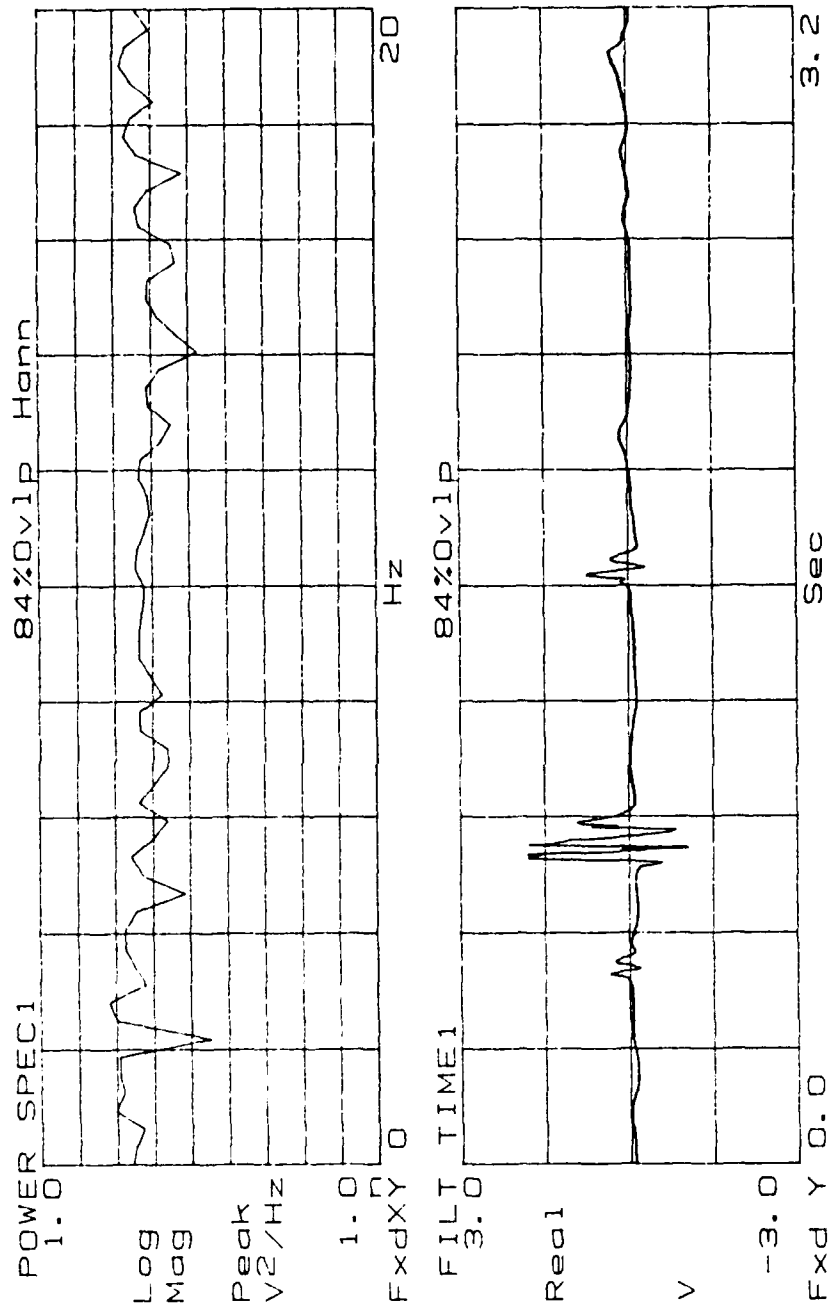


Figure 168.  $Re = 1696$ ,  $f_{osc} = 1$  Hz.

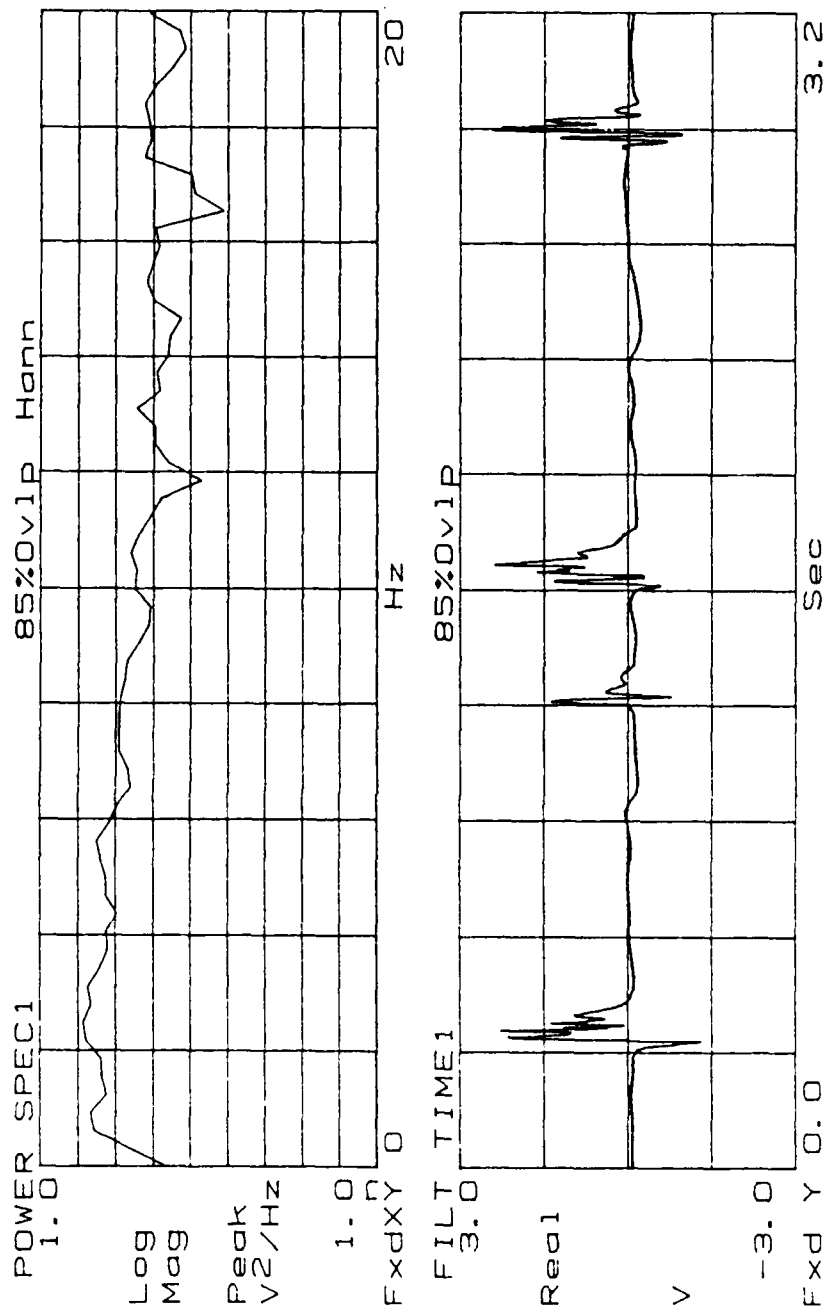


Figure 169.  $Re = 1742$ ,  $f_{osc} = 1$  Hz.

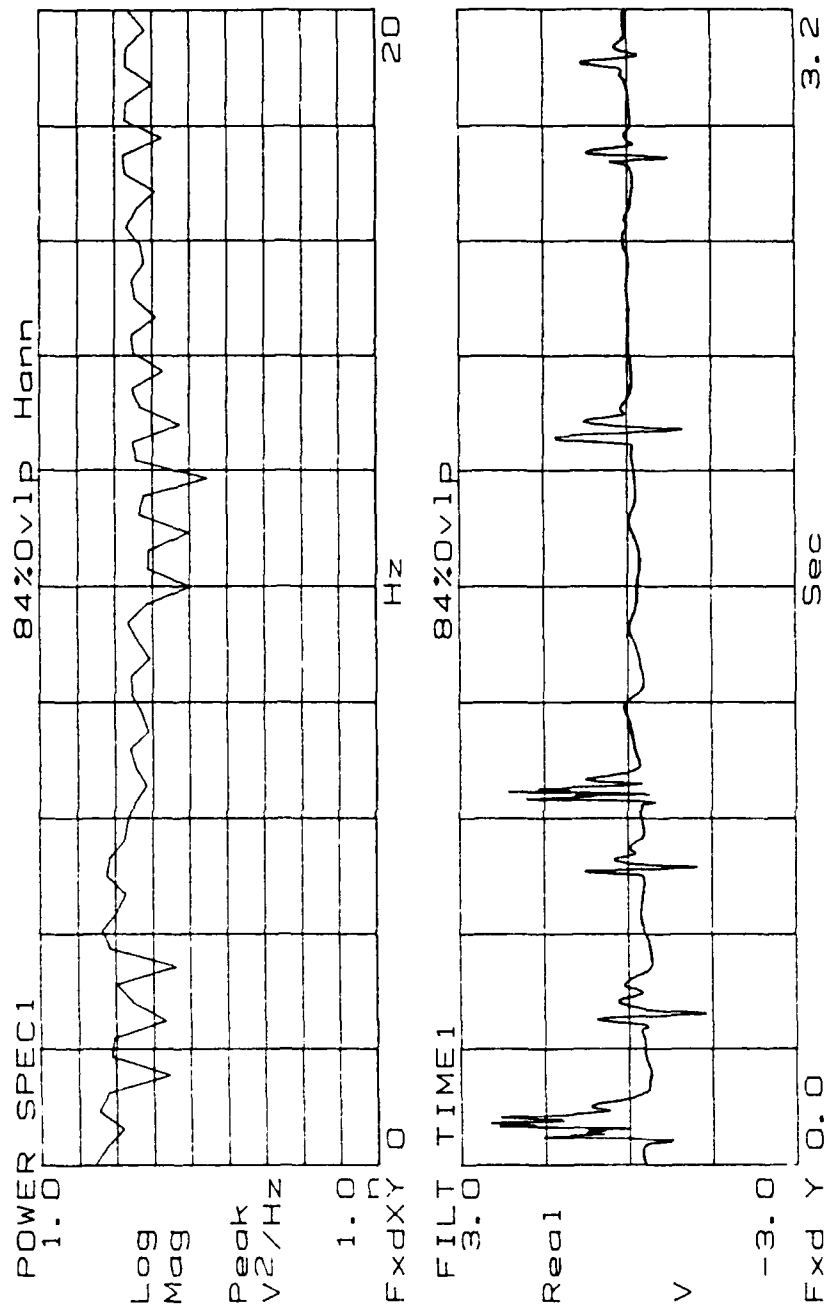


Figure 170.  $Re = 1796$ ,  $f_{osc} = 1$  Hz.

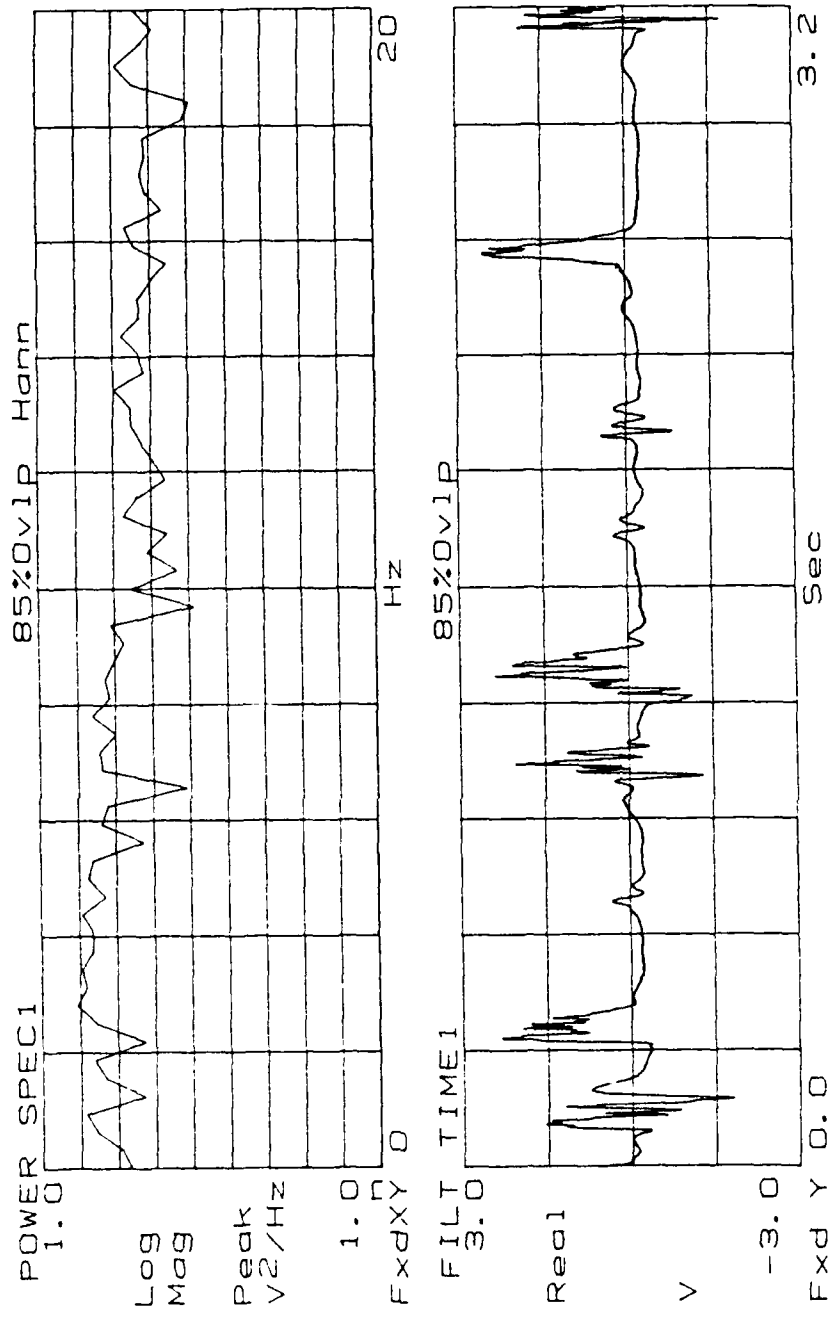


Figure 171. Re = 1905,  $f_{osc} = 1$  Hz.

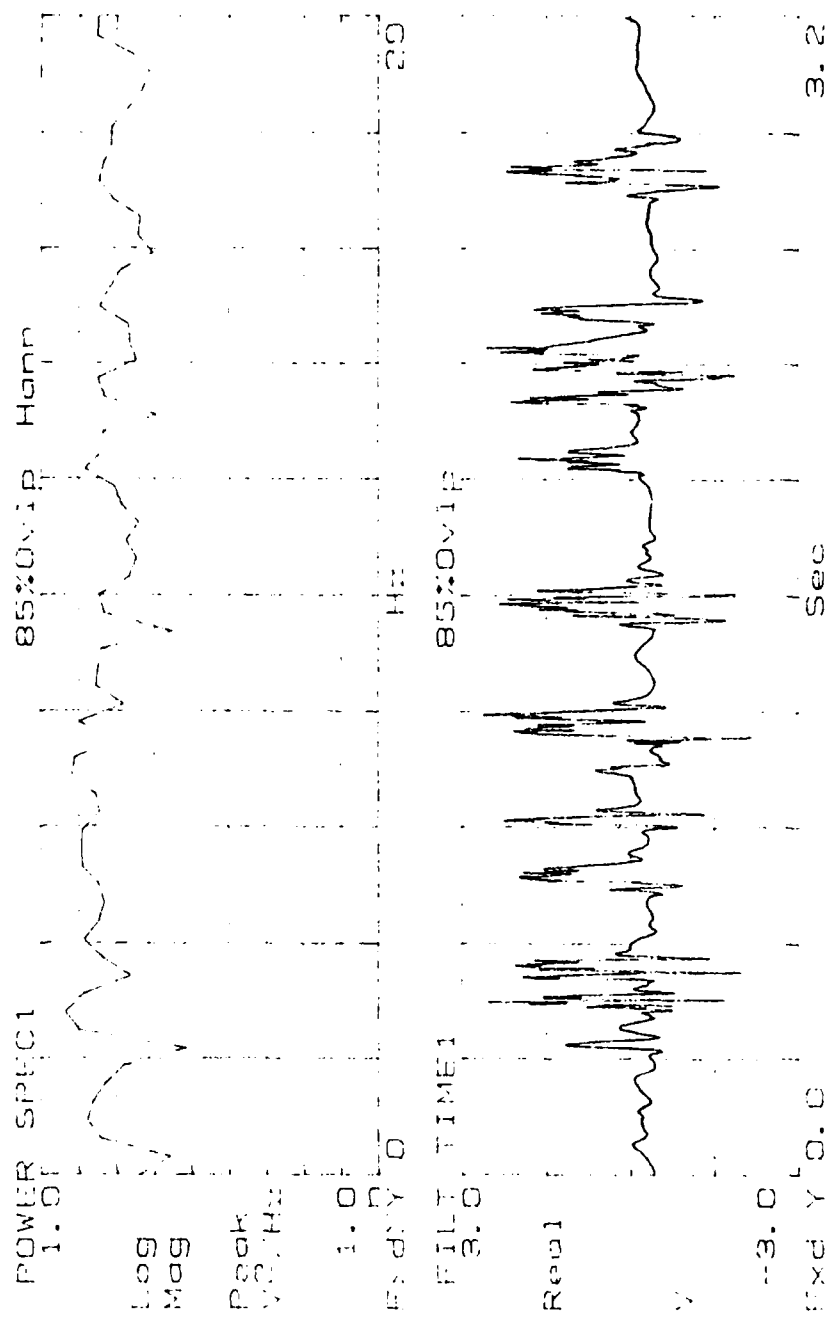


Figure 172. Re = 2005,  $f_{osc} = 1$  Hz.

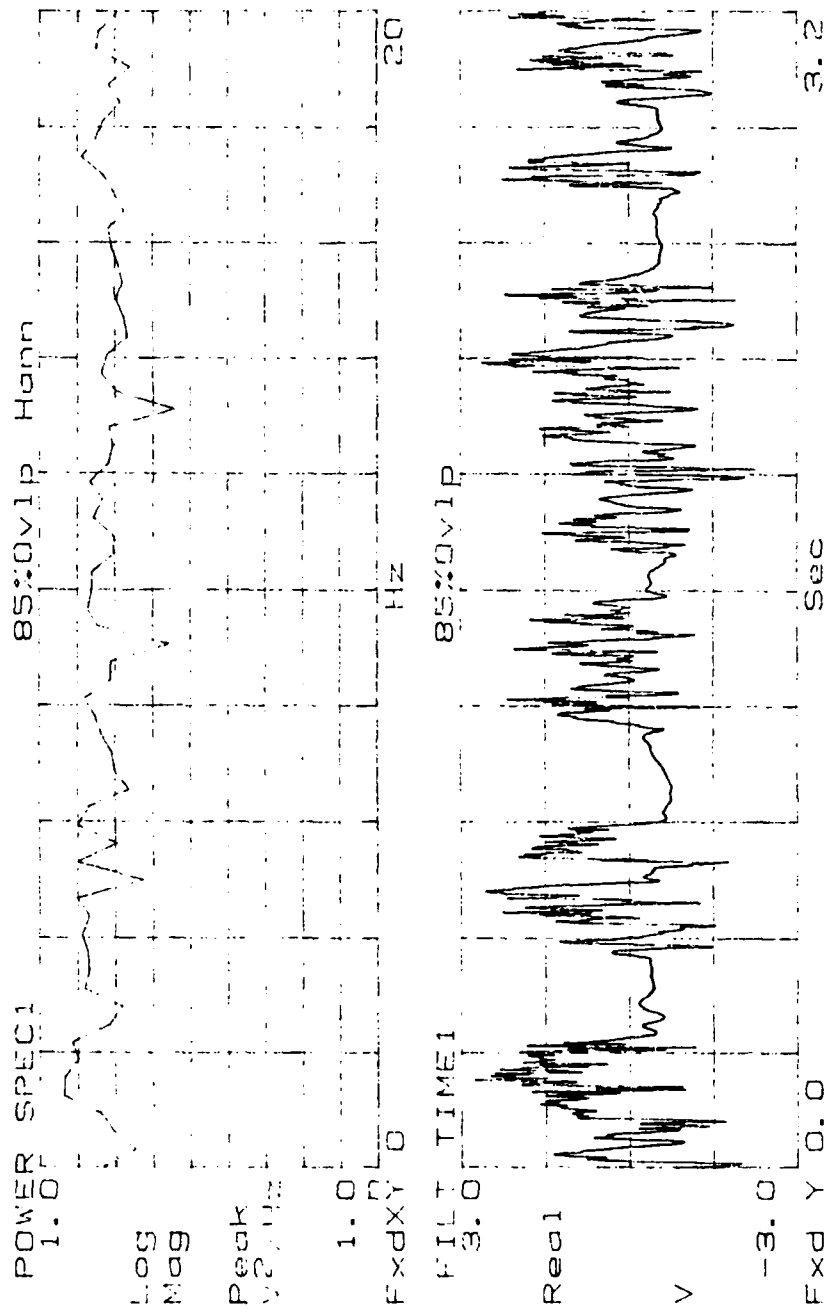


Figure 173.  $Re = 2097$ ,  $f_{osc} = 1$  Hz.

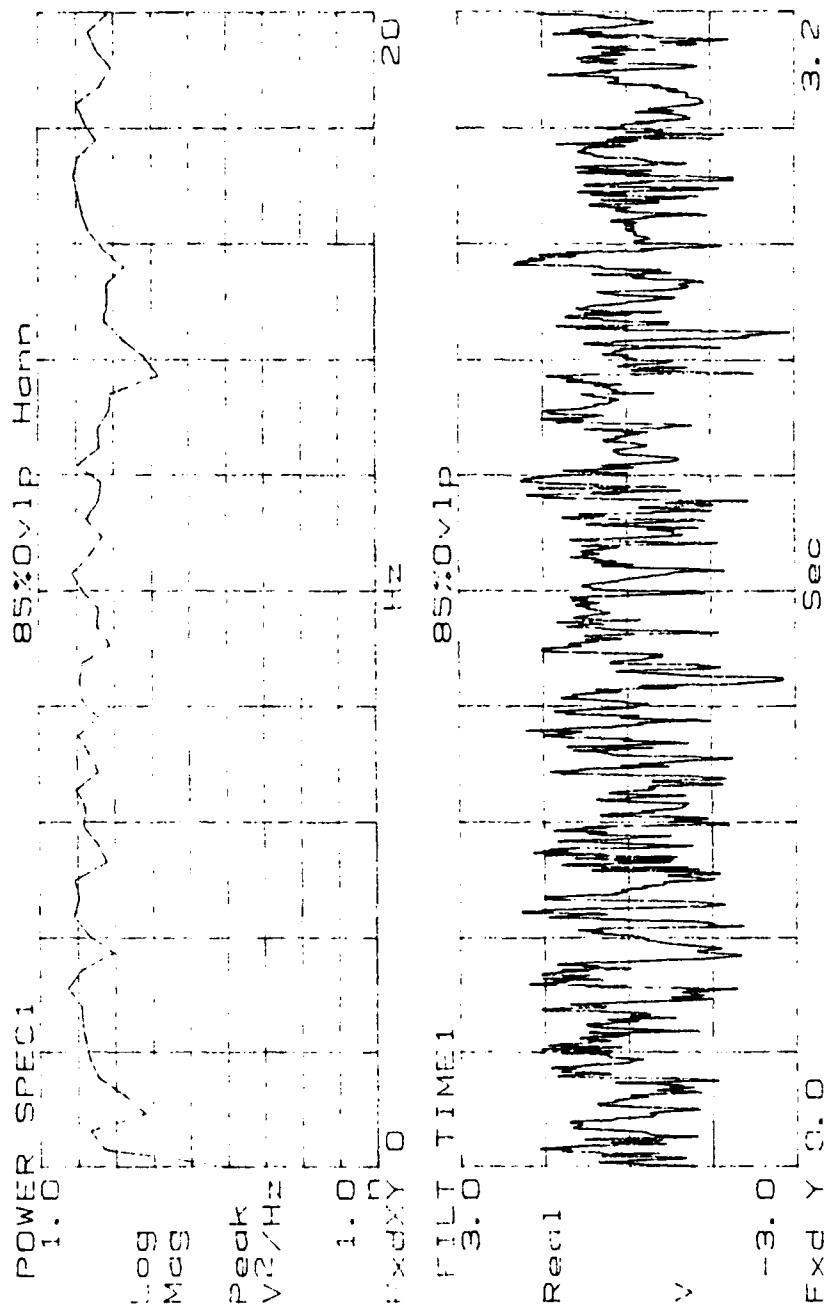


Figure 174.  $Re = 2197$ ,  $f_{osc} = 1$  Hz.

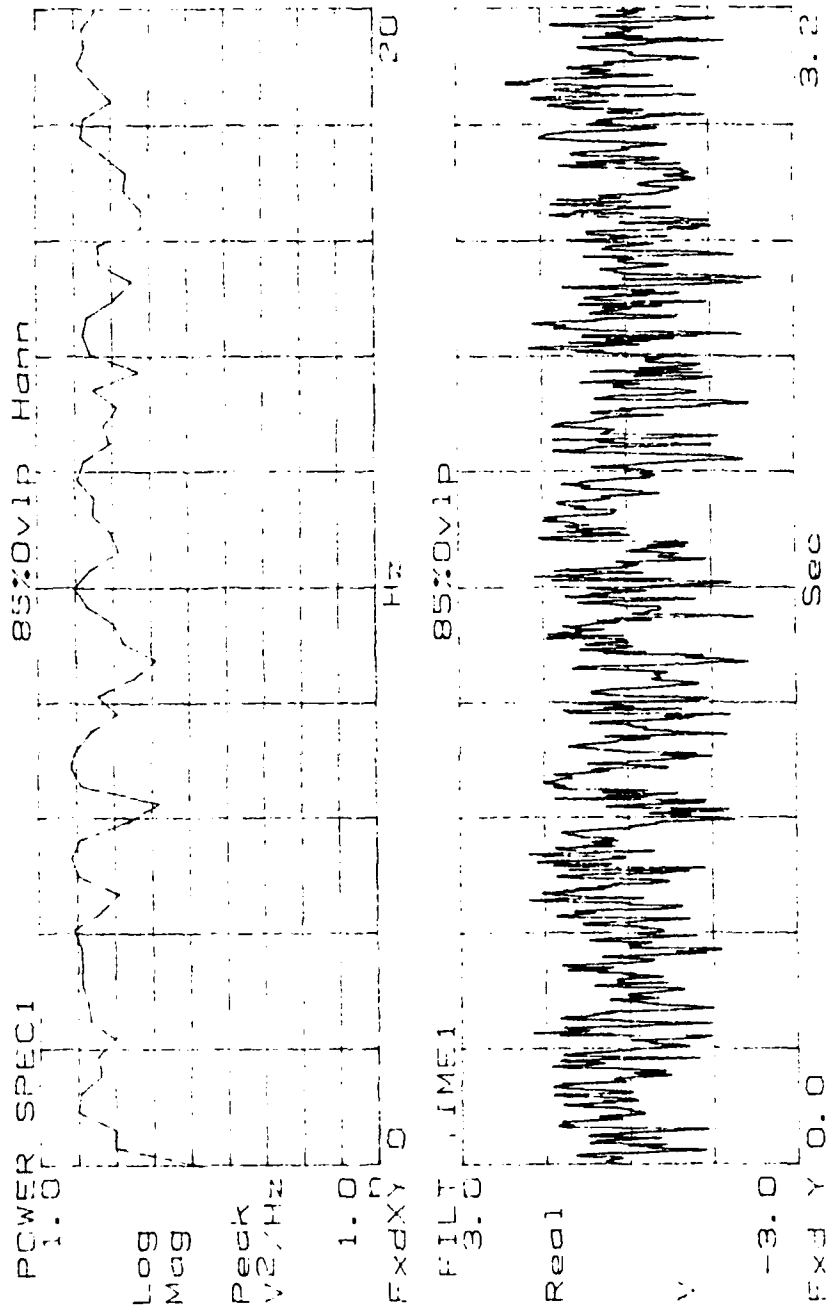


Figure 175.  $Re = 2298$ ,  $f_{osc} = 1$  Hz.



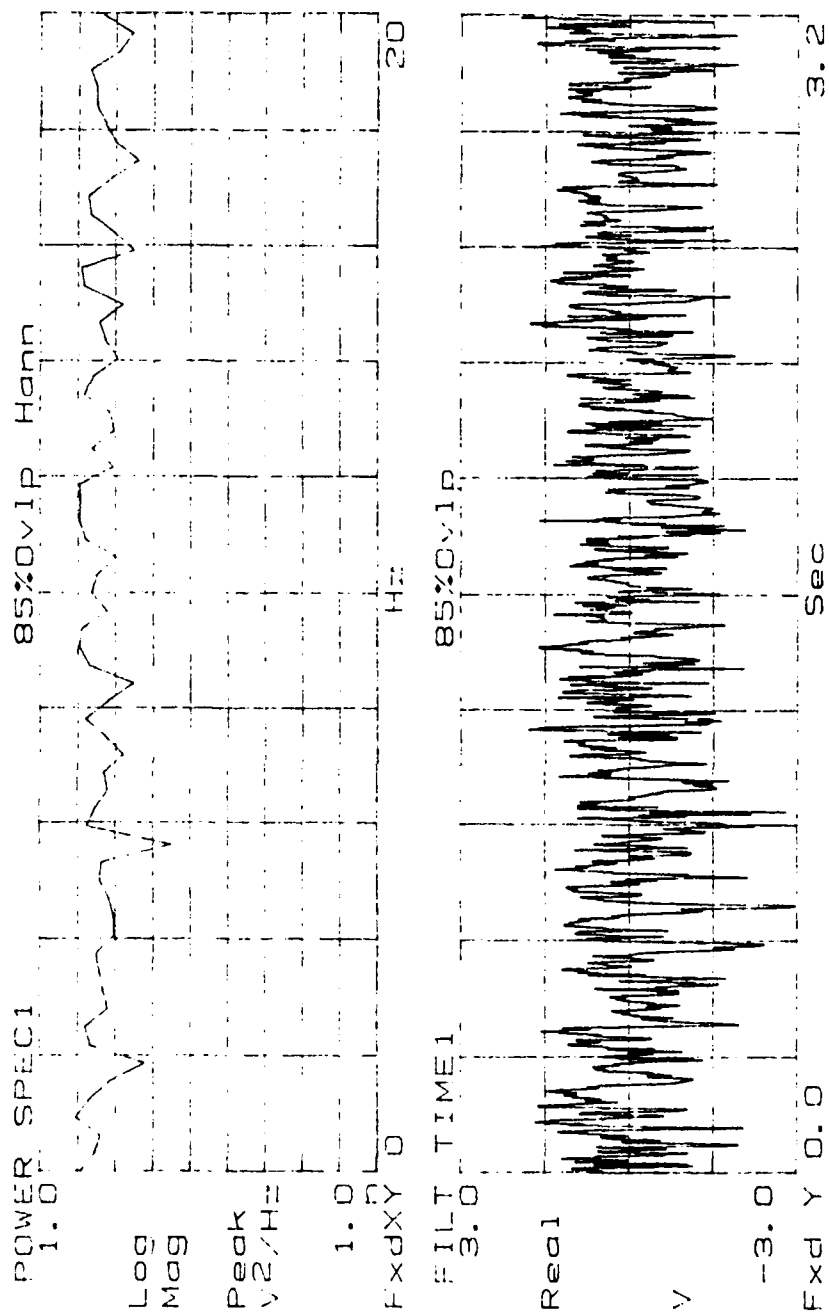


Figure 176.  $Re = 2402$ ,  $f_{osc} = 1$  Hz.

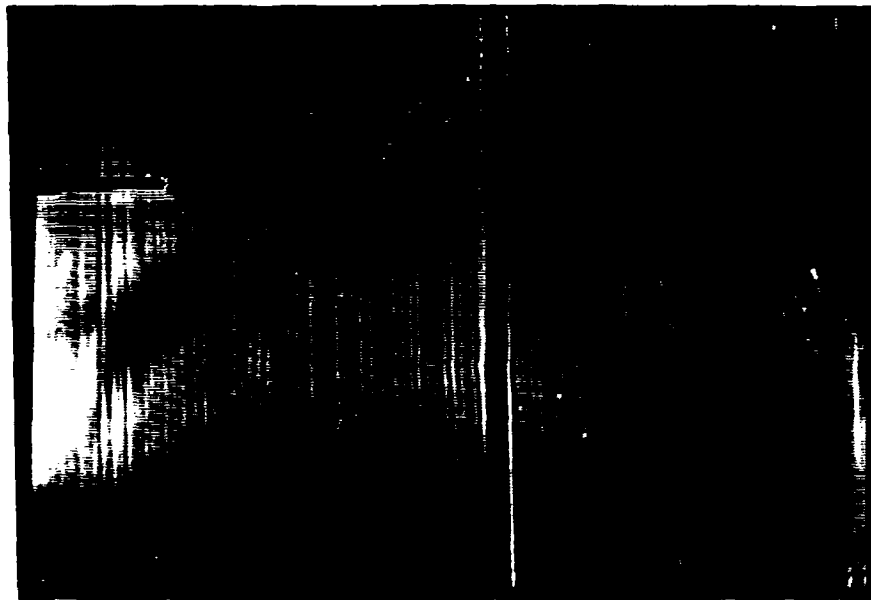
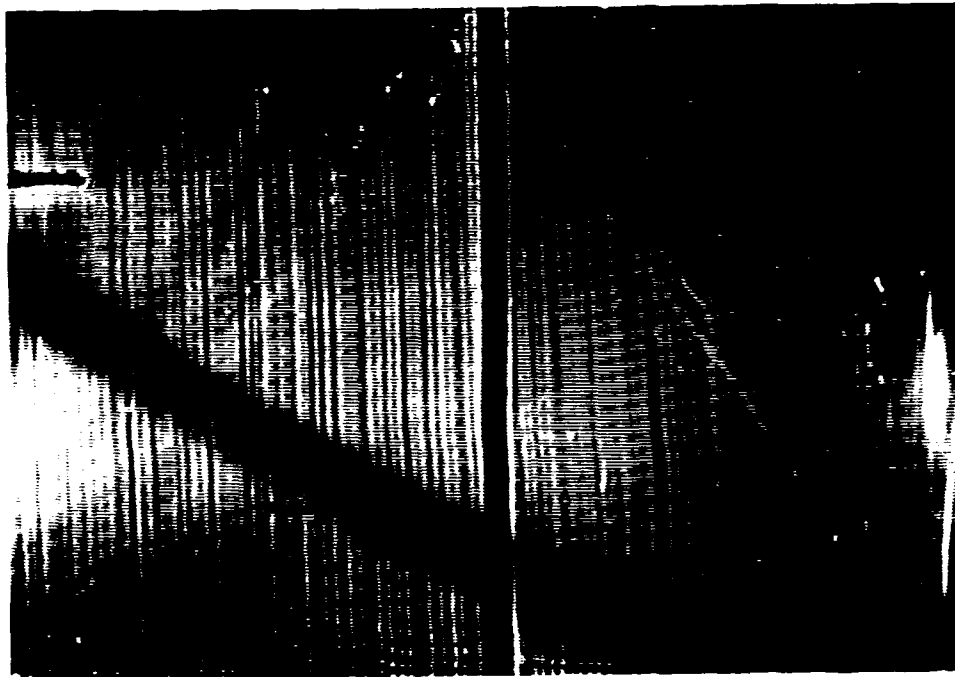


Figure 177. Smoke-wire patterns for  $Re = 1604$ , steady

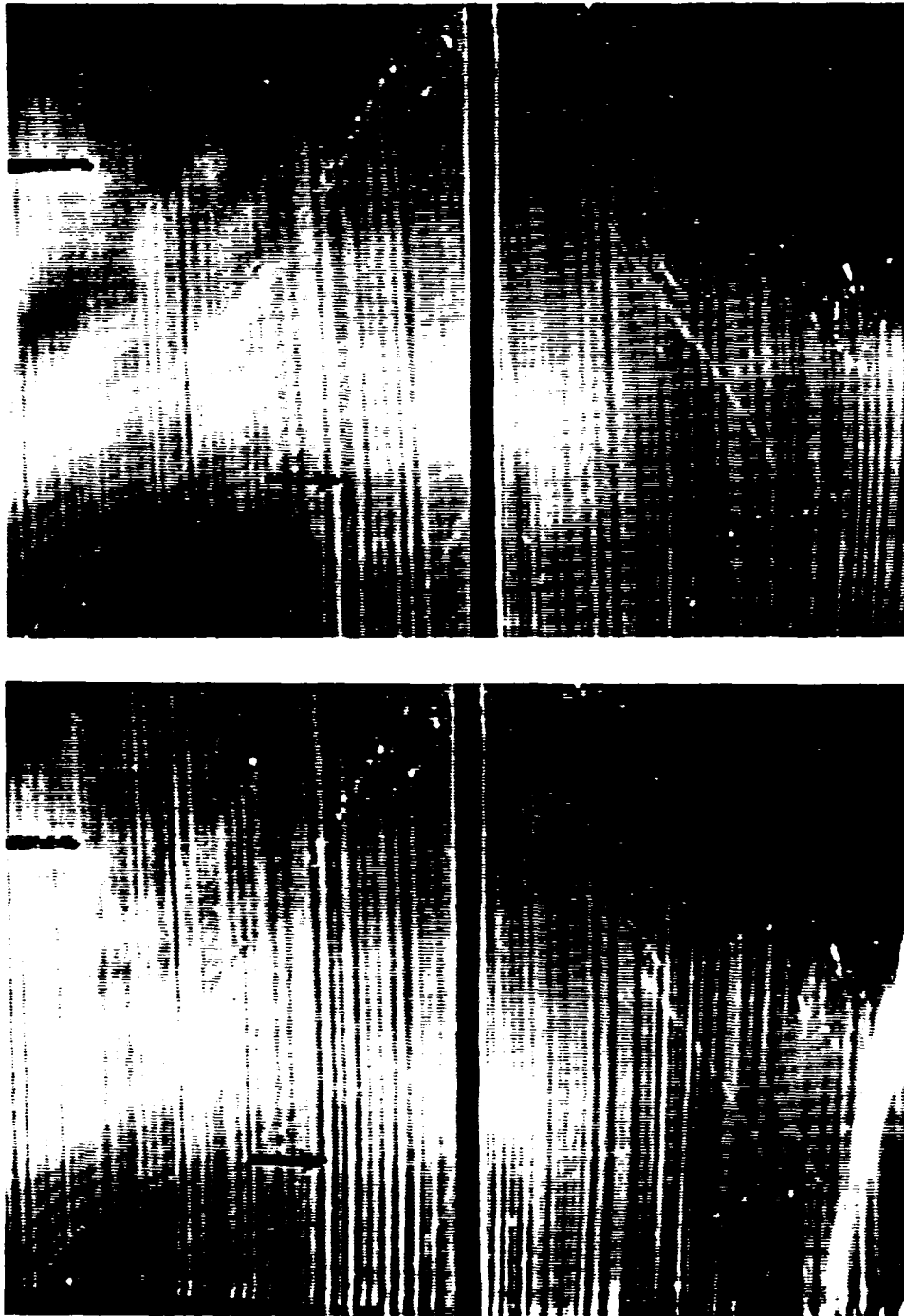


Figure 178. Smoke-wire patterns for  $Re = 1696$ , steady flow

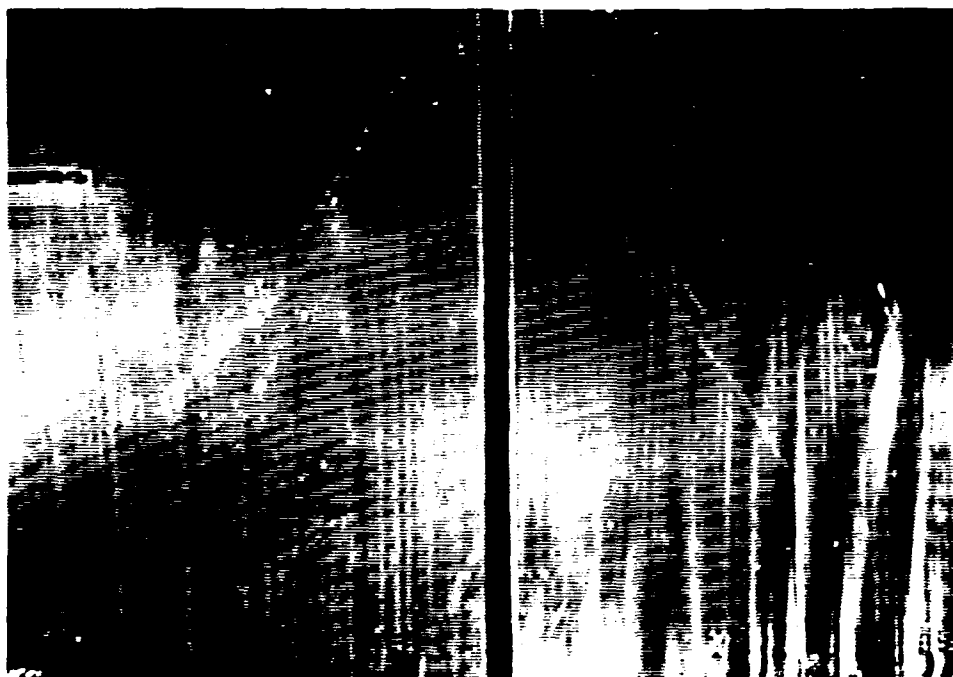
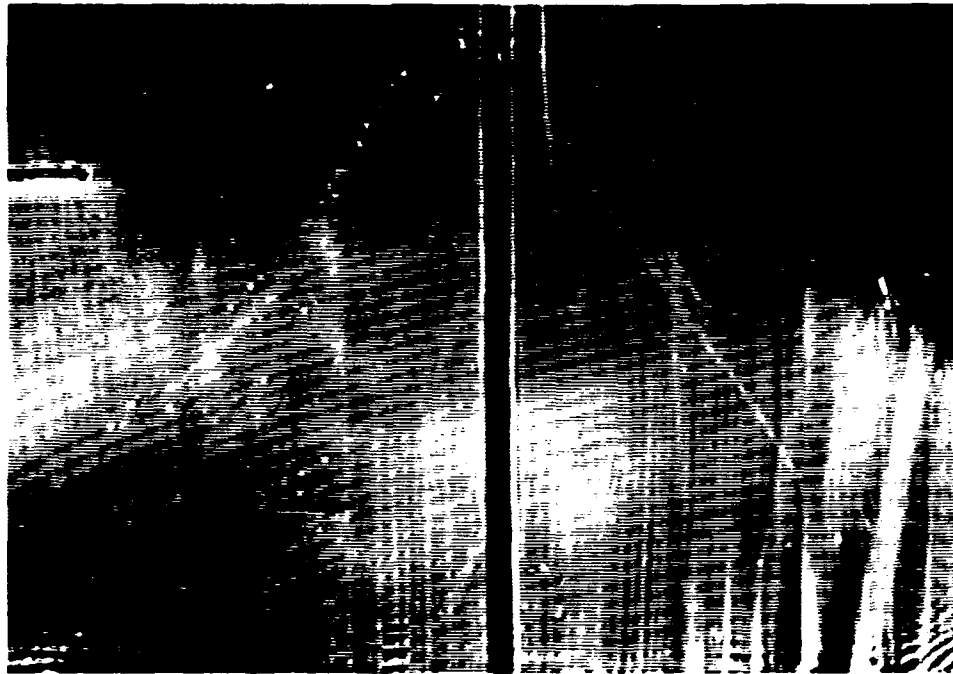


Figure 179. Smoke-wire patterns for  $Re = 1696$ ,  $f_{osc} = 1$  Hz

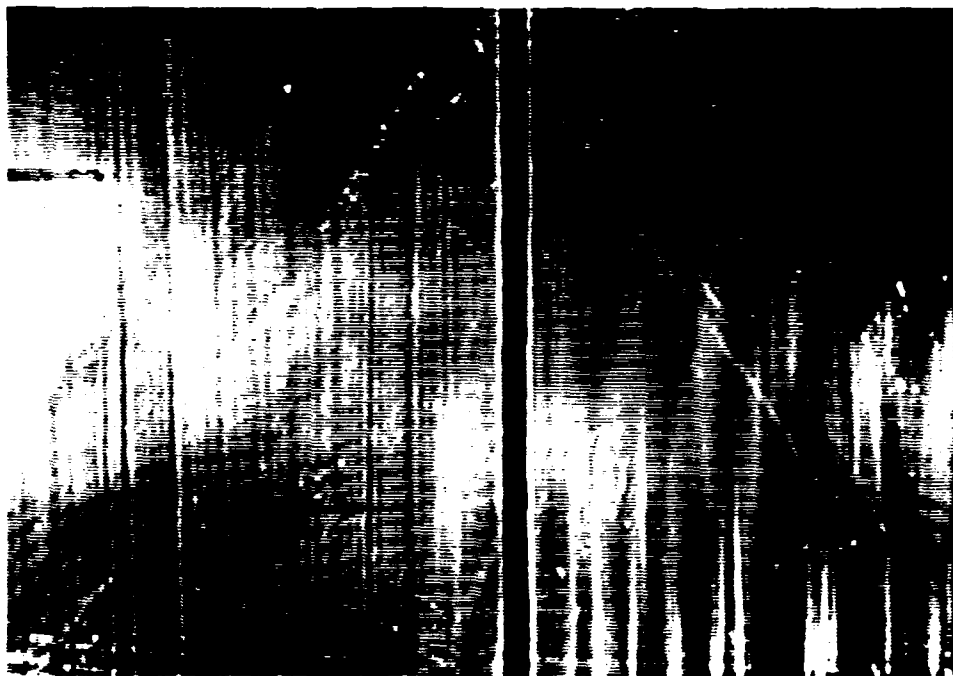


Figure 180. Smoke-wire patterns for  $Re = 1905$ ,  $f_{osc} = 1$  Hz

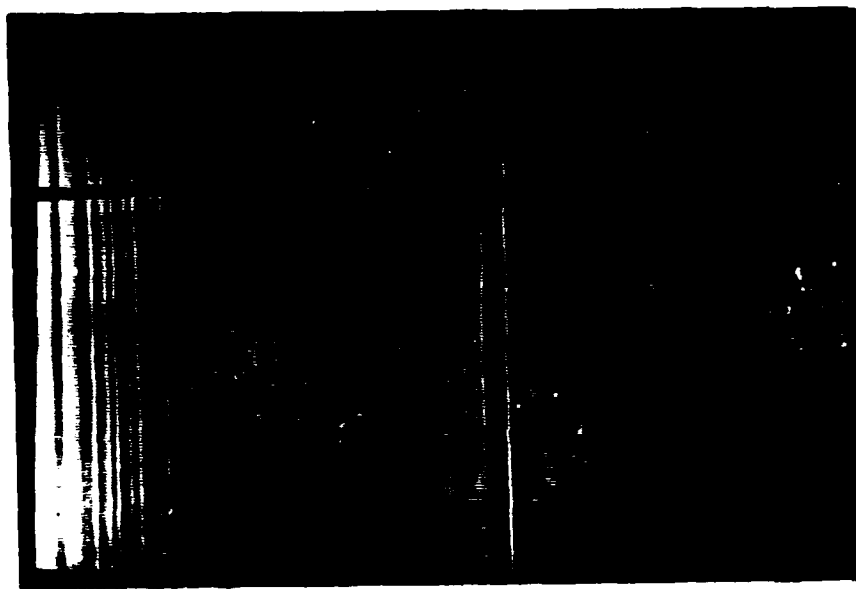
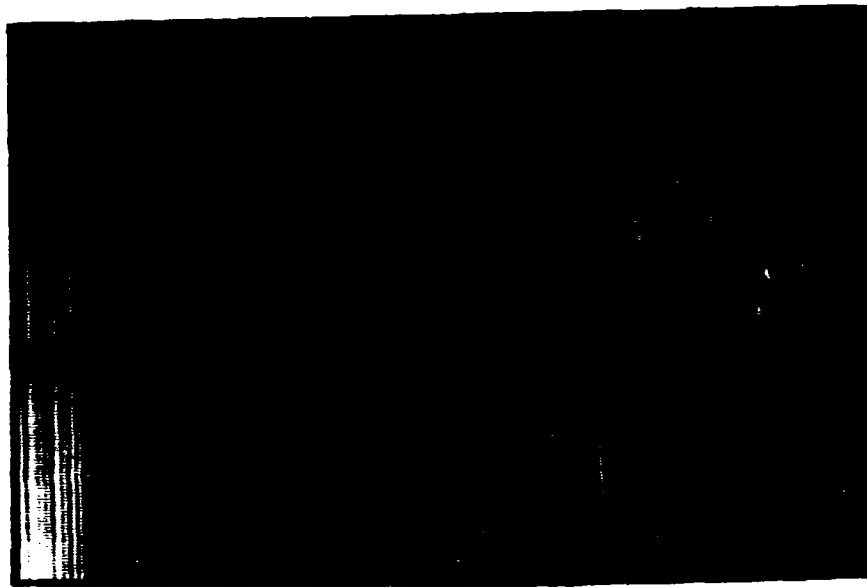


Figure 181. Smoke-wire patterns for  $Re = 1604$ ,  $f_{osc} = 2 \text{ Hz}$ ,  $3 \text{ Hz}$

## LIST OF REFERENCES

1. Shemer, L., "Laminar- Turbulent Transition in a Slowly Pulsating Pipe Flow", *Phys.Fluids*, 28, pp. 3506-3509, 1985.
2. Tu, S. W. and Ramaprian, B. R., "Fully Developed Periodic Turbulent Pipe Flow. Part I. Main Experimental Results and Comparisons with Predictions", *J. Fluid Mech.*, 137, pp. 31-58, 1983.
3. Ramaprian, B. R. and Tu, S. W., "An Experimental Study of Oscillatory Pipe Flow At Transitional Reynolds Numbers", *J. Fluid Mech.*, 100, pp. 513-544, 1980.
4. Stettler, J. C. and Hussain, A. K. M. F., "On Transition of the Pulsatile Pipe Flow", *J. Fluid Mech.*, 170, pp. 169-197, 1986.
5. Merkli, P. and Thomann, H., "Transition to Turbulence in Oscillating Pipe Flow", *J. Fluid Mech.*, 68, pp. 567-575, 1975.
6. Sergeev, S. I., "Fluid Oscillations in Pipes at Moderate Reynolds Numbers", *Fluid Dyn. (Mekh 2H)* 1, pp. 21-22, 1966.
7. Hino, M. and Sawamoto, M., "Linear Stability Analysis of an Oscillatory Flow Between Parallel Plates", *Proc. 7th Symposium on Turbulence*. H. Sato and M. Ohji, Eds., pp. 1-7. Inst. of Space & Aeronautics, Univ. of Tokyo, 1975.
8. Hino, M., Sawamoto, M. and Takasu, S., "Experiments on Transition to Turbulence in an Oscillatory Pipe Flow", *J. Fluid Mech.*, 75, pp. 193-207, 1976.

9. Gerrard, J. H., "An Experimental Investigation of the Pulsating Turbulent Water Flow in a Tube", *J. Fluid Mech.*, 46, pp. 43-64, 1971.
10. Gilbrech, D. A. and Combs, G.D., "Critical Reynolds Numbers for Incompressible Pulsating Flow in Tubes," in *Developments in Theoretical and Applied Mechanics*, I. New York, Plenum Press, 1963.
11. Sarpakaya, T., "Experimental Determination of the Critical Reynolds Number for Pulsating Poiseuille Flow", *Trans. A.S.M.E. D. J. Basic Engrg.*, 88, pp. 589-598, 1966.
12. Simpson, R. L., Sallas, J. J. and Nasburg, R. E., "Tailoring the Wave Form of a Periodic Flow with a Programmable Damper", *J. Fluids Engrg.*, 100, pp. 287-290. 1978.
13. Grosch, C. E. and Salwen, H., "The Stability Of Steady And Time-Dependent Plane Poiseuille Flow", *J. Fluid Mech.*, 34, pp.177-205, 1968.
14. Herbert, D. M., "The Energy Balance in Plane Poiseuille Flow", *J. Fluid Mech.*, 56, pp. 73-80, 1972.
15. Hall, P., "The Stability of Plane Poiseuille Flow Modulated at High Frequency", *ProcR. Soc. Lond. A.*, 344, pp. 453-464, 1975.
16. von Kerczek, C. H., "The Instability of Oscillatory Plane Poiseuille Flow", *J. Fluid Mech.*, 116, pp. 91-114, 1982.
17. Singer, B., Ferziger, J. H. and Reed, H., *Numerical Simulation of Laminar-Turbulent Transition in the Plane Channel*, Report TF- 31, Thermosciences Division, Department of Mechanical Engineering, Stanford University, Stanford, May 1987.



18. Singer, B., Ferziger, J. H. and Reed, H., "Numerical Simulation of Transition in Oscillatory Plane Channel Flow", *J. Fluid Mech.*, 208, pp. 45-66, 1989.
19. Tozzi, J. T., Ph. D. Thesis, Catholic University, 1982.
20. Davies, S., "Stability of Time Periodic Flows", *Ann. Rev. Fluid Mech.*, 8, pp. 57-74, 1976.
21. Schlichting, H. , *Boundary Layer Theory*, McGraw-Hill Book Company, Seventh Edition. New York, 1979.
22. Subramanian, C. S., Ligrani, P. M., Coumes, T. M., Greco, F. J., Koth, H. and Longest, J. M., "Study of the Imposition of Bulk Flow Oscillations on a Plane Channel Flow at Low Strouhal Numbers", submitted to the *Int'l J. of Experiments in Thermal & Fluid Sciences* in March 1990.
23. Longest, J., *Flow Visualization Studies in (1) a Curved Rectangular Channel With 40 to 1 Aspect Ratio and (2) a Straight Channel With Bulk Flow Unsteadiness*, Master's Thesis, Naval Postgraduate School, Monterey, California, June 1989.
24. Coumes, T. M., *The Effects of 1 Hz imposed Unsteadiness on laminar / Turbulent Transition in a Straight Channel Flow* Master's Thesis, Naval Postgraduate School, Monterey, California, December 1989.
25. Greco F., *The Effects of 2 Hz imposed Unsteadiness on laminar / Turbulent Transition in a Straight Channel Flow* Master's Thesis, Naval Postgraduate School, Monterey, California, December 1989.

26. Zang, T. A. and Krist, S. E., "Numerical Experiments on Stability and Transition in Plane Channel Flow", *Theoretical and Computational Fluid Dynamics*, 1, pp. 41 - 64, 1989.
27. Coles, D., *Proc. Indian Acad. Sci. (Engng Sci.)*, 4, p. 111, 1981.
28. Wygnanski, I. J. and Champagne, F. H., *J. Fluid Mech.*, 59, p. 281, 1973.
29. Rubin, Y., Wygnanski, I. and Haritonidis, J. H., *IUTAM Symp. on Laminar Turbulent Transition* (ed. R. Eppler & H. Fasel), p. 17, Springer, 1980.
30. Kline, S. J., and McClintock, F. A., "Describing Uncertainties in Single-Sample Experiments", *Mech. Engrg.*, pp. 3-8, 1953.
31. Moffat, R. J., "Describing the Uncertainties in Experimental Results", *Exp. Therm. Fluid Sci.*, 1, 1, pp. 11-18, 1988.

## INITIAL DISTRIBUTION LIST

1. Defense Technical Information Center 2  
Cameron Station  
Alexandria, Virginia 22304-6145
2. Library, Code 0142 2  
Naval Postgraduate School  
Monterey, California 93943-5002
3. Professor P. M. Ligrani, Code 69Li 4  
Department of Mechanical Engineering  
Naval Postgraduate School  
Monterey, California 93943-5000
4. Department Chairman, Code 69 1  
Department of Mechanical Engineering  
Naval Postgraduate School  
Monterey, California 93943-5000
5. Naval Engineering Curricular Officer, Code 34 1  
Department of Mechanical Engineering  
Naval Postgraduate School  
Monterey, California 93943-5000
6. Professor C. S. Subramanian, Code 69Su 2  
Department of Mechanical Engineering  
Naval Postgraduate School  
Monterey, California 93943-5000
7. Professor Y. S. Joshi, Code 69Ji 2  
Department of Mechanical Engineering  
Naval Postgraduate School  
Monterey, California 93943-5000
8. LT Howard E. Koth 4  
8984 N Crass Rd.  
Tomahawk, Wisconsin 54487